THE UNIVERSITY OF ALBERTA

THE PREDICTION OF THE MINIMUM MISCIBILITY PRESSURE

by

Akli NOUAR

©

A THESIS

SUBMITTED TO THE FACULTY OF GRADUATE STUDIES AND RESEARCH

IN PARTIAL FULFILMENT OF THE REQUIREMENTS FOR THE DEGREE

OF Doctor of Philosophy

IN

Petroleum Engineering

MINING, METALLURGICAL AND PETROLEUM ENGINEERING

EDMONTON, ALBERTA

Fall, 1987

Permission has been granted to the National Library of Canada to microfilm this thesis and to lend or sell copies of the film.

The author (copyright owner) has reserved other publication rights, and neither the thesis nor extensive extracts from it may be printed or otherwise reproduced without his/her written permission.

L'autorisation a été accordée à la Bibliothèque nationale du Canada de microfilmer cette thèse et de prêter ou de vendre des exemplaires du film.

L'auteur (titulaire du droit d'auteur) se réserve les autres droits de publication; ni la thèse ni de longs extraits de celle-ci ne doivent être imprimés ou autrement reproduits sans son autorisation écrite.

ISBN 0-315-41166-X

THE UNIVERSITY OF ALBERTA

RELEASE FORM

NAME OF AUTHOR Akli NOUAR

TITLE OF THESIS THE PREDICTION OF THE MINIMUM MISCIBILITY PRESSURE

DEGREE FOR WHICH THESIS WAS PRESENTED Doctor of Philosophy

YEAR THIS DEGREE GRANTED Fall, 1987

Permission is hereby granted to THE UNIVERSITY OF ALBERTA LIBRARY to reproduce single copies of this thesis and to lend or sell such copies for private, scholarly or scientific research purposes only.

The author reserves other publication rights, and neither the thesis nor extensive extracts from it may be printed or otherwise reproduced without the author's written permission.

(SIGNED) A. N. Nouar

PERMANENT ADDRESS:

26 Rue Parmentier
Hydra Alger
ALGERIE - ALGERIA

DATED Oct. 15 1987

THE UNIVERSITY OF ALBERTA

FACULTY OF GRADUATE STUDIES AND RESEARCH

The undersigned certify that they have read, and recommend to the Faculty of Graduate Studies and Research, for acceptance, a thesis entitled THE PREDICTION OF THE MINIMUM MISCIBILITY PRESSURE submitted by Akli NOUAR in partial fulfilment of the requirements for the degree of Doctor of Philosophy in Petroleum Engineering.

D.L. Flock

Supervisor

Ramon Bentsen

A E Mather

M. M. Oguztoreli

J M Whiting

External Examiner

Date Oct. 15, 1987

ABSTRACT

The need for the development of a reliable method for the prediction of the minimum miscibility pressure (MMP) for lean hydrocarbon and nitrogen vaporizing gas drives is becoming more obvious considering the time and expense required to perform laboratory evaluations. A new approach for predicting the MMP for a lean hydrocarbon vaporizing gas drive is presented. The method has a theoretical basis, since it relies on thermodynamic criteria that have been set forth in the case of ternary systems and, thereby, removes some of the empiricism attached to most of the correlations used to predict the MMP.

In order to predict the MMP for a nitrogen vaporizing gas drive of an oil containing an appreciable amount of methane, one needs to consider the two light components, methane and nitrogen, as two separate entities, since each of them has a characteristic influence on the phase behavior of the system. The ternary representation of a multicomponent system will necessarily leave one component for the representation of the oil which, therefore, must give rise to large quantitative errors. An order of magnitude better representation can be achieved, however, if quaternary diagrams are used, allowing a more realistic represenation of the oil composition into a light (C1), and intermediate (C2-C6) and a heavy fraction ($C7^+$).

For nitrogen vaporizing gas drives, the proposed method involves the extension of the concepts used in the previous ternary system approach to quaternary systems. It considers methane and nitrogen as two separate components. This new predictive method consists of determining and correlating the MMP's for quaternary systems, based upon rigorous thermodynamic criteria. The MMP of a vaporizing gas drive of a multicomponent oil by nitrogen is then predicted using quaternary systems as building blocks.

AKNOWLEDGEMENTS

The author is especially grateful to Dr. D.L. Flock for his guidance and support in this study.

Thanks are due to the ALBERTA OIL SANDS TECHNOLOGY AND RESEARCH AUTHORITY, the PETROLEUM AID TO EDUCATION and the MINING, METALLURGICAL AND PETROLEUM ENGINEERING DEPARTMENT for partial financial support.

Thanks are also due to Messrs. J. Gibeau and B. Smith who helped in the set up of the experimental apparatus.

Table of Contents

Chapter Page

1. Introduction 1

2. Phase Behavior of Multicomponent Systems 3

2.1 Introduction. 3

2.2 Qualitative Phase Behavior. 4

2.3 Phase Behavior of Ternary Systems. 6

2.4 Phase Behavior of Quaternary systems. 9

3. Concept of Minimum Miscibility Pressure 17

3.1 Introduction. 17

3.2 Basic Displacement Mechanisms of a Vaporizing Gas Drive. 18

3.2.1 Immiscible Case. 18

3.2.2 Multiple-contact Miscible Case (or Dynamic Miscibility). 21

3.2.3 First-contact Miscible Case. 23

3.3 Basic Displacement Mechanisms of a Condensing Gas Drive. 25

3.3.1 Immiscible Case. 25

3.3.2 Multiple-contact Miscible Case. 27

3.4 Definition of the Minimum Miscibility Pressure for Ternary Systems. 27

3.5 Extension of the Concept of MMP to Quaternary Systems. 28

3.5.1 Immiscible Case. 30

3.5.2 Multiple-contact Miscible Case. 32

3.5.3 Definition of the Minimum Miscibility Pressure for Quaternary Systems. 32

4. Methods For Estimating The Minimum Miscibilty Pressure 34

4.1 Introduction 34

4.2 Pseudo-Ternary Diagram Method 35

4.3 Empirical Correlations 38

4.4 Slim-Tube Test Method 40

4.5 Line of Investigation 42

5. Formulation of the Criteria Defining the MMP 44

5.1 Introduction 44

5.2 Phase Equilibria for Multicomponent Systems 45

5.2.1 Gibbs Free Energy Analysis of a Binary System 47

5.2.2 Gibbs Free Energy Analysis of a Ternary System 51

5.3 Equation of the Limiting Tie Line of a Ternary System 55

5.4 Equation of the Quaternary Limiting Tie Line 64

5.5 Selection of the Equation of State 72

6. Minimum Miscibility Predictions for Methane and Nitrogen Vaporizing Gas Drives ... 75

6.1 Introduction 75

6.2 Methane Vaporizing Gas Drives 75

6.2.1 Correlation of Generated Data 79

6.2.2 Procedure for Predicting the MMP of a Ternary System 82

6.2.3 Procedure for Predicting the MMP of a Multicomponent System 83

6.2.4 Comparison of Predicted and Experimental MMP's 87

6.3 Nitrogen Vaporizing Gas Drives 95

6.3.1 Correlation of Generated Data 99

6.3.2 Procedure for Predicting the MMP of a Quaternary System 99

6.3.3 Extension to Multicomponent Systems 100

6.3.4 Effect of Reservoir Oil Composition on the MMP 101

6.3.5 Effect of Temperature on the MMP 105

6.3.6 Comparison Between Predicted and Experimental MMP's 107

SUMMARY AND CONCLUSIONS 111

REFERENCES 113

Appendix 1
Application of the Fractional Flow Theory
to Vaporizing and Condensing Gas Drives 118

Appendix 2
Properties of Extensive Variables 141

Appendix 3
Stability Analysis of Homogeneous Phases 145

Appendix 4
Gibbs Free Energy From Soave-Redlich and Kwong
Equation of State and Related Partial Derivatives 148

Appendix 5
A New Equation of State for Pure Components 151

Appendix 6
Prediction of the MMP of a Methane VGD
Numerical Application and Related Table and Figures 170

Appendix 7
Experimental Apparatus & Experimental Procedure 184

Appendix 8
Fortran Program for the Determination of the MMP
of a Nitrogen VGD 190

List of Tables

Table	Description	Page
1	Experimental Procedures and Criteria for MMP Determination	41
2	Initial Estimates and Number of Iterations for Convergence (Method 1 vs. Method 2)	63
3	Binary Interaction Coefficients	74
4	Comparison of Experimental and Predicted MMP's (Lean hydrocarbon vaporizing gas drive)	90
5	Comparison of Experimental and Predicted MMP's (nitrogen vaporizing gas drive)	107
1-1	Input Data for Condensing Gas Drive	132
1-2	Input Data for Vaporizing Gas Drive	137
5-1	Acentric Coefficients and Critical Properties	154
5-2	Comparison between Calculated and Experimental PVT Data	156
5-3	Comparison Between Calculated and Experimental Saturated Properties	157
6-1	Coefficients of Equations 58 and 59 (lean hydrocarbon vaporizing gas drive)	172
6-1	(continued) - Coefficients of Equations 58 and 59 (lean hydrocarbon vaporizing gas drive)	173
7-1	Slim-tube Physical Characteristics	186

List of Figures

Figure		Page
1	Pressure-Temperature Diagram for Various Binary Systems	5
2-a	Phase Behavior of Ternary System:C1-C3-C10 T=60 °C Representation on a Ternary Diagram T,P fixed	7
2-b	Phase Behavior of Ternary System:C1-C3-C10 T=60 °C Phase Envelopes at Various Pressures T,fixed	7
3	Representation of the Quaternary System N2-C1-C3-C10 on a Tetrahedron	10
4	Phase Diagram of Quaternary System:N2-C1-C3-C10 at T=60 °C P=11 MPa, low pressure case	11
5	Phase Diagram of Quaternary System:N2-C1-C3-C10 at T=60 °C P=18 MPa, medium pressure case	14
6	Phase Diagram of Quaternary System:N2-C1-C3-C10 at T=60 °C P=41 MPa, high pressure case	15
7-a	Starting Stage of Immiscible VGD	19
7-b	Final Stage of Immiscible VGD	19
8-a	Starting Stage of Multiple Contact Miscible VGD	22
8-b	Final Stage of Multiple Contact Miscible VGD	22
9-a	Idealized Representation of Porous Media	24
9-b	Representation of the Effect of Convective Mixing on a Phase Diagram	24
10-a	Final Stage of Immiscible CGD	26
10-b	Final Stage of Multiple Contact Miscible CGD	26

11 Quaternary Limiting Tie Lines of System: N2-C1-C3-C10 at T=60 °C and P= 25MPa 29

12 Final Stage of Immiscible VGD Case of a Quaternary System 31

13-a Normalized Gibbs Free Energy of Binary System: Methane, n-Pentane T=87 °C P=8 MPa 48

13-b Second Partial Derivative of the Normalized Gibbs Free Energy as a Function of n-Pentane Mole Fraction 48

14 Inverted Gibbs Free Energy of a Ternary System - T,P fixed 52

15 Generation of Bubble and Dew point Curves of a Ternary System T,P fixed 60

16 Critical Curves of Various Binaries - Experiments vs. Predictions, using SRK EOS 73

17 Comparison of Experimental and Prediction of Critical Points and Limiting Tie Lines - System: Methane n-Butane Decane - T=71 °C 78

18 Minimum Miscibility Pressure vs. Intermediate Mole Fraction at Critical Point - T=30 °C MWI=44 81

19-a Effect of MWH on MMP - T=60 °C 86

19-b Effect of MWI on MMP - T=60 °C 86

19-c Effect of T on MMP 86

20 Effect of Tube Length and Injection Rate on Recovery vs. Pressure after 1.2 PV injection 88

21 Recovery vs Pressure Curve (after 1.17 PV injection) Methane Displacement 92

22 Intersection of Quaternary Limiting Tie Lines with the Hydrocarbon Composition Plane (Limiting Curves) 98

23 Effect of Molecular Weight of Intermediates and Heavies on MMP 102

24 Effect of Methane Mole Fraction in Oil on MMP 104

25 Effect of Temperature on MMP 106

26 Recovery vs. Pressure Curve (after 1.08 PV injection)
Nitrogen Displacement 109

1-1 Projections of Composition Routes on Composition Plane 126

1-2 Condensing Gas Drive Case: Composition Route 133

1-3 Condensing Gas Drive Case: Phase Composition and Normalized Velocity
vs. Dimensionless Length (at 0.5 Pore Volume Injection) 134

1-4 Condensing Gas Drive Case:
Oil Saturation vs. Dimensionless Length (at 0.5 Pore Volume Injection)
% Recovery of In-Place n-Decane vs. Pore Volume Injection 135

1-5 Vaporizing Gas Drive Case: Composition Route 138

1-6 Vaporizing Gas Drive Case: Phase Composition and Normalized Velocity
vs. Dimensionless Length (at 0.5 Pore Volume Injection) 139

1-7 Vaporizing Gas Drive Case:
Oil Saturation vs. Dimensionless Length (at 0.5 Pore Volume Injection)
% Recovery of In-Place n-Decane vs. Pore Volume Injection 140

5-1 Comparison of PVT Data: Methane
Experiments - Prediction (Eq. 5-1) 158

5-2 Comparison of PVT Data: Nitrogen
Experiments - Prediction (Eq. 5-1) 159

5-3 Comparison of PVT Data: Ethane
Experiments - Prediction (Eq. 5-1) 160

5-4 Comparison of PVT Data: Propane
Experiments - Prediction (Eq. 5-1) 161

5-5 Comparison of PVT Data: n-Butane
Experiments - Prediction (Eq. 5-1) 162

5-6 Comparison of PVT Data: n-Pentane
Experiments - Prediction (Eq. 5-1) 163

5-7 Comparison of PVT Data: n-Hexane
Experiments - Prediction (Eq. 5-1) 164

5-8 Comparison of PVT Data: n-Heptane
Experiments - Prediction (Eq. 5-1) 165

5-9 Comparison of PVT Data: n-Octane
Experiments - Prediction (Eq. 5-1) 166

5-10 Comparison of PVT Data: n-Nonane
Experiments - Prediction (Eq. 5-1) 167

5-11 Comparison of PVT Data: n-Decane
Experiments - Prediction (Eq. 5-1) 168

5-12 Comparison of Vapor Pressures
Experiments - Prediction (Eq. 5-1) 169

6-1-a Minimum Miscibility Pressure vs. Intermediate Mole Fraction
at Critical Point - T=30 °C - MWI=44 174

6-1-b Minimum Miscibility Pressure vs. Intermediate Mole Fraction
at Critical Point - T=30 °C - MWI=58 174

6-2-a Minimum Miscibility Pressure vs. Intermediate Mole Fraction
at Critical Point - T=30 °C - MWI=72 175

6-2-b Minimum Miscibility Pressure vs. Intermediate Mole Fraction
at Critical Point - T=30 °C - MWI=86 175

6-3-a Minimum Miscibility Pressure vs. Intermediate Mole Fraction
at Critical Point - T=45 °C - MWI=44 176

6-3-b Minimum Miscibility Pressure vs. Intermediate Mole Fraction
at Critical Point - T=45 °C - MWI=58 176

6-4-a Minimum Miscibility Pressure vs. Intermediate Mole Fraction
at Critical Point - T=45 °C - MWI=72 177

6-4-b Minimum Miscibility Pressure vs. Intermediate Mole Fraction at Critical Point - T=45 °C - MWI=86 177

6-5-a Minimum Miscibility Pressure vs. Intermediate Mole Fraction at Critical Point - T=60 °C - MWI=44 178

6-5-b Minimum Miscibility Pressure vs. Intermediate Mole Fraction at Critical Point - T=60 °C - MWI=58 178

6-6-a Minimum Miscibility Pressure vs. Intermediate Mole Fraction at Critical Point - T=60 °C - MWI=72 179

6-6-b Minimum Miscibility Pressure vs. Intermediate Mole Fraction at Critical Point - T=60 °C - MWI=86 179

6-7-a Minimum Miscibility Pressure vs. Intermediate Mole Fraction at Critical Point - T=75 °C - MWI=44 180

6-7-b Minimum Miscibility Pressure vs. Intermediate Mole Fraction at Critical Point - T=75 °C - MWI=58 180

6-8-a Minimum Miscibility Pressure vs. Intermediate Mole Fraction at Critical Point - T=75 °C - MWI=72 181

6-8-b Minimum Miscibility Pressure vs. Intermediate Mole Fraction at Critical Point - T=75 °C - MWI=86 181

6-9-a Minimum Miscibility Pressure vs. Intermediate Mole Fraction at Critical Point - T=90 °C - MWI=44 182

6-9-b Minimum Miscibility Pressure vs. Intermediate Mole Fraction at Critical Point - T=90 °C - MWI=58 182

6-10-a Minimum Miscibility Pressure vs. Intermediate Mole Fraction at Critical Point - T=90 °C - MWI=72 183

6-10-b Minimum Miscibility Pressure vs. Intermediate Mole Fraction at Critical Point - T=90 °C - MWI=86 183

7-1 Slim-Tube Apparatus Schematic 185

NOMENCLATURE

AAD% = Average absolute deviation (%)

Ac = Parameter characterizing a pure fluid

A_i^* = Ideal gas molar Helmholtz free energy of component i (J/mole)

C1-N2 = methane, nitrogen

C2-C4 = ethane to butane

C2-C6 = ethane to hexane

$C5^+$ = pentane plus

$C7^+$ = heptane plus

CGD = condensing gas drive

K = intrinsic permeability, m^2

K_{rgm} = permeability to gas at irreducible oil saturation, m^2

K_{rom} = permeability to oil at irreducible gas saturation, m^2

MMP = minimum miscibility pressure, MPa

MWI = Molecular weight of intermediate component (g/mole)

MWH = Molecular weight of heavy component (g/mole)

P = Pressure (MPa)

R = Gas constant = 8.31434 (kPa·liter)/(K·mole)

S_o = oil saturation, fraction

S_{or} = irreducible oil saturation, fraction

T = Temperature (°C, K)

v = Molar volume (liter/mole)

Vc = critical velocity, m/s

Vd = Darcy velocity, m/s

VGD = vaporizing gas drive

X_i = Mole fraction of component i

X_I^{oil} = Mole fraction of the intermediate fraction of the oil

X_H^{oil} = Mole fraction of the heavy fraction of the oil

X_L^{oil} = Mole fraction of the light fraction of the oil

X_{Ic} = Mole fraction of intermediate component at critical point

X_{Lc} = Mole fraction of light component at critical point

ρ_g = gas density, kg/m³

ρ_o = oil density, kg/m³

μ_g = gas viscosity, Pa·s

μ_o = oil viscosity, Pa·s

ϕ = porosity, fraction

θ = angle of dip of reservoir, negative radians

: = Symbol signifying that the vectors are collinear

Superscripts: l = liquid

v = vapor

1. Introduction

Enhanced oil recovery methods have been developed in order to alleviate the problem of low recovery associated with primary depletion of oil and gas condensate reservoirs. One approach is to eliminate or at least reduce the effect of interfacial phenomena to improve the displacement efficiency. To achieve this goal, the injection of a fluid which is completely miscible with the reservoir fluid, for instance a solvent, has been extensively investigated and applied to many pools. However, the choice of fluids miscible with crude oil is severly limited in practice by economic considerations. Different processes have been proposed; they are briefly outlined below.

The Displacement by a Slug of Rich Gas Followed by Dry Gas: In this type of displacement, a predetermined volume of liquified petroleum gas (mainly propane and butane) is first injected, which in turn is driven by an inexpensive lean gas. The slug acts as a buffer zone, mutually miscible with the displacing and displaced fluids.

The Vaporizing Gas Drive Process: In this case, the mechanism consists of an enrichment of the lean displacing gas (by the stripping of the intermediate hydrocarbons present in the oil) until miscibility is dynamically initiated. Conditions favorable to this type of displacement are usually encountered in reservoirs with rather volatile light oils and at high pressures.

The Condensing Gas Drive Process: This type of displacement is similar to the previous case, in the sense that miscibility is dynamically initiated through multiple contacts between the co-currently flowing phases. However, the enrichment process is reversed, and consists of a condensation of the intermediate hydrocarbons present in the wet gas, upon contact with the reservoir oil. Conditions favorable to this type of displacement are found in reservoirs with medium API gravity oil and moderate pressures.

In order to evaluate the possibilities of applying a lean hydrocarbon gas or nitrogen vaporizing gas drive to an oil reservoir (the vaporizing gas drive process), it is necessary to determine the minimum miscibility pressure (MMP). At present, there are two ways of accomplishing this, experimentally and empirically. The experimental approach is both time consuming and costly, whereas the empirical techniques require the use of two correlations based on a limited number of experimental data points. More specifically, one of the correlations deals with a vaporizing gas drive by a lean hydrocarbon gas, while the other assumes that the minimum miscibility pressure is the same whether the oil is displaced by a lean hydrocarbon gas or nitrogen. These methods were intended to be simple screening tools.

The object of this study was to develop a more refined predictive method for the determination of the minimum miscibility pressure of a vaporizing gas drive by a lean hydrocarbon gas or nitrogen, based on rigorous thermodynamic criteria. The method is flexible enough that it may be readily extended to the case of condensing gas drives. The case of lean hydrocarbon gas vaporizing gas drives is treated in terms of ternary systems for the phase behavior representation of the displaced and displacing fluids. In order to adequately describe the phase relationships of nitrogen-hydrocarbon systems whereby nitrogen and methane are dealt with as two separate components, quaternary systems are considered when nitrogen is the displacing fluid. These ternary and/or quaternary systems are then used as building blocks for the prediction of the minimum miscibility pressure of multicomponent hydrocarbon systems. The work will be presented under five subject headings, including the phase behavior of multicomponent systems, the concept of minimum miscibility pressure (MMP), methods of estimating the MMP, formulation of the thermodynamic criteria defining the MMP and the results of predictions for the methane and nitrogen vaporizing miscible gas drive processes.

2. Phase Behavior of Multicomponent Systems

2.1 Introduction.

High pressure gas displacement is a process by which the reservoir oil is displaced by a gas at high pressure and is characterized by a mass transfer between the phases which, initially, are not in thermodynamic equilibrium. When such displacements are conducted in the field, the composition of the injected fluid and of the displaced oil and the reservoir temperature are fixed, the only operating variable being the displacement pressure. In the case of vaporizing or condensing gas drives, mass transfer occurs between the co-currently flowing phases until thermodynamic equilibrium is established. Thermodynamic considerations, such as the phase behavior of the hydrocarbon system of interest and the effect of the prevailing pressure on the phase relationships, should therefore be accounted for.

Field hydrocarbon systems are generally complex in nature, consisting of hundreds of components. The representation of the phase behavior of such systems would require an n-1 dimensional space at some fixed pressure and temperature, n being the number of components. In practice, the composition of a complex hydrocarbon system is divided into three pseudo-groups, namely:

the light ends, C1-N2,
the intermediates, C2-C6, CO2,
and the heavy ends, $C7^+$.

At some fixed pressure and temperature, the phase behavior of a multicomponent hydrocarbon system can then be conveniently represented on a ternary diagram by means of these pseudo-groups. However, one must keep in mind that such a representation is not rigorous in a thermodynamic sense. For the purpose of describing the phase relationships of a hydrocarbon system, ternary and quaternary systems will be considered. At constant pressure and temperature, such systems can be respectively represented on a two and three dimensional space. In the following discussion, two-phase equilibrium (liquid-vapor) will be considered, since it is the commonly encountered type of phase relationship for field hydrocarbon systems at reservoir temperatures.

2.2 Qualitative Phase Behavior.

A pressure-temperature diagram can be very useful to qualitatively describe the phase relationships of multicomponent systems. Such a diagram is shown in Figure 1, for various binary systems (C1-C3, C1-C10, C3-C10, N2-C1 and N2-C10). In general, the P-T diagram of each binary system is delimited by the vapor pressure curves of the constituting components and the critical curve joining their respective critical points. The inner region represents pressure and temperature conditions at which two-phase equilibrium may result for certain compositions of the binary system. The outer region corresponds to P-T conditions for all possible compositions of the binary system to remain in the single phase region. However, when the temperature of the system approaches the triple point temperature of the heavy constituent of the binary system, complex phase behavior may result, with multiphase equilibrium, such as liquid-liquid-vapor or solid-liquid-liquid-vapor equilibrium[1]. Such behavior can be expected for the system C1-C10 at low temperatures, for example. A study of Figure 1 shows that the critical curve of the C1-C10 binary system, originating from the critical point of decane, does not end at the critical point of methane, but eventually crosses the methane vapor pressure curve towards a region where complex phase behavior occurs. Although the P-T diagrams shown in Figure 1 were generated from the Soave-Redlich and Kwong equation of state[2] (SRK EOS), such behavior has been observed experimentally for the methane-n-hexane system[3]. Fortunately, at normally encountered reservoir temperatures, 30 to 90 °C, such complex phase behavior is not present for hydrocarbon systems, and therefore will not be considered any further. It should be mentioned, however, that for the case where CO2 is considered as the injection fluid, liquid-liquid-vapor equilibrium may result when mixed with reservoir oil at temperatures as high[4] as 50 °C.

Consider the ternary system C1-C3-C10 at some reservoir temperature, TR, and pressure P1 (see Figure 1). The binary systems C1-C3 and C3-C10 are both in the single phase region. However, certain compositions of the C1-C10 binary will be in the two-phase

Figure 1

Pressure–Temperature Diagram For Various Binary Systems

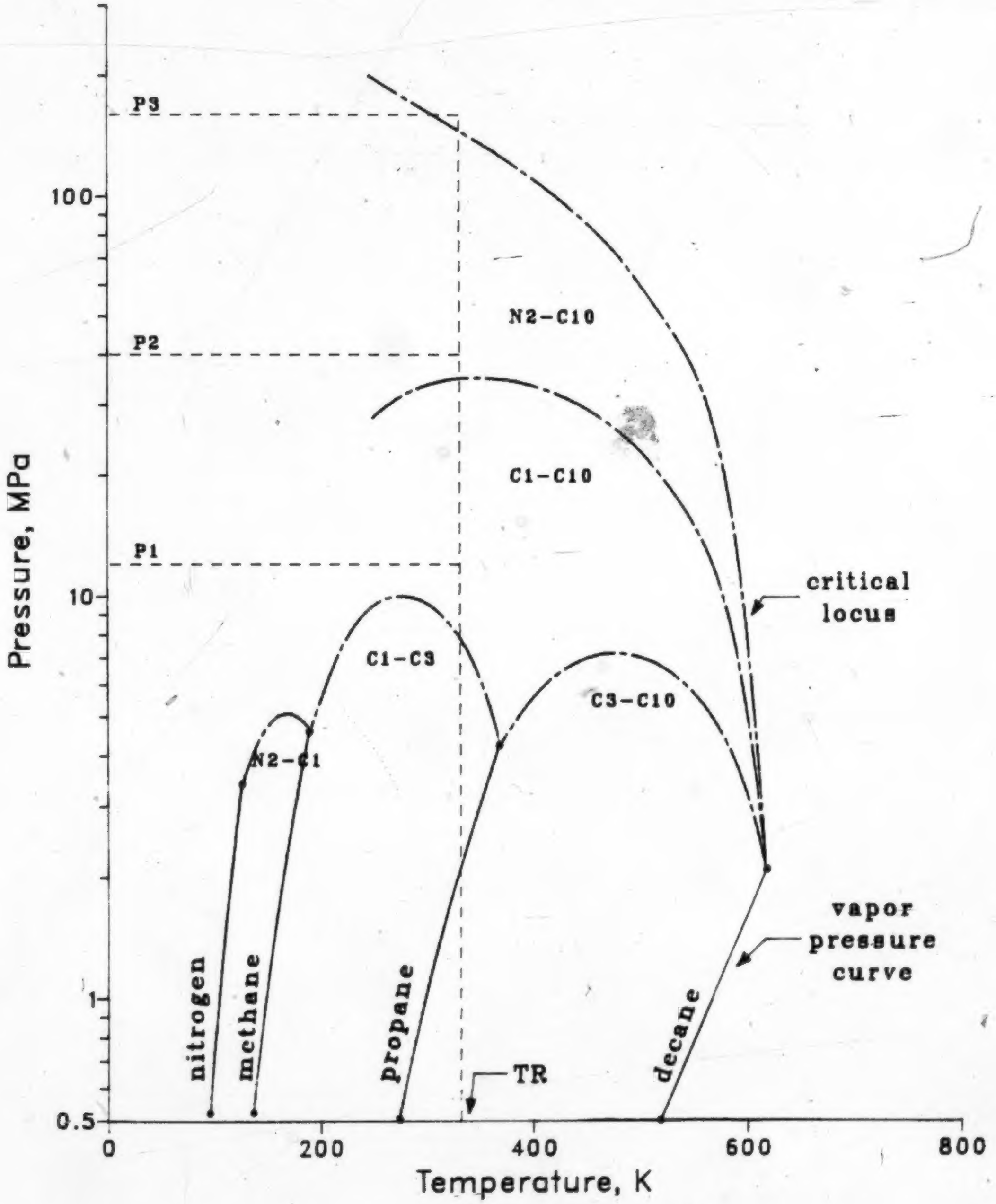

region, as well as certain compositions of the ternary system C1-C3-C10. If the pressure is increased to P2, the system C1-C10 will be in the single phase region, and consequently, so will be the ternary system C1-C3-C10. From this analysis, one may infer that an increase in pressure will be followed by a shrinkage of the two-phase region of the ternary system C1-C3-C10 at the fixed temperature TR.

At pressure P2 and Temperature TR, some compositions of the system N2-C10 will fall in the two-phase region, and consequently, a two-phase region will be present for certain compositions of the quaternary system N2-C1-C3-C10. This two-phase region region will vanish upon an increase in pressure to P3. One may also note that, at some fixed temperature, the critical pressure of a binary system increases as the critical temperature of the light component decreases or the critical temperature of the heavy component increases. For example, the critical pressure of the system N2-C10 at a temperature of 60 °C is 146 MPa, which may exceed the fracturing pressure of most oil reservoirs (the pressure at which the formation rock will fracture). First-contact miscibility (displaced and displacing fluids miscible in all proportions) is, therefore, seldom expected when a lean gas is used to displace a reservoir oil at normal operating pressures.

From the analysis of a P-T diagram, one can infer whether or not to expect a two-phase region for a particular system and determine the pressure at which it will vanish, given the system temperature. The same procedure can be readily extented to any other multicomponent system.

2.3 Phase Behavior of Ternary Systems.

At some fixed pressure and temperature, the phase behavior of a ternary system can be represented on a ternary diagram. Figure 2-a is such a representation for the system C1-C3-C10 at a temperature of 60 °C and a pressure of 25 MPa. The ternary diagram is a compositional diagram, with each apex of the triangle corresponding to one of the pure constituting components. Suppose that Ng moles of a fluid from region (A) are brought into contact with Nl moles of a fluid from region (C) and that thermodynamic equilibrium is

Phase Behavior of Ternary System: C1–C3–C10

T=60°C

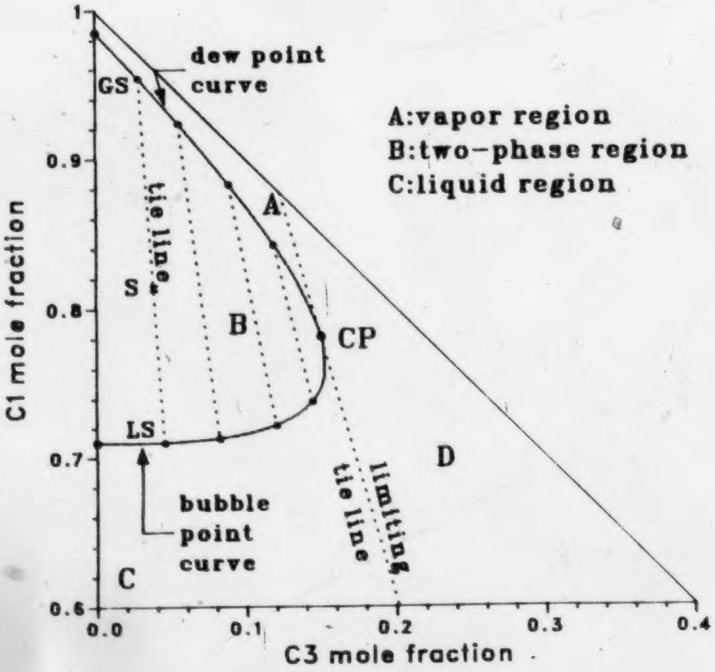
Representation
on a Ternary Diagram
T,P fixed

Fig. 2–a

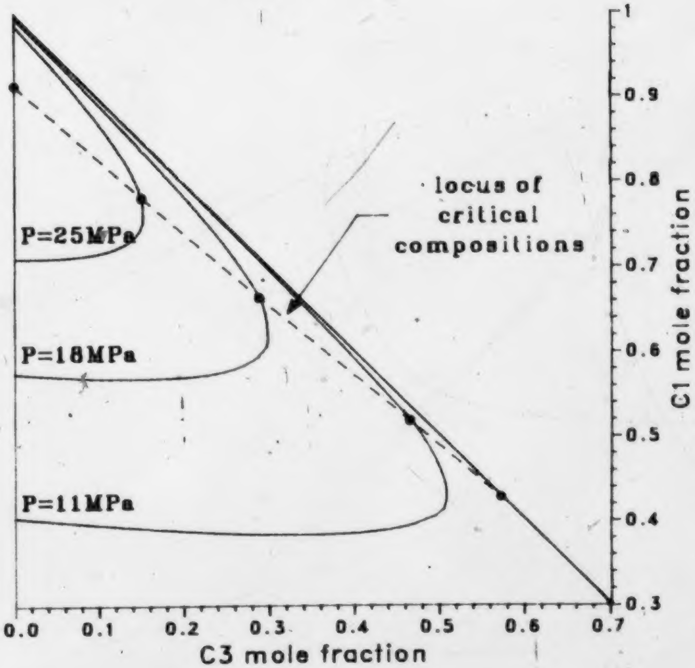
Phase Envelopes
at Various Pressures
T,fixed

Fig. 2–b

attained. The resulting system, depending on its overall composition, may be located in the liquid region (C), the two-phase region (B), or the vapor region (A). As more gas from region (A) is added to the system, there will be a transition in the phase behavior of such a system from an initial liquid state to a coexistence of vapor and liquid phases, and eventually to a single vapor phase. The two-phase region is bounded by the phase envelope which comprises the dew point curve (locus of points where the vapor phase is in equilibrium with an infinitesimal amount of liquid) and the bubble point curve (locus of points where the liquid phase is in equilibrium with an infinitesimal amount of vapor). If the pressure and temperature considered are such that the binary systems C1-C3 and C3-C10 are in the single phase region of their respective P-T composite diagrams, while the binary system C1-C10 is not (corresponding to pressure P1 and temperature TR in Figure 1), the bubble and dew point curves meet at the critical point (CP) where all the properties of the coexisting liquid and vapor phases become identical.

If a hydrocarbon system has a composition that places it inside the phase envelope, two phases will result at equilibrium. The point representing the composition of the vapor phase will be located on the dew point curve, and the point representing the liquid phase composition, on the bubble point curve. The line connecting theses points is referred to as a tie line. Each point (S) on this tie line represents the overall composition of a system which, at equilibrium, will have coexisting vapor and liquid phases of composition corresponding to that of the intersection point of the tie line with the dew point and bubble point curves, respectively (GS,LS). Various tie lines are shown in Figure 2-a. At the limit, as the critical point is approached, the tie line coincides with the tangent to the phase envelope at the critical point, and is referred to as the limiting tie line. In region (D), one cannot distinguish a vapor from a liquid phase. A liquid phase can be distinguished from a vapor phase only in the context of two phases coexisting at equilibrium. In the single phase region, a liquid or vapor should be more appropriately termed fluid, since one can follow a path from region (A) to region (C) without crossing the two phase region, thus going from a light fluid to a denser fluid while remaining as a single phase at all times.

From the analysis of the P-T diagrams, it can be inferred that an increase in pressure at a fixed temperature is followed by a shrinkage of the phase envelope. Figure 2-b illustrates the effect of pressure on the C1-C3-C10 system at a temperature of 60 °C. The phase envelopes were generated at various pressures using the SRK equation of state[2] (a new way of rapidly generating the bubble point and dew point curves without using empirical initial estimates will be discussed in the context of chapter 5). It is observed that an increase in pressure at constant temperature is accompanied by a shrinkage of the phase envelope. Also, the critical point composition moves from the critical point of the C1-C3 binary to that of the C1-C10 binary as the pressure is increased from the critical pressure of the C1-C3 binary to the one of the C1-C10 binary at the set temperature, at which point the two-phase region vanishes.

2.4 Phase Behavior of Quaternary systems.

In order to analyse how the phase behavior of a ternary system is affected by the addition of another component, N2 was selected as the fourth component along with the previously selected ternary system (C1-C3-C10). In a vaporizing gas drive, N2 may be considered as the driving gas, and the question arises as to whether or not nitrogen is to be included in the light fraction.

At constant pressure and temperature, a ternary system can be represented by a ternary diagram, as is shown in Figure 2-a. However, by adding one more component, the dimensionality is increased by one, in which case the quaternary system can only be represented by a tetrahedron, as is shown in Figure 3. Each apex of the tetrahedron corresponds to a pure component, viz., nitrogen (N2), methane (C1), the intermediate (C3) and the heavy component (C10). The front face of the tetrahedron corresponds to the hydrocarbon ternary system (C1-C3-C10), while the bottom face corresponds to the N2-C3-C10 ternary system. The left and right side faces are the N2-C1-C10 and N2-C1-C3 ternary systems, respectively. Figure 4 is a phase diagram illustrating the phase relationships of the above quaternary system at a low pressure of 11 MPa and a temperature of 60 °C. Now

Figure 3

REPRESENTATION OF THE QUATERNARY SYSTEM N2-C1-C3-C10 ON A TETRAHEDRON

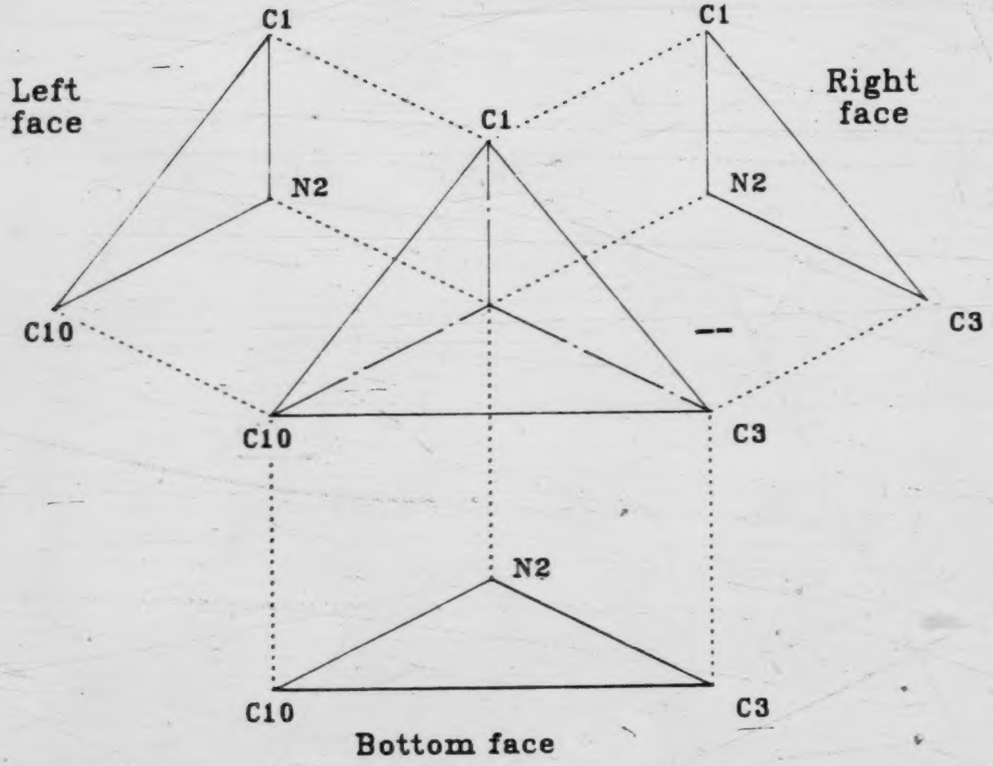

2

Figure 4
Phase Diagram of Quaternary
System:N2-C1-C3-C10 at T=60C
P=11MPa, low pressure case

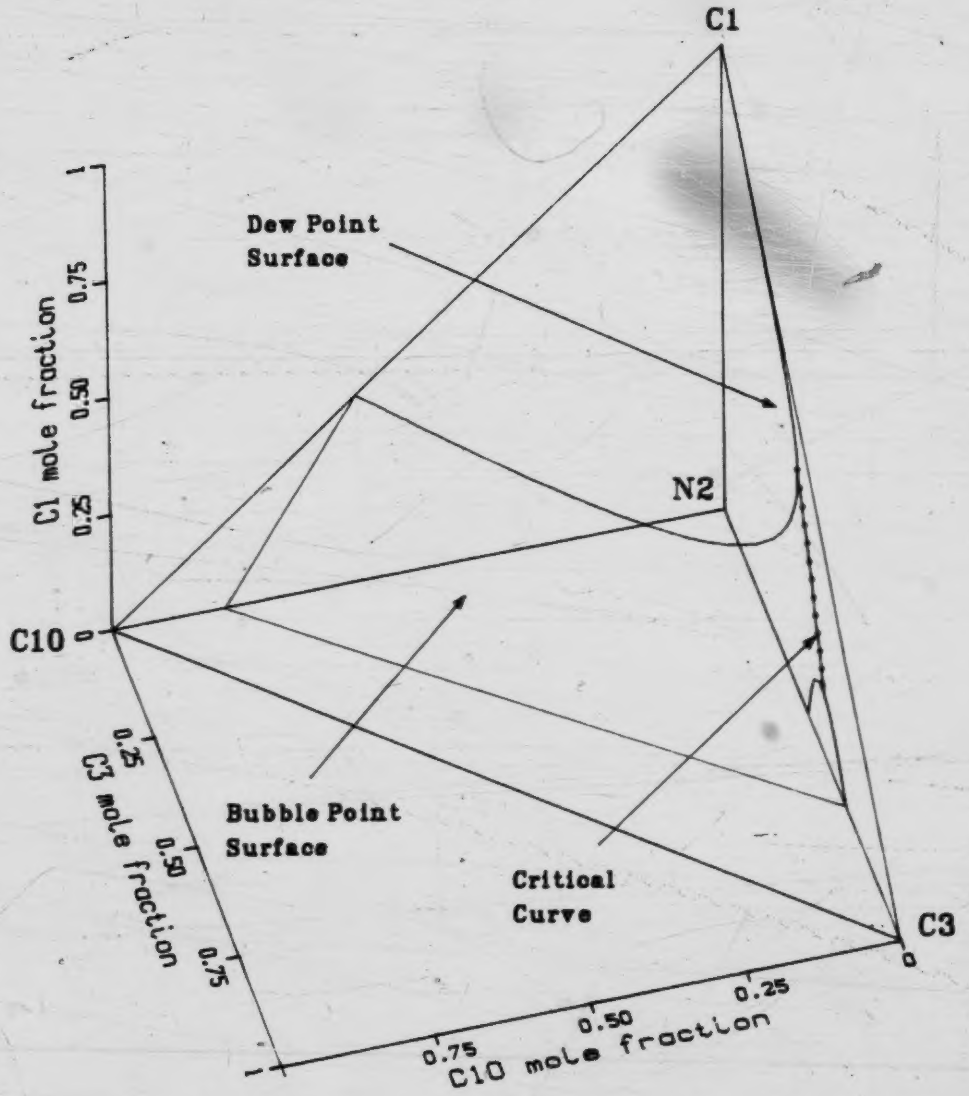

it can be seen that, by treating nitrogen and methane as two separate components, several new features are displayed. The familiar bubble point curve, dew point curve and the critical point of a ternary system are respectively replaced by a bubble point surface, a dew point surface and a critical point curve for a quaternary system. This can be deduced directly from the Gibbs phase rule[5]:

$$F=n-p+2$$

$$\text{or } F'=n-1$$

where F is the degrees of freedom, p is the number of coexisting phases and n is the number of components. The second equality defines the degrees of freedom (F') for a system to remain in a critical state. The degrees of freedom is two for a quaternary system in a saturated liquid state (bubble point) or a saturated vapor state (dew point) at constant pressure and temperature, which corresponds to the bubble point surface and dew point surface, respectively. However, the degrees of freedom is one for a quaternary system at its critical point at constant pressure and temperature, corresponding to the critical point curve shown in Figure 4.

The phase diagram, shown in Figure 4, was again generated using the SRK equation of state[2] (no complete experimental data for quaternary nitrogen-hydrocarbon systems are available in the literature at some fixed pressure and temperature). It may be observed that the two-phase region of the N2-C3-C10 ternary is considerably larger than that of the C1-C3-C10 ternary system. The pressure selected was lower than the critical pressure of the binary N2-C3 at the set temperature and, therefore, the dew point curve and bubble point curve of the N2-C3-C10 ternary system do not meet at a critical point, but intersect the N2-C3 axis respectively at the dew point and bubble point of the N2-C3 binary at the set pressure and temperature. The two-phase region is seen to extend even onto the N2-C1-C3 face of the tetrahedron, which clearly shows that the addition of nitrogen considerably enlarges the two-phase region. The critical point curve, which separates the dew point surface from the bubble point surface, connects the critical point of the C1-C3-C10 ternary system to the critical point of the N2-C1-C3 ternary system.

The effect of pressure, at constant temperature, on the two-phase region was also investigated for the case of the above quaternary system. Figure 5 shows that an increase in pressure to 18 MPa (greater than the critical pressure of the N2-C3 binary system) is followed by a shrinkage of the phase envelope, with complete disappearance of the two-phase region from the N2-C1-C3 side of the tetrahedron which was present at the lower pressure of 11 MPa. The critical point curve is now seen to extend from the critical point of the N2-C3-C10 ternary system to the critical point of the C1-C3-C10 ternary system. It may be observed that the two-phase region of the N2-C3-C10 ternary system remains considerably larger than that of the C1-C3-C10 ternary system. A comparison of Figures 4 and 5 shows that the shrinkage is more pronounced on the bubble point side of the phase envelope than on the dew point side which departs slightly from the N2-C1-C3 side of the tetrahedron. At the high pressure of 41 MPa and same temperature, the size of the two-phase region has decreased considerably, as is shown in Figure 6. The specified pressure in this case exceeds the critical pressure of the C1-C10 binary system, corresponding to pressure P2 on the P-T composite diagram shown in Figure 1. Consequently, the C1-C3-C10 system is now in the single phase region, while the two-phase region of the quaternary system extends from the N2-C1-C10 side to the N2-C3-C10 side of the tetrahedron. Also, the critical point curve now connects the critical point of the N2-C1-C10 ternary system to the critical point of the N2-C3-C10 ternary system.

The study of quaternary systems is enlightening in the sense that it demonstrates that lumping components into pseudo-groups or fractions may result in an oversimplification of the phase relationships of a multicomponent system. This would be especially true for the light fraction, as may be deduced from the analysis of the P-T composite diagram shown in Figure 1. It may be observed that, at normally encountered reservoir temperatures (30-90 °C), the reservoir temperature is lower than the critical temperature of propane and heavier components. Thus, any hydrocarbon system that does not contain components lighter than propane will remain as a single phase (the only requirement being that the pressure be greater than the vapor pressure of propane at the reservoir temperature). The controlling factor on

Figure 5
Phase Diagram of Quaternary
System:N2–C1–C3–C10 at T=60C
P=18MPa, medium pressure case

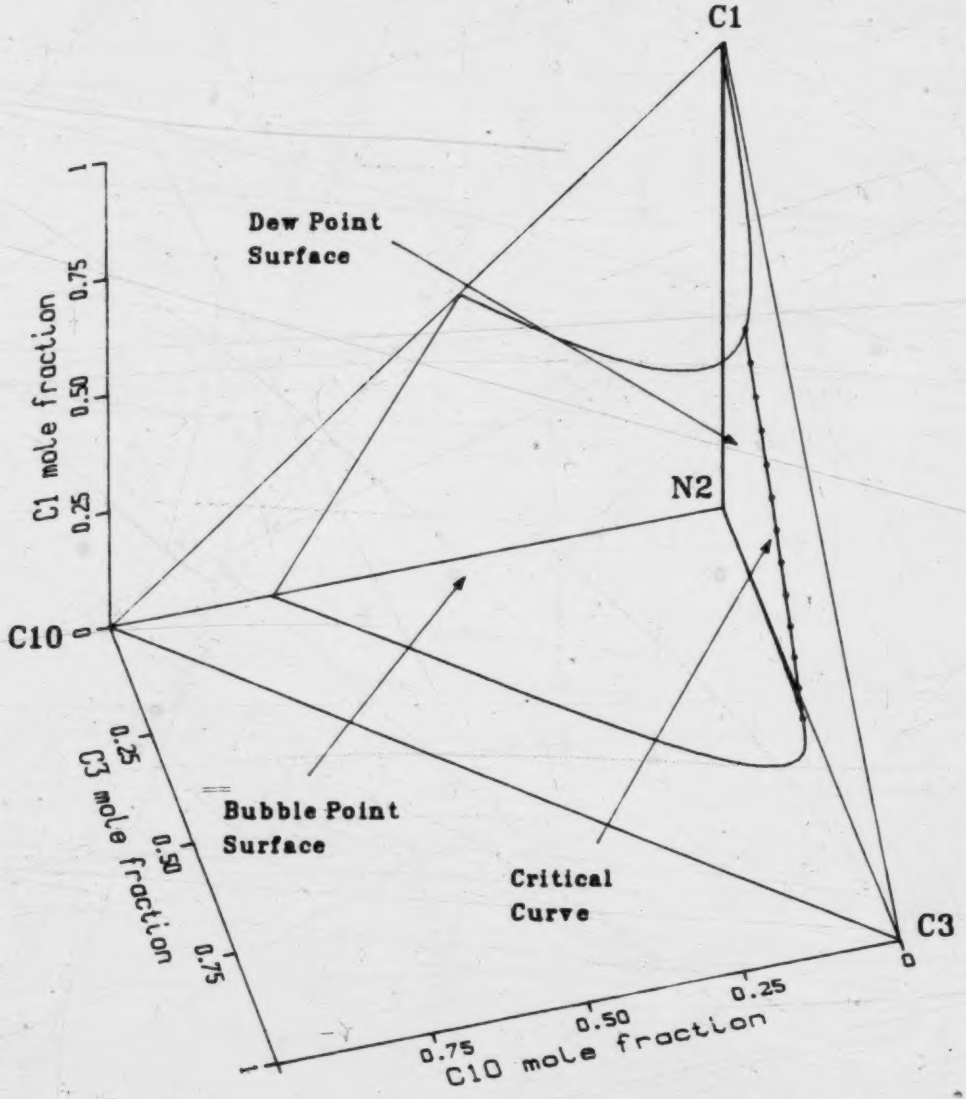

Figure 6
Phase Diagram of Quaternary
System:N2–C1–C3–C10 at T=60C
P=41MPa, high pressure case

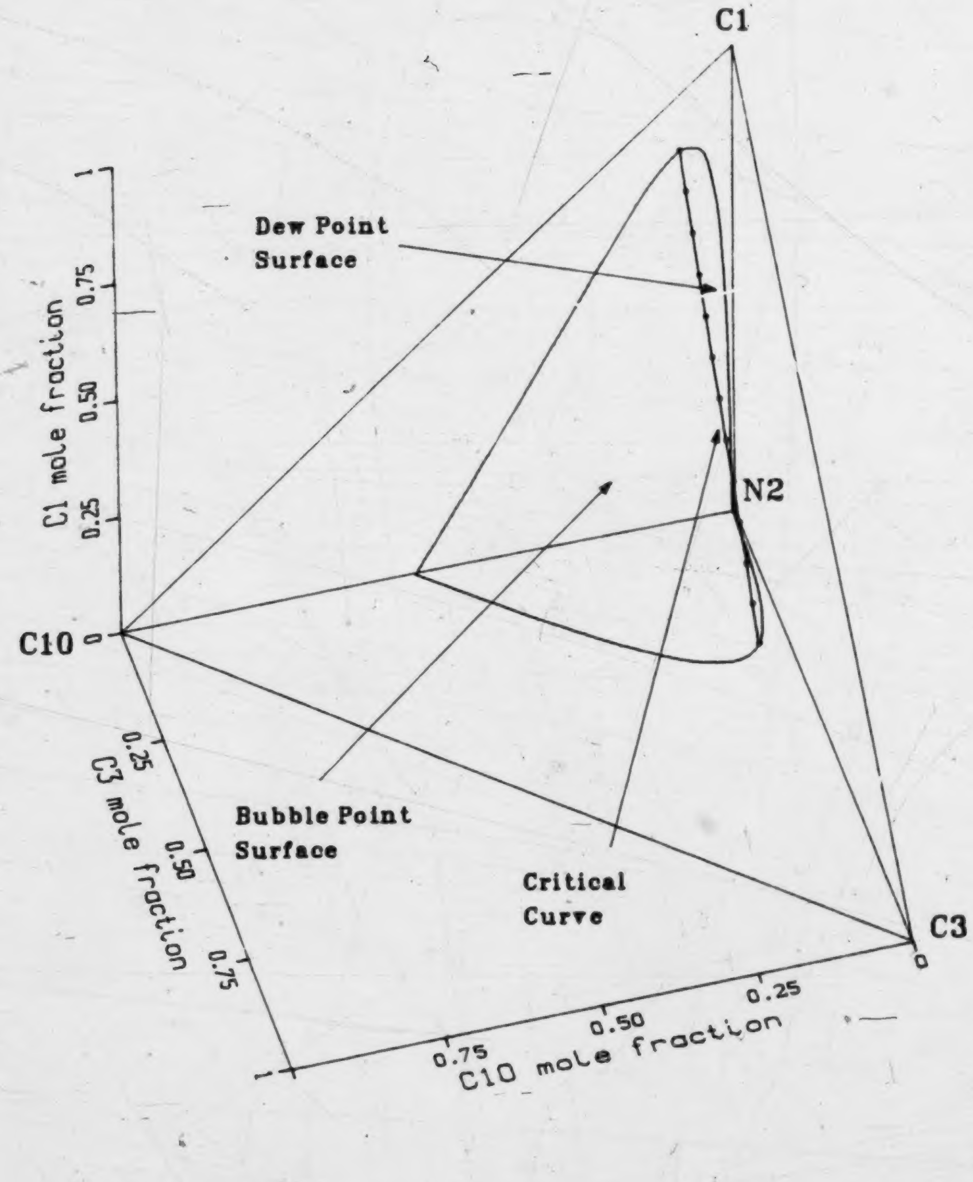

the size, the appearance or the disappearance of the two-phase region is related to the interaction of the light components with the heavier components, depending upon whether the pressure is less or greater than the critical pressure of the light-heavy binary system. For example, a study of Figure 1 shows that at normally encountered reservoir temperatures the critical pressure of the N2-C10 binary is considerably higher than the critical pressure of the C1-C10 binary. Therefore, a two-phase region will exist at higher pressures when nitrogen is present in the hydrocarbon system than would be the case if methane were the only light component present. This effect is better illustrated when comparing figures 4 to 6 discussed earlier.

3. Concept of Minimum Miscibility Pressure

3.1 Introduction.

The purpose of the following discussion is to describe the basis for the criteria defining the Minimum Miscibility Pressure for a vaporizing or condensing gas drive, which will be referred to from hereon as the MMP. The above gas drives are processes by which oil is displaced by a gas and are characterized by mass transfer between the two phases which, initially, are not in thermodynamic equilibrium. Depending on the compositions of the injected gaseous phase and the displaced oil, and the average operating conditions of pressure and temperature, three types of displacements may occur, namely, immiscible, multiple-contact miscible or first-contact miscible displacements.

In the case of a vaporizing gas drive, the injected gas would be lean in the intermediate components, C2-C6, while the oil would be rich in these components. The mass transfer between the co-currently flowing phases consists essentially of a stripping of these intermediate components by the gas phase, as well as the solution of the light ends, C1-N2, in the oil, until thermodynamic equilibrium is established. For the condensing gas drive, the injected gas would be rich in the intermediate components, while the oil would be lean in these components. In this case, condensation of the intermediates present in the injected gaseous phase into the displaced oil will occur.

In order to introduce the concept of MMP, a thorough understanding of the displacement mechanism, which consists essentially of the coupling of the two-phase flow mechanism with the phase behavior of the system of fluids considered, is necessary. For the sake of simplicity, the case of a ternary system will be considered first, wherein the representation on a ternary diagram of its phase behavior, at some fixed pressure and temperature, is thermodynamically rigorous. The concepts developed for the case of a ternary system will then be extended to the more complex case of a quaternary system.

3.2 Basic Displacement Mechanisms of a Vaporizing Gas Drive.

In the case of a vaporizing gas drive, the temperature and the displacing and displaced fluid compositions are fixed. The only variable which can be altered is the displacement pressure. Depending on the prevailing pressure, three types of displacements may occur, namely: immiscible, multiple-contact miscible or first-contact miscible displacements. Differentiation between these cases[6,7,8] can best be represented on a ternary diagram. For the sake of simplicity, consideration will be given to the case of a ternary hydrocarbon system composed of a light, an intermediate and a heavy component. Hence, the phase behavior of such a system at some fixed pressure and temperature can be rigorously described on a plane ternary diagram.

3.2.1 Immiscible Case.

Suppose that the displacement is conducted at the pressure P1 and temperature T, wherein the displacing fluid is a lean gas (G), while the displaced fluid is an oil (O) relatively rich in the intermediate component, (see Figure 7-a). At the beginning of the displacement, the displacing and displaced fluids are not in thermodynamic equilibrium. Under the influence of the viscous and capillary forces, the displacement will be of the Buckley-Leverett[9] type with the addition of mass transfer between the co-currently flowing phases. The saturation diagram (Figure 7-a) represents an idealized saturation profile in the diphasic zone before thermodynamic equilibrium is established. One may visualize the porous medium as a series of cells. On this diagram it may be observed that the relative amount of gas to oil decreases going from cell 1 to cell 3. This is reflected on the phase diagram by the overall composition of each cell, namely points 1, 2 and 3. Assuming that thermodynamic equilibrium is established, the composition of each phase in each cell will change to that corresponding to equilibrium conditions. Drawing the tie-lines passing through points 1, 2 and 3 the following is obtained:

cell 1: gas (G1) in equilibrium with oil (O1)

cell 2: gas (G2) in equilibrium with oil (O2)

Fig. 7–a
Starting Stage of
Immiscible VGD

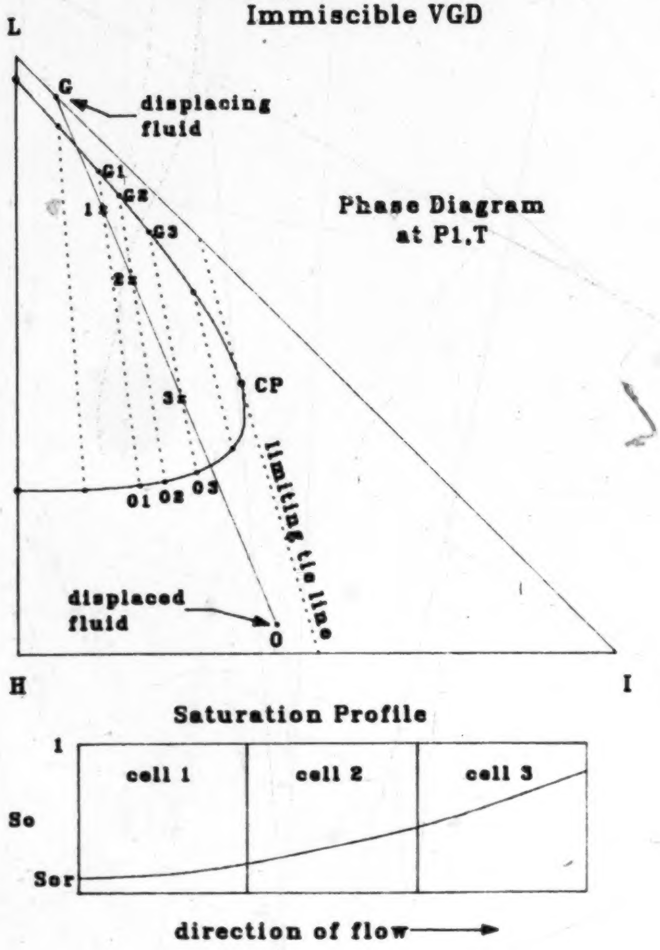

Fig. 7–b
Final Stage of
Immiscible VGD

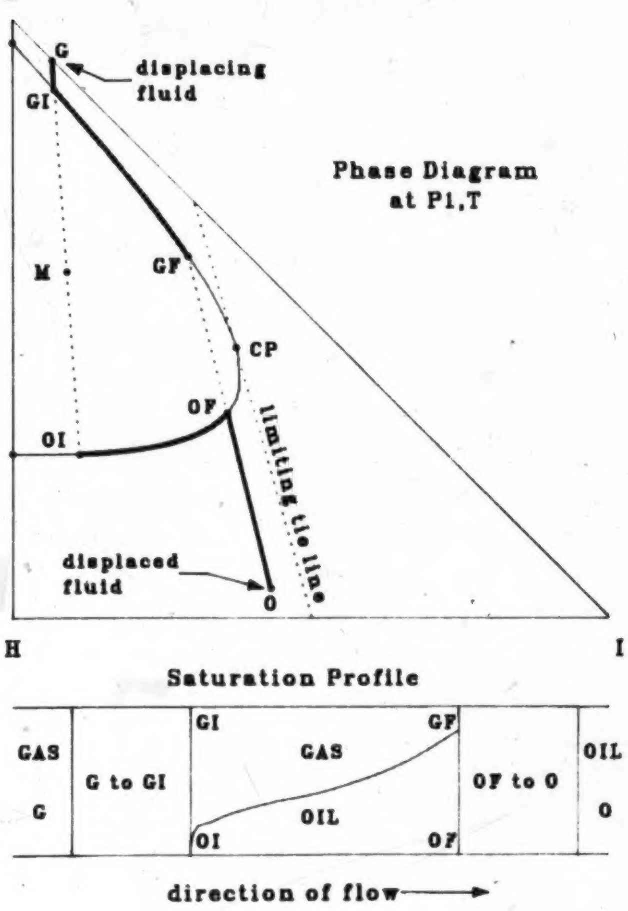

cell 3: gas (G3) in equilibrium with oil (O3).

Referring to Figure 7-b, as the displacement proceeds, the oil left behind will be contacted by the original displacing lean gas, and will be further stripped of its intermediate component. Its composition path will follow the bubble-point curve, in the direction of lesser intermediate component, until it reaches the limiting composition (OI). This limit is characterized by the particular tie-line passing through (G) and the equilibrium gas (GI). Suppose now that oil (OI) is at the irreducible oil saturation, thus immobile. Oil (OI) will always be in contact with more gas (G). Let (M) be the point representing the overall composition of Ng moles of gas (G) being in contact with Nl moles of oil (OI) before equilibrium is established. From the lever rule, one obtains

$$\frac{Ng}{Nl} = \frac{MOI}{MG}$$

where

MOI = distance between point (M) and point (OI)

MG = distance between point (M) and point (G)

At equilibrium, some oil will evaporate and the gas phase composition will change to (GI). The relative amount of gas to oil is therefore changed to

$$\frac{Ng \text{ equilibrium}}{Nl \text{ equilibrium}} = \frac{MOI}{MGI}$$

and Ng equilibrium $>$ Ng, since MGI $<$ MG.

where

MGI = distance between point (M) and point (GI)

As the oil (OI) is contacted by more lean gas (G), the evaporation process will continue until all the oil has evaporated. This correponds to the evaporation front. One may observe that an evaporation front will exist only if the original displacing gas phase has a composition that does not fall on the dew-point curve. Otherwise a residual oil saturation will always be present.

Similarly, the gas at the front will contact more virgin oil (O) and becomes more enriched in the intermediate component. Its composition path will follow the dew-point curve, in the direction of higher intermediate component, until it reaches the limiting composition (GF). This limit is characterized by the particular tie-line passing through the original oil (O) and the equilibrium oil (OF). For this case, the saturation distribution as a function of length is illustrated in Figure 7-b and the displacement is clearly immiscible as the gas at the front (GF) is immiscible with the oil being displaced.

3.2.2 Multiple-contact Miscible Case (or Dynamic Miscibility).

Suppose now that the displacement is conducted at a higher pressure P2, and at the same temperature T. Any increase in pressure will be followed by a shrinkage of the phase envelope. Suppose that, as is shown in Figure 8-a, the pressure is high enough so that the same displaced fluid (O) has a composition that places it just to the right of the limiting - tie-line. At the beginning of the displacement, the mechanism will be similar to that of the immiscible case, as the line joining point (O) to point (G) crosses the phase envelope. This line is the locus of the compositions of all possible combinations of gas (G) and oil (O). Viscous and capillary forces will play the same role and the displacement will be of the Buckley-Leverett type in its initial stage, with the addition of mass transfer between the co-currently flowing phases. The oil left behind will be contacted by the displacing lean gas (G) and will be stripped further of its intermediate component. Its composition path will follow the bubble-point curve, in the direction of lesser intermediate component, until it reaches the limiting composition (OI) (see Figure 8-b). As discussed earlier, oil (OI) will evaporate in the contacting lean gas (G), until it is completely evaporated. This corresponds to the evaporation front.

Similarly, the gas at the front will contact more virgin oil (O), and thus will further be enriched as the displacement proceeds. Its composition path will follow the dew-point curve in the direction of the higher intermediate component, until it reaches the limiting miscibility composition (GM). This limiting composition is characterized by the tangent to the phase envelope passing through point (O). Gas (GM) is now completly miscible with the oil ahead, as the line joining it to point (O) does not cross the phase envelope. At this point,

Fig. 8-a
Starting Stage of Multiple
Contact Miscible VGD

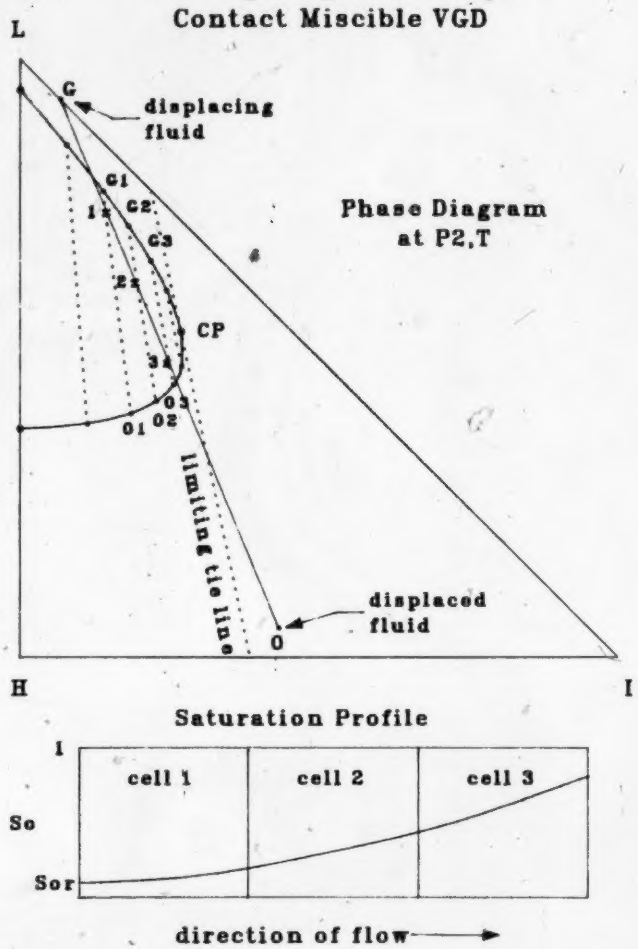

Fig. 8-b
Final Stage of Multiple
Contact Miscible VGD

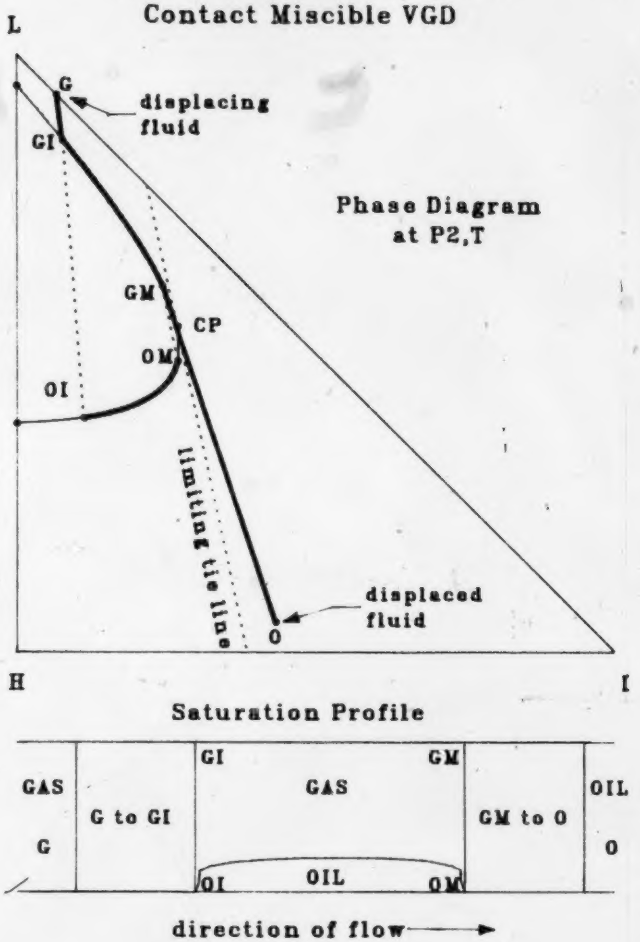

miscibility has been initiated.

Under the influence of dispersion and/or some perturbing phenomena (viscous fingering or gravity override), this displacement will be characterized by the continuous breakdown and reformation of the miscible front. Thus a residual oil saturation will be left behind, resulting in an incomplete displacement of the oil[10]. Consider the effect of convective mixing in the gas zone just behind the miscible front (see Figure 8-b). The composition of the contiguous gases forming this zone falls on the dew-point curve. An explanation of convective mixing is necessary at this point of the discussion. A porous medium may be represented by a bundle of interconnected dissimilar flow channels. Therefore, different interstitial velocities will exist for different flow paths. Consequently gases of different compositions may come in contact, as illustrated by the idealized system shown in Figure 9-a. Suppose that leaner gas of composition (G1) travels faster in flow path 1 than richer gas (G2) in flow path 2. At the intersection of the flow paths, gas (G1) may mix with gas (G2), resulting in a mixture of composition (MX) which just falls inside the phase envelope (see Figure 9-b). This will result in the condensation of some oil (OX) which is in equilibrium with gas (GX). The same process will disperse the gas of composition (GM) (see Figure 8-b), resulting in a leaner gas contacting the oil ahead, with the consequent loss of miscibility. Similarly, under the influence of some perturbing phenomena (viscous fingering or gravity override), leaner gas will come into contact with the oil ahead and an immiscible displacement will occur. The same displacement mechanism previously discussed will be repeated with the subsequent reformation of a miscible front.

3.2.3 First-contact Miscible Case.

Suppose now that the displacement is conducted at still a higher pressure P3, and at the same temperature T, and that the shrinkage of the phase envelope is such that the line connecting the points (O) and (G) does not cross the phase envelope. The connecting line (G)-(O) is the locus of all possible compositions encountered in the region where the two fluids are in contact with each other. As this line does not cross the phase envelope, the two

Fig. 9–a
Idealized Representation of Porous Media

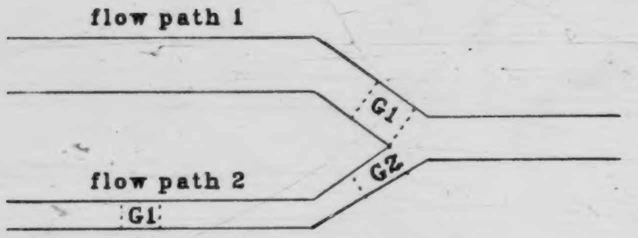

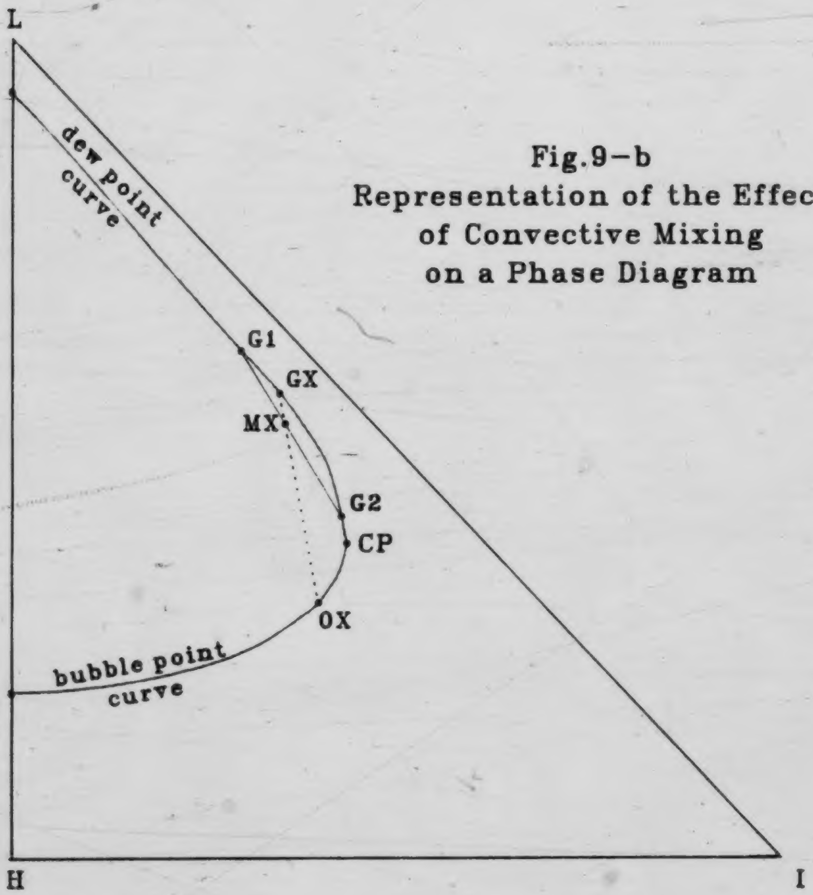

Fig.9–b
Representation of the Effect of Convective Mixing on a Phase Diagram

fluids are miscible in all proportions, and the displacement is referred to as a first-contact miscible displacement.

3.3 Basic Displacement Mechanisms of a Condensing Gas Drive.

This case becomes analogous to the preceding one, upon inverting the roles of the displaced and displacing fluids. Now the mass transfer consists essentially of a condensation of the intermediates present in the rich displacing gas into the displaced oil which is lean in these components.

3.3.1 Immiscible Case.

Figure 10-a illustrates the composition paths followed by the gaseous and liquid phases in the transition zone, once thermodynamic equilibrium is established. The point representing the composition of the displacing fluid (G), rich in the intermediate component, is located to the left of the limiting tie line at the pressure P1. As the displacement proceeds, the oil left behind will be contacted by the original displacing rich gas, and will be enriched further in its intermediate component. Its composition path will follow the bubble point curve, in the direction of higher intermediate component, until it reaches the limiting composition (OI). This limit is characterized by the particular tie-line passing through (G) and the equilibrium gas (GI). Similarly, the gas at the front will contact more virgin oil (O) and becomes more stripped of its intermediate component. Its composition path will follow the dew point curve, in the direction of lesser intermediate component, until it reaches the limiting composition (GF). This limit is charaterized by the particular tie-line passing through the original oil (O) and the equilibrium oil (OF). For this case, the displacement is clearly immiscible since the gas in the transition zone is at all times immiscible with the oil being displaced.

Fig. 10–a
Final Stage of
Immiscible CGD

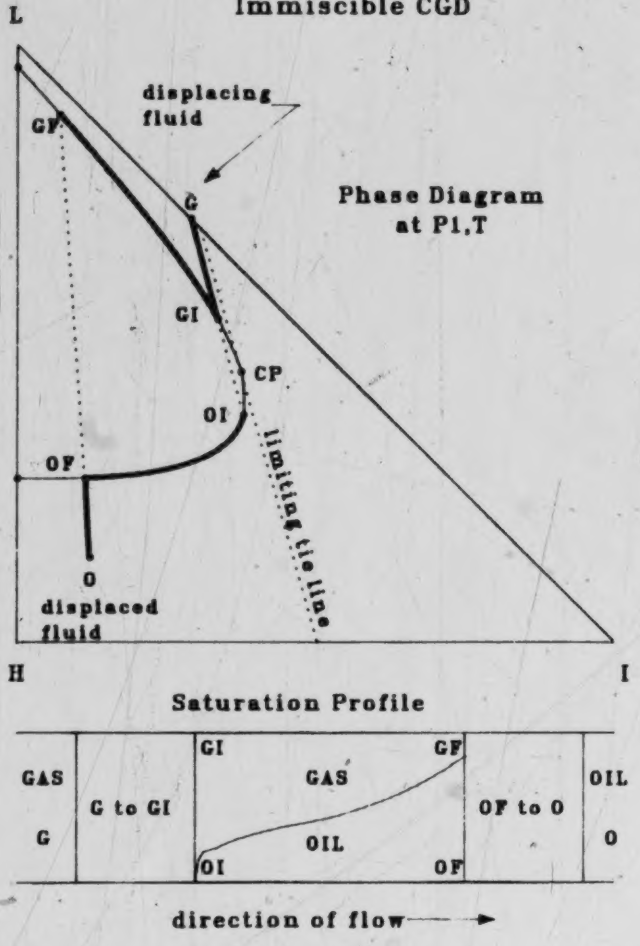

Fig. 10–b
Final Stage of Multiple
Contact Miscible CGD

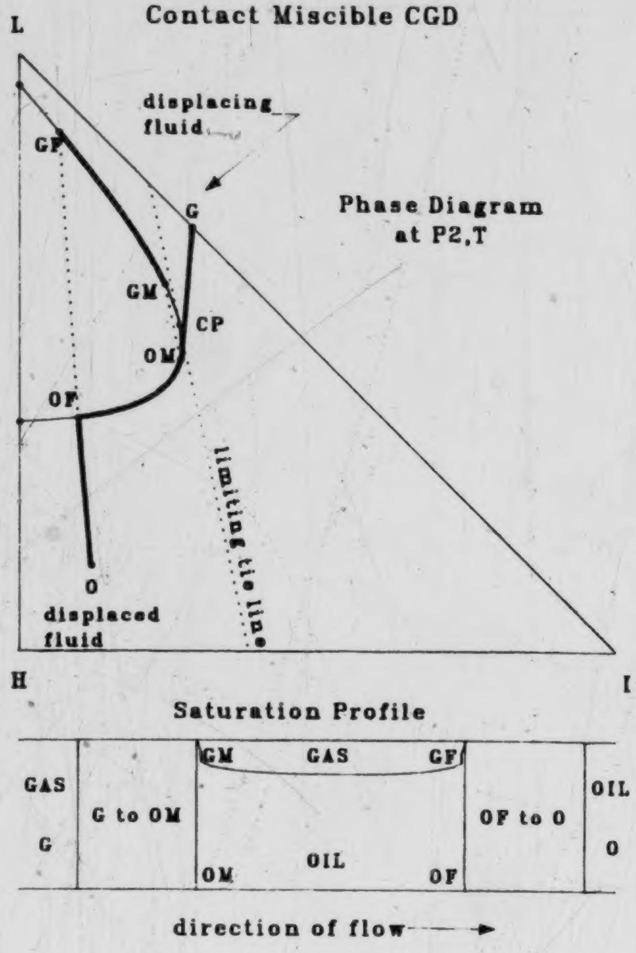

3.3.2 Multiple-contact Miscible Case.

Figure 10-b illustrates the composition paths followed by the gaseous and liquid phases in the transition zone at a higher displacement pressure P2, once thermodynamic equilibrium is established. It may be observed that the point representing the composition of the displacing fluid (G) is now located to the right of the limiting tie line. As the displacement proceeds, the oil left behind will be contacted by the displacing rich gas (G) and will be enriched further. Its composition path will follow the bubble point curve, in the direction of higher intermediate component, until it reaches the limiting miscibility composition (OM). This limiting composition is characterized by the tangent to the phase envelope passing through point (G). Gas (G) is now completely miscible with the oil ahead, as the line joining it to point (OM) does not cross the phase envelope. It may be observed that for the case of a condensing gas drive, miscibility is initiated at the upstream end of the transition zone, and is also referred to as rear miscibility.

An analytical treatment of the coupling of the two-phase flow mechanism and mass transfer is presented in Appendix 1. The model discusses the stationary solutions attained by the above gas drives for the case of an immiscible displacement.

3.4 Definition of the Minimum Miscibility Pressure for Ternary Systems.

The MMP of a gas drive may now be defined as the minimum displacement pressure necessary to initiate miscibility through a multiple-contact process between the displacing and displaced fluids. For the case of a vaporizing gas, the MMP will correspond to the pressure necessary for the limiting tie-line to pass through the point representing the composition of the displaced fluid. Below this pressure, a larger two-phase region will cause the point representing the oil composition to be located to the left of the limiting tie line, resulting in an immiscible displacement.

Similarly, for the condensing gas drive, one may define the MMP as the pressure necessary for the limiting tie-line to pass through the point representing the composition of the displacing gas. However, in this case, dynamic miscibility can also be achieved by injecting a gas rich enough in the intermediate component. The minimum enrichment required would be such that, at reservoir pressure, the limiting tie-line must pass through the point representing the composition of the injected gas.

Consider the case where the displacement is immiscible. Behind the front, a diphasic flow regime will exist, leaving a residual oil saturation. For the case where multiple-contact miscibility is initiated, convective mixing between fluids with compositions lying on the dew-point curve, will result in mixtures which barely fall within the two-phase region, thereby leaving a small amount of immobile liquid behind the front. Also, any reformation of the miscible front after its breakdown (through dispersion etc...) will be at the cost of even more oil being left behind, though small compared to the amount left behind during an immiscible displacement. This suggests that going from an immiscible to a multiple-contact miscible displacement will result in a sharp decrease in the residual oil saturation at gas breakthrough, or a sharp increase in the recovery of the initial oil in place, and that the overall character of the displacement will change from diphasic to monophasic flow. An experimental technique, referred to as the slim-tube test, uses the above conclusions as criteria for the experimental determination of the MMP.

3.5 Extension of the Concept of MMP to Quaternary Systems.

The general phase relationships of a quaternary system were discussed in Chapter 2. It was seen that the bubble point curve, the dew point curve and the critical point of a ternary system were respectively replaced by a bubble point surface, a dew point surface and a critical point curve for a quaternary system, at constant pressure and temperature. Also, the familiar limiting tie line of a ternary system is now replaced by the ruled surface generated by all the quaternary limiting tie lines, each one passing through a point of the critical point curve, as is shown in Figure 11 for the system N2-C1-C3-C10 at a pressure of 25 MPa and a temperature of 60 °C. This ruled surface may be generated by determining the compositions of a sufficient number of points on the critical curve and the directions of the quaternary limiting tie lines passing through each of these points.

Figure 11
Quaternary Limiting Tie Lines
of System:N2–C1–C3–C10
at T=60C and P=25MPa

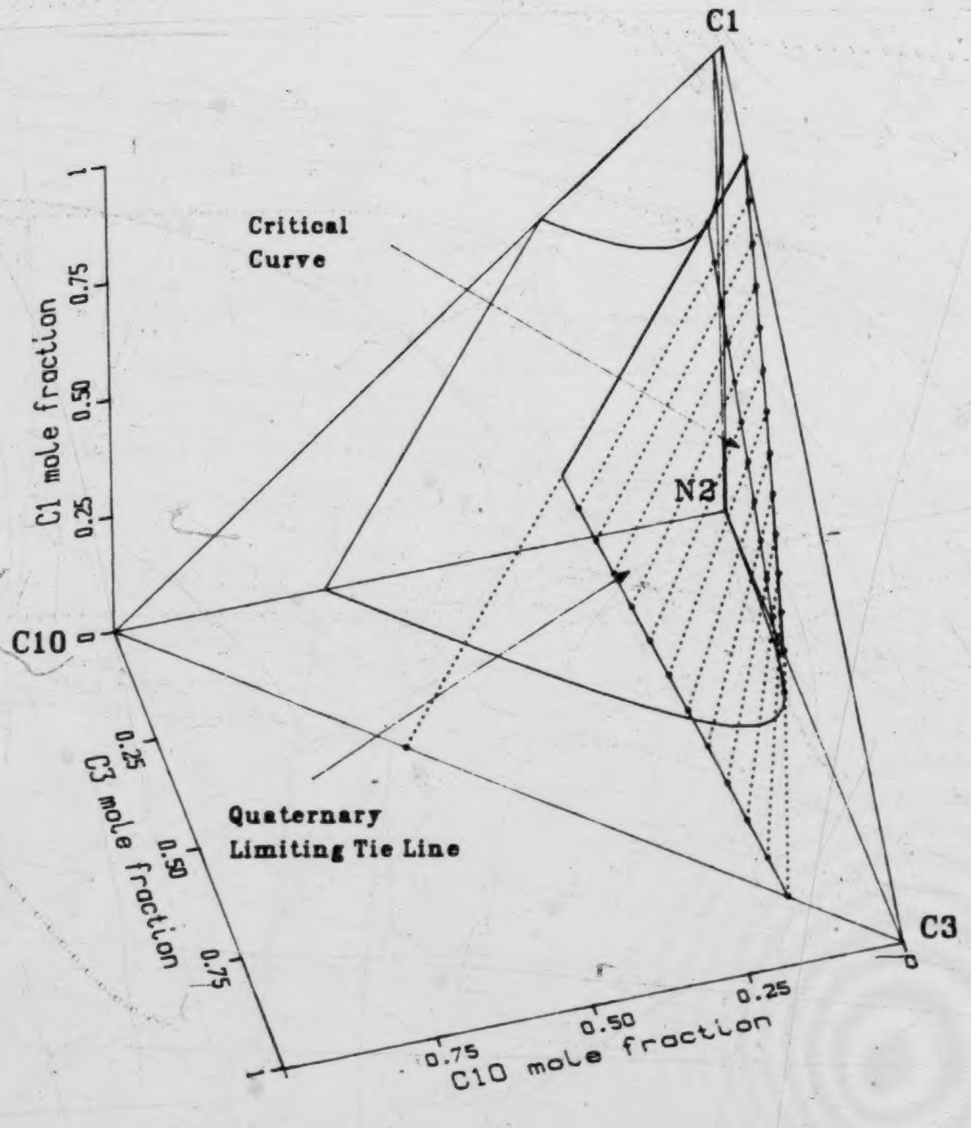

The mechanism of multiple-contact miscible displacement for a quaternary system[6,11] may be explained in a similar way to the previous ternary case. The discussion will be limited to the case of a vaporizing gas drive. Similar reasoning may be adopted for the condensing gas drive by inverting the roles of the displaced and displacing fluids.

3.5.1 Immiscible Case.

Let the displacing fluid be a lean gaseous phase (G) from the region of the tetrahedron, shown in Figure 11, delimited by the dew point surface and the ruled surface generated by the quaternary limiting tie lines, and the displaced fluid be a liquid phase (O), rich in the intermediate component, from the region of the tetrahedron delimited by the bubble point surface and the above ruled surface. The line connecting these points, which represents all the possible combinations of gas (G) and liquid (O), necessarily crosses the two phase region. Figure 12 illustrates the final composition paths of the displacing and displaced phases in the transition zone once thermodynamic equilibrium is established. This figure represents a portion of the phase envelope shown in Figure 11. It may be observed that the points representing the compositions of the displaced and displacing fluids are located on the extension of two different quaternary tie lines.

As the displacement of liquid (O) by the gas (G) proceeds, the gas at the front contacts more liquid (O) and becomes further enriched in the intermediate component. Its composition path will follow the dew point surface in the direction of higher intermediate component concentration, until the limiting composition (GF) is reached. This limit is characterized by the particular quaternary tie line passing through (O) and point (OF) which is in equilibrium with (GF). Similarly, the oil left behind will be contacted by the displacing lean gas (G) and will be further stripped of its intermediate component. Its composition path will follow the bubble point surface until it reaches the limiting composition (OI). This limit is again characterized by the particular quaternary tie line passing through (G) and (GI) which is in equilibrium with (OI). During the contacting mechanism, the path (GI) to (GF), shown in Figure 12, will fluctuate, but will eventually reach a stationary position[6]. Due to the

Figure 12

Final Stage of Immiscible VGD
Case of a Quaternary system

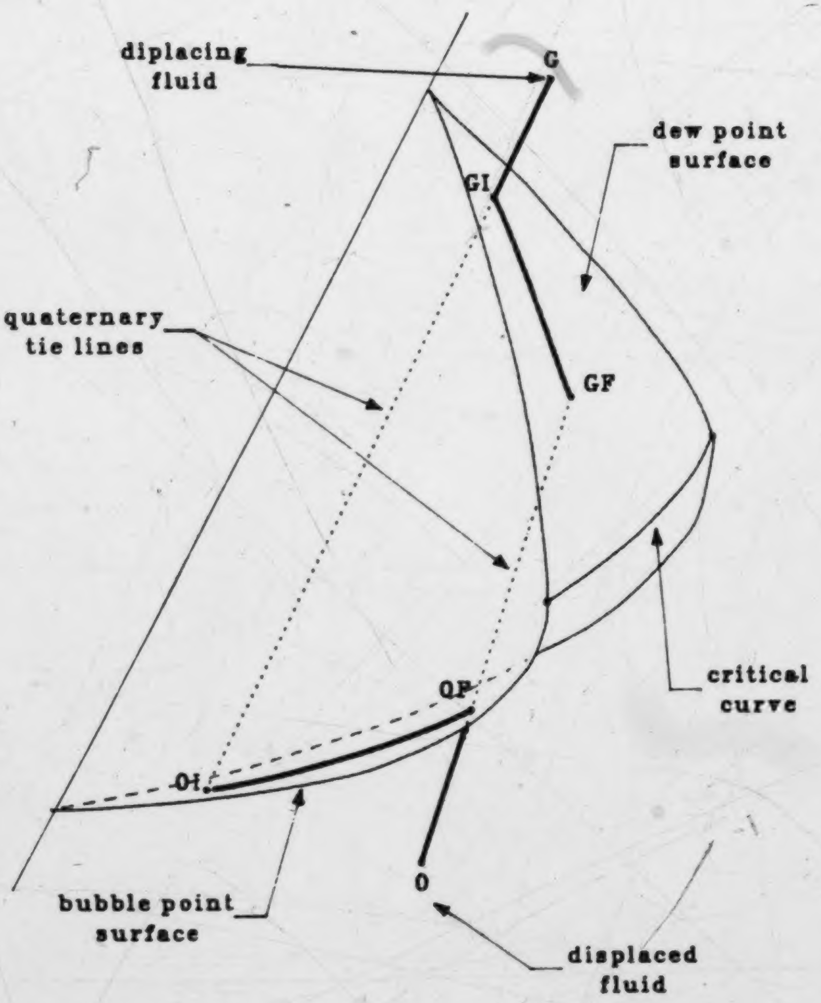

higher mobility of the gaseous phase and its lower density, one may expect a much larger degree of dispersion in the gaseous phase than in the liquid phase present in the transition zone. Since the mixing of contiguous gases on the path (GI)-(GF) located on the dew point surface results in some condensation, the resulting gas at equilibrium will not necessarily be located on the curve (GI)-(GF), and consequently a fluctuation of the path linking (GI) to (GF) will occur. A stationary position will be attained, however, when each quaternary tie line passing through each point of the path (GI)-(GF) is in the osculating plane of the curve (GI)-(GF) at that point.

3.5.2 Multiple-contact Miscible Case:

From the discussion on the phase relationships of a quaternary system (see Chapter 2) it was concluded that, at constant temperature, an increase in pressure is followed by a shrinkage of the phase envelope. Therefore, at a sufficiently high pressure, the point representing the composition of liquid (O) will be located on the ruled surface generated by the quaternary limiting tie lines. In this case, through the multiple-contact mechanism, the gas at the front will be enriched in the intermediate component to the point where it reaches a critical composition corresponding to the quaternary limiting tie line passing through point (O). Miscibility will then be initiated since the line connecting the point representing the composition of the gas at the front to that of the displaced fluid (O) does not cross the two-phase region. This displacement will again be characterized by the continuous breakdown and reformation of the miscible front, due to the effect of dispersion and/or some perturbing phenomena (viscous fingering or gravity override).

3.5.3 Definition of the Minimum Miscibility Pressure for Quaternary Systems.

The MMP of a vaporizing gas drive of an oil may now be defined as the minimum pressure, at the prescribed temperature, at which the point representing the oil composition lies on the ruled surface generated by the quaternary limiting tie lines. This surface separates oils that may be miscibly displaced by a lean gas through a multiple-contact process, from those that may not.

Similarly, for the condensing gas drive, one may define the MMP as the minimum pressure, at the prescribed temperature, at which the point representing the composition of the gas lies on the above ruled surface. Dynamic miscibility may also be initiated by injecting a gas rich enough in the intermediate component. The minimum enrichment required would be such that, at the prescribed pressure and temperature, the point representing the composition of the injected gas lies on the ruled surface generated by the quaternary limiting tie lines.

It may be concluded from this discussion that the MMP of a vaporizing or condensing gas drive may be solely determined from thermodynamic considerations, for the case of ternary or quaternary systems. The criteria defining the MMP, which have been set forth for the above systems, may now be used for the development of a reliable method for the prediction of the MMP based on the phase relationships of the displaced and displacing fluids.

4. Methods For Estimating The Minimum Miscibilty Pressure

4.1 Introduction

It may be recalled that the MMP is that minimum miscibility pressure necessary to initiate a multiple contact miscible displacement at constant reservoir temperature for fixed compositions of the reservoir oil and the injected gas. For the case of a three-component hydrocarbon system, the phase behavior of which can be rigorously represented on a ternary diagram at some fixed pressure and temperature, the MMP corresponds to the pressure at which the limiting tie line passes through the point representing the composition of the reservoir oil for a vaporizing gas drive, or that of the injected fluid for a condensing gas drive. For the case of complex field hydrocarbon systems, the MMP may be estimated or determined by means of pseudo-ternary diagrams, which will be referred to as the pseudo-ternary diagram method, empirical correlations and experimentally using the slim-tube test method.

The pseudo-ternary diagram method has been used essentially for the determination of the minimum enrichment of the injected gas for condensing gas drives. Two empirical correlations are available for the estimation of the MMP of a vaporizing gas drive. More specifically, one of the correlations[12] deals with a vaporizing gas drive utilizing a lean hydrocarbon gas and is based upon experimental data for nine oils. The other correlation[13] was intended to be a simple screening tool. It assumes that the MMP is the same whether the oil is displaced by a lean hydrocarbon gas or by nitrogen. From the discussion of the phase behavior of quaternary systems (refer to section 2-4), it was concluded that a two-phase region will exist at substantially higher pressures when nitrogen is present in the hydrocarbon system than would be the case if methane were the only light component present. Thus, the above assumption will result in an oversimplification of the problem when nitrogen is the displacing fluid, since the effect of nitrogen on the phase behavior of the system is not specifically taken into account. Furthermore, the correlation is based on twelve experimental data points of which only two involved displacements by nitrogen.

4.2 Pseudo-Ternary Diagram Method

This method treats any complex hydrocarbon system as being composed of three pseudo-components, the light end, C1, the intermediate and the heavy fractions. The grouping of components into these fractions is arbitrary. Benham et al.[14] and Craig and Zana[15] considered a C2-C4 and $C5^+$ split, while others[7,16] used a C2-C6 and $C7^+$ split for the intermediate and heavy fractions, respectively. The method is used to determine the minimum enrichment of the injected gas necessary to initiate a multiple contact miscible displacement for a condensing gas drive. However, the adopted approach differed from one investigator to another.

For the purpose of describing the process of multiple contact miscibility, Benham et al.[14] used the NGAA[17] equilibrium constants to generate a phase envelope by considering various mixtures of the above pseudo-components and performing a flash calculation for each mixture. For the case where the mixture results in the coexistence of liquid and vapor phases at equilibrium, the composition of the coexisting phases is then represented in terms of the above pseudo-groups and a tie line is drawn on the pseudo-ternary diagram. The phase envelope, which separates the single phase from the two-phase region is obtained by repeating the above procedure to other mixtures, assuming that the compositions of the C2-C4 and $C5^+$ fractions remain the same as those of the reservoir oil.

There are, however, severe limitations to this approach as described by Benham et al.[14]. It has been seen that in the case of a multiple contact miscible displacement, a transition zone will develop between the original injected gas and the displaced reservoir oil. Therefore, across the transition zone, the character of the intermediate and heavy-ends groups will vary from that of the injected gas to that of the reservoir oil. Hence, pseudo-ternary diagrams based on the character of these groups in only one of the phases will not describe all the stages involved in the initiation of miscibility. Benham et al.[14] suggested a way of overcoming this problem for the case of a condensing gas drive. They argued that if consideration is limited to the region close to the critical point and the associated limiting tie line, and if it is assumed that the characteristics of the intermediates and heavy-ends of the critical point are close to those of the injected and displaced fluids, respectively, a pseudo-ternary diagram, drawn using intermediates having characteristics similar to that of the injected gas and heavy ends having characteristics similar to that of the reservoir oil, will have quantitative significance in the region of the critical point and its associated limiting tie line.

Based on the preceeding assumptions and also assuming a limiting tie line of infinite slope (parallel to the C1-$C5^+$ edge of the pseudo-ternary diagram), they developed a simple method for estimating the minimum enrichment of the gas at some prescribed pressure and temperature. The procedure consisted of estimating the critical pressure and temperature of various mixtures of lean gas (C1), intermediates having characteristics similar to the intermediate fraction to be used to enrich the lean gas, and heavy-ends having characteristics similar to the $C5^+$ fraction of the reservoir oil. The Davis et al.[11] empirical method, was used to evaluate the critical pressure and temperature of each mixture. The mixture, the critical temperature and pressure of which corresponded to the reservoir conditions of temperature and pressure, was then used to obtain the minimum enrichment of the lean gas. Since the limiting tie line associated with the critical mixture was assumed to be of infinite slope (parallel to the C1-$C5^+$ edge of the pseudo-ternary diagram), the minimum enrichment corresponded to the mole percentage of the C2-C4 fraction of the critical mixture. The procedure was repeated for various molecular weights of the intermediate and heavy fractions, and the results cross-plotted to obtain the conditions for miscibilty at constant pressures for a given reservoir fluid, injection fluid and reservoir temperature. The graphical correlation was put into equation form by Glasø[19]. It may be seen that the Benham et al.[14] method relies on an empirical correlation for the estimation of the critical pressure and temperature and furthermore the restrictive assumption of a vertical limiting tie line, which in general has a negative slope, results in a conservative estimate of the minimum enrichment.

With the advent of new equations of state[2,20] and their computer implementation, the prediction of phase behavior has become easier and more reliable. Craig and Zana[15] used the Peng and Robinson (PR) equation of state[20] to perform flash calculations for various mixtures of the light fraction (C1), the intermediates (C2-C6) and heavy-ends ($C7^+$) having characteristics similar to that of the reservoir fluid, at fixed conditions of pressure and temperature. The results were then used to draw tie lines on a pseudo-ternary diagram, thereby generating a phase envelope. Using the above data, the critical point and limiting tie line were obtained by extrapolation. The limiting tie line obtained was then used to establish the minimum enrichment of the injected gas required to initiate a multiple-contact miscible condensing gas drive at the prescribed pressure and temperature.

Based on suggestions made by Benham et al.[14] with respect to the characterization of the intermediate and heavy fractions, Cohen and Shirer[16] considered various mixtures of the light fraction (C1), the intermediate fraction (having characteristics similar to the intermediate fraction used to enrich the injection fluid) and the reservoir fluid to generate a phase envelope on a pseudo-ternary diagram, at some prescribed pressure and temperature. In this case, the Exxon Benedict-Webb-Rubin-Starling (BWRS) equation of state[21] was used to perform the flash calculations. The critical point and the associated limiting tie line were again obtained by extrapolation, and used to determine the minimum enrichment of the injected gas.

These equations of state based methods have the advantage of removing the restrictive assumption of a vertical limiting tie line made by Benham et al.[14]. However, they do not lend themselves to the development of a practical method for the prediction of the MMP. The disadvantage is that the determination of the limiting tie line requires the generation of the complete phase envelope. Moreover, both investigations[15,16] reported difficulties in the determination of the critical point and convergence problems in the flash calculations when the mixtures were close to the critical point. Furthermore, the concept of pseudo-ternary diagrams is not rigorous from a thermodynamic standpoint as is immediately apparent from the phase rule. The limitations of the pseudo-ternary approach have been described by Hutchinson and Braun[7]. Basic to the pseudo-ternary method is the fact that the distribution of the individual components within each group is not given. Since components within a group have different volatilities, they are not distributed in each group the same way in coexisting gas and liquid phases. Also, they have shown that the slopes of the tie lines differ depending on the overall composition which in turn is set by the process used to reach equilibrium. For example, one set of tie lines was obtained from a multiple batch-contact study. A reservoir fluid L1 was mixed with a gas G1 which, at equilibrium, resulted in the coexistence of gas G2 and liquid L2. The liquid L2 obtained was then mixed with the original gas G1 which, at equilibrium, resulted in the coexistence of gas G3 and liquid L3, and this mixing procedure was repeated for other batch-contact experiments. Another experiment involved the actual displacement of liquid L1 by gas G1 in a porous medium at the same conditions of pressure and temperature. The tie line obtained for a sample produced at one stage during the multiple contact process was shown to have a slope significantly different than the trend obtained from the previous set of experiments.

The limitations of the pseudo-ternary approach become even more pronounced when a non-hydrocarbon component is involved. For instance, when nitrogen is considered as the driving gas, the question arises as to whether or not nitrogen is to be included in the light fraction. It has been observed that in general, at some fixed pressure and temperature, an increase in size of the two-phase region of the light-intermediate-heavy ternary system will result when nitrogen is the light component (refer to chapter 2). One could speculate that, to adequately describe the phase relationships of nitrogen-hydrocarbon systems, it would be necessary to deal with nitrogen and methane as two separate components.

4.3 Empirical Correlations

At present, two correlations for the determination of the MMP of vaporizing gas drives have been published in the literature[12,13]. Blackwell's correlation[12], which based upon experimental data for nine oils, applies to displacements by a lean hydrocarbon gas and may be expressed mathematically as

$$MMP = Ps(X + 4.09068)/(2.252354\ X)$$

where

$$X = Wi \cdot Wl \cdot Tr / W7^{+}$$

and

MMP= minimum miscibility pressure, Psia

Ps = oil saturation pressure at reservoir temperature, Psia

Wl = Lbs methane+nitrogen per Lb-mole oil

Wi = Lbs of C2-C6 fraction+CO2+H2S per Lb-mole oil

$W7^+$= Lbs of $C7^+$ fraction per Lb-mole oil

Tr = reduced temperature of reservoir fluid.

The correlation was tested with four data points not included in the data base used for its development. The average deviation between estimated and experimental MMP's was 260 Psia with a maximum deviation of 640 Psia. Stalkup[12] points out that this correlation should be used with caution and for screening purposes only, since so few data points were used in its development.

Recently, another correlation[13] was presented. It consists of a correlation of the MMP as a function of a parameter X and may be expressed as

$$MMP = 9433 - 188\text{x}10^3\, X + 1430\text{x}10^3\, X^2$$

where

$$X = (C2\text{-}C5)/(C7^+M.wt)/(T^{0.25})$$

and

C2-C5 = mole% of intermediate fraction C2-C5

$C7^+$M.wt= molecular weight of heavy fraction $C7^+$

T = temperature in °F.

This correlation assumes that the MMP is the same whether the oil is being displaced by a lean hydrocarbon gas or by nitrogen. It has been seen that the presence of nitrogen in a hydrocarbon system results generally in a considerably larger two-phase region (see chapter 2) and, therefore, the above assumption is an oversimplication considering that the correlation is based on twelve experimental data points, of which only two involved displacements by nitrogen. Aside from their empirical nature, correlations depend heavily on the experimental procedure used to determine the MMP.

4.4 Slim-Tube Test Method

The minimum miscibility pressure required for the development of a multiple contact miscible displacement is often determined experimentally by what is referred to as the slim-tube displacement test. In this method, the reservoir oil is displaced by the potential lean gas at reservoir temperature and at various pressures. The experiments are carried out in an elongated small diameter tube packed with glass beads or silica sand.

Before going any further, it is important to note[22,23] that the sand-packed tube displacement apparatus is a device for bringing about multiple contacts between co-currently flowing phases. It is not intended to simulate reservoir fluid displacement conditions. Hence, slim-tube tests are not indicative of ultimate recovery, macroscopic sweep efficiency, transition zone length, etc..., to be achieved in an actual reservoir.

As discussed earlier, the basic criteria defining the MMP rely on the theoretical conclusions that for a value of the pressure greater or equal to the MMP, an increase in recovery should be observed and that the character of the displacement changes from diphasic to monophasic flow. However, as observed by Orr et al.[24], the experimental procedures vary from one investigator to another with displacement lengths ranging from 1.5 m to 25.6 m, flow geometries varying from vertical to flat coils to spirals, and flow velocities varying over nearly two orders of magnitude. Moreover, no general consensus exists as to the experimental criteria defining the MMP. These criteria are not clearly defined except for those researchers[6,22] who conducted vertical displacements. Table 1 summarizes some of the published experimental procedures and criteria utilized for MMP definition.

A parametric analysis of the MMP, as determined by the slim-tube test method, was conducted by Flock and Nouar[26]. It was concluded that, because the recovery was found to be affected by system length and injection rate, one should not use as a sole criterion that for

Table 1
Experimental Procedures and Criteria for MMP Determination

Experimenter	Experimental procedure	Stability criterion	Criteria defining MMP
Deffrenne et al[6]	vertical displacement tube length = 1.5m tube diameter = 0.01m packing material: 60-65 mesh glass beads	$Vd \leq Vc$ $Vc = Kg\frac{(\rho o - \rho g)}{(\mu_o - \mu_g)}$	Plot of recovery vs pressure at gas breakthrough or after 1 to 1.2 PV injection should show a clear break in slope for a value of P = MMP.
Yellig and Metcalfe[23]	flat coil (horizontal displacement) tube length = 12.2m tube diameter = 0.457cm packing material: 160-200 mesh sand	none Injection rate: 12.2 m/d up to 70% PV inj 24.4 m/d up to 1.2 PV inj	Define miscible displacements as those in which recovery at 1.2 PV was very near maximum recovery obtained in a series of displacements and in which transition-zone fluids appeared in a sight glass. They took as an indication of a multiple-contact miscible process, color gradation from dark oil to a yellow fluid. Floods that produce clear vapor and dark oil were judged immiscible.
Holm and Josendal[25]	Flat coil (horizontal displacement) tube length = 14.6-25.6m tube diameter = 0.457cm	none Injection rate: 91.5 m/d	Define miscible displacements as those that recover more than 80% of the IOIP at gas breakthrough, and that more than 94% of IOIP is recovered ultimately.

the determination of the MMP, the recovery should be greater than some arbitrarily fixed value at some pore volume injection. It was recommended that the system length should be as long as possible in order that the minimum length of immiscible displacement, necessary for miscibility to be dynamically initiated, will not mask the overall effect of the multiple contact miscible displacement. It was also found that a moderately high injection rate is preferable in order to obtain a better differentiation between immiscible and multiple contact miscible displacements.

An examination of these observations clearly shows that any MMP correlation would be strongly affected by the data base used in its development. Any inconsistency in the experimental procedure will also be reflected in the correlation, thereby increasing the uncertainty of such correlations.

4.5 Line of Investigation

It has been seen that the methods available for the estimation of the MMP are either too cumbersome or too simplistic. The pseudo-ternary approach lacks rigor from the thermodynamic point of view and does not take specifically into account the effect of non-hydrocarbon components on the phase relationships. Furthermore, it requires the complete generation of phase envelopes and does not lend itself to the development of a practical method. Empirical correlations are as good as the data base from which they are developed. They require a large data base and consistency in the experimental procedure and criteria used in the determination of the MMP. Considering the time and expense necessary to perform laboratory tests, it is apparent that the development of a sound predictive method is necessary.

In view of the above, the object of this study was to develop a more refined predictive method for the determination of the MMP of a vaporizing gas drive by a lean hydrocarbon gas or nitrogen, based on rigorous thermodynamic criteria. The method may also be extended to the case of condensing gas drives.

The development of the method for predicting the MMP is based on the thermodynamic criteria set forth in chapter 3. It involves the formulation of these criteria in terms of rigorous equations and their solutions for simple ternary and quaternary systems. The method is then to be extended to complex systems using ternary or quaternary systems as building blocks. The formulation of the problem is presented in the following chapter.

5. Formulation of the Criteria Defining the MMP

5.1 Introduction

From the discussion of the mechanism of a vaporizing gas drive, for a ternary system at constant temperature, it was concluded that if the displacement pressure is high enough for the limiting tie line to pass through the point representing the oil composition, multiple contact miscibility could be initiated. This pressure was referred to as the MMP. Similarly, for a condensing gas drive, it is necessary for the limiting tie line to pass through the point representing the rich gas composition for the initiation of dynamic miscibility. It may be seen that the determination of the MMP necessitates the evaluation of the critical point composition and the slope of the limiting tie line as a function of pressure for the selected system and temperature. The MMP is determined by evaluating the pressure at which the limiting tie line passes through the point representing the oil composition for a vaporizing gas drive, or the rich gas composition for a condensing gas drive.

For the case of a quaternary system, the MMP of a vaporizing gas drive was defined as the minimum pressure, at the prescribed temperature, at which the point representing the oil composition lies on the ruled surface generated by the quaternary limiting tie lines. Similarly, the composition of the rich gas would have to lie on the above ruled surface for a multiple contact miscible condensing gas drive. In this case, the determination of the MMP necessitates the generation of the ruled surface at various pressures for the selected system and temperature. At each pressure, the ruled surface may be determined by evaluating the compositions of a sufficient number of points on the critical curve and the directions of the quaternary limiting tie lines passing through each of these points. The MMP is obtained by determining the pressure, at the prescribed temperature, at which the ruled surface passes through the point representing the oil composition for a vaporizing gas drive, or the rich gas composition for a condensing gas drive.

The above criteria defining the MMP will be formulated in terms of rigorous equations for ternary systems. The approach used will then be extended to the case of quaternary systems. The formulation of the problem is based on geometrical properties of the Gibbs surface in the neighborhood of a critical point. However, before addressing the specific derivation of the equations pertinent to the problem, it would appear appropriate to discuss the thermodynamic relationships existing between phases in equilibrium for a multicomponent system.

5.2 Phase Equilibria for Multicomponent Systems

The conditions that have to be satisfied for a multicomponent system to be stable (homogeneous) or unstable (coexistence of phases) at equilibrium were first described by Gibbs[5]. These conditions are derived from the criterion for equilibrium enunciated by him: "For the equilibrium of any isolated system it is necessary and sufficient that in all possible variations of the state of the system which does not alter its internal energy, the variation of its entropy shall either vanish or be negative". In other words, equilibrium requires that the entropy of an isolated system be a maximum. Under the conditions of constant pressure and temperature, an equivalent statement of the above criterion is for the Gibbs free energy of a system to be a minimum at equilibrium[5]. Since multicomponent systems at constant pressure and temperature are the ones considered, the description of phase equilibria will be discussed in terms of the Gibbs free energy. Let the Gibbs free energy of a system containing $N_1, N_2, \ldots, N_n$ moles of components $1, 2, \ldots, n$ at some pressure P and temperature T be:

$$G(T, P, N_1, N_2, \ldots, N_n).$$

If the total number of moles of the system is fixed, the number of independent variables is reduced by one, since the composition is uniquely defined by specifying the mole fractions $X_1, X_2, \ldots, X_{n-1}$ of the components $1, 2, \ldots, n-1$ $(X_n = 1 - X_1 - X_2 - \ldots - X_{n-1})$. One may, therefore, consider possible variations of the composition of the system in terms of the molar Gibbs free energy:

$$g(T, P, X_1, X_2, \ldots, X_{n-1}).$$

At constant pressure and temperature, the relationship between the molar Gibbs free energy and the composition of the system may be represented, in an n-dimensional space, by a hypersurface which, hereafter, will be referred to as the Gibbs surface. For simple systems such as binaries this relationship corresponds to a curve, and for ternary systems, a 2-dimensional surface.

An important consequence of the criterion of equilibrium is the requirement that the Gibbs surface, which represents equilibrium states, be above its tangent plane at any of its points. Such a property may be readily explained in terms of a composite system[27]. Consider a point on the Gibbs surface corresponding to a mixture M at equilibrium, hence, requiring that its Gibbs free energy is a minimum. Further suppose that the tangent plane to the Gibbs surface at that point cuts the surface at some other point. A portion of the surface will necessarily be located below the tangent plane. If such is the case, the system M does not represent an equilibrium state and, therefore, does not belong to the Gibbs surface, as shown below. Now consider a composite system M' consisting of two parts, one representing a point on the portion of the Gibbs surface located above the tangent plane and the other, a point on the portion of the surface located below the tangent plane, with the same overall composition as the original system M. The Gibbs free energy of the system M' is the sum of the Gibbs free energy of each of its parts. One may, therefore, obtain a composite system M' having a Gibbs free energy smaller than the Gibbs free energy of the original System M, which contradicts the previous assumption that the Gibbs free energy of the original system is a minimum for that system to be in equilibrium. Hence, the requirement that the Gibbs surface is above its tangent plane at any of its points in order for those points to represent equilibrium states.

Unstable mixtures result in the coexistence of two or more phases at equilibrium, in order to lower the Gibbs free energy of the system at some fixed pressure and temperature, thereby tending toward the most stable state. The phases in equilibrium must satisfy the criteria of equality of the chemical potentials[5] of each component in all the phases present, as well as the uniformity of temperature and pressure throughout the system. At equilibrium, there are no driving forces to cause a net movement of any component from one phase to any other phase. For an n-component system resulting, for instance, in a liquid-vapor equilibrium at some pressure and temperature, these criteria may be expressed in terms of partial derivatives of the Gibbs free energy as follows:

$$\mu_1^l = \mu_1^v$$

$$\mu_2^l = \mu_2^v$$

$$\vdots$$

$$\mu_n^l = \mu_n^v$$

and

$$\mu_i = \frac{\partial G}{\partial N_i}$$

where μ_i refers to the chemical potential of component i, and superscripts l and v refer to the liquid and vapor phases of the system, respectively.

If one expresses the above relationships in terms of the molar Gibbs free energy, it may be shown (refer to Appendix 2) that the point on the Gibbs surface representing the above system is located on a common plane tangent to the Gibbs surface at the points representing the individual phases of the system, in this case the liquid and vapor phases. The Gibbs free energy of a system at constant pressure and temperature is a homogeneous function of degree one and it is shown in Appendix 2 that the above result may be derived from the properties of homogeneous functions. These concepts are illustrated below for the case of binary and ternary systems, since these are the only systems for which a representation of the Gibbs surface, in a three-dimensional space, is possible.

5.2.1 Gibbs Free Energy Analysis of a Binary System

At constant pressure and temperature, the molar Gibbs free energy of a binary system composed of components 1 and 2 may be represented by a curve, since the only independent variable is the mole fraction of one of the components 1 or 2, for instance X_1 ($g(X_1)$). Figure 13-a illustrates such a representation for the system methane-n-pentane at a temperature of 87 °C and a pressure of 8 MPa, calculated using the SRK equation of state[2]. In this figure, the normalized molar Gibbs free energy is graphically represented as a function of the n-pentane mole fraction. The normalized molar Gibbs free energy being defined as

$$gn = (g - gmin)/(gmax - gmin)$$

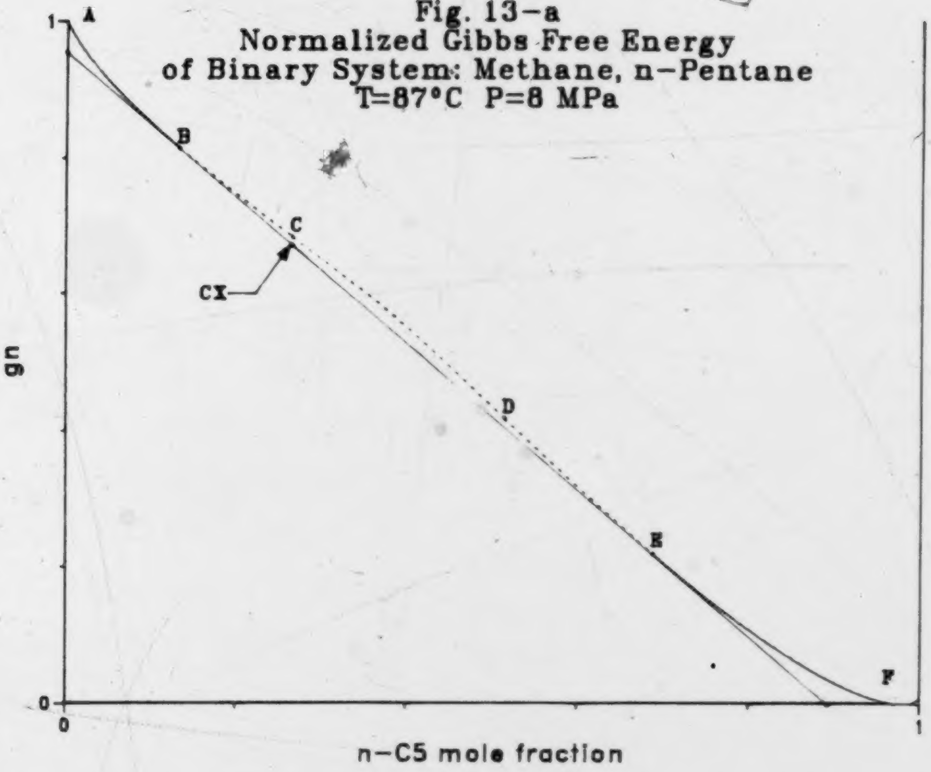

Fig. 13−a
Normalized Gibbs Free Energy
of Binary System: Methane, n−Pentane
T=87°C P=8 MPa

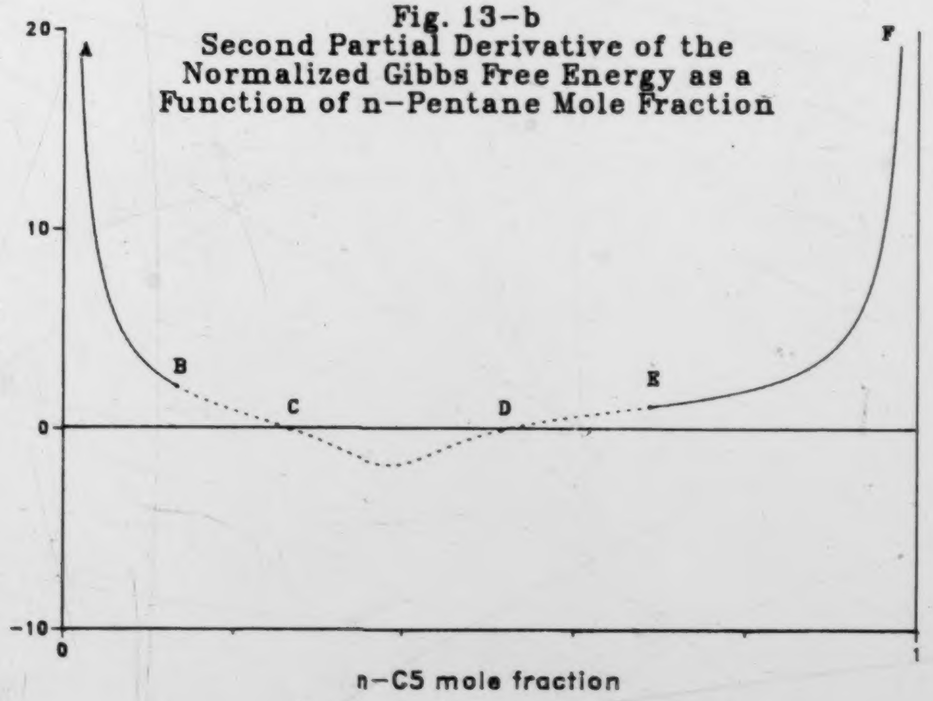

Fig. 13−b
Second Partial Derivative of the
Normalized Gibbs Free Energy as a
Function of n−Pentane Mole Fraction

where gmin and gmax are the minimum and maximum molar Gibbs free energy, respectively, for all the possible mixtures varying from pure methane to pure n-pentane. The curve A to F has been referred to as the primitive curve[5], since not all of its points satisfy the equilibrium criterion as it is explained below. As previously mentioned, in order for a point on the Gibbs curve to represent an equilibrium state, it is necessary for the curve to be above its tangent line at that point. The portions AB and EF satisfy such a requirement and correspond to stable equilibrium states. This is not the case for points on the portion BE of the curve, since a portion of the curve will be below the tangent line to the curve at any point between B and E. Consider for instance point C. There exists a composite system, CX, having the same overall composition as the system C with, however, a lower molar Gibbs free energy. Such a system may consist of two parts, one corresponding to system B and the other to system E. The overall molar Gibbs free energy of such a system will correspond to that of point CX, and it is clearly observed in Figure 13-a that it is lower than the molar Gibbs free energy of the original system C. The systems represented by points on the curve BCDE are unstable systems and will form heterogeneous systems at equilibrium in order to lower their molar Gibbs free energies. In this case, the resulting systems, at equilibrium, will consist of the coexistence of two phases represented by points B and E in the proportions dictated by the component material balance. As previously mentioned, the points B and E, which represent the phases in equilibrium, are located on the same line tangent to the primitive curve at both points. The segment BE, which is referred to as the derived curve, corresponds to two-phase equilibrium states for mixtures having overall compositions varying from that of system B to that of system E. This segment, along with the portions AB and EF of the primitive curve, correspond to true equilibrium states, with the portion AB representing the homogeneous vapor state (high methane concentration), the portion EF representing the homogeneous liquid state (high n-pentane concentration), while the segment BE corresponds to a two-phase state varying from 100% vapor (B being the dew point) to 100% liquid (E being the bubble point). Points B and E may be found by rolling a tangent line on the primitive curve until it makes a double-contact with the curve at these points, the primitive curve being at all times above this tangent line.

Figure 13-b illustrates the graphical representation of the second partial derivative of the molar Gibbs free energy with respect to the n-pentane mole fraction for the same methane-n-pentane system and at the same conditions of pressure and temperature. In other words, this relationship defines the convex and concave portions of the primitive curve, depending on the sign of the second partial derivative. The portions AB and EF of the primitive curve are necessarily convex in order to satisfy the criterion that the primitive curve be above the tangent line at any point corresponding to stable equilibrium states. The portions BC and DE of the primitive curve have also the same characteristic. However, although the criterion of stability is satisfied locally (i.e. in the neighborhood of a point belonging to portions BC and DE, the primitive curve is above the tangent line at that point), this criterion is not satisfied globally as any tangent line to the primitive curve at a point belonging to portions BC and DE will be above a portion of the curve. The portions BC and DE refer to metastable states (supersaturated vapor or liquid). These states may be reached experimentally[1,5,27], but will result in a heterogeneous state if disturbed (unstable to the nucleation of some other phase). In particular, the curvature vanishes at points C and D. These points are referred to as the limit of essential stability or spinodal points[27]. Between these points, the primitive curve is concave. The points belonging to the portion CD of the primitive curve correspond to completely unstable systems, as the stability criterion is not even satisfied locally (these states can not be reached experimentally). For the case of a smooth primitive curve (as is shown in Figure 13-a), it may be observed that it is necessary for a portion of the curve to have a negative second partial derivative in order for some mixtures to result in a heterogeneous state at equilibrium. If the second partial derivative is at all times positive, the first partial derivative of the molar Gibbs free energy will be a monotonic function of the mole fraction of one of the components of the binary system. Hence, all the points of the curve will represent homogeneous states. For the system shown in Figure 13.a, the temperature being between the critical temperatures of the constituting components, a critical point may be reached by increasing the pressure of the system. As the critical pressure is approached, point B will come closer to point E and at the critical pressure, these points will coincide so that one cannot distinguish the vapor phase (B) and the liquid phase (E). At the critical point, the second partial derivative of the primitive curve will vanish since upon a slight reduction of the pressure a two-phase system will result for some mixtures and a portion of the primitive curve will necessarily have a negative second partial derivative. Hence, at the critical pressure, the second partial derivative will be positive for all points of the primitive curve, being zero at the point representing the critical mixture. It follows also that the critical point will correspond to a minimum for the curve shown in Figure 13.b, thus, the third partial derivative of the molar Gibbs free energy will also vanish at that point. These are the criteria to be satisfied by a critical binary mixture (the vanishing of the second and third partial derivatives of the molar Gibbs free energy) and were first derived by Gibbs[5].

5.2.2 Gibbs Free Energy Analysis of a Ternary System

For a ternary system composed of components 1,2 and 3 at constant pressure and temperature, the molar Gibbs free energy may be represented by a surface with the independent variables being, for instance, the mole fractions of components 1 and 2 ($g(X_1,X_2)$). Figure 14 illustrates such a representation for the methane-propane-n-pentane system at a temperature of 87 °C and a pressure of 8 MPa, using the SRK equation of state[2]. In order to display those portions of the surface that would be otherwise hidden from the viewer, the negative molar Gibbs free energy (-g) is represented as a function of the mole fractions of propane and n-pentane, thereby allowing the salient features of such a surface to be shown to the viewer. In this figure, the negative Gibbs free energy was also normalized according to the procedure utilized for the case of a binary system.

One may observe that the criteria given in section 4.2 should be reversed when the inverted Gibbs surface is considered, i.e. at equilibrium a system tends to maximize the negative of its molar Gibbs free energy. Also, the tangent plane criterion (stability criterion) that has to be satisfied by a stable system requires that the inverted surface be below the

Figure 14
Inverted Gibbs Free Energy Surface
of a Ternary System
T,P fixed

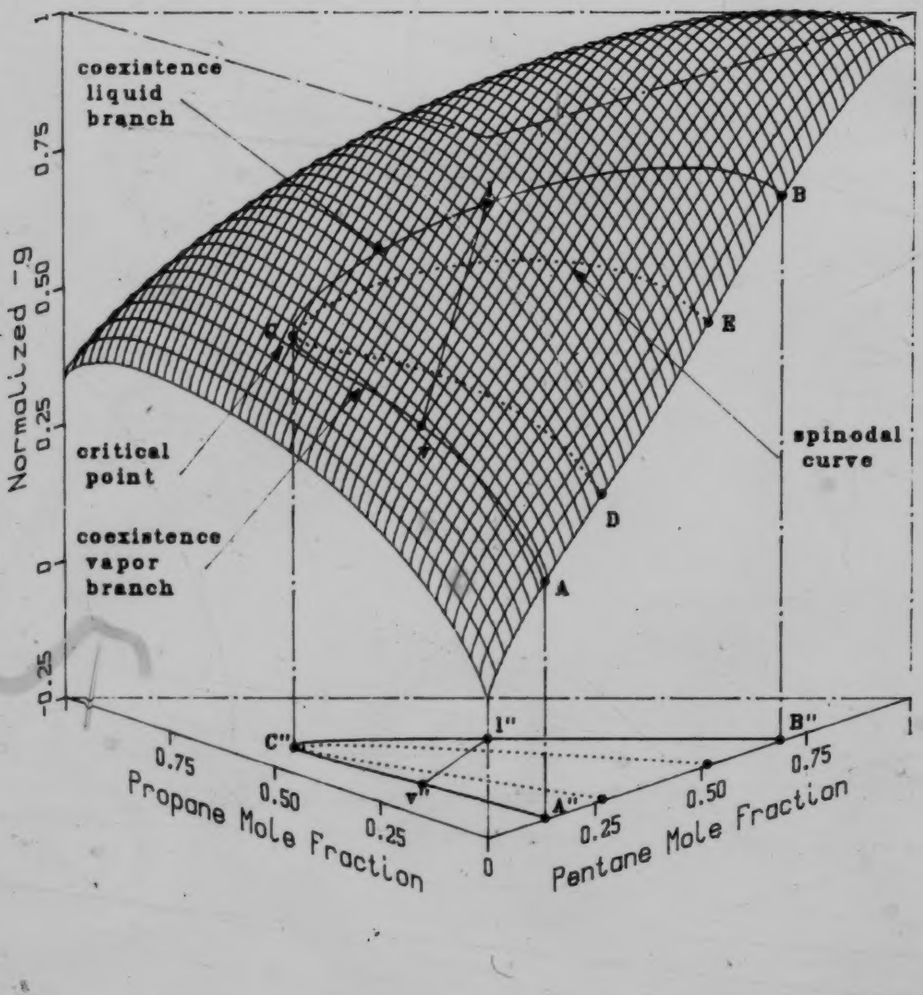

tangent to the surface at the point representing such a system. The surface shown in Figure 14 is referred to as the primitive surface and not all points on this surface satisfy the equilibrium criterion. The unstable systems avoid instability through a phase split, in this case a vapor-liquid equilibrium. As shown in Appendix 2, the points representing these phases in equilibrium are located on a common plane tangent to the primitive surface at each of these points. Furthermore, in order to satisfy the equilibrium criterion, it is required that this double-tangent plane be at all times above the primitive inverted Gibbs surface, making contact with the surface only at the points representing the phases in equilibrium. It may be seen now that the points representing the equilibrium phases may be found by rolling a double-tangent plane onto the primitive surface as described by Gibbs[5]. Two coexistence curves are thereby generated by those points corresponding to the liquid branch (BC) and the vapor branch (AC) on the surface shown in Figure 14. The inner region of the primitive surface delimited by the above curves corresponds to non-equilibrium systems. This region is now replaced by a coexistence surface (also referred to as the derived surface) which consists of the line segments, or generators, joining the points representing the phases in equilibrium (for instance, segment l-v in Figure 14). Each generator is necessarily part of the double-tangent plane to the primitive surface at contact points corresponding to the end points of the generator. Geometrically speaking, each generator is located at the intersection of two infinitesimally close double-tangent planes to the primitive surface. It follows that the coexistence surface corresponds to the portion, delimited by the coexistence curves, of the ruled surface generated by the envelope of this family of double-tangent planes. The liquid and vapor branches, shown in Figure 14, meet at the critical point (C) where the vapor and liquid phases coalesce. On the more familiar ternary diagram, corresponding to the composition plane spanned by the propane and n-pentane mole fraction axes, the projections A"C" and B"C" of the curves AC and BC correspond to the dew-point and bubble-point curves, respectively, which meet at the critical point composition represented by point C". Also, the projection of the generator l-v onto the composition plane correponds to the familiar tie line l"-v".

The curve ECD, shown in Figure 14, corresponds to the limit of essential stability and is referred to as the spinodal curve. As previously discussed, metastable systems satisfy locally but not globally the tangent plane criterion. The metastable region is delimited by the coexistence curve and the spinodal curve, and corresponds to supersaturated liquid or vapor states which may be reached experimentally. These metastable systems are unstable to the nucleation of another phase and degenerate into a heterogeneous state upon a small disturbance of the system. An analysis of the stability of homogeneous phases is given in Appendix 3, wherein the criteria that need to be satisfied for systems to be locally stable are considered. It may be shown[5,27] (refer to Appendix 3) that in order for an n-component system at constant pressure and temperature to locally satisfy the tangent plane criterion, the following determinant:

$$U = \begin{vmatrix} g_{11} & g_{1j} & g_{1,n-1} \\ \vdots & \vdots & \vdots \\ g_{i1} & g_{ij} & g_{i,n-1} \\ \vdots & \vdots & \vdots \\ g_{n-1,1} & g_{n-1,j} & g_{n-1,n-1} \end{vmatrix} \qquad (1)$$

as well as all its principal minors must be positive, where the general element g_{ij} of the above determinant corresponds to the second partial derivative of the molar Gibbs free energy with respect to the mole fractions of components i and j.

At the limit of essential stability, the determinant U vanishes, which is the condition satisfied by the points on the spinodal curve ECD shown in Figure 14. The spinodal curve makes a tangent contact with the coexistence curve (ACB) at the critical point C and necessarily lies inside the coexistence curve, since it represents the limit of essential stability. As first derived by Gibbs[5], for the general case of an n-component system, a critical phase is only capable of n-1 variations and, therefore, must satisfy another criterion, along with the vanishing of the above determinant U, which may be expressed by requiring that the following determinant be zero:

$$V = \begin{vmatrix} g_{11} & g_{1j} & g_{1,n-1} \\ \vdots & \vdots & \vdots \\ g_{i1} & g_{ij} & g_{i,n-1} \\ \vdots & \vdots & \vdots \\ g_{n-2,1} & g_{n-2,j} & g_{n-2,n-1} \\ U_1 & U_j & U_{n-1} \end{vmatrix} \qquad (2)$$

where U_j is the partial derivative of determinant U with respect to the mole fraction of component j.

The analysis presented in this section may be extended to any other multicomponent system, by following the same equilibrium principles. These principles may now be used to formulate the problem of interest to this investigation, i.e. the criteria defining the MMP. The approach considered is addressed below, first for the case of a ternary system.

5.3 Equation of the Limiting Tie Line of a Ternary System

For the case of a ternary system at constant temperature, the development of a multiple contact miscible vaporizing gas drive requires that the point representing the oil composition be at least located on the limiting tie line, corresponding to a pressure which was referred to as the minimum miscibility pressure (with similar considerations for a condensing gas drive). Thus, in order to formulate the above criterion, one needs to derive an equation for the limiting tie line. By definition, the limiting tie line corresponds to the limiting position attained by the ternary tie lines as the critical point is approached. Therefore, one needs to develop a general equation of a tie line in order to consider its limit as the critical point is approached. In order to do so, the results of the previous analysis of the Gibbs surface of a ternary system, at any fixed pressure and temperature, are considered in the region where two phases (liquid, vapor) coexist.

For a ternary system composed of species 1,2 and 3 at constant pressure and temperature, the equation of a generator may be developed in terms of the molar Gibbs free energy. For a two-phase transition, liquid(l)-vapor(v) equilibrium, and considering the mole fractions of components 1 and 2 as the independent variables, the following must be satisfied (refer to Appendix 2):

$$g_1^l = g_1^v$$

$$g_2^l = g_2^v$$

and

$$g^l - \sum_{i=1}^{2} X_i^l g_i^l = g^v - \sum_{i=1}^{2} X_i^v g_i^v \tag{3}$$

where g refers to the molar Gibbs free energy, g_i, its partial derivative with respect to the mole fraction of component i, and X_i^l and X_i^v refer to the compositions of the liquid (l) and vapor (v) phases in equilibrium, respectively.

As previously discussed, from the equalities 3, one concludes that the coexistence curve (liquid and vapor branches) is generated by rolling a double-tangent plane onto the primitive surface $g(X_1,X_2)$, and the coexistence surface is the envelope of this family of planes delimited by the coexistence curve.

Considering its liquid branch, let the coexistence curve be given by the following parametric form

$$X_1 = x^l$$

$$X_2 = f(x^l)$$

$$g(X_1,X_2) = g(x^l,f(x^l)) = \psi(x^l) \tag{4}$$

where x^l is the parameter, and the partial derivatives of the molar Gibbs free energy on the coexistence curve be given by

$$g_1(x^l,f(x^l)) = \psi_1(x^l) \tag{5-a}$$

$$\text{and } g_2(x^l,f(x^l)) = \psi_2(x^l) \tag{5-b}$$

The coexistence tangent planes form a family of planes, of parameter x^l, given by

$$F(X_1,X_2,g;x^l) = (X_1-x^l)g_1 + (X_2-f(x^l))g_2 - (g-\psi(x^l)) = 0 \tag{6}$$

where $[g_1,g_2,-1]$ is the normal to the Gibbs surface on the coexistence curve.

The equation of the characteristic line (intersection of two infinitesimally close tangent planes), or generator of the envelope of this family of planes is given by

$$F(X_1,X_2,g;x_1^l) = 0 \tag{7-a}$$

and

$$\frac{\partial F}{\partial x_1^l} = 0 \tag{7-b}$$

which may be written as

$$(X_1-x_1^l)g_1 + (X_2-f(x_1^l))g_2 - (g-\psi(x_1^l)) = 0 \tag{8-a}$$

and

$$(X_1-x_1^l)\frac{d\psi_1}{dx_1^l} + (X_2-f(x_1^l))\frac{d\psi_2}{dx_1^l} - g_1 - g_2\frac{df(x_1^l)}{dx_1^l} + \frac{d\psi(x_1^l)}{dx_1^l} = 0 \tag{8-b}$$

and from the chain rule of differentiation,

$$-g_1 - g_2\frac{df(x_1^l)}{dx_1^l} + \frac{d\psi(x_1^l)}{dx_1^l} = 0 \tag{9}$$

It follows from Equations 8 to 9 that the vector $[X_1-x_1^l, X_2-f(x_1^l), g-\psi(x_1^l)]$ is orthogonal to the vectors $\vec{u}$ and $\vec{v}$, where

$$\vec{u} = [g_1, g_2, -1]$$

$$\text{and } \vec{v} = [\frac{d\psi_1}{dx_1^l}, \frac{d\psi_2}{dx_1^l}, 0]$$

The direction of the generator is then given by the cross product of these vectors, $\vec{u} \times \vec{v}$.

$$\begin{bmatrix} X_1-x_1^l \\ X_2-f(x_1^l) \\ g-\psi(x_1^l) \end{bmatrix} : \begin{bmatrix} x_1^v-x_1^l \\ x_2^v-x_2^l \\ g^v-g^l \end{bmatrix} : \begin{bmatrix} \frac{d\psi_2}{dx_1^l} \\ -\frac{d\psi_1}{dx_1^l} \\ g_1\frac{d\psi_2}{dx_1^l} - g_2\frac{d\psi_1}{dx_1^l} \end{bmatrix} \tag{10}$$

where (x_1^v, x_2^v) is the vapor composition which is in equilibrium with the liquid of composition (x_1^l, x_2^l) and is located at the contact point of the generator with the vapor branch of the coexistence curve (the symbol ":" signifying that the vectors are collinear).

The direction of the projection of the generator onto the composition plane (spanned by the component mole fraction axes), or the direction of the tie line, is given by

$$\begin{bmatrix} x_1^v-x_1^l \\ x_2^v-x_2^l \end{bmatrix} : \begin{bmatrix} \frac{d\psi_2}{dx_1^l} \\ -\frac{d\psi_1}{dx_1^l} \end{bmatrix} \tag{11}$$

From the chain rule of differentiation, one obtains

$$\frac{d\psi_1}{dx_1^\ell} = g_{11} + g_{12}\frac{df}{dx_1^\ell} \qquad (12\text{-a})$$

$$\text{and } \frac{d\psi_2}{dx_1^\ell} = g_{12} + g_{22}\frac{df}{dx_1^\ell} \qquad (12\text{-b})$$

As the critical point is approached, point (x_1^ℓ, x_2^ℓ) tends toward point (x_1^v, x_2^v) so that in the limit, i.e. at the critical point (x_1^c, x_2^c)

$$g_{11} + g_{12}\frac{df}{dx_1^\ell} = 0 \qquad (13\text{-a})$$

$$\text{and } g_{12} + g_{22}\frac{df}{dx_1^\ell} = 0 \qquad (13\text{-b})$$

For the simple case of a ternary system, the tie lines are in the osculating plane of the coexistence curve. Thus, the direction of the limiting tie line coincides with the direction of the tangent line to the coexistence curve at the critical point and is given by the vector $\vec{t}$

$$\vec{t} = [1, a] \qquad (14\text{-a})$$

and

$$a = \frac{df}{dx_1^\ell}(x_1^c, x_2^c) = -\frac{g_{11}}{g_{12}} = -\frac{g_{12}}{g_{22}} \qquad (14\text{-b})$$

In Equation 14-b, the slope of the limiting tie line, a, is formulated in terms of partial derivatives of the molar Gibbs free energy. However, one needs the coordinates of a point on the limiting tie line in order to define its equation, and the natural choice is the critical point. As previously discussed, at constant pressure and temperature, the critical point composition is defined by the following equations

$$U(x_1^c, x_2^c) = \begin{vmatrix} g_{11} & g_{12} \\ g_{21} & g_{22} \end{vmatrix} = 0 \qquad (15)$$

and

$$V(x_1^c, x_2^c) = \begin{vmatrix} g_{11} & g_{12} \\ U_1 & U_2 \end{vmatrix} = 0 \qquad (16)$$

The equation of the limiting tie line is obtained by solving Equations 15 and 16 for the critical composition at which point the slope of the limiting tie line is evaluated using Equation 14-b, which is given by

$$a = \frac{X_2 - x_2^c}{X_1 - x_1^c} \qquad (17)$$

The conditions defining the MMP may now be formulated for a ternary system at a fixed temperature. For the case of a vaporizing gas drive, the MMP corresponds to the pressure at which Equation 17 is satisfied by the composition of the displaced oil (X_1^{oil}, X_2^{oil}), signifying that the point representing the oil composition is on the limiting tie line so that

$$a = \frac{X_2^{oil} - x_2^c}{X_1^{oil} - x_1^c} \tag{18}$$

Similarly, for a condensing gas drive, the point representing the injected gas composition (X_1^{gas}, X_2^{gas}) has to lie on the limiting tie line at the pressure corresponding to the MMP, in which case

$$a = \frac{X_2^{gas} - x_2^c}{X_1^{gas} - x_1^c} \tag{19}$$

Before extending these concepts to the case of a quaternary system, it is interesting to note that Equation 11, which is a general formulation of a tie line, may be used in an in an efficient way to generate the phase envelope of a ternary system at constant pressure and temperature without the use of an empirical equation to provide initial estimates of the equilibrium ratios[30] (K values) when a flash calculation is performed. Given a point on the dew point curve and its corresponding point on the bubble point curve (end points of a tie line), the approach consists of obtaining the initial estimates of the composition of the adjacent point on the dew point curve and its corresponding point on the bubble point curve, using Equation 11. This procedure is illustrated in Figure 15, wherein a ternary system composed of components 1,2 and 3 at constant pressure and temperature is considered. Let Z_i (Z_1, Z_2) represent the overall composition of a system which, at equilibrium, results in the coexistence of a vapor phase of composition Y_i (Y_1, Y_2) on the dew point curve and a liquid phase of composition X_i (X_1, X_2) on the bubble point curve. The adjacent point Y_i^* on the dew point curve, displaced by an amount ΔY_2 from the previous point Y_i, and its corresponding point on the bubble point curve X_i^* may be estimated as is shown in the following. The respective slopes of the dew point and bubble point curves (f_1^l, f_1^v in Figure 15) at the dew point Y_i and bubble point X_i may be evaluated using Equation 11 and are given by

Figure 15

Generation of Bubble and Dew point Curves of a Ternary System T,P fixed

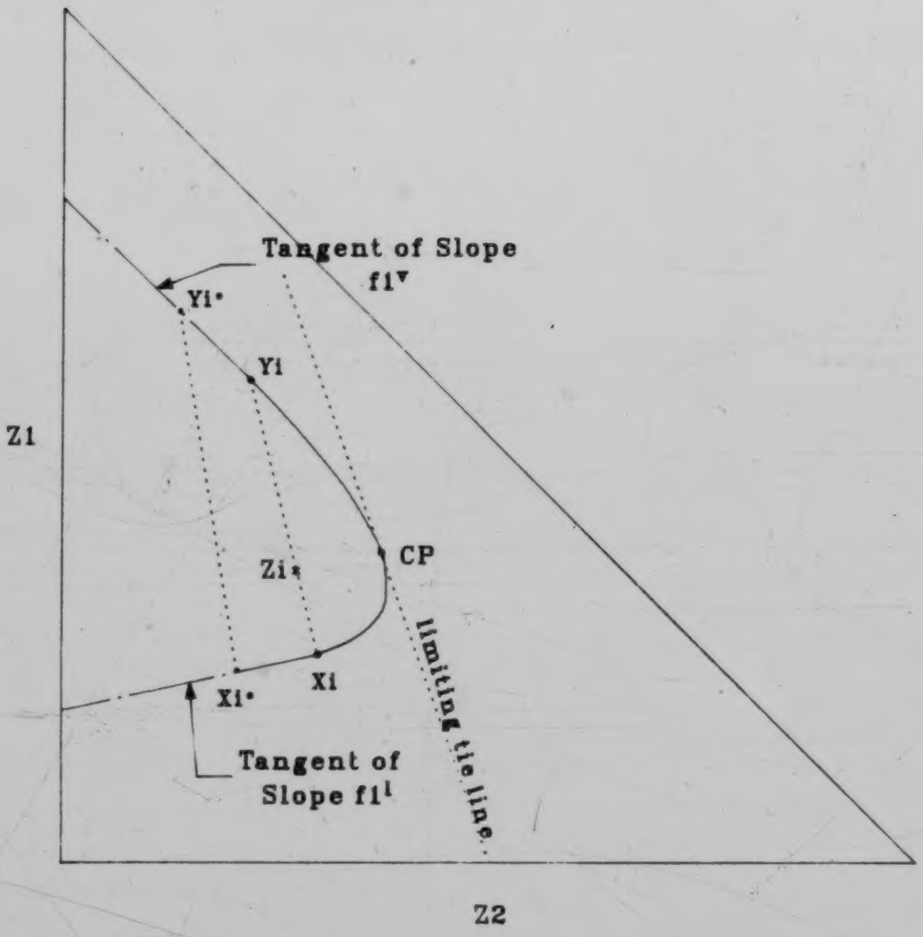

$$f_1^v = \frac{-g_{12}^v(Y_2-X_2)-g_{11}^v(Y_1-X_1)}{g_{12}^v(Y_1-X_1)+g_{22}^v(Y_2-X_2)} \tag{20}$$

and

$$f_1^l = \frac{-g_{12}^l(Y_2-X_2)-g_{11}^l(Y_1-X_1)}{g_{12}^l(Y_1-X_1)+g_{22}^l(Y_2-X_2)} \tag{21}$$

where g_{ij}^v and g_{ij}^l are evaluated at the dew point Y_i and bubble point X_i, respectively. Thus, the adjacent point Y_i^* on the dew point curve, displaced by an amount ΔY_2 from the previous point Y_i, is given by

$$\begin{bmatrix} Y_1^* \\ Y_2^* \end{bmatrix} = \begin{bmatrix} Y_1+\dfrac{\Delta Y_2}{f_1^v} \\ Y_2+\Delta Y_2 \end{bmatrix} \tag{22}$$

If ΔY_2 is not too large, a good estimate of the slope of the tie line passing through Y_i^* may be taken as

$$m = \frac{Y_2-X_2}{Y_1-X_1} \tag{23}$$

Finally, the corresponding point X_i^* on the bubble point curve may be estimated by the intersection point of the tie line passing through Y_i^* and the tangent line to the bubble point curve at point X_i, and is given by

$$\begin{bmatrix} X_1^* \\ X_2^* \end{bmatrix} = \begin{bmatrix} (Y_2^* - Y_1^* m - X_2 + X_1 f_1^l)/(f_1^l - m) \\ (f_1^l(Y_2^* - Y_1^* m) - m(X_2 - X_1 f_1^l))/(f_1^l - m) \end{bmatrix} \tag{24}$$

A flash calculation for a system consisting of a mixture of phase Y_i^* and phase X_i^*, for instance with an overall composition given by $Z_i = (X_i^* + Y_i^*)/2$, is then performed to obtain the exact compositions of the equilibrium phases (such that the equality of the chemical potentials of each component in all phases is satisfied). The initial estimates for the K values are taken as Y_i^*/X_i^*. The procedure is then repeated until the generation of the phase envelope is completed.

In the conventional way, the phase envelope is generated by performing flash calculations on various mixtures inside the phase envelope, for instance on a horizontal segment linking the critical point to the ordinate Z_1 in Figure 15, using the following empirical correlation[28] to obtain an initial estimate for the K values,

$$K_i = \frac{\exp[5.37(1+\omega_i)(1-1/Tr_i)]}{Pr_i} \qquad (25)$$

where ω_i ,Tr_i and Pr_i are respectively the acentric factor, the reduced temperature and the reduced pressure of component i.

The results of the flash calculations for the various mixtures used to generate the phase envelope of the nitrogen-methane-propane system at a temperature of 60 °C and a pressure of 10 MPa are shown in Table 2. In this table, method 1 refers to the case where the initial estimates of the K values are obtained using Equations 22 and 24, while in method 2 the initial estimates of the K values are evaluated using the empirical relationship given by Equation 25. For each mixture considered, the successive substitution method[29] was used to solve for the compositions of the vapor and liquid phases at equilibrium. The procedure is assumed to converge when the following condition is satisfied

$$\sum_i \left(\frac{K_i^{m+1}}{K_i^m} - 1\right)^2 < 10^{-12} \qquad (26)$$

where K_i is the equilibrium ratio of component i and superscripts m and m+1 refer to successive iterates.

For each system composition (mixtures 1 to 11 in Table 2), it may be observed that the initial estimates of the composition of the liquid and vapor phases (X_i° ,Y_i°) obtained by method 1 are very close to the converged values (X_i,Y_i), while the estimates obtained from method 2 are very far from the final solution. The convergence of the successive substitution method is very slow[30] as is indicated by the number of iterations needed to satisfy the condition given by Equation 26, even when the initial estimates are close to the final solution as in method 1. It may also be observed that the number of iterations increases as the critical point is approached (mixture 1 being close to the critical point, while mixture 13 is far away from it). It is also interesting to note that the successive substitution method is robust in the sense that it does not require good initial estimates to achieve convergence as is the case of method 2. However, solution techniques that converge rapidly (such as those derived from the Newton-Raphson method) generally require good initial estimates to avoid divergence problems, and it is expected that convergence will be reached in fewer iterations when such techniques are used in conjunction with method 1 for obtaining the initial estimates.

Table 2

Initial Estimates and Number of Iterations for Convergence

(Method 1 vs. Method 2)

Mixture	Method	Initial Estimates				Equilibrium composition				Number of iterations
		$X_1^\bullet$	$X_2^\bullet$	$Y_1^\bullet$	$Y_2^\bullet$	X_1	X_2	Y_1	Y_2	
1	1	0.19736	0.16830	0.27936	0.21425	0.20962	0.17782	0.26986	0.20603	203
	2	0.04413	0.07228	0.47424	0.33579	0.20962	0.17782	0.26986	0.20603	222
2	1	0.21082	0.16772	0.28028	0.20024	0.21091	0.16880	0.28100	0.19951	96
	2	0.04535	0.06939	0.48731	0.32236	0.21092	0.16880	0.28100	0.19951	181
3	1	0.21245	0.15953	0.29047	0.19372	0.21241	0.16058	0.29129	0.19300	75
	2	0.04649	0.06667	0.49959	0.30974	0.21242	0.16058	0.29130	0.19300	155
4	1	0.21415	0.15184	0.30019	0.18721	0.21403	0.15288	0.30107	0.18648	62
	2	0.04760	0.06405	0.51147	0.29753	0.21404	0.15288	0.30108	0.18648	138
5	1	0.21589	0.14453	0.30957	0.18069	0.21573	0.14556	0.31050	0.17993	53
	2	0.04868	0.06148	0.52308	0.28561	0.21574	0.14557	0.31051	0.17993	124
6	1	0.22156	0.12139	0.33508	0.16256	0.22116	0.12488	0.33789	0.15978	57
	2	0.05186	0.05391	0.55729	0.25046	0.22116	0.12489	0.33789	0.15978	98
7	1	0.22742	0.10256	0.36072	0.14241	0.22669	0.10601	0.36385	0.13954	44
	2	0.05494	0.04660	0.59033	0.21650	0.22669	0.10601	0.36386	0.13955	83
8	1	0.23313	0.08488	0.38568	0.12217	0.23222	0.08835	0.38901	0.11918	37
	2	0.05794	0.03946	0.62262	0.18332	0.23222	0.08835	0.38902	0.11918	73
9	1	0.23872	0.06810	0.41017	0.10181	0.23771	0.07159	0.41365	0.09870	34
	2	0.06090	0.03244	0.65437	0.15069	0.23771	0.07159	0.41366	0.09870	66
10	1	0.24422	0.05203	0.43432	0.08133	0.24312	0.05555	0.43793	0.07810	32
	2	0.06382	0.02550	0.68573	0.11847	0.24312	0.05555	0.43793	0.07810	60
11	1	0.24960	0.03658	0.45823	0.06073	0.24845	0.04010	0.46193	0.05741	30
	2	0.06671	0.01864	0.71677	0.08658	0.24845	0.04010	0.46193	0.05741	56
12	1	0.25489	0.02163	0.48194	0.04004	0.25370	0.02517	0.48573	0.03663	29
	2	0.06957	0.01183	0.74755	0.05495	0.25370	0.02517	0.48573	0.03663	52
13	1	0.26008	0.00713	0.50551	0.01926	0.25886	0.01067	0.50936	0.01577	28
	2	0.07241	0.00507	0.77811	0.02355	0.25886	0.01067	0.50936	0.01577	49

5.4 Equation of the Quaternary Limiting Tie Line

In the case of a quaternary system at fixed pressure and temperature, one needs to formulate the equation of the ruled surface generated by the quaternary limiting tie lines passing through each point of the critical point curve. As previously discussed, this surface separates oils that may be miscibly displaced through a multiple-contact process from those that may not in a vaporizing gas drive (with similar considerations for a condensing gas drive). This ruled surface may be generated by determining the compositions of a sufficient number of points on the critical point curve and the directions of the quaternary limiting tie lines passing through each of these points. As in the case of a ternary system, one needs to develop the general equation for a quaternary tie line in order to consider its limiting position as a critical point is approached. The same methodology used in the case of a ternary system may be extented to the case of a quaternary system, keeping in mind that the dimensionality of the Gibbs space is increased by one.

For a quaternary system composed of components 1, 2, 3 and 4 at constant pressure and temperature, the equation of a generator of the coexistence Gibbs hypersurface may be developed in terms of the molar Gibbs free energy. For a two-phase transition, liquid(l) vapor(v) equilibrium, considering the mole fractions of components 1, 2 and 3 as the independent variables, the following must be satisfied (refer to Appendix 2)

$$g_1^l = g_1^v$$

$$g_2^l = g_2^v$$

$$g_3^l = g_3^v$$

and

$$g^l - \sum_{i=1}^{3} X_i^l g_i^l = g^v - \sum_{i=1}^{3} X_i^v g_i^v \qquad (27)$$

From the equalities 27, it may be concluded that the coexistence hypersurface (of dimension 3) may be generated by rolling a double-tangent hyperplane onto the primitive hypersurface, $g(X_1,X_2,X_3)$, where the resulting coexistence hypersurface will be comprised of the envelope of the tangent hyperplanes.

Let the liquid side of the coexistence surface (bubble point surface) be given by the following parametric form

$$X_1 = x_1^\ell$$

$$X_2 = x_2^\ell$$

$$X_3 = f(x_1^\ell, x_2^\ell)$$

$$g(X_1, X_2, X_3) = g(x_1^\ell, x_2^\ell, f(x_1^\ell, x_2^\ell)) = \psi(x_1^\ell, x_2^\ell) \tag{28}$$

where x_1^ℓ and x_2^ℓ are the parameters, and the partial derivatives of the molar Gibbs free energy on the coexistence surface are given by

$$g_1(x_1^\ell, x_2^\ell, f(x_1^\ell, x_2^\ell)) = \psi_1(x_1^\ell, x_2^\ell) \tag{29-a}$$

$$g_2(x_1^\ell, x_2^\ell, f(x_1^\ell, x_2^\ell)) = \psi_2(x_1^\ell, x_2^\ell) \tag{29-b}$$

$$g_3(x_1^\ell, x_2^\ell, f(x_1^\ell, x_2^\ell)) = \psi_3(x_1^\ell, x_2^\ell) \tag{29-c}$$

The coexistence tangent hyperplanes form a double family of hyperplanes, with parameters x_1^ℓ and x_2^ℓ, given by

$$F(X_1, X_2, X_3, g; x_1^\ell, x_2^\ell) =$$

$$(X_1 - x_1^\ell)g_1 + (X_2 - x_2^\ell)g_2 + (X_3 - f(x_1^\ell, x_2^\ell))g_3 - (g - \psi(x_1^\ell, x_2^\ell)) = 0 \tag{30}$$

where $[g_1, g_2, g_3, -1]$ is the normal to the g-hypersurface on the coexistence hypersurface. Let the parameter x_2^ℓ be related to the parameter x_1^ℓ by any differentiable function h. The intersection, for the chosen direction (h), of two infinitesimally close tangent hyperplanes is given by

$$F(X_1, X_2, X_3, g; x_1^\ell, x_2^\ell) = 0 \tag{31-a}$$

and

$$\frac{\partial F}{\partial x_1^\ell} + \frac{\partial F}{\partial x_2^\ell} \cdot \frac{dh}{dx_1^\ell} = 0 \tag{31-b}$$

The coexistence tangent hyperplanes will intersect in unique lines of parameters x_1^ℓ and x_2^ℓ, whatever the functional form of h, when

$$\frac{\partial F}{\partial x_1^\ell} = 0 \quad \text{and} \quad \frac{\partial F}{\partial x_2^\ell} = 0 \tag{32}$$

These characteristic lines, or generators, constitute the envelope of this family of hyperplanes which is the coexistence hypersurface defined by the following equations

$$(X_1-x_1^\ell)g_1 + (X_2-x_2^\ell)g_2 + (X_3-f(x_1^\ell,x_2^\ell))g_3 - (g-\psi(x_1^\ell,x_2^\ell)) = 0 \tag{33-a}$$

$$(X_1-x_1^\ell)\frac{\partial\psi_1}{\partial x_1^\ell} + (X_2-x_2^\ell)\frac{\partial\psi_2}{\partial x_1^\ell} + (X_3-f(x_1^\ell,x_2^\ell))\frac{\partial\psi_3}{\partial x_1^\ell} - g_1 - g_3\frac{\partial f}{\partial x_1^\ell} + \frac{\partial\psi}{\partial x_1^\ell} = 0 \tag{33-b}$$

$$(X_1-x_1^\ell)\frac{\partial\psi_1}{\partial x_2^\ell} + (X_2-x_2^\ell)\frac{\partial\psi_2}{\partial x_2^\ell} + (X_3-f(x_1^\ell,x_2^\ell))\frac{\partial\psi_3}{\partial x_2^\ell} - g_2 - g_3\frac{\partial f}{\partial x_2^\ell} + \frac{\partial\psi}{\partial x_2^\ell} = 0 \tag{33-c}$$

By applying the chain rule of differentiation to Equation 28 one obtains

$$-g_1 - g_3\frac{\partial f}{\partial x_1^\ell} + \frac{\partial\psi}{\partial x_1^\ell} = 0 \tag{34-a}$$

$$\text{and } -g_2 - g_3\frac{\partial f}{\partial x_2^\ell} + \frac{\partial\psi}{\partial x_2^\ell} = 0 \tag{34-b}$$

Thus, from Equations 33 and 34, it may be concluded that the vector $[X_1-x_1^\ell,X_2-x_2^\ell,X_3-f(x_1^\ell,x_2^\ell),g-\psi(x_1^\ell,x_2^\ell)]$ is othogonal to the vectors $\vec{u}$, $\vec{v}$ and $\vec{w}$, where

$$\vec{u} = [g_1,g_2,g_3,-1]$$

$$\vec{v} = [\frac{\partial\psi_1}{\partial x_1^\ell},\frac{\partial\psi_2}{\partial x_1^\ell},\frac{\partial\psi_3}{\partial x_1^\ell},0]$$

$$\vec{w} = [\frac{\partial\psi_1}{\partial x_2^\ell},\frac{\partial\psi_2}{\partial x_2^\ell},\frac{\partial\psi_3}{\partial x_2^\ell},0]$$

The direction of the generator is then given by the vector which is orthogonal to the vectors $\vec{u}$, $\vec{v}$ and $\vec{w}$. Its projection onto the X_1,X_2,X_3 composition plane, or direction of the quaternary tie line is then given by

$$\begin{bmatrix} X_1-x_1^\ell \\ X_2-x_2^\ell \\ X_3-f(x_1^\ell,x_2^\ell) \end{bmatrix} : \begin{bmatrix} x_1^y-x_1^\ell \\ x_2^y-x_2^\ell \\ x_3^y-x_3^\ell \end{bmatrix} : \begin{bmatrix} A \\ B \\ C \end{bmatrix} \tag{35}$$

where

$$A = \frac{\partial\psi_3}{\partial x_1^\ell}\cdot\frac{\partial\psi_2}{\partial x_2^\ell} - \frac{\partial\psi_2}{\partial x_1^\ell}\cdot\frac{\partial\psi_3}{\partial x_2^\ell}$$

$$B = \frac{\partial\psi_1}{\partial x_1^\ell}\cdot\frac{\partial\psi_3}{\partial x_2^\ell} - \frac{\partial\psi_3}{\partial x_1^\ell}\cdot\frac{\partial\psi_1}{\partial x_2^\ell}$$

$$C = \frac{\partial\psi_2}{\partial x_1^\ell}\cdot\frac{\partial\psi_1}{\partial x_2^\ell} - \frac{\partial\psi_1}{\partial x_1^\ell}\cdot\frac{\partial\psi_2}{\partial x_2^\ell}$$

and (x_1^y,x_2^y,x_3^y) is the vapor composition which is in equilibrium with the liquid of composition $(x_1^\ell,x_2^\ell,x_3^\ell)$ and is located at the contact point of the quaternary tie line with the vapor side of the coexistence surface or the dew point surface (the symbol ":" signifying that the vectors are collinear).

Using the chain rule of differentiation, the expressions of A, B and C in terms of the partial derivatives of the molar Gibbs free energy are given by

$$\begin{aligned} A = {} & g_{13}g_{22} + g_{13}g_{23}f_2 + g_{33}g_{22}f_1 \\ & - g_{12}g_{23} - g_{12}g_{33}f_2 - g_{23}g_{23}f_1 \end{aligned} \qquad (36\text{-a})$$

$$\begin{aligned} B = {} & g_{11}g_{23} + g_{11}g_{33}f_2 + g_{13}g_{23}f_1 \\ & - g_{13}g_{12} - g_{13}g_{13}f_2 - g_{33}g_{12}f_1 \end{aligned} \qquad (36\text{-b})$$

$$\begin{aligned} C = {} & g_{12}g_{12} + g_{12}g_{13}f_2 + g_{23}g_{12}f_1 \\ & - g_{11}g_{22} - g_{11}g_{23}f_2 - g_{13}g_{22}f_1 \end{aligned} \qquad (36\text{-c})$$

where

$$f_i = \frac{\partial f}{\partial x_i^\ell} \quad i=1,2$$

$$\text{and } g_{ij} = \frac{\partial^2 g}{\partial X_i \partial X_j}\left(x_1^\ell, x_2^\ell, f(x_1^\ell, x_2^\ell)\right) \quad i,j=1,3$$

As a critical point is approached, point $(x_1^\ell, x_2^\ell, x_3^\ell)$ tends toward point (x_1^v, x_2^v, x_3^v). In the limit, i.e. at the critical point, the direction of the limiting tie line is given by

$$\lim_{x_i^\ell \to x_i^c} \begin{bmatrix} 1 \\ \dfrac{x_2^\ell - x_2^v}{x_1^\ell - x_1^v} \\ \dfrac{x_3^\ell - x_3^v}{x_1^\ell - x_1^v} \end{bmatrix} = \lim_{x_i^\ell \to x_i^c} \begin{bmatrix} 1 \\ B/A \\ C/A \end{bmatrix} \qquad (37)$$

where A, B and C are given by Equation 36 and (x_i^c) is the critical point (x_1^c, x_2^c, x_3^c) being approached.

In the case of a quaternary system, the phase envelope is represented by a surface and not simply by a curve as in the case of a ternary system. Thus, a plane is tangent to the coexistence surface at the critical point (the normal vector to this plane being $[f_1, f_2, -1]$) and the direction of the limiting quaternary tie line on this plane is given by Equation 37. One may observe that the ratios of the components of the vectors in Equation 37 are indeterminate, since the numerator and the denominator of each ratio tend to zero as the critical point is approached. The limiting value of these ratios may be obtained following a path on the liquid side of the coexistence surface leading to a critical point. Let this path be represented by the following parametric form, with parameter x_1^ℓ.

$$\begin{aligned} X_1 &= x_1^\ell \\ X_2 &= h(x_1^\ell) \\ X_3 &= f(x_1^\ell, h(x_1^\ell)) = \psi(x_1^\ell) \end{aligned} \tag{38}$$

Since the quaternary tie line originating from a point on the liquid side of the coexistence surface is unique, its limiting position near a critical point is independent of the path followed to approach that critical point. One may, therefore, choose a particular path by specifying the function h, for instance

$$\begin{aligned} X_1 &= x_1^\ell \\ X_2 &= x_2^c \\ X_3 &= f(x_1^\ell, x_2^c) = \Phi(x_1^\ell) \end{aligned} \tag{39}$$

i.e., following a path on the liquid side of the coexistence surface such that the mole fraction of component 2 is held constant to its value at the critical point being approached. On this path, the values of A, B and C are given by the following parametric form

$$A(x_1^\ell, x_2^c, f(x_1^\ell, x_2^c)) = \Phi_a(x_1^\ell) \tag{40-a}$$

$$B(x_1^\ell, x_2^c, f(x_1^\ell, x_2^c)) = \Phi_b(x_1^\ell) \tag{40-b}$$

$$C(x_1^\ell, x_2^c, f(x_1^\ell, x_2^c)) = \Phi_c(x_1^\ell) \tag{40-c}$$

and the direction of the limiting tie line is given by

$$\vec{D} = \lim_{x_1^\ell \to x_1^c} \begin{bmatrix} 1 \\ \Phi_b(x_1^\ell)/\Phi_a(x_1^\ell) \\ \Phi_c(x_1^\ell)/\Phi_a(x_1^\ell) \end{bmatrix} \tag{41}$$

At this point one may invoke l'Hopital's rule to remove the indeterminate value of the ratios in the relationship 41, in the limit

$$\vec{D} = \lim_{x_1^l \to x_1^c} \begin{bmatrix} 1 \\ \dfrac{d\Phi_b}{dx_1^l} \Big/ \dfrac{d\Phi_a}{dx_1^l} \\ \dfrac{d\Phi_c}{dx_1^l} \Big/ \dfrac{d\Phi_a}{dx_1^l} \end{bmatrix} = \begin{bmatrix} 1 \\ \alpha \\ \beta \end{bmatrix} \tag{42}$$

Using the chain rule of differentiation, the numerator and denominator of the ratio defining α are given by

$$\begin{aligned} \frac{d\Phi_a}{dx_1^l} = {} & (g_{113}+g_{133}f_1)g_{22} + (g_{122}+g_{223}f_1)g_{13} \\ & + (g_{113}+g_{133}f_1)g_{23}f_2 + (g_{123}+g_{233}f_1)g_{13}f_2 + g_{13}g_{23}f_{12} \\ & + (g_{133}+g_{333}f_1)g_{22}f_1 + (g_{122}+g_{223}f_1)g_{33}f_1 + g_{33}g_{22}f_{11} \\ & - (g_{112}+g_{123}f_1)g_{23} - (g_{123}+g_{233}f_1)g_{12} \\ & - (g_{112}+g_{123}f_1)g_{33}f_2 - (g_{133}+g_{333}f_1)g_{12}f_2 - g_{12}g_{33}f_{12} \\ & - (g_{123}+g_{233}f_1)g_{23}f_1 - (g_{123}+g_{233}f_1)g_{23}f_1 - g_{23}g_{23}f_{11} \end{aligned} \tag{43}$$

and $$\begin{aligned} \frac{d\Phi_b}{dx_1^l} = {} & (g_{111}+g_{113}f_1)g_{23} + (g_{123}+g_{233}f_1)g_{11} \\ & + (g_{111}+g_{113}f_1)g_{33}f_2 + (g_{133}+g_{333}f_1)g_{11}f_2 + g_{11}g_{33}f_{12} \\ & + (g_{113}+g_{133}f_1)g_{23}f_1 + (g_{123}+g_{233}f_1)g_{13}f_1 + g_{13}g_{23}f_{11} \\ & - (g_{113}+g_{133}f_1)g_{12} - (g_{112}+g_{123}f_1)g_{13} \\ & - (g_{113}+g_{133}f_1)g_{13}f_2 - (g_{113}+g_{133}f_1)g_{13}f_2 - g_{13}g_{13}f_{12} \\ & - (g_{133}+g_{333}f_1)g_{12}f_1 - (g_{112}+\underline{g_{123}}f_1)g_{33}f_1 - g_{33}g_{12}f_{11} \end{aligned} \tag{44}$$

where

$$f_{ij} = \frac{\partial^2 f}{\partial X_i \partial X_j}(x_1^c, x_2^c) \qquad i,j=1,2$$

and $$g_{ijk} = \frac{\partial^3 g}{\partial X_i \partial X_j \partial X_k}(x_1^c, x_2^c, x_3^c) \qquad i,j=1,3$$

and the expressions given in Equations 43 and 44 are evaluated at the critical point.

Since the quaternary limiting tie line is on the tangent plane to the coexistence surface at the critical point, one obtains the following relationship for β

$$\beta = f_1 + \alpha f_2 \tag{45}$$

It may be recalled that the limit of essential stability is given by the points satisfying the condition that the determinant U be zero (refer to Equation 1) and which in the case of a quaternary system is given by the following

$$U(X_1,X_2,X_3) = \begin{vmatrix} g_{11} & g_{12} & g_{13} \\ g_{21} & g_{22} & g_{23} \\ g_{31} & g_{32} & g_{33} \end{vmatrix} = 0 \tag{46}$$

The relationship 46 describes a surface S, referred to as the spinodal surface, and is given by the following implicit form

$$U(X_1,X_2,X_3=S(X_1,X_2)) = 0 \tag{47}$$

As discussed in the case of a ternary system, the spinodal surface of a quaternary system is enclosed in the coexistence surface and is tangent to it on the critical point curve. Consequently, in the neighborhood of a critical point, the coexistence surface, $f(X_1,X_2)$, may be represented by the spinodal surface, $S(X_1,X_2)$. Using the chain rule of differentiation one obtains from Equation 47

$$f_i = -\frac{U_i}{U_3} \qquad i=1,2 \tag{48}$$

and

$$f_{ij} = -\frac{(U_{ij}U_3 - U_{j3}U_i)}{U_3{}^2} \qquad i,j=1,2 \tag{49}$$

U_i and U_{ij} being respectively the first and second partial derivatives of the determinant U given in Equation 46, and evaluated at the critical point.

Consequently, the direction of the quaternary limiting tie line, $\vec{D}$, may be expressed in terms of partial derivatives of the molar Gibbs free energy using Equations 43, 44, 45, 48 and 49.

For a quaternary system at constant pressure and temperature, a critical point composition must satisfy the following equations

$$U(x_1^c, x_2^c, x_3^c) = \begin{vmatrix} g_{11} & g_{12} & g_{13} \\ g_{21} & g_{22} & g_{23} \\ g_{31} & g_{32} & g_{33} \end{vmatrix} = 0 \qquad (50)$$

and

$$V(x_1^c, x_2^c, x_3^c) = \begin{vmatrix} g_{11} & g_{12} & g_{13} \\ g_{21} & g_{22} & g_{23} \\ U_1 & U_2 & U_3 \end{vmatrix} = 0 \qquad (51)$$

The simultaneous solution of Equations 50 and 51 describes the critical point curve. It may be seen now that the ruled surface may be generated by determining the compositions of a sufficient number of points on the critical point curve and the directions, $\vec{D}$, of the quaternary limiting tie lines passing through each of these points.

The conditions defining the MMP may now be formulated for a quaternary system at constant temperature. For the case of a vaporizing gas drive, the MMP corresponds to the pressure at which the above ruled surface passes through the point representing the compositions of the displaced oil. Similarly, for a condensing gas drive, the point representing the injected gas composition must lie on the above ruled surface at a pressure corresponding to the MMP.

The above methodology may be extended to any other multicomponent system. However, in the present investigation, the analysis will be restricted to ternary and quaternary systems which will then be used as building blocks for the prediction of the MMP of a multicomponent system. The approach considered will be discussed in the context of chapter 6. So far, it has been seen that for ternary and quaternary systems the criteria defining the MMP may be formulated in terms of the molar Gibbs free energy. In order to apply the above formulation, one needs an analytical expression for the molar Gibbs free energy which can be constructed, for instance, from any pressure explicit equation of state.

5.5 Selection of the Equation of State

In this investigation, the Soave-Redlich and Kwong equation of state[2] (SRK EOS) was used, and is given by

$$P = \frac{RT}{(v-b)} - \frac{a}{v(v+b)} \tag{52}$$

with the following mixing rules

$$b = \sum_i\sum_j X_i X_j b_{ij}, \quad b_{ij} = \frac{b_i + b_j}{2} \tag{53}$$

and

$$a = \sum_i\sum_j X_i X_j a_{ij}, \quad a_{ij} = \sqrt{a_i a_j}\cdot(1-\delta_{ij}) \tag{54}$$

The construction of the molar Gibbs free energy using a pressure explicit equation of state has been thoroughly discussed by Chao and Greenkorn[31] and may be expressed as

$$g(T,P,X_i) = \int_{\infty}^{v} [\frac{RT}{v} - P]dv - RTLn(\frac{v}{RT}) + \sum_i X_i A_i^{*} + RT\sum_i X_i LnX_i + Pv \tag{55}$$

The expressions for the molar Gibbs free energy and its partial derivatives with respect to the mole fraction X_i, derived from the SRK EOS, are given in Appendix 4. The choice of the equation of state was based on the premise that in order to predict the critical region of ternary and quaternary systems, the region of interest in this investigation, the equation of state should first be capable of giving a good representation of the critical locus of the constituting binary systems. A comparison of the experimental and predicted (SRK EOS) critical loci for various binary systems is shown in Figure 16. It may be seen that the SRK equation of state represents the critical loci of the binary systems considered reasonably well. Given the available experimental data, the interaction coefficients δ_{ij} of the binary systems composed of component i and j were obtained by best fitting the experimental critical points. The values of the interaction coefficients are given in Table 3. For the case where only meager or approximate data were available, the interaction coefficients were set to zero.

An attempt was made to develop a new equation of state constrained to the three conditions satisfied by the critical point of a pure component. This equation, presented in

Figure 16

Critical Curves of Various Binaries Experiments vs Predictions, using SRK EOS

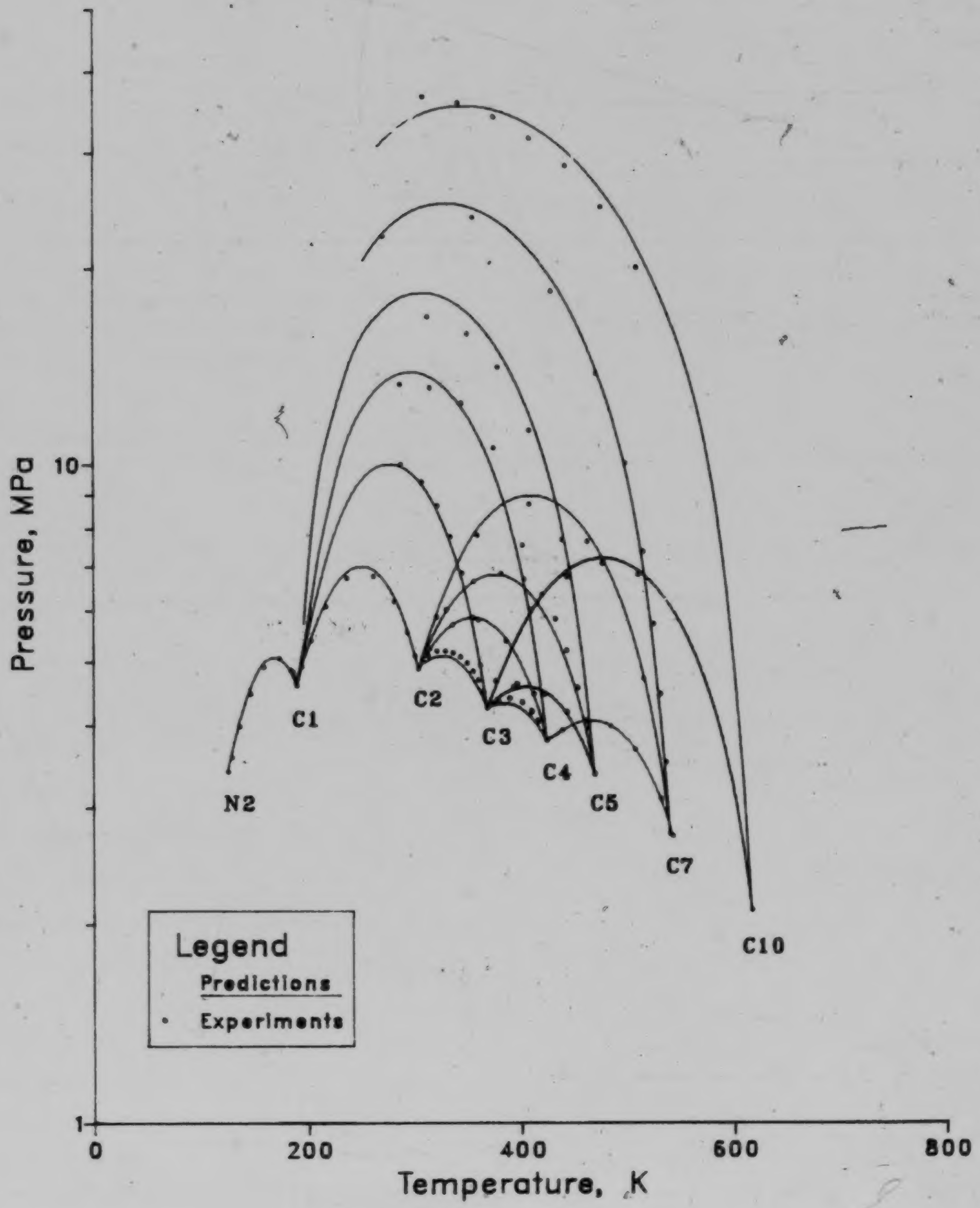

Table 3

Binary Interaction Coefficients

Binary System	δ_{ij}	Source
methane-nitrogen	0.0030	32
methane-ethane	0.0020	33
methane-propane	-0.0010	34
methane-n-butane	-0.0010	35
methane-n-pentane	0.0200	36
methane-n-heptane	-0.0040	37
methane-n-decane	0.0030	38
ethane-propane	-0.0070	39
ethane-n-butane	0.0050	40
ethane-n-pentane	0.0010	41
ethane-n-heptane	0.0160	42
propane-n-butane	-0.0030	43
propane-n-pentane	0.0120	44
propane-n-decane	0.0200	45
n-butane-n-heptane	0.0050	46

Appendix 5, appears to reproduce the PVT relationships of pure components with good accuracy. However, additional work is necessary for the development of appropriate mixing rules in order to extend its application to mixtures.

With the aim of developing a predictive method for the determination of the MMP, the above developed concepts were applied to various ternary and quaternary systems at various pressures and temperatures. The generated data were then used as a basis for the prediction of the MMP for multicomponent systems using ternary and quaternary systems as building blocks.

6. Minimum Miscibility Predictions for Methane and Nitrogen Vaporizing Gas Drives

6.1 Introduction

In the following, a method is proposed for the determination of minimum miscibility pressures for methane and nitrogen vaporizing gas drives. The case of methane vaporizing gas drives is treated in terms of ternary systems for the representation of the phase behavior of the displaced and displacing fluids, while quaternary systems are considered when nitrogen is the displacing fluid in order to adequately describe the phase relationships of nitrogen-hydrocarbon systems whereby nitrogen and methane are dealt with as two separate components.

Specifically, when methane is the displacing fluid, the development of the method consists of the following:

i. the determination and correlation of the MMP's of ternary systems based upon the formulation of the necessary conditions for the initiation of dynamic miscibility,

ii. the prediction of the MMP of a multicomponent hydrocarbon system using ternary systems as building blocks.

When nitrogen is the displacing fluid, a similar approach is considered in terms of quaternary systems.

The method requires a knowledge of the composition of the oil in terms of the light fraction (methane), the intermediate fraction (ethane to hexane) and the heavy fraction (heptane$^+$). The intermediate and heavy fractions are characterized in terms of their apparent molecular weights.

6.2 Methane Vaporizing Gas Drives

For ternary systems in which methane is the injected gas, the MMP may be correlated as a function of temperature, molecular weight of the intermediate components and of the heavy components, where the components are:

light component	C1
intermediate component	C3-C4-C5-C6
heavy component	C8-C10-C12-C15

Five temperatures were selected in the range of normally encountered reservoir temperatures, varying from 30 to 90 °C. Sixteen ternaries were considered at the above temperatures, with the molecular weight of the intermediate ranging from 44 to 86 and that of the heavy component from 114 to 212. For each system at constant temperature, the critical point composition and slope of the limiting tie line were calculated at 7 pressures, ranging from the critical pressure of the light-intermediate binary to the critical pressure of the light-heavy binary.

It has been experimentally observed[47] that a simple pattern exists for the critical point curve of a ternary system at constant temperature. It was found that the critical point curve could be closely approximated by a line segment joining the points representing the critical compositions of two of the constituting binaries of the ternary system. This information is valuable when an estimate for the critical composition is desired. Equations 15 and 16 defining the critical composition of a ternary system at constant temperature and pressure are non-linear and may only be solved using numerical solution techniques which usually require a good initial estimate in order to avoid divergence problems. For the ternary systems and temperatures considered, the critical point curve joins the point representing the critical composition of the light-intermediate binary to that of the light-heavy binary. When solving for a critical composition at some pressure between the critical pressures of the above binaries, an initial estimate was obtained by minimizing the absolute value of the determinant U given by Equation 15 along a straight path joining the points representing the critical compositions of the above binaries at the prescribed temperature. Equations 15 and 16 were then solved using the Newton-Raphson method.

In order to apply the above procedure, one has to determine the critical points of the above binaries. For a binary system at fixed temperature, a critical system is invariant, i.e. it consists of a single point. Therefore, one may solve for the critical pressure and critical composition simultaneously using the two criteria defining the critical point

$$\frac{\partial^2 g}{\partial X_1^2}(X_1,P) = 0 \tag{56}$$

and

$$\frac{\partial^3 g}{\partial X_1^3}(X_1,P) = 0 \tag{57}$$

where X_1 is the mole fraction of one of the components of the binary system considered. Equations 56 and 57 are also non-linear; hence, they require an initial estimate for the variables X_1 and P when solved numerically. Based on the knowledge that, for a binary system at constant temperature, the critical pressure is the maximum pressure at which two phases may coexist, Spear et al.[48] developed a method to obtain a close estimate of the critical point. The method consists of determining the point on the curve described by Equation 56 (the limit of essential stability) which maximizes the pressure (correponding to the critical pressure) by varying the composition of the binary system. Using the above method for the evaluation of the initial estimates, Equations 56 and 57 were then solved simultaneously (Newton-Raphson method) to obtain the critical composition and pressure of the light-intermediate and light-heavy binaries, for the considered ternary system and temperature.

For a particular ternary system, at some prescribed pressure and temperature, the slope of the limiting tie line is determined using Equation 14-b by evaluating the expressions of the partial derivatives of the molar Gibbs free energy at the critical point. For these conditions, the equation of the limiting tie line is determined. The procedure is repeated for other pressures, ranging from the critical pressure of the light-intermediate binary to that of the light-heavy binary, enabling a complete sweep of the composition plane by the limiting tie lines. Thus, for the system and temperature considered, the MMP may be determined by considering the pressure at which the corresponding limiting tie line passes through the point representing the composition of the displaced oil. This may be done by correlating the generated data, critical point composition, slope of the limiting tie line and pressure.

Before going into the discussion of the correlating procedure, it would be interesting to compare experimental and predicted results. Figure 17 shows such a comparison of critical

Figure 17
Comparison of Experimental and Prediction of Critical Points and Limiting Tie Lines
System: Methane n–Butane Decane
T=71°C

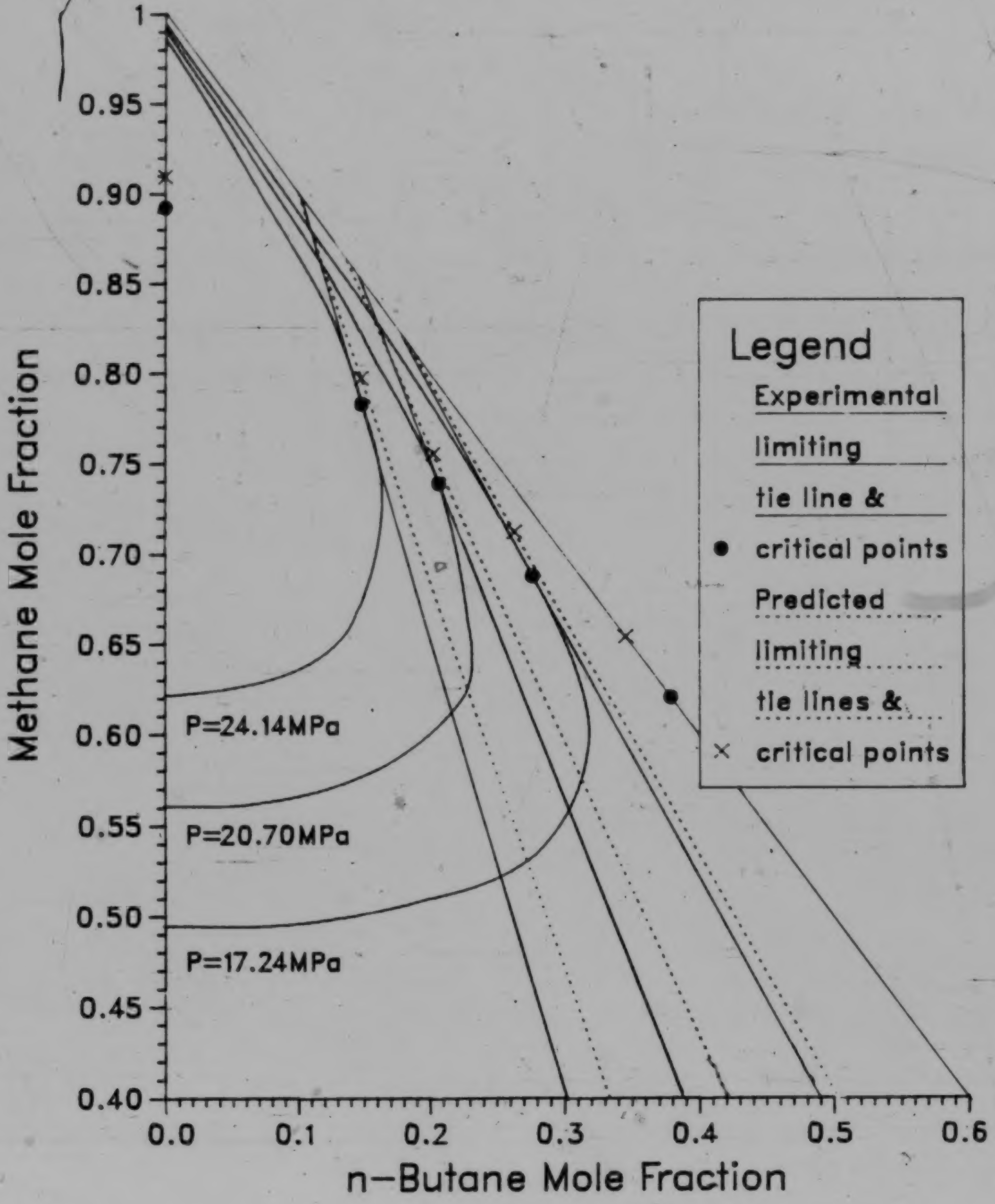

points and limiting tie lines for the methane-n-butane-decane system at a temperature of 71 °C and various pressures. The phase behavior (two-phase equilibrium data) of the above system has been thoroughly investigated experimentally by Sage and Lacey[49]. The experimental critical points and limiting tie lines are only estimates since no actual measurements of critical points were made by Sage and Lacey[49]. For the above system, estimates of critical point compositions, at the conditions of pressure and temperature considered, were obtained from Reamer et al[50]. At constant pressure and temperature, the slope of the experimental tie lines was correlated with a parameter corresponding to the n-butane mole fraction of the point of intersection of the tie line with the line parallel to the abscissa and passing through the critical point. The slope of the limiting tie line was obtained by extrapolation of the above relationship at a value of the parameter equal to the n-butane mole fraction of the critical point. This procedure made the extrapolation scheme less prone to errors since the value of the parameter at the critical point was within 8% of the maximum value of the parameter for the experimental tie lines.

A study of Figure 17 shows that the agreement between the predictions and the experimental data is good considering the fact that the latter are only estimates. It may also be observed that for the above system the MMP predictions will be on the conservative side since the predicted limiting tie lines tend to be shifted to the left of the experimental ones. One may note that the present method does not require the generation of the entire phase envelope since it evaluates directly the variables necessary for determining the MMP, i.e. the critical point composition and slope of the limiting tie line, with the result of considerable savings of computer time.

6.2.1 Correlation of Generated Data

For each system and temperature, the data generated were correlated as follows:

1. the mole fraction of the light component at the critical point (X_{Lc}) was correlated as a function of the intermediate mole fraction (X_{Ic}) by means of the following linear equation

$$X_{Lc} = 1 - xic + b_1(X_{Ic} - xic) \qquad (58)$$

2. using the same correlating variable, the slope of the limiting tie line, a, was correlated employing the following quadratic equation

$$a = -[1 + a_1(X_{Ic} - xic) + a_2(X_{Ic} - xic)^2] \qquad (59)$$

where xic is the intermediate component mole fraction at the critical point of the light-intermediate binary.

The values of a_1, a_2, b_1 and xic are given in Table 6-1 of Appendix 6. The coefficients a_1, a_2, b_1 and xic are tabulated as a function of temperature (T), molecular weight of the intermediate component (MWI) and molecular weight of the heavy component (MWH). Equations 58 and 59 were also compared with the computed data. For a total 560 data points, the absolute average deviation for Equation 58 was 0.15% and for Equation 59, 2.6%.

3. The critical pressure was also correlated graphically as a function of the intermediate mole fraction at the critical point (refer to Figures 6-1 to 6-10 in Appendix 6). Figures 6-1 to 6-10 are correlations with the same variables. For example, Figure 18 (the equivalent of Fig. 6-1-a of Appendix 6) corresponds to the case where the temperature is 30 °C and the molecular weight of the intermediate is 44. This figure consists of a graphical representation of the critical pressure as a function of the intermediate mole fraction at the critical point. Four curves are shown, each one representing a specific system identified by the molecular weight of the heavy component. For example, the solid curve is the minimum miscibility pressure-compositional representation of the methane-propane-n-octane system at a temperature of 30 °C. The value of X_{Ic} on the abscissa varies from 0 to xic which corresponds to the mole fraction of the intermediate component of the light-intermediate binary. This is why all the curves converge to the same point representing the critical pressure and composition of the light-intermediate binary at the specified temperature, while each curve intersects the ordinate at a point representing the critical pressure of the corresponding light-heavy binary. The ordinate was labelled "MMP,MPa" instead of "Critical Pressure" as becomes evident in the

Figure 18
Minimum Miscibility Pressure vs Intermediate Mole Fraction at Critical Point
T=30°C MWI=44

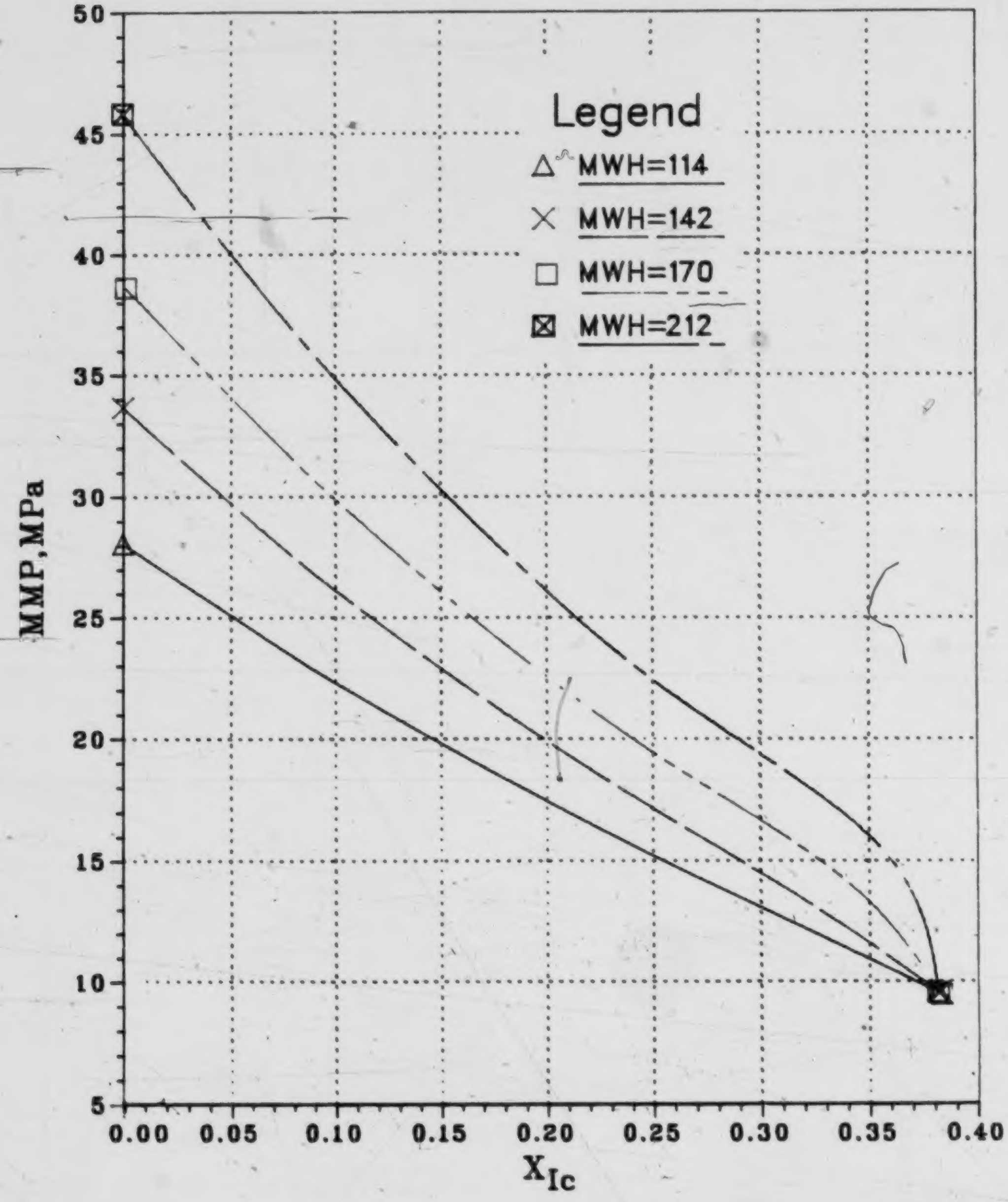

following section. Table 6-1 and Figures 6-1 to 6-10 constitute the base data for predicting the MMP for a multicomponent system.

6.2.2 Procedure for Predicting the MMP of a Ternary System

For a specified ternary system at a fixed temperature, the coefficients a_1, a_2, b_1 and xic (refer to Equations 58 and 59), can be read from Table 6-1 in Appendix 6. The above coefficients having been specified, Equations 58 and 59 permit the evaluation of the mole fraction of the light component at the critical point and the slope of the limiting tie line, respectively, as a function of the mole fraction of the intermediate component at the critical point. Given the displaced oil composition (X_L^{oil}, X_I^{oil}), dynamic miscibility may be initiated if the point representing the oil composition satisfies the equation of the limiting tie line, or

$$a = \frac{X_I^{oil} - X_{Ic}}{X_L^{oil} - X_{Lc}} \qquad (60)$$

Substituting Equations 58 and 59 into Equation 60, one obtains the following cubic equation in terms of the mole fraction of the intermediate component at the critical point (X_{Ic})

$$\Phi(X_{Ic}) = C_0 + C_1 X_{Ic} + C_2 X_{Ic}^2 + C_3 X_{Ic}^3 = 0 \qquad (61)$$

where

$$C_0 = -X_I^{oil} - (1 - a_1 xic + a_2 xic^2) \cdot (X_L^{oil} - 1 + xic + b_1 xic)$$

$$C_1 = 1 + b_1 \cdot (1 - a_1 xic + a_2 xic^2) - (a_1 - 2a_2 xic) \cdot (X_L^{oil} - 1 + xic + b_1 xic)$$

$$C_2 = b_1 \cdot (a_1 - 2a_2 xic) - a_2 \cdot (X_L^{oil} - 1 + xic + b_1 xic)$$

$$C_3 = a_2 b_1$$

The first step is to solve Equation 61 for X_{Ic}. The value of X_{Ic} satisfying Equation 61 verifies that the point representing the composition of the oil satisfies the equation of the limiting tie line. Therefore, the critical pressure corresponding to the calculated value of X_{Ic} represents the MMP for the methane vaporizing gas drive of the above oil. This is why the ordinate of the graphs of Figures 6-1 to 6-10, presented in Appendix 6, was labelled "MMP,MPa" instead of "Critical Pressure".

The second step is to refer to the appropriate figure (Figures 6-1 to 6-10) representing the selected ternary system and temperature. Given the molecular weights of the intermediate and heavy components, the MMP is then read from the appropriate curve at the value obtained for X_{Ic}.

Equation 61 can be solved analytically or numerically using the Newton-Raphson method. The numerical solution converges rapidly (3 to 4 iterations for a specified tolerance of 10^{-8}). The value of X_{Ic} is bounded by 0 and xic. Therefore, if the numerical solution approach is used, the initial estimate of X_{Ic} has to be within the above interval. One could choose, for instance, an initial value of xic/2.

6.2.3 Procedure for Predicting the MMP of a Multicomponent System

Field oil systems are generally very complex consisting of hundreds of components. The MMP of a methane vaporizing gas drive of such systems will be function of the composition of the oil and temperature:

$$MMP = f(T, X_j^{oil}, j=1,n-1)$$

where X_j^{oil} is the mole fraction of the j^{th} component of the oil.

It would be impossible to precisely define such a functional relationship when dealing with hundreds of components. Instead, it is proposed to simplify the above relationship by approximating the composition of complex oils in terms of the light fraction (C1), the intermediate fraction (C2-C6) and the heavy fraction ($C7^+$), the intermediate and heavy fractions being characterized by their respective apparent molecular weights. In other words, the above functional relationship is approximated by the following one

$$MMP = f(T, X_I^{oil}, X_H^{oil}, AMI, AMH)$$

where

X_I^{oil} = mole fraction of the intermediate fraction of the oil,

X_H^{oil} = mole fraction of the heavy fraction of the oil,

AMI = apparent molecular weight of the intermediate fraction,

AMH = apparent molecular weight of the heavy fraction.

With the above representation of complex oil systems, the previously considered ternary systems may be used as building blocks for the prediction of the MMP of a multicomponent system.

For the case of a multicomponent system (more than 3 components) and given the composition of the oil and the reservoir temperature, the MMP may be predicted using the following procedure:

1. The first step consists of grouping the intermediate and heavy components of the oil so as to obtain an average mole fraction and apparent molecular weight of the intermediate and heavy fractions, (X_I^{oil}, X_H^{oil}, AMI, AMH). The grouping into C2-C6 and C7+ for the intermediate and heavy fractions, respectively, is used in the present method.
2. The second step is to obtain the MMP by interpolation of the four MMP's obtained by selecting the four ternary systems, previously specified, that circumscribe the above hypothetical ternary system based on the molecular weight of the intermediate and heavy components, i.e.,

   a) select C_I^1, C_I^2, such that $MWC_I^1 < AMI^{oil} < MWC_I^2$

   select C_H^1, C_H^2, such that $MWC_H^1 < AMH^{oil} < MWC_H^2$

   where

   C_I^1, C_I^2

   are the intermediate components, the molecular weights of which circumscribe the apparent molecular weight of the intermediate fraction of the oil,

   C_H^1, C_H^2

   are the heavy components, the molecular weights of which circumscribe the apparent molecular weight of the heavy fraction of the oil.

   b) obtain the four MMP's, using the procedure for ternary systems (refer to section 6.2.2), of the four ternaries given by:

   $$MMP^{ij} = MMP(C_L, C_I^i, C_H^j) \quad i=1,2 \; ; \; j=1,2$$

   where MMP^{ij} is the MMP of the ternary system C_L-C_I^i-C_H^j at the reservoir temperature, C_L being the light component, in this case methane.

and

c) obtain the MMP by interpolation of the MMP^{ij} based on the molecular weights of the intermediate and heavy components and evaluated at the AMI and AMH of the oil.

For the case where the temperature does not correspond to any of the temperatures listed in Table 6-1 of Appendix 6, an interpolation scheme may be used. This would involve the calculation of the MMP using the above procedure at two temperatures, selected from Table 6-1, in order to bracket the reservoir temperature. A linear interpolation may then be used to determine the MMP at the desired temperature. A numerical application of the method, showing the various steps involved, when predicting the MMP of a multicomponent oil displaced by a lean hydrocarbon gas is described in Appendix 6.

At this point, one may question the validity of a linear interpolation scheme. The variation of the MMP of a three-component oil as a function of the molecular weight of the intermediate component, molecular weight of the heavy component and temperature was investigated using the previously specified ternary systems. The composition of the oil considered is composed of 40 mole % of the light component, 35 mole % of the intermediate component and 25 mole % of the heavy component. The effect of the molecular weight of the heavy component on the MMP is shown in Figure 19-a for two cases. In one case the molecular weight of the intermediate component was fixed at a value of 44 and in the other, at a value of 58. It may be observed that the MMP increases almost linearly with increases in the molecular weight of the heavy component. Figure 19-b illustrates the effect of the molecular weight of the intermediate component for the case where the molecular weight of the heavy component is fixed (two values were considered for the molecular weight of the heavy component: 170 and 212). The behavior of the MMP vs. MWI relationship is seen to deviate more from linearity. The effect of temperature on the MMP was investigated for two cases wherein the molecular weight of the intermediate component was fixed at a value of 44, while that of the heavy component was considered at two values: 170 and 212. For these cases

Effect of MWH, MWI and Temperature on MMP

Fig. 19-a
Effect of MWH on MMP
T=60°C

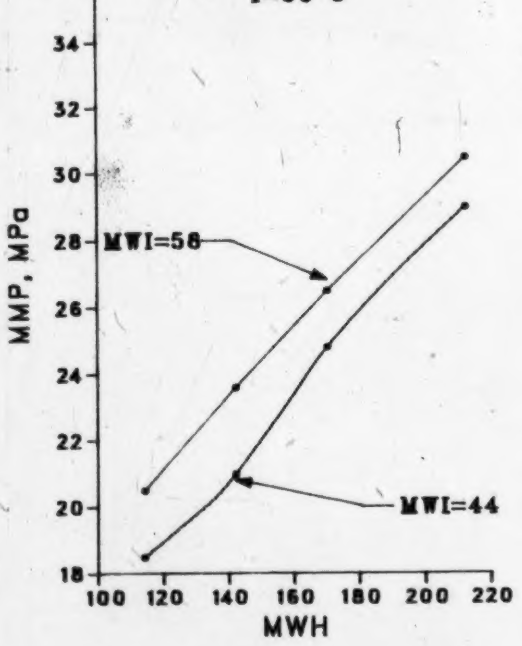

Fig. 19-b
Effect of MWI on MMP
T=60°C

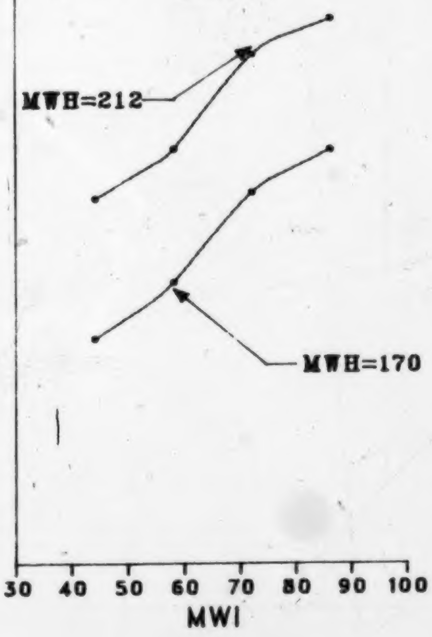

Fig. 19-c
Effect of T on MMP

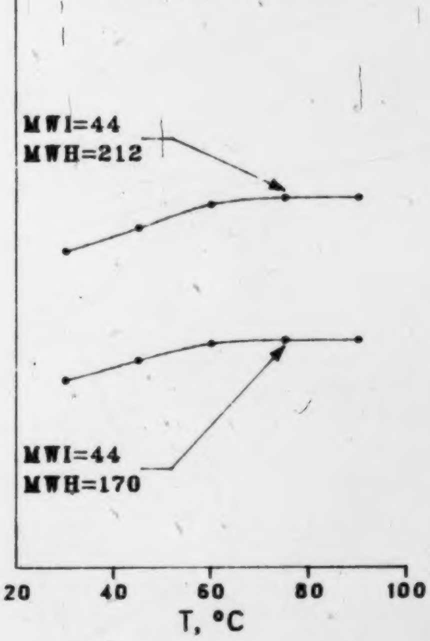

the temperature effect is shown in Figure 19-c. In both cases, the MMP is observed to increase up to a temperature of 70 °C. Beyond a temperature of 70 °C, the MMP appears to be independent of temperature. A study of Figures 19-a to 19-c shows that interpolating between two consecutive points that bracket a particular variable will not introduce a significant error.

6.2.4 Comparison of Predicted and Experimental MMP's

Very few experimental MMP's for a vaporizing gas drive by a lean hydrocarbon gas have been reported in the literature. Available experimental data will be reported along with procedures used to obtain them and criteria employed to estimate the MMP. As previously mentioned, the experimental procedures vary from one investigator to another and no general consensus exists as to the best experimental criteria for defining the MMP. In order to assess the consequences of such a variation in the experimental procedure, the results of a parametric analysis[26] are shown in Figure 20 (reproduced from reference 26) for two extreme cases:

case (a): shortest slim-tube length, lowest injection rate
case (b): longest slim-tube length, highest injection rate.

This figure represents the recovery after 1.2 pore volume injection as a function of displacement pressure for an oil system, composed of 64 mole % of n-butane and 36 mole % of decane, displaced by methane. An examination of these cases results in the following observations:

i. an upward shift of the recovery vs pressure relationship by as much as 10% observed when the displacement conditions of case (a) are changed to those of case (b),

ii. while the recovery curve of case (b) shows a clear break in slope (characteristic of of the initiation of multiple-contact miscibility), case (a) shows almost no change in slope.

It was concluded[26] that because the recovery was found to be affected by system length and injection rate, one should not use as a sole criterion, a recovery greater than some arbitrarily

Figure 20
Effect of Tube Length and Injection Rate on Recovery vs. Pressure after 1.2 PV injection

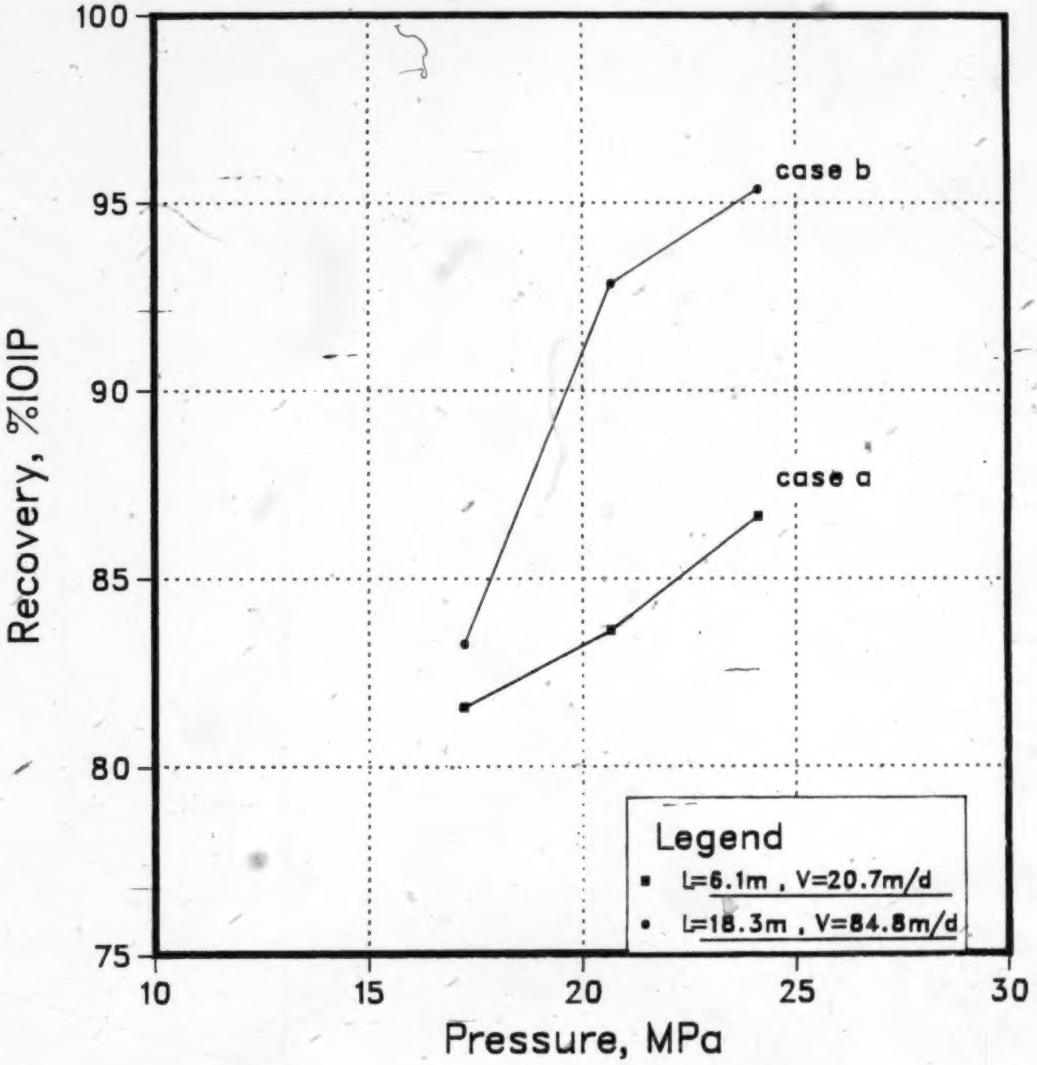

fixed value at some pore volume injection, in order to determine experimentally the MMP. For instance, if one uses a criterion of 90% recovery of the IOIP at 1.2 pore volume injection to define the experimental MMP, the experimental conditions for case (a) will result in an overestimation of the MMP by as much as 5 MPa as compared to the one obtained when the experimental conditions are those of case (b), an error as large as 25% (see Figure 20). In the above study, it was recommended that the length of the system should be as long as possible in order that the minimum length of immiscible displacement necessary for miscibility to be dynamically created will not mask the overall effect of the multiple-contact miscible displacement.

The experimental MMP's for various oils are shown in Table 4. Each oil is characterized by the average mole fraction and the apparent molecular weight of the intermediate fraction (C2-C6) and the heavy fraction ($C7^+$). Oil systems O-1 and O-2 are reported by Firoozabadi and Aziz[13]. The only description of the apparatus reported in the paper was the slim-tube length: 7 m (23 ft). The recovery curves and the criteria used to estimate the MMP were not given. For such a short system length, one may expect the estimated MMP to be conservative. As shown in the preceding discussion, the use of short slim-tubes results in overestimations of the MMP, whether an arbitrary recovery criterion (such as a value of 94% at 1.2 pore volume injection) or the break in slope of the recovery curve is used to experimentally determine the MMP.

For oil systems O-3 and O-4, Glasø[19] defined the MMP using a recovery criterion of 95% after 1.2 pore volume injection because the recovery curve did not show a break in slope. Moreover, the MMP for oil O-4 was found by extrapolation of the recovery curve. A 16.5 m (54 ft) slim-tube with an inside diameter of 0.05 cm was used. The pore volume for the reported slim-tube (porosity of 39%) was 1.26 cm^3, while the reported injection rate was 60 cm^3/h. It appears then that the experiments were completed in a matter of minutes. Furthermore, a great uncertainty in the results might have been expected when dealing with such a small pore volume and when an arbitrary recovery criterion is used to define the MMP.

Table 4
Comparison of Experimental and Predicted MMP's
(lean hydrocarbon vaporizing gas drive)

Oil system	mole% C2-C6	mole% C7+	AMI	AMH	T,°C	MMP_{exp} (MPa)	MMP_{pred} (MPa)	% deviation
O-1	22.16	22.76	48.56	209	93.3	40.10	34.86	13.0
O-2	22.49	27.12	46.42	250	107.2	41.48	40.37	2.7
O-3	30.94	24.91	47.83	231	98.9	35.27	33.03	6.3
O-4	15.55	42.93	50.70	215	78.9	47.24	41.05	13.1
O-5	28.35	29.48	51.34	193	103.0	33.79	31.59	6.5
O-6	28.75	28.48	51.31	204	102.0	35.00	31.90	8.9
O-7	22.37	17.53	49.64	191	106.0	37.90	30.74	18.9
O-8	36.00	21.30	48.00	191	60.0	24.23	26.10	-7.7
O-9	39.00	26.15	46.83	190	120.0	26.21	26.00	0.8
O-10	39.00	61.00	44.00	100	105.0	18.24	17.60	3.5
O-11	35.00	35.00	44.00	142	60.0	22.10	22.50	-1.8
O-12	25.37	28.91	53.82	190	125.0	<37.34	32.07	
O-13	28.83	54.10	54.30	222	42.8	>27.70	37.20	
O-14	22.30	33.17	48.70	268	85.6	>41.47	43.90	
							AAD=	7.5%

The MMP's of 3 reservoir fluids (O-5, O-6, O-7) of the Brazeau River Field were reported by Lee and Reitzel[51]. The characteristics of the slim-tube used were not given. They reported that when the recovery curve did not show a clear break in slope, a recovery criterion of 94% at 1.2 pore volume injection was used to define the MMP. No sight-glass obervations of the effluent were reported to substantiate the above assumption.

A 37.5 m (123 ft) long slim-tube was used by Koch and Hutchinson[11] for the experimental determination of the MMP of oil O-8. They defined the MMP at the point where a break in slope of the recovery curve occurs, which is characteristic of the pressure at which dynamic miscibility is initiated. They also distinguished miscible from immiscible displacement by observing the phase condition of the effluent through a sight glass located at the outlet of the slim-tube apparatus.

The MMP of oil O-9 (Hassi-Messaoud Field) was reported by Deffrenne et al.[6], while the detailed composition of the reservoir fluid was given by Giraud et al.[52]. The test apparatus consisted of a 1.5 m long vertical sand packed tube with an inside diameter of 1 cm. A vertical system was used to eliminate poor sweep efficiency caused by gravity segregation. A displacement velocity lower than the critical velocity Vc was used to minimize viscous fingering, where

$$Vc = \frac{Kg(\rho_o - \rho_g)}{(\mu_o - \mu_g)}$$

The break in slope of the recovery curve was used to identify the MMP. Deffrenne et al.[6] also reported the MMP of a propane-n-heptane mixture (reported as oil O-10 in Table 4).

The MMP of a ternary mixture composed of methane, propane and decane, oil O-11, displaced by methane was determined in the present investigation. The slim-tube apparatus was the same as the one used in a previous study[53]. A description of the apparatus is also given in Appendix 7. The slim-tube was 24.4 m long (80 ft) with an inside diameter of 0.457 cm and a total pore volume of 159 cm^3. An injection rate of 30 cm^3/h was used. This injection rate was selected based on the results of a parametric analysis[26,53], as it was found that a moderately high injection rate was preferable (provided that the slim-tube length is sufficiently long) in order to obtain a better differentiation between immiscible and multiple-contact miscible displacements. Figure 21 is a representation of the percent recovery of the IOIP at 1.17 pore volume injection as a function of displacement pressure. At breakthrough of the transition zone, the observation of the effluent through a sight glass located at the outlet of the slim-tube permitted making a judgement as to whether the displacement achieved miscibility. For an immiscible displacement, a clear interface was observed between the displacing and the displaced fluids, while no interface was observed for displacements that achieved miscibility. These sight-glass observations are also indicated in Figure 21. The recovery curve shows a clear break in slope when the character of the displacement changes from that of an immiscible displacement to that of a multiple-contact miscible displacement. The minimum miscibility pressure is estimated at the intersection point of tangent lines extended from the straight portions of the recovery curve in the immiscible

Figure 21
Recovery vs. Pressure Curve
(after 1.17 PV injection)
Methane Displacement

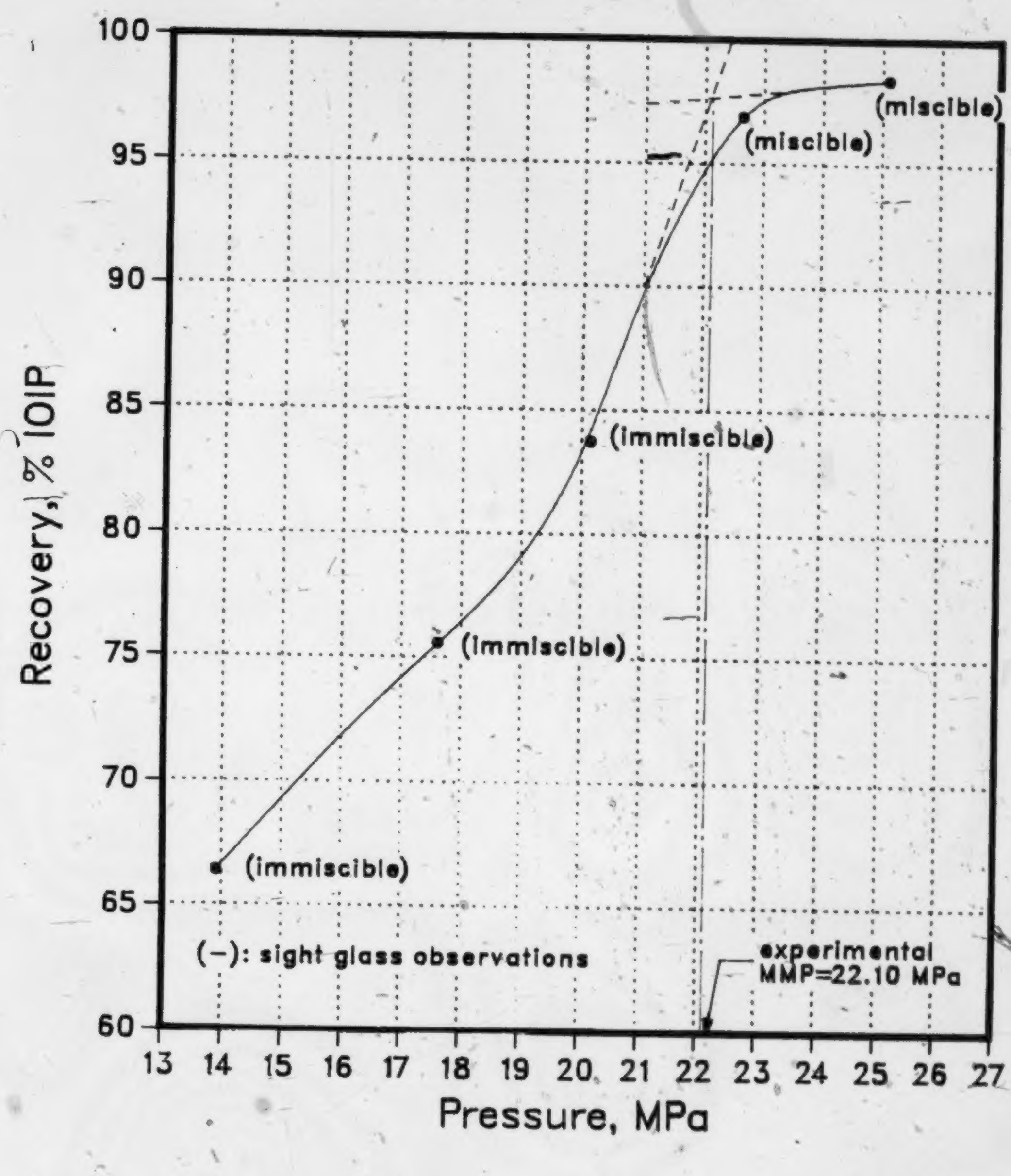

and miscible regions, respectively (see Figure 21). It is estimated that the reported value of the MMP is within ±0.4 MPa depending on the extreme positions that may be attained by these tangent lines (by considering the tangent lines drawn at various points on the miscible and immiscible portions of the recovery curve that bracket the MMP).

Meltzer et al.[54] reports the result of a single displacement at a pressure of 37.3 MPa (5414 Psia) of oil O-12 (Raleigh Field) that recovered 95% of the oil in place upon injection of 1.1 pore volumes of a lean hydrocarbon gas. The characteristics of the displacement apparatus were not reported. It is assumed[12] that the MMP is lower than the above test pressure.

Rathmell et al.[55] reported that methane displacements of oil O-13 at a pressure of 27.7 MPa (4014 Psia) and of oil O-14 at a pressure of 41.47 MPa (6014 Psia) were immiscible, and that the MMP would be above the displacement pressure considered for each oil.

From the above discussion, one may conclude that some uncertainty is associated with the reported values of the MMP's for oils O-1 to O-7, as a result of the experimental procedure and criteria used to define the MMP. As previously explained, these values were shown to be overestimates of the MMP's.

The predicted MMP's for oils O-1 to O-14 by the present method are also given in Table 4. A comparison between the predicted and experimental MMP's for oils O-1 to O-7 shows that the predicted values are lower than the reported experimental ones. It appears then that the predicted results are consistent with the fact that for these oils the experimental MMP's were overestimates.

Considering the care taken in the experimental procedure and better criteria used to estimate the MMP, it has been concluded that the reported values of the MMP's for oils O-8 to O-10 involved a much lesser degree of uncertainty. For these oils the predicted MMP's seem to agree favorably with the experimental ones.

A comparison between the predicted and experimental MMP for oil O-11 (obtained in the present investigation), further supports that better agreement is obtained when appropriate procedures and criteria are used to experimentally determine the MMP. It has been seen then that it was necessary to examine closely how the experimental MMP's were obtained in order to make an objective judgement when predicted MMP's were compared to experimental ones. For those cases where the experimental MMP's were considered to be overestimates, oils O-1 to O-7, an average deviation of 9.9% is observed between experimental and predicted values. On the other hand, the average deviation is reduced to -0.4% for those cases, oils O-8 to O-11, in which the experimental determination of the MMP involved a lesser degree of uncertainty. The overall average absolute deviation between experimental and predicted values is 7.5%.

To further investigate the predictive capability of the present method, oils O-12 to O-14 were also included in Table 4. For these oils, the experimental test consisted of a displacement at a single pressure, in order to examine whether or not dynamic miscibility was achieved. The test pressure of 37.3 MPa (5414 Psia) for oil O-12 was reported to be above the MMP. The predicted value of 32.07 MPa (4650 Psia) also showed that the test pressure was above the MMP. The MMP's for oils O-13 and O-14 were reported to be higher than 27.7 MPa (4014 Psia) and 41.47 MPa (6014 Psia), respectively. For these oils, the predicted values of 37.2 MPa (5394 Psia) for oil O-13 and 43.9 MPa (6367 Psia) for oil O-14 again agree with the above experimental observations.

In general, it appears that the predictions agree reasonably well with the experimental evidence. Furthermore, for those cases where a closer examination of the experimental procedure and criteria, used to determine the MMP, indicated that the reported values were overestimates of the MMP's, the predicted values were consistently lower than the experimental ones. This makes the present predictive method more reliable than an empirical correlation which would be strongly affected by the quality of the data base used in its development.

6.3 Nitrogen Vaporizing Gas Drives

The case of nitrogen vaporizing gas drives was treated using quaternary systems, wherein nitrogen and methane are considered as two separate components in order to adequately describe the phase relationships of nitrogen-hydrocarbon systems. For quaternary systems, the MMP for a nitrogen vaporizing gas drive was defined as the minimum pressure, at the prescribed temperature, at which the point representing the oil composition lies on the ruled surface generated by the quaternary limiting tie lines. Furthermore, since most reservoir oils contain a negligible amount of nitrogen, one only needs to consider the intersection of the above ruled surface with the hydrocarbon face of the tetrahedron corresponding to the ternary system methane-propane-decane shown in Figure 11 (refer to chapter 3). The intersection of this ruled surface with the hydrocarbon face of the tetrahedron results in a curve which is hereinafter referred to as the limiting curve. This curve separates oils that may be miscibly displaced by nitrogen through a multiple-contact process from those that may not. The MMP is obtained by determining the pressure, at the prescribed temperature, at which the limiting curve passes through the point representing the oil composition.

Given the direction of the quaternary limiting tie line (Equation 42) and the composition of the corresponding critical point, one can readily determine the point of intersection of the quaternary limiting tie line with the methane-intermediate-heavy composition plane. This procedure may be repeated, for various points on the critical curve, so as to obtain a sufficient number of points of intersection on the methane-intermediate-heavy composition plane. As stated before, the curve passing through these intersection points is the limiting curve.

Thus, it has been shown that, given a quaternary system at some fixed pressure and temperature, one can determine the limiting curve on the hydrocarbon composition plane, which separates oils that may be miscibly displaced by nitrogen through a multiple-contact process, from those that may not. This procedure may be repeated for a sequence of pressures. That pressure, at the fixed reservoir temperature, at which the corresponding limiting curve passes through the point representing the oil composition is then the MMP for that system.

To test these concepts, limiting curves were determined at various pressures and temperatures for the following quaternary systems, wherein the injected gas is nitrogen:

C1 - N2 - C3 - C12
C1 - N2 - C3 - C13
C1 - N2 - C3 - C14
C1 - N2 - C4 - C12
C1 - N2 - C4 - C13
C1 - N2 - C4 - C14

Three temperatures were selected in the range of normally encountered reservoir temperatures. The values selected were 30, 60 and 90 °C. Twelve pressures were selected, varying from 17.5 MPa (2500 Psia) to 70.0 MPa (10100 Psia). The six quaternary systems were considered at the above temperatures and pressures, with the molecular weight of the intermediate ranging from 44 to 58 and that of the heavy component from 170 to 198.

For each system at constant pressure and temperature, the limiting curve was determined as follows. Twelve critical point compositions, on the critical point curve, were calculated by applying the Newton-Raphson method to Equations 50 and 51. Estimates of the composition of successive points on the critical point curve were obtained from a knowledge of the direction of the tangent to the critical curve at any of its points. For a quaternary system at constant temperature and pressure, the only independent variables are the mole fractions of three of the four constituting components, for instance: X_1, X_2 and X_3. The critical point curve may then be represented by the following parametric form

$$X_1 = x$$
$$X_2 = f(x)$$
$$X_3 = h(x)$$

where x is the parameter.

On the critical point curve, the determinants U and V defined by Equations 50 and 51 are only a function of the chosen parameter, x.

$$U(x,f(x),h(x)) = r(x) = 0$$

$$V(x,f(x),h(x)) = s(x) = 0$$

Applying the chain rule of differentiation to the above equations, one readily obtains the direction of the tangent line to the critical curve at a point given by

$$\vec{t} = [1,f'(x),h'(x)]$$

where

$$f'(x) = (V_1 \cdot U_3 - U_1 \cdot V_3) / (U_2 \cdot V_3 - V_2 \cdot U_3)$$

$$h'(x) = (U_1 \cdot V_2 - V_1 \cdot U_2) / (U_2 \cdot V_3 - V_2 \cdot U_3)$$

and U_i and V_i are the partial derivatives of the determinants U and V with respect to the mole fraction X_i of component i.

The direction of the quaternary limiting tie line passing through each of the critical points was calculated using Equation 42 by evaluating the expressions of the partial derivatives of the molar Gibbs free energy at each critical point. The intersection points of the quaternary limiting tie lines with the hydrocarbon composition plane were used as the generating points for the limiting curve.

Figure 22 is a graphical representation of the limiting curves on the hydrocarbon composition plane for the nitrogen-methane-propane-n-tridecane system, at a temperature of 60 °C and various pressures. For example, at a pressure of 35 MPa, oils having compositions represented by points located to the left of the 35 MPa limiting curve may not be miscibly displaced by nitrogen, through a multiple-contact process. One may observe that there is a characteristic break in the slope of the limiting curve. This break occurs when the critical point of the methane-propane-n-tridecane is approached along the critical curve, at which point the quaternary limiting tie line becomes identical with the ternary limiting tie line. At high pressures, the limiting curve intersects the ordinate. This will occur whenever the set pressure exceeds the critical pressure of the methane-heavy component binary system, at the prescribed temperature. The ordinate intercept of the limiting curve (at P=50 MPa) corresponds to the intersection of the limiting tie line of the nitrogen-methane-n-tridecane system with the hydrocarbon composition plane. From Figure 22 it may be noted that

Figure 22
Intersection of Quaternary Limiting Tie Lines with the Hydrocarbon Composition Plane (Limiting Curves)

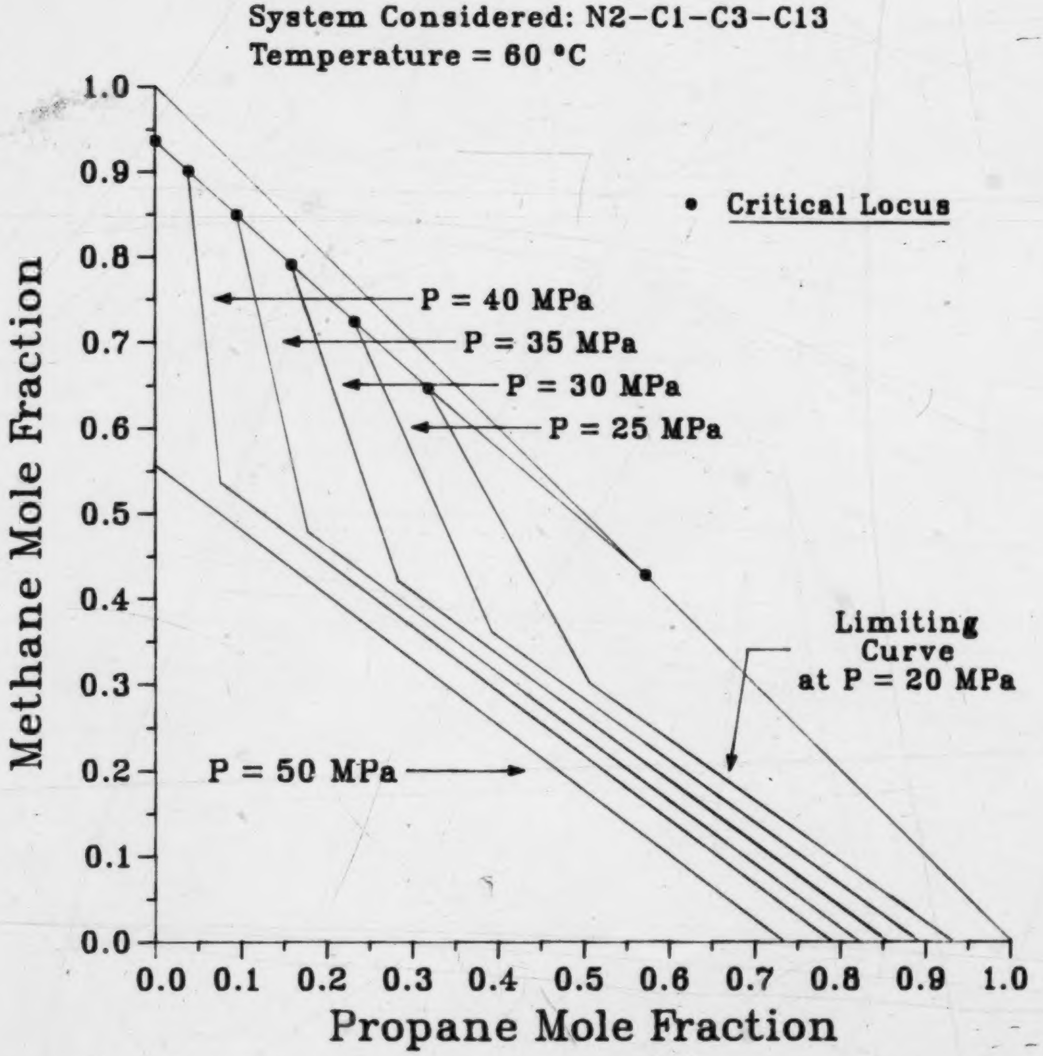

increases in pressure tend to shift the limiting curves to the left. This is to be expected, since leaner oils may be miscibly displaced by nitrogen, through a multiple-contact process, as the displacement pressure is increased.

As stated before, this method does not require the generation of the entire phase envelope, since it evaluates the variables necessary for the calculation of the MMP directly, i.e. the critical point compositions and directions of the quaternary limiting tie lines, which results in considerable savings in computer time.

6.3.1 Correlation of Generated Data

For each temperature, pressure and system combination, the limiting curves generated were approximated by two line segments:

an upper segment given by: $X_{C1} = a + bX_I$

and a lower one given by: $X_{C1} = a' + b'X_I$

where X_{C1} and X_I are the mole fraction of methane and of the intermediate component, respectively.

A total of 864 coefficients (a, b, a' and b') were evaluated by considering all the possible temperature, pressure and system combinations. The average absolute deviation between the generated and calculated data points was less than 0.001%. A program which uses the above coefficients was designed to calculate the MMP of a nitrogen vaporizing gas drive of a multicomponent oil, given the reservoir temperature, the molar composition of the oil in terms of the light fraction (methane), the intermediate fraction (ethane to hexane) and the heavy fraction (heptane$^+$), as well as the apparent molecular weight of the intermediate and heavy fractions. This program is presented in Appendix 8.

6.3.2 Procedure for Predicting the MMP of a Quaternary System

For a specified quaternary system at a fixed temperature from those selected in this investigation, the coefficients a, b, a' and b' are retrieved for all the twelve pressures considered. The routine then goes through a search procedure to circumscribe the point representing the composition of the oil on the hydrocarbon composition plane by two consecutive limiting curves. The MMP is then calculated by interpolating the circumscribing limiting curves. The pressure, at which the interpolated limiting curve passes through the oil composition point, is the required MMP.

6.3.3 Extension to Multicomponent Systems

The same procedure described for the case of a ternary system is applied using, however, quaternary systems as building blocks to predict the MMP of a multicomponent system. Given the composition of the oil and the reservoir temperature, the MMP can be predicted using the following procedure:

1. Group the intermediate and heavy components of the oil so as to obtain an average mole fraction and apparent molecular weight of the intermediate and heavy fractions, (X_I^{oil}, X_H^{oil}, AMI, AMH). The grouping into C2-C6 and C7+ for the intermediate and heavy fractions, respectively, is used in the present method.
2. Obtain the MMP by interpolation of the four MMP's obtained by selecting the four quaternary systems, previously specified, that circumscribe the above hypothetical quaternary system based on the molecular weight of the intermediate and heavy components, i.e.,

   a) select C_I^1, C_I^2, such that $MWC_I^1 < AMI^{oil} < MWC_I^2$

   select C_H^1, C_H^2, such that $MWC_H^1 < AMH^{oil} < MWC_H^2$

   where

   C_I^1, C_I^2

   are the intermediate components, the molecular weights of which circumscribe the apparent molecular weight of the intermediate fraction of the oil and

   C_H^1, C_H^2

   are the heavy components, the molecular weights of which circumscribe the apparent molecular weight of the heavy fraction of the oil.

   b) obtain the four MMP's, using the procedure for quaternary systems (refer to section 6.3.2), of the four quaternaries given by

$$MMP^{ij} = MMP(C1, N2, C_I^i, C_H^j) \quad i=1,2 \; ; \; j=1,2$$

where MMP^{ij} is the MMP of the quaternary system $C1\text{-}N2\text{-}C_I^i\text{-}C_H^j$ at the reservoir temperature.

and

c) obtain the MMP by interpolation of the MMP^{ij} based on the molecular weights of the intermediate and heavy components and evaluated at the AMI and AMH of the oil.

If the AMI^{oil}, AMH^{oil} or temperature falls outside the previously specified range, linear extrapolation may be used to obtain the MMP. The computer program has been formulated to perform this function (see Appendix 8).

6.3.4 Effect of Reservoir Oil Composition on the MMP

In order to investigate the effect on the MMP of the molecular weight of the intermediates and the heavies, two extreme cases, among the quaternary systems investigated, were considered:

Case 1. Light oil, represented by the methane-propane-dodecane system,

Case 2. Medium oil, represented by the methane-butane-tetradecane system.

Figure 23 is a graphical representation of the limiting curves, on the hydrocarbon composition plane, for each of the above systems at a temperature of 60 °C and 3 pressures (20 MPa, 35 MPa and 70 MPa). The results indicate that increases in the molecular weight of the intermediate and heavy components tend to shift the limiting curves to the right, for any given pressure. This is to be expected since heavier oil systems have higher MMP's. In order to further elaborate on this point, it may be recalled that the limiting curve separates oils that can be miscibly displaced by nitrogen, through a multiple-contact process, from those that can not. That is, oils having a composition represented by a point located to the left of the limiting curve may be immiscibly displaced by nitrogen, while those located to the right of the limiting curve may be miscibly displaced, the limiting curve being the boundary of miscibility.

Figure 23
Effect of Molecular Weight of Intermediates and Heavies on MMP

Temperature = 60 °C

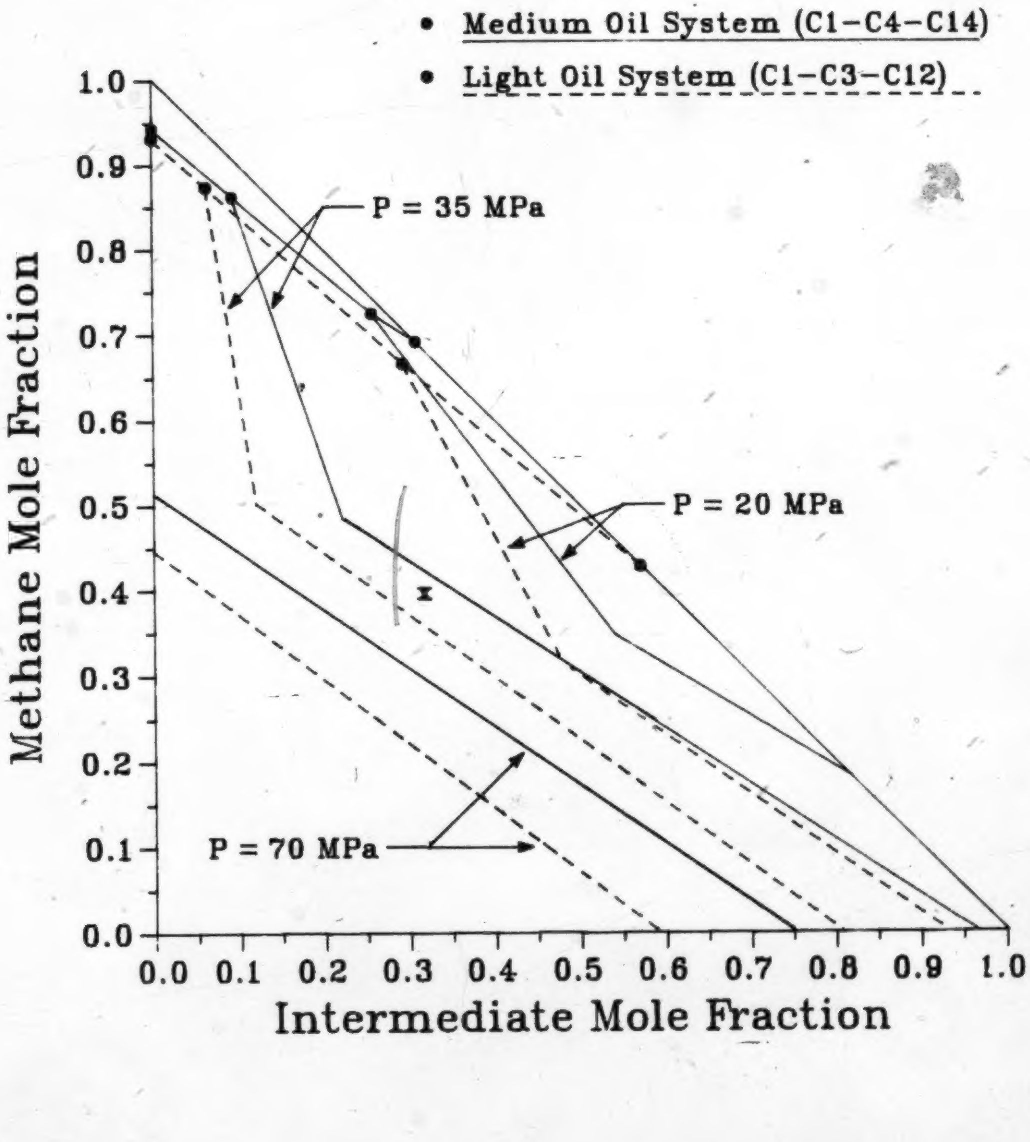

For example, consider an oil having a methane mole fraction of 0.40 and an intermediate mole fraction of 0.30 (represented by "x" in Figure 23). If the character of the intermediates and heavies of this oil is represented by the light oil system, multiple-contact miscible displacement by nitrogen will occur at a pressure of 35 MPa, since the point representing the composition of the oil is located to the right of the limiting curve (dashed curve in Figure 23). On the other hand, if the character of the intermediates and heavies of the oil is represented by the medium oil system, immiscible displacement by nitrogen will result at the same pressure of 35 MPa, since the point representing the oil composition is located to the left of the corresponding limiting curve (solid curve in Figure 23).

The effect of the methane mole fraction in the oil on the MMP for this drive process was also investigated. The quaternary system considered was the nitrogen-methane-propane-tridecane at a temperature of 60 °C. In order to study the effect of the methane concentration in the oil, the mole fraction of the intermediate component was fixed at a value of 0.40, while the methane mole fraction was increased from a value of 0.15 to 0.45. The solid curve, shown in Figure 24, is a graphical representation of the MMP of the nitrogen vaporizing gas drive of the above oil as a function of the methane mole fraction of the oil. An examination of this figure shows that a sharp decrease in the MMP occurs for nitrogen displacements, when the methane content of the oil is increased from 0.15 to 0.35, followed by a smaller decrease above a methane mole fraction of 0.35 (solid curve in Figure 24).

Through the analysis of their experimental results, Koch and Hutchinson[11] concluded that "the spread in the MMP between nitrogen and lean hydrocarbon gas injection decreases with increasing methane in the reservoir oil (keeping the intermediate mole fraction fixed)". To verify the above statement, the MMP of a methane vaporizing gas drive, under the same conditions as in the case of the nitrogen displacement, was determined and also plotted as a function of the methane mole fraction in the oil (dashed curve in Figure 24). From this figure, it may be seen that the spread in the MMP between nitrogen and methane displacement decreases as the methane mole fraction in the oil is increased. This is in complete agreement with the findings of Koch and Hutchinson[11]. Furthermore, one may observe that

Figure 24
Effect of Methane Mole Fraction in Oil on MMP

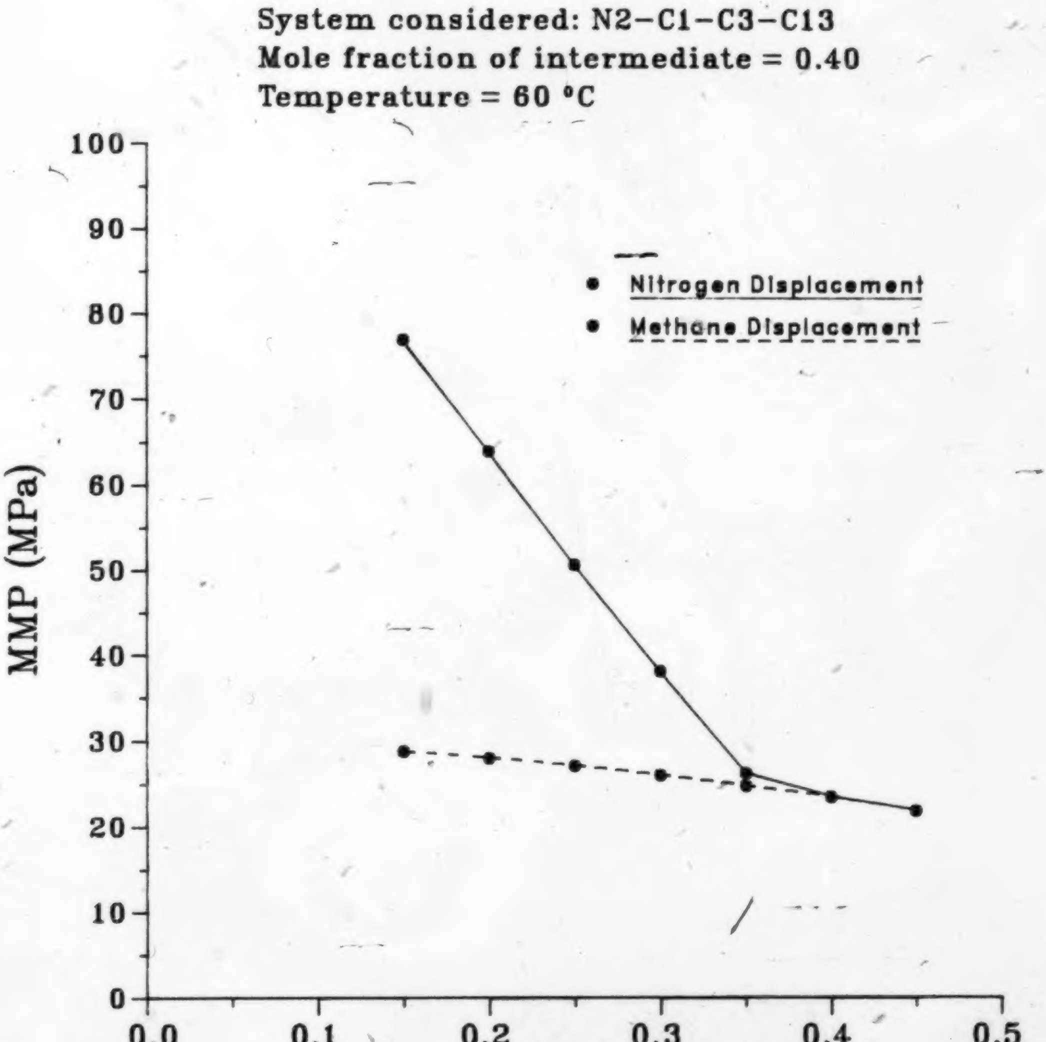

when the methane mole fraction of the oil exceeds a particular value (0.37 in Figure 24), the MMP's of nitrogen and methane displacement coincide. This is to be expected, since during the multiple-contact process of a high methane content oil by nitrogen, methane, being very volatile, will be the first component in the oil to be vaporized, thereby creating a high methane concentration buffer zone between the displaced oil and the injected nitrogen. In essence, the displacement will proceed as if the oil were being displaced by methane.

6.3.5 Effect of Temperature on the MMP

In his monograph on miscible displacement, Stalkup[12] states that "the MMP for a lean hydrocarbon gas increases with increasing temperature because the solubility of methane in hydrocarbons decreases with increasing temperature, which in turn causes the size of the two-phase region to increase. However, nitrogen miscibility pressure decreases with increasing temperature at temperatures of practical interest in reservoirs because the solubility of nitrogen in hydrocarbon increases for temperatures higher than 100 °F (39 °C)".

In order to investigate the above contention, the same system (N2 - C1 - C3 - C13), previously used to investigate the effect on the MMP of methane concentration in the oil, was considered. The mole fraction of the intermediate was again fixed at a value of 0.4.

The effect of temperature on the MMP for nitrogen displacement was investigated for two oil compositions:

one with a low methane content (methane mole fraction of 0.2),
and the other with a high methane content (mole fraction of 0.4).

As previously mentioned, at a fixed temperature, nitrogen displacement of a high methane content oil will behave as if methane were the displacing fluid, while for the case of a low methane content oil, the displacement is more characteristic of that by nitrogen, with a high MMP. The results obtained are presented in Figure 25. The results in this figure illustrates the MMP vs. temperature relationship for the low methane content oil (solid curve), and that for a high methane content oil (dashed curve). It may be observed that an increase in temperature from 30 °C to 90 °C results in a sharp decrease of the MMP for the low methane content oil,

Figure 25
Effect of Temperature on MMP

System considered: N2–C1–C3–C13
Mole fraction of intermediate = 0.40

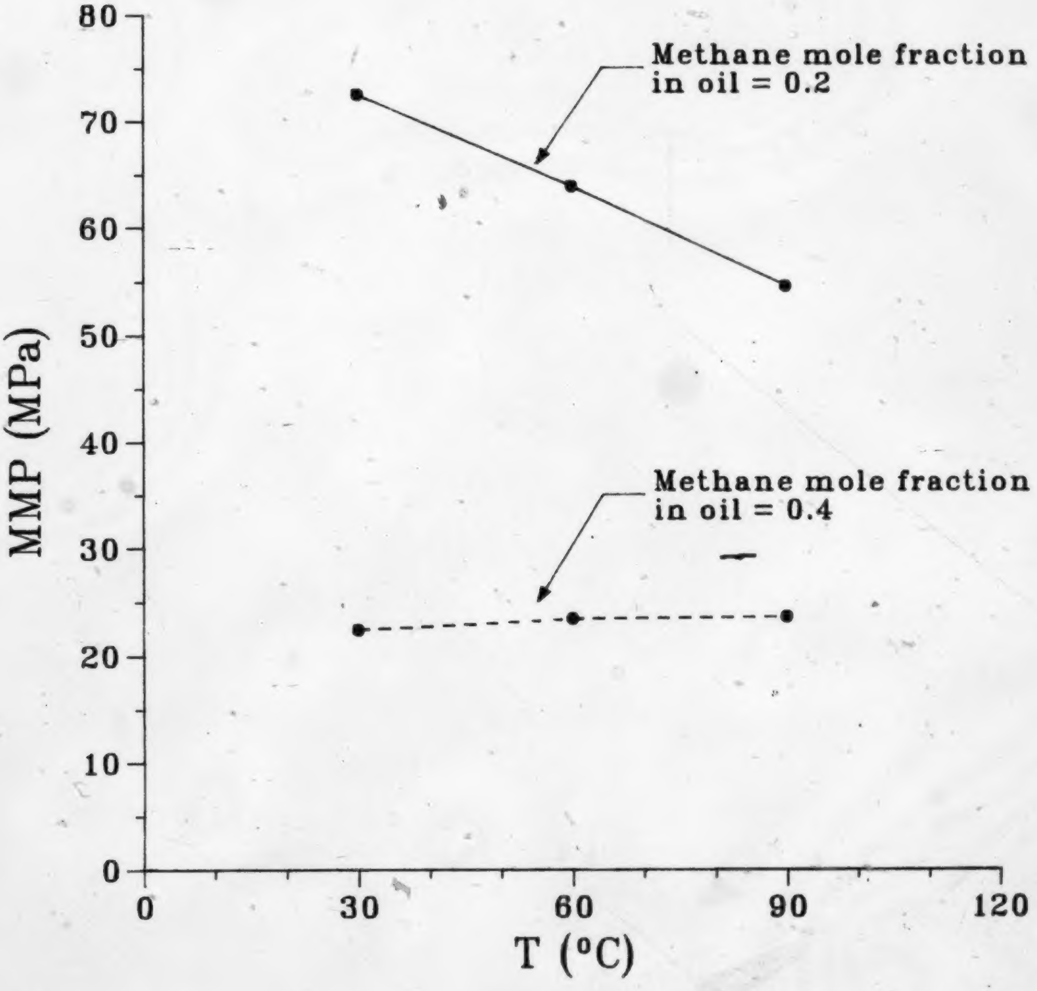

while a slight increase in the MMP is observed for the high methane content oil. These results agree with Stalkup's[12] observation. That is, the displacement of the low methane content oil by nitrogen is characteristic of nitrogen displacement, in that it demonstrates the expected decrease in the MMP with an increase in temperature. On the other hand, displacement of the high methane content oil is more characteristic of methane displacement, as is indicated by a slight increase in MMP with temperature.

6.3.6 Comparison Between Predicted and Experimental MMP's

Very few experimental data for nitrogen vaporizing gas drives have been reported in the literature. The experimental MMP's for 4 oils are shown in Table 5, each oil being characterized by the average mole fraction and apparent molecular weight of the intermediate fraction (C2-C6) and the heavy fraction ($C7^+$).

Table 5

Comparison of Experimental and Predicted MMP's

(nitrogen vaporizing gas drive)

Oil system	mole% C2-C6	mole% $C7^+$	AMI	AMH	T,°C	MMP_{exp} (MPa)	MMP_{pred} (MPa)	% deviation
O-1	36.00	21.30	48.00	191	60.0	26.70	26.34	1.3
O-2	39.00	26.15	46.83	190	120.0	25.17	23.27	7.5
O-3	26.59	17.77	44.38	193	73.3	29.52	29.32	0.7
O-4	35.00	35.00	44.00	142	60.0	31.34	32.83	-4.7
							AAD=	3.5%

The experimental procedure used for the case of oil O-1 and O-2 has been discussed in Section 6.2.4. The MMP of the nitrogen displacement of oil O-1, which has the same composition as oil O-8 reported in Table 4, has been reported by Koch and Hutchinson[11]. The MMP of oil O-2 (Hassi-Messaoud Field), reported by Deffrenne et al.[6], has the same composition as oil O-9 reported in Table 4. Peterson[56] conducted a nitrogen displacement of oil O-3 (Painter Field) at a displacement pressure of 29.52 MPa (4280 Psia). For this test, the recovery was 91% at 1.2 pore volume injection and Peterson[56] concluded that the displacement pressure corresponded to the MMP, assuming that miscibility is generated if at least 90% of the initial oil in place was recovered at 1.2 pore volume injection. The test was conducted in a 17 m (56 ft) long slim-tube. Since only one test was performed, the above value of the MMP is only approximate. The MMP of oil O-4, a ternary mixture of methane, propane and decane (same composition as oil O-11 in Table 4), was determined in the present investigation, using the apparatus described in Appendix 7. Figure 26 is a representation of the percent recovery of the IOIP (at 1.08 pore volumes injection) as a function of displacement pressure. For each displacement pressure, the test was completed after 1.08 pore volumes injection since a negligible amount was produced after breakthrough of the transition zone. Koch and Hutchinson[11] observed that when nitrogen was the displacing fluid, the recoveries were smaller than for the case of a methane displacement. They showed that with nitrogen more contacts between the displacing and displaced fluids were necessary before the development of multiple-contact miscibility and that a longer path of immiscible displacement was necessary before initiation of miscibility. The same behavior is observed when the results in Figure 26 are compared to those in Figure 20. This observation further confirms that in order to identify the MMP, one should not use as a sole criterion that the recovery be greater than some arbitrarily fixed value at some pore volume injected. The MMP for oil O-4 was determined using the same method discussed in Section 6.2.4. The break in slope of the recovery curve, which occurs at approximately a value of 31.34 MPa, agrees with the sight glass observation of the displacement being near miscibility conditions at a pressure of 31.21 MPa. The presence of a diffused and poorly defined interface is characteristic of near miscibility conditions. As discussed by Yellig and Metcalfe[23], when the displacement pressure approaches the MMP, the developed transition zone, through a multiple-contact process,

Figure 26
Recovery vs. Pressure Curve
(after 1.08 PV injection)
Nitrogen Displacement

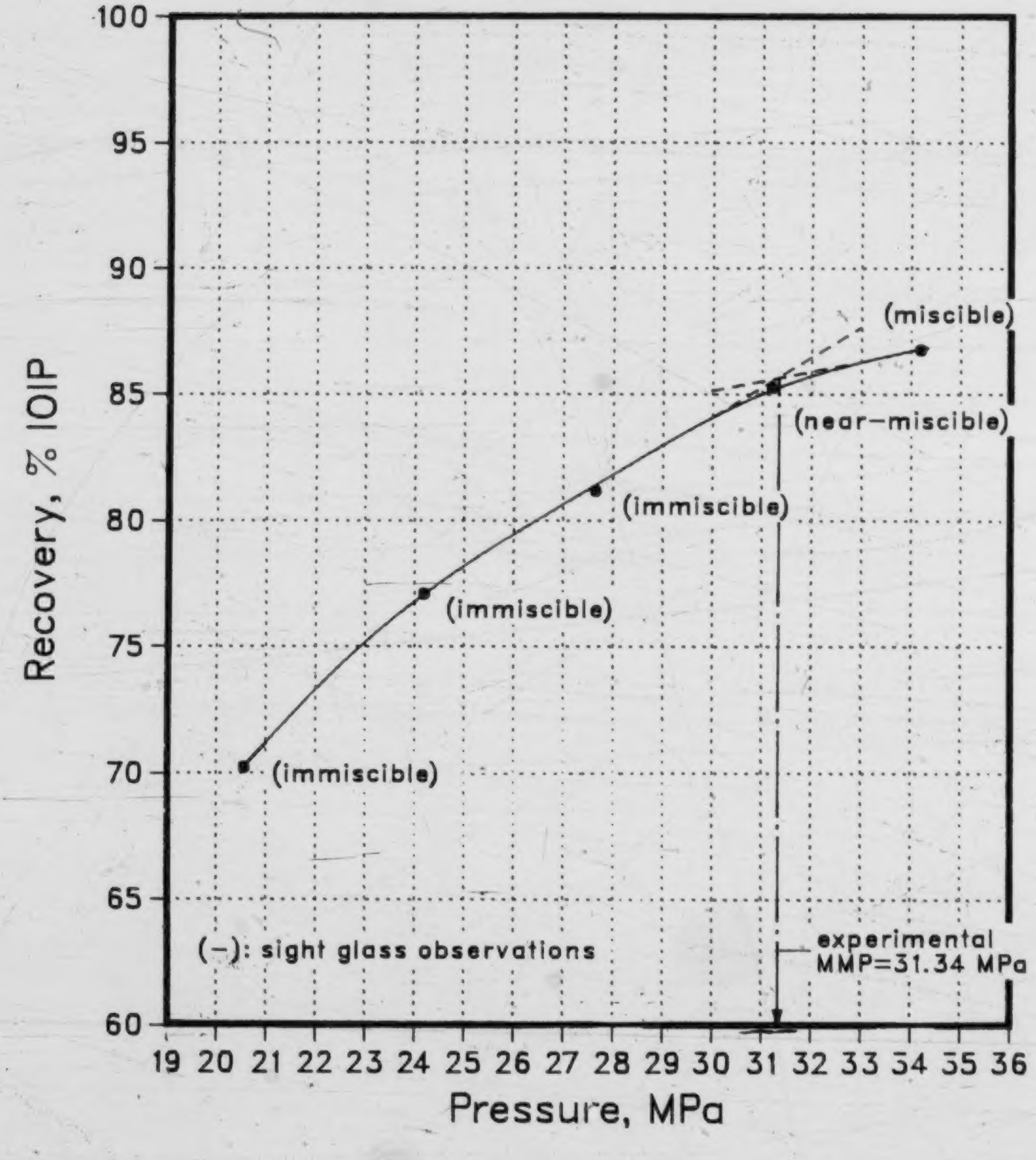

contains near critical fluids which have a very low interfacial tension resulting in a broad and not sharply defined interface.

The predicted values of the MMP's by the present method are also shown in Table 5. For the systems considered, the predicted MMP's agree favorably with the experimental ones with an average absolute deviation of 3.5% and a maximum deviation of 7.5%. It is interesting to note that for oil O-2 (Hassi-Messaoud Field), the experimental MMP of a methane displacement was 26.2 MPa (3800 Psia), while for a nitrogen drive, a lower value of 25.17 MPa (3650 Psia) was reported. As shown previously, the MMP for nitrogen vaporizing gas drives decreases with increasing temperature. The predicted values of the MMP for oil O-2 show the same trend, being 26.0 MPa (3770 Psia) for a methane vaporizing gas drive and 23.27 MPa (3374 Psia) for a nitrogen drive. One may also observe that for oil O-4, an oil with a relatively low methane content (30 mole%), the experimental MMP for a nitrogen drive of 31.34 MPa (4544 Psia) is substantially higher than the MMP of a methane drive of 22.10 MPa (3205 Psia). The predicted MMP's (32.83 MPa and 22.5 MPa respectively for a nitrogen and methane displacement) show the same trend. This further substantiates the previous observation that low methane content oils have higher MMP's when displaced by nitrogen than with methane.

SUMMARY AND CONCLUSIONS

In summary, a refined method for predicting the MMP of methane and nitrogen vaporizing gas drives has been developed.

- This new predictive method consists of the following:
  1. the determination and correlation of the MMP's of ternary and quaternary systems based upon rigorous thermodynamic criteria,
  2. the prediction of the MMP of methane vaporizing gas drives of multicomponent hydrocarbon systems, using ternary systems as building blocks,
  3. the prediction of the MMP of nitrogen vaporizing gas drives of multicomponent hydrocarbon systems, using quaternary systems as building blocks.
- The method has a theoretical basis, hence, removing the empiricism inherent in the previously used correlations. This makes the present method more reliable than an empirical correlation which would be strongly affected by the quality of the data base from which it was developed.
- A much improved representation of the phase relationships between nitrogen and hydrocarbon systems was obtained by treating nitrogen and methane as two separate components. Such a representation has shown that the hypothesis that the MMP is the same whether the driving gas is methane or nitrogen is unfounded.
- The predicted effects of reservoir oil composition and temperature on the MMP are in agreement with the published experimental observations. The results indicate that:
  1. increases in the molecular weight of the intermediate and heavy components result in increases in the MMP,
  2. the spread in the MMP between nitrogen and methane displacement decreases as the methane mole fraction in the oil increases,
  3. the MMP's of nitrogen and methane displacement coincide once the methane mole fraction in the oil exceeds a particular value,
  4. for nitrogen displacements, a sharp decrease in the MMP with an increase in temperature is predicted for low methane content oils, while a slight increase in

the MMP was predicted for high methane content oils,

5. for methane displacements, an increase in the MMP with an increase in temperature was predicted, the effect of temperature becoming less pronounced as temperature increases,
6. based upon the fact that the MMP's evaluated for a number of cases agreed reasonably well with experimentally observed values (ie. the average absolute deviation was 7.5% for lean hydrocarbon gas drives and 3.5% for nitrogen displacements), it has been concluded that this prediction technique is reliable.

•The accuracy could be improved through the use of a more accurate equation of state, and by further adjusting the interaction coefficients as more data for the critical point curve of binaries (especially for light-heavy binaries) become available.

REFERENCES

1. Rowlinson, J.S., and Swinton, F.L., "Liquids and Liquid Mixtures", Third Edition, Butterworths Monographs in Chemistry, London, (1982).

2. Soave, G., "Equilibrium Constants from a Modified Redlich-Kwong Equation of State", Chem. Eng. Sci., Vol. 27, p. 1197, (1972).

3. Chen, R.J.J., Chappelear, P.S., and Kobayashi, R., "Dew-Point Loci for Methane-n-Hexane and Methane-n-Heptane", J. Chem. Eng. Data, Vol. 21, p. 213, (1976).

4. Orr, F.M., Yu, A.D., and Lein, C.L., "Phase Behavior of CO2 and Crude Oil in Low Temperature Reservoirs", SPE J., Vol. 21, No. 4, p. 480, (Aug. 1981).

5. Gibbs, J.W., "On the Equilibrium of Heterogeneous Substances", (Oct. 1876 - May. 1877), "Collected Works", Vol. 1, Yale Univ. Press, New Haven, Conn., (1928).

6. Deffrenne, P., Marle, C., Pacsirsky, J., and Jantet, M., "La Détermination des Pressions de Miscibilité", Revue IFP XVI, No. 6, p. 678, (June. 1961).
"The Determination of Pressures of Miscibility", 36th Annual Fall Meeting of SPE of AIME, Dallas, Oct. 8-11, 1961. SPE No. 116.

7. Hutchinson, C.A. Jr., and Braun, P.H., "Phase Relations of Miscible Displacement in Oil Recovery", AIChE J., Vol. 17, p. 64, (March. 1961).

8. Slobod, R.L., and Koch, H.A., "High-Pressure Gas Injection - Mechanism of Recovery Increase", Drill. and Prod. Prac., p. 82, API(1953).

9. Buckley, S.E., and Leverett, M.C., "Mechanism of Fluid Displacements in Sands", Trans. AIME, Vol. 146, p. 107, (1942).

10. Giraud, A., and Thomere, R., "Miscibilité Dynamique. Contribution à l'Étude des Zones de Mélanges", Revue IFP, p. 619, (May. 1968).

11. Koch, H.A., and Hutchinson, C.A. Jr., "Miscible Displacements of Reservoir Oil Using Flue Gas", Trans. AIME, Vol. 213, p. 7, (1958).

12. Stalkup, F.I. Jr., "Miscible Displacement", Monograph Vol. 3, Henry L. Doherty Series, Society of Petroleum Engineers, (1983).

13. Firoozabadi, A., and Aziz, K., "Analysis and Correlation of Nitrogen and Lean-Gas Miscibility Pressure", SPE J., Vol. 1, No. 6, p. 575, (Nov. 1986).

14. Benham, A.L., Dowden, W.E., and Kunzman, W.J., "Miscible Fluid Displacement - Prediction of Miscibility", Trans. AIME, Vol. 216, p. 388, (1959).

15. Craig, A.W., and Zana, E.N., "Use of the Peng-Robinson Equation of State to Predict Hydrocarbon Phase Behavior and Miscibility for Fluid Displacement", First Joint SPE/DOE Symposium on Enhanced Recovery, Tulsa, Oklahoma, Apr. 20-23, 1980. SPE No. 8817.

16. Cohen, G.S., and Shirer, J.A., "Prediction of Conditions Necessary for Multiple-Contact Miscibility", 58th Annual Technical Conference and Exhibition, San Fransisco, CA., Oct. 5-8, 1983. SPE No. 12111.

17. Engineering Data Book, Natural Gasoline Supply Men's Association, (1957).

18. Davis, P.C., Bertuzzi, A.F., Gore, T.L., and Kurata, F., "Phase and Volumetric Behavior of Natural Gases at Low Temperatures and High Pressures", Trans. AIME, Vol. 201, p. 245, (1954).

19. Glasø, Ø., "Generalized Minimum Miscibility Pressure Correlation", SPE J., Vol. 25, No. 6, p. 927, (Dec. 1985).

20. Peng, D.Y., and Robinson, D.B., "A New Two-Constant Equation of State", Ind. Eng. Chem. Fund., Vol. 15, p. 59, (1976).

21. Lin, C.J., and Hopke, S.W., "Application of the BWRS Equation to Methane, Ethane, Propane, and Nitrogen Systems", Thermodynamics - Data and Correlations, AIChE Symposium Series, Vol. 70, No. 140, p. 37, (1974).

22. Rutherford, W.M., "Miscibility Relationships in the Displacement of Oil by Light Hydrocarbons", Trans. AIME, Vol. 222, p. II-340, (1962).

23. Yellig, Y.F., and Metcalfe, R.S., "Determination and Prediction of CO2 Minimum Miscibility Pressures", JPT, Vol. 32, No. 1, p. 160, (Jan. 1980).

24. Orr, F.M., Silva, M.K., Lien, C.L., and Pelletier, M.T., "Laboratory Experiments to Evaluate Field Prospects for CO2 Flooding", JPT, Vol. 26, p.888, (Apr. 1982).

25. Holm, L.W., and Josendal, V.A., "Mechanism of Oil Displacement by Carbon Dioxide", JPT, p. 1427, (Dec. 1974).

26. Flock, D.L., and Nouar, A., "Parametric Analysis on the Determination of the Minimum Miscibility Pressure in Slim-Tube Displacements", JCPT, Vol. 23, p. 80, (Sept-Oct. 1984).

27. Tisza, L., "Generalized Thermodynamics", M.I.T. Press, Cambridge, Massachusetts, (1966).

28. Wilson, G.M., "A Modified Redlich-Kwong Equation of State, Application to General Physical Data Calculations", Paper 15C presented at the 65th AIChE National Meeting, Cleveland, OH., (May. 4-7, 1969).

29. Heidemann, R.A., "Computation of High Pressure Phase Equilibria", Fluid Phase Equilibria, Vol. 14, p. 55, (1983).

30. Nghiem, L.X., Aziz, K., and Li, Y.K., "A Robust Iterative Method for Flash Calculations Using The Soave-Redlich-Kwong or the Peng-Robinson Equation of State", SPE J., Vol.23, No. 3, p. 521, (June. 1983).

31. Chao, K.C., and Greenkorn, R.A., "Thermodynamics of Fluids, An Introduction to Equilibrium Theory", Marcel Dekker, Inc., New York, (1975).

32. Bloomer, O.T., and Parent, J.D., "Liquid-Vapor Phase Behavior of the Methane-Nitrogen System", Chem. Eng. Prog., Symposium Series No. 6, Vol. 49, p. 11, (1953).

33. Ellington, R.T., Eakin, B.E., Parent, J.D., Gami, D.C., and Bloomer, O.T., "Vapor-Liquid Phase Equilibria in the Binary Systems of Methane, Ethane and Nitrogen", Thermodynamic and Transport Properties of Gases, Liquids and Solids,

ASME, New York, p. 180, (1959).

34. Reamer, H.H., Sage, B.H., and Lacey, W.N., "Volumetric and Phase Behavior of the Methane-Propane System", Ind. Eng. Chem., Vol. 42, p. 534, (1950).

35. Sage, B.H., Hicks, B.L., and Lacey, W.N., "The Methane-n-Butane System in the Two-Phase Region", Ind. Eng. Chem., Vol. 32, p. 1085, (1940).

36. Sage, B.H., Reamer, H.H., Olds, R.H., and Lacey, W.N., "Volumetric and Phase Behavior of the Methane-n-Pentane System", Ind. Eng. Chem., Vol. 34, p. 1108, (1942).

37. Reamer, H.H., Sage, B.H., and Lacey, W.N., "Phase Equilibria in Hydrocarbon Systems - Volumetric and Phase Behavior of the Methane-n-Heptane System", Chem. Eng. Data Series, Vol. 1, p. 29, (1956).

38. Reamer, H.H., Olds, R.H., Sage, B.H., and Lacey, W.N., "Phase Equilibria in Hydrocarbon Systems - Methane-Decane System", Ind. Eng. Chem., Vol. 34, p. 1526, (1942).

39. Matschke, E., and Thodos, G., "Vapor-Liquid Equilibria for the Ethane-Propane System", J. Chem. Eng. Data, Vol. 7, p. 232, (1962).

40. Kay, W.B., "Liquid-Vapor Equilibrium Relations in Binary Systems - The Ethane-n-Butane System", Ind. Eng. Chem., Vol. 32, p. 353, (1940).

41. Reamer, H.H., Sage, B.H., and Lacey, W.N., "Phase Equilibria in Hydrocarbon Systems - Volumetric and Phase Behavior of the Ethane-n-Pentane System", J. Chem. Eng. Data, Vol. 5, p. 44, (1960).

42. Kay, W.B., "Liquid-Vapor Equilibrium Relations in the Ethane-n-Heptane System", Ind. Eng. Chem., Vol. 30, p. 459, (1938).

43. Nysewander, C.N., Sage, B.H., and Lacey, W.N., "Phase Equilibria in Hydrocarbon Systems - The Propane-n-Butane System in the Critical Region", Ind. Eng. Chem., Vol. 32, p. 118, (1940).

44. Sage, B.H., and Lacey, W.N., "Phase Equilibria in Hydrocarbon Systems - Propane-n-Pentane System", Ind. Eng. Chem., Vol. 32, p. 992, (1940).

45. Sage, B.H., and Berry, V.M., "Phase Equilibria in Hydrocarbon Systems", Monograph on API Research Project 37, p. 105, API, (1971).

46. Kay, W.B., "Liquid-Vapor Equilibrium Relations in Binary Systems - n-Butane-n-Heptane System", Ind. Eng. Chem., Vol. 33, p. 590, (1941).

47. Grieves, R.B., and Thodos, G., "The Critical Temperatures of Ternary Hydrocarbon Systems", Ind. Eng. Chem., Fundam. No. 1, Vol. 1, p. 45, (1962).

48. Spear, R.L., Robinson, R.L., and Chao, K.C., "Critical States of Ternary Mixtures and Equations of State", Ind. Eng. Chem. Fundam., Vol. 10, p. 588, (1971).

49. Sage, B.H., and Lacey, W.N., "Thermodynamic Properties of the Lighter Paraffin Hydrocarbons and Nitrogen", Monograph on API Research Project 37, p. 203, API, (1950).

50. Reamer, H.H., Sage, B.H., and Lacey, W.N., "Phase Equilibria in Hydrocarbon Systems

- Methane-n-Butane-Decane System at 40°F", Ind. Eng. Chem., Vol. 44, p. 1671, (1952).

51. Lee, J.I., and Reitzel, G.A., "High Pressure, Dry Gas Miscible Flood - Brazeau River Nisku oil Pools", JPT, Vol. 34, No. 11, p. 2503, (Nov. 1982).

52. Giraud, A., Thomere, R., Gard, J., and Charles, M., "A Laboratory Investigation Confirms the Relative Inefficiency of True Miscible Drives, and Outlines New Concepts for Maximizing Oil Recovery by Gas Injection", 46th Annual Fall Meeting, New Orleans, La., (Oct. 3-6, 1971). SPE No. 3486.

53. Nouar, A., M.Sc. Dissertation, U. of Alberta, Edmonton, (1983).

54. Meltzer, B.D., Hurdle, R.W., and Cassingham, R.W., "An Efficient Gas Displacement Project - Raleigh Field, Mississipi", JPT, Vol. 17, p. 509, (May 1965).

55. Rathmell, J.J., Stalkup, F.I., and Hassinger, R.C., "A Laboratory Investigation of Miscible Displacement by Carbon Dioxide", 46th Annual Fall Meeting of SPE of AIME, New Orleans, La., Oct. 3-6, 1971. SPE No. 3483.

56. Peterson, A.V., "Optimal Recovery Experiments with N2 and CO2", Petroleum Engineer International, p. 40, (Nov. 1978).

57. Welge, H.J., Johnson, E.F., Ewing, S.P., and Brinkman, F.H., "The Linear Displacement of Oil by Enriched Gas", JPT, Vol. 13, p. 787, (Aug. 1961).

58. Helfferich, H.J., "General Theory of Multicomponent, Multiphase Displacement in Porous Media", SPE J., p. 51, (Feb. 1981).

59. Dumore, J.M., Haggort, J., and Risseeuw, A.S., "An Analytical Model for One-Dimensional Three-Component Condensing and Vaporizing Gas Drives", SPE J., Vol. 24, No. 2, p. 169, (Apr. 1984).

60. Lee, A.L., Gonzalez, M.H., and Eakin, B.E., "The Viscosity of Natural Gases", JPT, Vol. 18, p. 997, (Aug. 1966).

61. Hankinson, R.W., and Thomson, G.H., "A New Correlation for Saturated Densities of Liquids and Their Mixtures", AIChE. J., Vol. 25, No. 4, p. 653, (July 1979).

62. Alani, G.H., and Kennedy, H.T., "Volumes of Liquid Hydrocarbons at High Temperatures and Pressures", Trans. AIME, Vol. 219, p. 288, (1960).

63. Lohrenz, J., Bray, B.G., and Clark, C.R., "Calculating Viscosities of Reservoir Fluids from their Composition", JPT, Vol. 16, p. 1171, (Oct. 1964).

64. Henderson, D., "Practical Calculations of the Equation of State of Fluids and Fluid Mixtures Using Perturbation Theory and Related Theories", Equations of State in Engineering and Research, Advances in Chemistry Series No. 182, ACS., Washington, D.C., (1979).

65. Goodwin, R.D., "The Thermophysical Properties of Methane, from 90 to 500 K at Pressures to 700 Bar", Nat. Bur. Stand. (U.S.), Tech. Note 653, (1974).

66. Goodwin, R.D., Roder, H.M., and Straty, G.C., "Thermophysical Properties of Ethane, from 90 to 600 K at Pressures to 700 Bar", Nat. Bur. Stand. (U.S.), Tech. Note 684, (1976).

67. Goodwin, R.D., and Haynes, W.M., "Thermophysical Properties of Propane, from 85 to 700 K at Pressures to 70 MPa", Nat. Bur. Stand. (U.S.), Monogr. 170, (1982).

68. Haynes, W.M., and Goodwin, R.D., "Thermophysical Properties of Normal Butane, from 135 to 700 K at Pressures to 70 MPa", Nat. Bur. Stand. (U.S.), Monogr. 169, (1982).

69. Das, T.R., Reed, C.O., and Eubank, P.T., "PVT Surface and Thermodynamic Properties of n-Pentane", J. Chem. Eng. Data, Vol. 22, p. 3, (1977).

70. Vargaftik, N.B., "Tables on the Thermophysical Properties of Liquids and Gases", John Wiley & Sons, Inc., New York, (1975).

71. Passut, C.A., and Danner, R.P., "Acentric Factor. A Valuable Correlating Parameter for the Properties of Hydrocarbons", Ind. Eng. Chem. Process Des. Develop., Vol. 12, No. 3, p. 365, (1973).

72. Jacobsen, R.T., and Stewart, R.B., "Thermophysical Properties of Nitrogen from the Fusion Line to 3500 R (1944 K) for Pressures to 150,000 Psia", Nat. Bur. Stand. (U.S.), Tech. Note 648, (1973).

73. Stewart, D.E., Sage, B.H., and Lacey, W.N., "Volumetric Behavior of n-Hexane in Liquid Phase", Ind. Eng. Chem., Vol. 46, p. 2529, (1954).

74. Carmichael, L.T., Sage, B.H., and Lacey, W.N., "Phase Equilibria in Hydrocarbon Systems - Volumetric Behavior of n-Nonane", Ind. Eng. Chem., Vol. 45, p. 2697, (1953).

Appendix 1

Application of the Fractional Flow Theory to Vaporizing and Condensing Gas Drives

1.1 Introduction

Several authors have attempted to analytically describe the coupling of two phase flow and phase behaviour in gas drives. The first successful attempt was made by Welge et al.[57]. Recently Helfferich[58] presented a general theory on one-dimensional multiphase, multicomponent flow in porous media. Dumore et al.[59] applied these concepts and presented an analytical model for the calculation of one-dimensional, three-component condensing and vaporizing gas drives, based on the method of characteristics. The model describes the following processes:

1)mass transfer between oil and gas

2)swelling and shrinkage

3)viscosity and density changes

4)gravity stabilization, and

5)rock-fluid interaction.

This model will be discussed, showing the main features of the solution procedure. The main assumptions of the model are:

1)instantaneous local thermodynamic equilibrium,

2)absence of dispersion and capillarity.

The above assumptions are needed to simplify the problem such that it becomes amenable to an analytical treatment.

1.2 Phase Behavior Description of a Three-component System

In the following, we will represent the composition of a mixture by the mole fractions of its individual components as follows:

Z_1=overall composition of light component

Z_2=overall composition of intermediate component

Z_3=overall composition of heavy component

and $Z_1+Z_2+Z_3=1$

If a mixture $[Z_1,Z_2,Z_3]$ lies in the two-phase region, it will separate in two phases which are in equilibrium:

a liquid phase, (X_i,no) $i=1,3$

a gas phase, (Y_i,ng) $i=1,3$ where,

X_i=mole fraction of ith component in liquid phase

Y_i=mole fraction of ith component in gas phase

no=liquid mole fraction(moles of liquid/ moles of mixture)

ng=gas mole fraction (moles of gas/ moles of mixture), and

$$X_1+X_2+X_3=1$$

$$Y_1+Y_2+Y_3=1$$

$$no+ng=1$$

The equilibrium ratios K_i are defined as: $K_i = Y_i/X_i$ $i=1,3$.

Given the pressure, temperature and the composition of a mixture lying in the two-phase region, the K-values can be obtained by three methods, viz.:

1)equation of state

2)convergence pressure method

3)directly from experimental data.

Thus, given Z_1 and Z_2, K_1, K_2 and K_3 can be evaluated, and the following unknowns X_i,Y_i,Z_3, no and ng can be determined by solving the following 9 equations:

(1) $\sum_i X_i=1$

(2) $\sum_i Y_i=1$

(3) $\sum_i Z_i=1$

(4-6) $K_i = Y_i/X_i$ $i=1,3$

(7-8) $Z_i=(1-ng)X_i + ngY_i$ $i=1,2$

(9) $no+ng=1$

1.3 Flow Equations

To make the problem amenable to an analytical treatment, the following assumptions and simplifications are introduced:

1)the flow is one-dimensional and isothermal,

2)the gas and oil phases are locally in thermodynamic equilibrium,

3)for the purpose of evaluating the thermodynamic properties of the fluids, the system is considered to be at uniform temperature and pressure,

4)capillary and dispersion effects in the flow direction are negligible,

5)the porous medium is homogeneous and may contain an inert, irreducible water saturation.

1.3.1 Multiphase Flow Equations

For two-phase flow in porous media, the oil and gas velocities are, respectively,

$$U_o = -\frac{KK_{ro}}{\mu_o}\left[\frac{dP}{dz} + \rho_o g\sin\theta\right] \quad \theta\leq 0 \tag{1-1}$$

$$U_g = -\frac{KK_{rg}}{\mu_g}\left[\frac{dP}{dz} + \rho_g g\sin\theta\right] \quad \theta\leq 0 \tag{1-2}$$

Let A be the constant cross-sectional area of the porous medium; the oil and gas flow rates are, respectively,

$$q_o = A\cdot U_o \tag{1-3}$$

$$q_g = A\cdot U_g \tag{1-4}$$

and the oil and gas mass flow rates are, respectively,

$$\dot{m}_o = \rho_o q_o \tag{1-5}$$

$$\dot{m}_g = \rho_g q_g \tag{1-6}$$

Since the oil and gas are in thermodynamic equilibrium, and given the overall composition of the oil-gas mixture contained in a volume portion of the porous medium, the oil and gas compositions can then be determined (X_i, Y_i). The oil and gas mole rates are, respectively,

$$\dot{N}_o = \frac{\dot{m}_o}{Mo} \tag{1-7}$$

$$\dot{N}_g = \frac{\dot{m}_g}{Mg} \tag{1-8}$$

where

Mo = apparent molecular weight of oil

Mg = apparent molecular weight of gas, given by

$$Mo = \sum_i X_i M_i \tag{1-9}$$

$$Mg = \sum_i Y_i M_i \tag{1-10}$$

and M_i is the molecular weight of the ith component.

The mole rates of the individual components in the oil and gas phases are, respectively,

$$\dot{N}_{oi} = \frac{\dot{m}_o}{Mo} X_i = \frac{\rho_o A U_o}{Mo} X_i \tag{1-11}$$

$$\dot{N}_{gi} = \frac{\dot{m}_g}{Mg} Y_i = \frac{\rho_g A U_g}{Mg} Y_i \tag{1-12}$$

The above expressions are needed to derive the continuity equation for each species i.

1.3.2 Continuity Equation for Each Species i

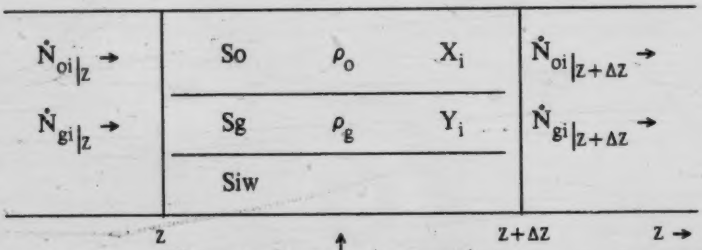

Element of pore volume = $\phi A \Delta z$

The material balance for each component i can be stated as follows:

[number of moles of component i entering volume element -

number of moles of component i leaving volume element]

over time Δt

=

[net accumulation of component i in volume element]

For the above pore volume element:

number of moles i in oil phase = $\phi A \Delta z \frac{So\rho_o}{Mo} X_i$

number of moles i in gas phase = $\phi A \Delta z \frac{Sg\rho_g}{Mg} Y_i$

and the material balance equation becomes

$$[(\dot{N}_{oi}-\dot{N}_{gi})_z - (\dot{N}_{oi}-\dot{N}_{gi})_{z+\Delta z}]\cdot\Delta t =$$

$$\phi A\Delta z[(\frac{So\rho_o}{Mo}X_i+\frac{Sg\rho_g}{Mg}Y_i)_{t+\Delta t} - (\frac{So\rho_o}{Mo}X_i+\frac{Sg\rho_g}{Mg}Y_i)_{\Delta t}] \qquad (1\text{-}13)$$

and taking the limit as the element of pore volume and the incremental time tend to zero, one obtains

$$\frac{\partial}{\partial z}[\dot{N}_{oi}+\dot{N}_{gi}] + \phi A\frac{\partial}{\partial t}[\frac{So\rho_o}{Mo}X_i+\frac{Sg\rho_g}{Mg}Y_i)] = 0 \quad i=1,3 \qquad (1\text{-}14)$$

Substituting the expressions for $\dot{N}_{oi}$ and $\dot{N}_{gi}$, one obtains

$$\frac{\partial}{\partial z}[\frac{\rho_o U_o}{Mo}X_i+\frac{\rho_g U_g}{Mg}Y_i)] + \phi\frac{\partial}{\partial t}[\frac{So\rho_o}{Mo}X_i+\frac{Sg\rho_g}{Mg}Y_i)] = 0 \quad i=1,3 \qquad (1\text{-}15)$$

Let $U=U_o+U_g$, total phase velocity, the fractional flow equation to oil is

$$f_o = \frac{U_o}{U} \qquad (1\text{-}16)$$

and eliminating the pressure gradients from the gas and oil velocities, one obtains

$$f_o = \frac{K_{ro}/\mu_o}{K_{ro}/\mu_o+K_{rg}/\mu_g}\cdot[1-\frac{KK_{rg}}{U\mu_g}(\rho_o-\rho_g)g\sin\theta] \qquad (1\text{-}17)$$

The continuity equation can be written in the following form

$$\frac{\partial}{\partial z}[U(\frac{\rho_o f_o}{Mo}X_i+\frac{\rho_g(1-f_o)}{Mg}Y_i)] + \phi\frac{\partial}{\partial t}[\frac{So\rho_o}{Mo}X_i+\frac{Sg\rho_g}{Mg}Y_i)] = 0 \quad i=1,3 \qquad (1\text{-}18)$$

defining

$$F_i = \frac{U}{\phi}[\frac{\rho_o f_o}{Mo}X_i+\frac{\rho_g(1-f_o)}{Mg}Y_i] \qquad (1\text{-}19)$$

$$G_i = \frac{So\rho_o}{Mo}X_i+\frac{Sg\rho_g}{Mg}Y_i \qquad (1\text{-}20)$$

the continuity equation is simplified to

$$\frac{\partial F_i}{\partial z}+\frac{\partial G_i}{\partial t} = 0 \quad i=1,3 \qquad (1\text{-}21)$$

where

$F_i=F_i(Z_j,U)$

$G_i=G_i(Z_j) \quad j=1,2$

and So and Sg are given by

$$So = \frac{no\ Mo\ \rho_g\ (1-Siw)}{no\ Mo\ \rho_g + ng\ Mg\ \rho_o} \qquad (1\text{-}22)$$

$$Sg = 1 - So - Siw \qquad (1\text{-}23)$$

1.4 Solution Procedure

The equations to be solved are

$$\frac{\partial F_i}{\partial z} + \frac{\partial G_i}{\partial t} = 0 \quad i=1,3$$

where

$$F_i=F_i(Z_j,U)$$

$$G_i=G_i(Z_j) \quad j=1,2$$

the unknowns being Z_1, Z_2 and U as a function of position and time. Thus, we have three unknowns for three equations. The boundary and initial conditions are as follows:

1)boundary conditions:

composition of injected gas

injection or production rate (constant)

2)initial conditions:

reservoir temperature and pressure

composition of in-place oil.

1.4.1 Solution Path in Hodograph Space

In the hodograph space, or the Z_1, Z_2, U space, the solution curve can be parametrized through a parameter λ,

$$Z_1 = Z_1(\lambda)$$

$$Z_2 = Z_2(\lambda)$$

$$U = U(\lambda)$$

where $\lambda = \lambda(z,t)$

thus,

$$F_i = F_i(Z_j(\lambda),U(\lambda)) = F_i(\lambda) = F_i(z,t)$$

$$G_i = G_i(Z_j(\lambda)) = G_i(\lambda) = G_i(z,t) \quad j=1,2 \quad i=1,3$$

Using the chain rule, the continuity equation can be written in the following form

$$\sum_j \frac{\partial F_i}{\partial Z_j} \cdot \frac{\partial Z_j}{\partial z} + \frac{\partial G_i}{\partial Z_j} \cdot \frac{\partial Z_j}{\partial t} + \frac{\partial F_i}{\partial U} \cdot \frac{\partial U}{\partial z} \qquad i=1,3 \quad j=1,2 \tag{1-24}$$

where

$$\frac{\partial Z_j}{\partial z} = \frac{dZ_j}{d\lambda} \frac{\partial \lambda}{\partial z} \tag{1-25}$$

$$\frac{\partial Z_j}{\partial t} = \frac{dZ_j}{d\lambda} \frac{\partial \lambda}{\partial t} \tag{1-26}$$

$$\frac{\partial U}{\partial z} = \frac{dU}{d\lambda} \frac{\partial \lambda}{\partial z} \tag{1-27}$$

or

$$\left[\sum_j \left(\frac{\partial F_i}{\partial Z_j} \frac{dZ_j}{d\lambda}\right) + \frac{\partial F_i}{\partial U} \frac{dU}{d\lambda}\right\} \frac{\partial \lambda}{\partial z} + \sum_j \left(\frac{\partial G_i}{\partial Z_j} \frac{dZ_j}{d\lambda}\right) \cdot \frac{\partial \lambda}{\partial t} = 0 \qquad i=1,3 \tag{1-28}$$

1.4.2 Propagation Rate of a Point of the Solution Curve

Since a single point $[Z_1, Z_2, U]$ of the solution curve is obtained given a particular value of λ, its propagation rate, V, is given by

$$V = \frac{dz}{dt}\Big|_\lambda \tag{1-29}$$

and, since $\lambda(z,t)=\text{constant}$, from the chain rule one obtains

$$V = \frac{dz}{dt}\Big|_\lambda = -\frac{\partial \lambda / \partial t}{\partial \lambda / \partial z} \tag{1-30}$$

and substituting in the continuity equation, one obtains

$$\left[\sum_j \left(\frac{\partial F_i}{\partial Z_j} \frac{dZ_j}{d\lambda}\right) + \frac{\partial F_i}{\partial U} \frac{dU}{d\lambda}\right] - V\left[\sum_j \left(\frac{\partial G_i}{\partial Z_j} \frac{dZ_j}{d\lambda}\right)\right] = 0 \qquad i=1,3 \tag{1-31}$$

let

$$F_{ij} = \frac{\partial F_i}{\partial Z_j} \tag{1-32}$$

$$G_{ij} = \frac{\partial G_i}{\partial Z_j} \tag{1-33}$$

$$F_{i3} = \frac{\partial F_i}{\partial U} \tag{1-34}$$

The above system of equations can be written in matrix form as

$$\underbrace{\begin{bmatrix} (F_{11}\text{-}VG_{11}) & (F_{12}\text{-}VG_{12}) & F_{13} \\ (F_{21}\text{-}VG_{21}) & (F_{22}\text{-}VG_{22}) & F_{23} \\ (F_{31}\text{-}VG_{31}) & (F_{32}\text{-}VG_{32}) & F_{33} \end{bmatrix}}_{[\,A\,]} \cdot \begin{bmatrix} dZ_1/d\lambda \\ dZ_2/d\lambda \\ dU/d\lambda \end{bmatrix} = \begin{bmatrix} 0 \\ 0 \\ 0 \end{bmatrix}$$

A non-trivial solution is obtained only if det[A]=0. Setting det[A]=0 results in a quadratic equation in V from which two characteristic propagation rates are obtained, V^- and V^+. The smaller root V^- corresponds to a slow path, and the larger root V^+, to a fast path. Given a point on the solution curve, $[Z_1^0, Z_2^0, U^0]$, the direction of the tangent line to the curve at that point is obtained by solving the above sytem, whereby the parameter λ is eliminated,

$$\vec{t} = [\,1,\ \frac{dZ_2}{dZ_1},\ \frac{dU}{dZ_1}\,]$$

where

$$\frac{dZ_2}{dZ_1} = \frac{[F_{23}(F_{31}\text{-}VG_{31}) - F_{33}(F_{21}\text{-}VG_{21})]}{[F_{33}(F_{22}\text{-}VG_{22}) - F_{23}(F_{32}\text{-}VG_{32})]}$$

$$\frac{dU}{dZ_1} = \frac{[(F_{21}\text{-}VG_{21})(F_{32}\text{-}VG_{32}) - (F_{22}\text{-}VG_{22})(F_{31}\text{-}VG_{31})]}{[F_{33}(F_{22}\text{-}VG_{22}) - F_{23}(F_{32}\text{-}VG_{32})]}$$

and for a small displacement ΔZ_1, the adjacent point $[Z_1+\Delta Z_1, Z_2+\Delta Z_2, U+\Delta U]$ is obtained by a first order approximation, where

$$\Delta Z_2 = \frac{dZ_2}{dZ_1}\,\Delta Z_1$$

$$\Delta U = \frac{dU}{dZ_1}\,\Delta Z_1$$

Thus, given the injection composition and injection rate $[Z_1, Z_2, U]$inj, the next point $[Z_1+\Delta Z_1, Z_2+\Delta Z_2, U+\Delta U]$ on the slow path (for $V=V^-$) may be obtained using the above procedure. Similarly the next point $[Z_1+\Delta Z_1, Z_2+\Delta Z_2, U+\Delta U]$ on the fast path ($V=V^+$) may also be determined. For a three-component system, the projections of the slow and fast paths on the composition plane are shown on Figure 1-1.

Figure 1–1
Projections of Composition Routes
on Composition Plane

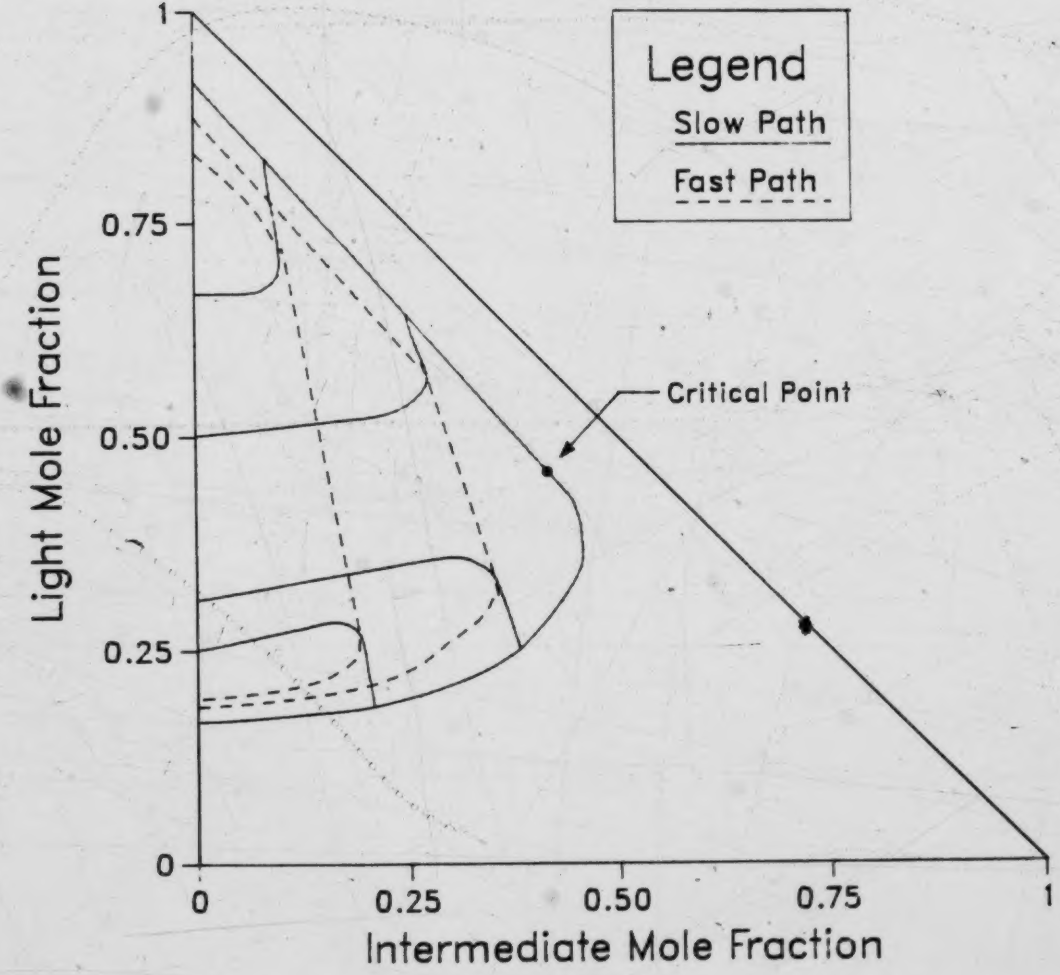

For the solution not to become multiple-valued the composition route, going from the injection point to the production point (see Fig 1-1), must follow a route in the sequence of increasing propagation velocities. Thus, for both cases (condensing or vaporizing gas drive), the composition route must follow the sequence slow to fast path.

Along a slow path or a fast path, it may happen that the propagation rate decreases. For the solution not to become multiple-valued, one must introduce a shock front (a step change in concentration and phase velocity) the shock velocity of which is determined from material balance considerations.

Each point in the two-phase region is at the intersection of a fast and slow path (see Fig 1-1). Each tie-line is composed of two sections of a slow path, separated by a fast path section and at the junction points, V^- is equal to V^+.

1.4.3 Solution Along Tie-line

Along a tie-line, the oil and gas compositions are fixed, only So varies:

X_i, Y_i, ρ_o, ρ_g, Mo and Mg being fixed.

The continuity equations for component i and j $(i \neq j)$ simplifies to (dividing by X_i and X_j):

let $mo = \rho_o / Mo$ and $mg = \rho_g / Mg$

i-component:

$$\frac{1}{\phi}\frac{\partial}{\partial z}\left[U(mof_o + mg(1-f_o)K_i)\right] + \frac{\partial}{\partial t}\left[S_o mo + S_g mgK_i\right] = 0 \tag{1-35}$$

j-component:

$$\frac{1}{\phi}\frac{\partial}{\partial z}\left[U(mof_o + mg(1-f_o)K_j)\right] + \frac{\partial}{\partial t}\left[S_o mo + S_g mgK_j\right] = 0 \tag{1-36}$$

Substracting Equation 1-36 from 1-35 and simplifying, one obtains

$$\frac{1}{\phi}\frac{\partial}{\partial z}\left[\,U(1-f_o)\,\right] + \frac{\partial S_g}{\partial t} = 0 \tag{1-37}$$

Equation 1-35 can also be written as

$$\frac{mo}{\phi}\frac{\partial}{\partial z}\left[\,Uf_o\,\right] + \frac{mg}{\phi}K_i\frac{\partial}{\partial z}\left[\,U(1-f_o)\,\right] + mo\frac{\partial S_o}{\partial t} + mgK_i\frac{\partial S_g}{\partial t} = 0 \tag{1-38}$$

multiplying Equation 1-37 by K_i and substracting it from 1-38 one obtains

$$\frac{1}{\phi}\frac{\partial}{\partial z}[\,Uf_o\,] + \frac{\partial S_o}{\partial t} = 0 \qquad (1\text{-}39)$$

adding Equations 1-37 and 1-39 results in $\partial U/\partial z=0$ (incompressible flow).

Thus, Equation 1-39 can be written as

$$\frac{U}{\phi}\frac{\partial f_o}{\partial z} + \frac{\partial S_o}{\partial t} = 0 \qquad (1\text{-}40)$$

Since U is constant along a tie-line, $f_o=f_o(S_o)$ and Equation 1-40 reduces to the Buckley-Leverett case, with the propagation rate of any saturation S_o given by

$$\left.\frac{dz}{dt}\right|_{S_o} = \frac{U}{\phi}\frac{df_o}{dS_o} \qquad (1\text{-}41)$$

Thus, if the injected gas and in-place oil lie on the dew point curve and bubble point curve, respectively, and if they are linked by the same tie-line, the solution reduces to the Buckley-Leverett case.

1.4.4 Entering or Exiting the Two-phase Region

Since we assume that no dispersion occurs within a phase, we must introduce a shock from the single phase point to the two-phase region. The material balance equation for a shock is derived as follows:

let

Z_i^+, U^+, F_i^+, G_i^+: downstream quantities of the shock

Z_i^-, U^-, F_i^-, G_i^-: upstream quantities of the shock

zs: position of the shock at time t

zs+Δzs: position of the shock at time t+Δt

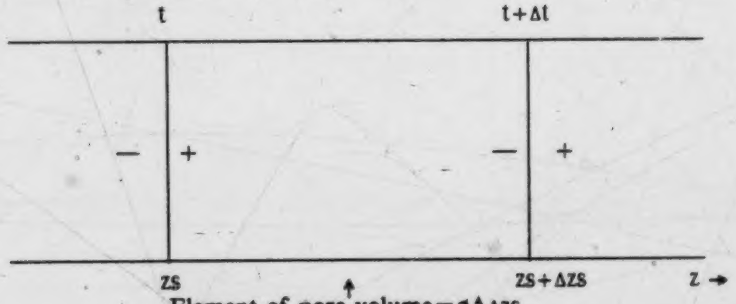

Element of pore volume=øAΔzs

The material balance equation on the above pore volume element can be stated as:

[leaving - entering] volume element over time Δt

+ accumulation in pore volume element over time Δt =0

or

$$[U^+(f_o^+mo^+X_i^+ + (1-f_o^+)mg^+Y_i^+) - U^-(f_o^-mo^-X_i^- + (1-f_o^-)mg^-Y_i^-)]A\Delta t$$
$$+ [(So^-mo^-X_i^- + Sg^-mg^-Y_i^-) - (So^+mo^+X_i^+ + Sg^+mg^+Y_i^+)]\phi A\Delta zs = 0 \qquad (1\text{-}42)$$

or

$$(F_i^+ - F_i^-)\cdot\Delta t + (G_i^+ - G_i^-)\cdot\Delta zs = 0 \quad i=1,3 \qquad (1\text{-}43)$$

Taking the limit as Δt tends to zero, one obtains the propagation rate of the shock wave

$$Vs = \lim_{\Delta t \to 0} \frac{\Delta zs}{\Delta t} = \frac{F_i^+ - F_i^-}{G_i^+ - G_i^-} \quad i=1,3 \qquad (1\text{-}44)$$

defining

$$\gamma = \frac{U}{\phi} f_o mo - VsSomo$$

$$\beta = \frac{U}{\phi}(1-f_o)mg - VsSgmg$$

Equation 1-42 can be written as

$$\gamma^+ X_i^+ + \beta^+ Y_i^+ = \gamma^- X_i^- + \beta^- Y_i^- \quad i=1,3 \qquad (1\text{-}45)$$

Suppose that the upstream phase is a gas, $X_i^-=0$, then

$$\gamma^+ X_i^+ + \beta^+ Y_i^+ = \beta^- Y_i^- \qquad (1\text{-}46)$$

and summation over i gives

$$\gamma^+ + \beta^+ = \beta^- \qquad (1\text{-}47)$$

or

$$\gamma^+[X_i^+ - Y_i^-] + \beta^+[Y_i^+ - Y_i^-] = 0 \rightarrow ([\overrightarrow{X_i^+ - Y_i^-}], [\overrightarrow{Y_i^+ - Y_i^-}] \text{ are linearly dependent}) \qquad (1\text{-}48)$$

Therefore, points (X_i^+, Y_i^+, Y_i^-) lie on the same straight line.

Thus, the landing point in the two-phase region due to the shock (downstream side of the shock) must lie on the tie-line the extension of which passes through injection point Y_i^-.

Using the same arguments, from the two-phase region to the liquid phase region, the exiting point (upstream side of the shock) must lie the tie-line the extension of which passes through the point representing the composition of the in-place oil.

A study of the general topology of the slow and fast paths (see Figure 1-1), shows that in order to follow the sequence slow to fast path, and given the two bounding tie-lines (respectively passing through the injection gas and the in-place oil compositions), the cross-over between the two bounding tie-lines must occur on a slow path for a condensing gas drive and a fast path for a vaporizing gas drive.

1.5 Example Calculations

To calculate the displacement of a three-component gas drive, a program was developed to determine the solution path in the hodograph space that connects the injection gas with the reservoir oil, following the previously outlined procedure. The volumetric and physical properties of the fluids were calculated using the following methods:

a) gas density: using the generalized compressibility chart

b) gas viscosity: Lee et al.[60] method

c) saturated liquid density: COSTALD method[61]

d) undersaturated liquid density: Alani and Kennedy[62] method

e) liquid viscosity: Lohrenz et al.[63] method

The relative permeabilities can be represented by the following parametric equations:

$$K_{rg} = K_{rgm}\left[\frac{S_g}{(1-S_{iw})}\right]^{N_g} \tag{1-49}$$

$$K_{ro} = K_{rom}\left[\frac{(S_o-S_{or})}{(1-S_{iw}-S_{or})}\right]^{N_o} \tag{1-50}$$

The results of an example calculation of a condensing and vaporizing gas drive in a vertical column for the three-component system methane, n-butane and n-decane are shown on Figures 1-2 to 1-7. The input data are summarized in Tables 1-1 and 1-2.

1.5.1 Condensing Gas Drive Case

Figure 1-2 shows the projection of the solution path on the composition plane. The composition route enters the two-phase region on a slow path at point A. It continues along the tie-line up to point B, where the slow path starts to deviate from the tie line. The composition route moves then to point C, the intersection of the slow path and the tie-line through the reservoir oil. At point C the composition changes from a slow path to a fast path. Along this path (bounding tie-line through reservoir oil), the Buckley-Leverett propagation rate is lower than the propagation rate of the slow path at point C. This means that the composition route cannot travel along the fast path and therefore, jumps straight to the composition of the reservoir oil.

The overall composition, total phase velocity and saturation profiles are shown on Figures 1-3 and 1-4. The jump from the injection gas composition to point A on the tie-line gives rise to a shock front called the evaporation front. From point A to B the changes are along the tieline; hence, the total phase velocity remains constant, only the saturation increases. The cross-over between the two bounding tie-lines occurs in a rather narrow zone. At the intersection of the slow and the fast path at point C, a bank is formed where all the variables have constant values. The recovery as a function of pore volumes injected is shown on Figure 1-4.

Table 1-1

Input Data for Condensing Gas Drive

Relative permeability data:

absolute permeability (darcy) = 0.100

maximum oil relative permeability = 0.800

maximum gas relative permeability = 0.800

N_o = oil relative permeability exponent = 3.0

N_g = gas relative permeability exponent = 3.0

irreducible oil saturation = 0.05

irreducible water saturation = 0.20

Reservoir data:

porosity = 0.25

length (m) = 100.0

gravitational acceleration (cm/s^2) = 981.0

angle of dip (rads) = 4.7124

Injection gas composition:

light component mole fraction = 0.840

intermediate component mole fraction = 0.160

In place oil composition:

light component mole fraction = 0.450

intermediate component mole fraction = 0.050

Injection phase velocity (m/day) = 0.450

Injection time (days) = 50.0

Figure 1–2

Condensing Gas Drive Case: Composition Route

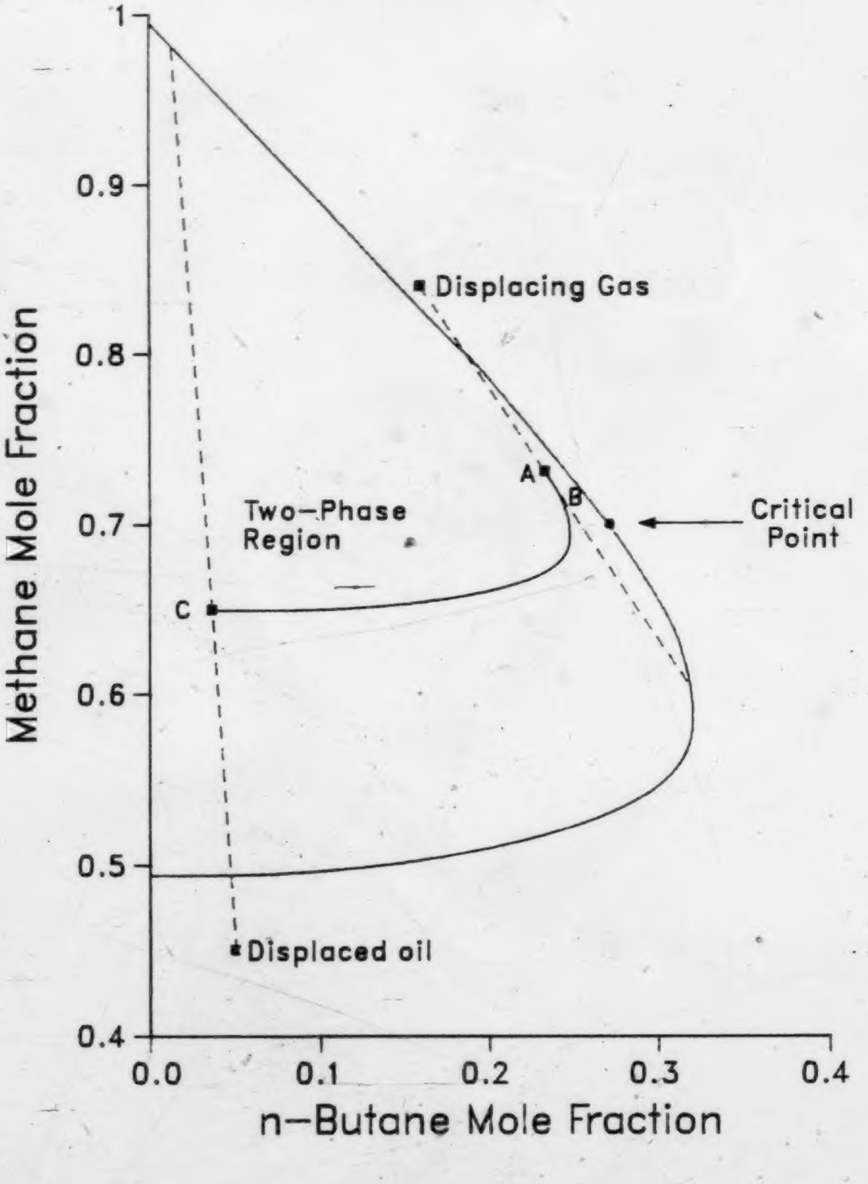

Figure 1–3
Condensing Gas Drive Case:
Phase Composition and Normalized Velocity
vs. Dimensionless Length (at 0.5 Pore Volume Injection)

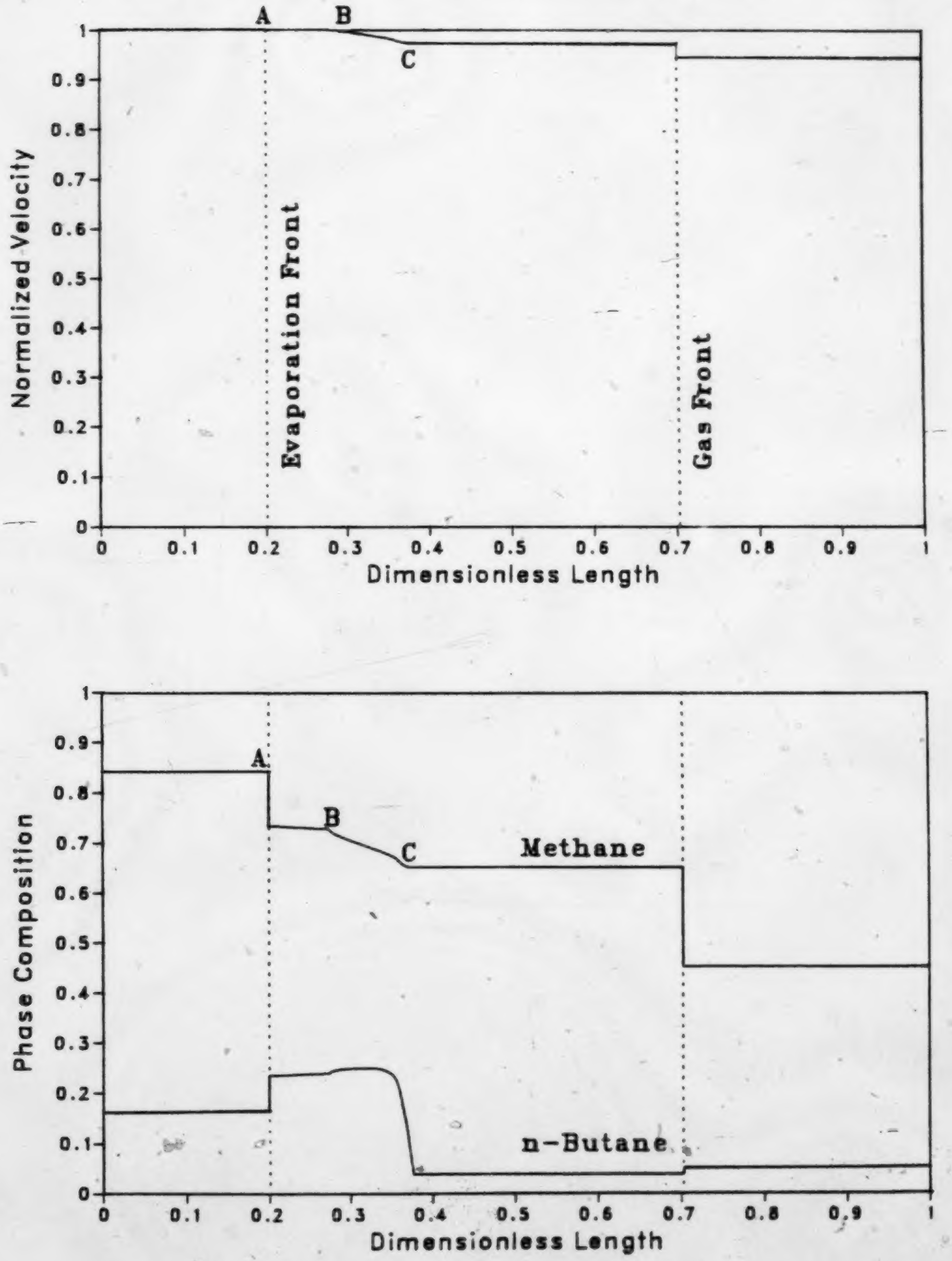

Figure 1–4
Condensing Gas Drive Case:

Oil Saturation vs. Dimensionless Length
(at 0.5 Pore Volume Injection)

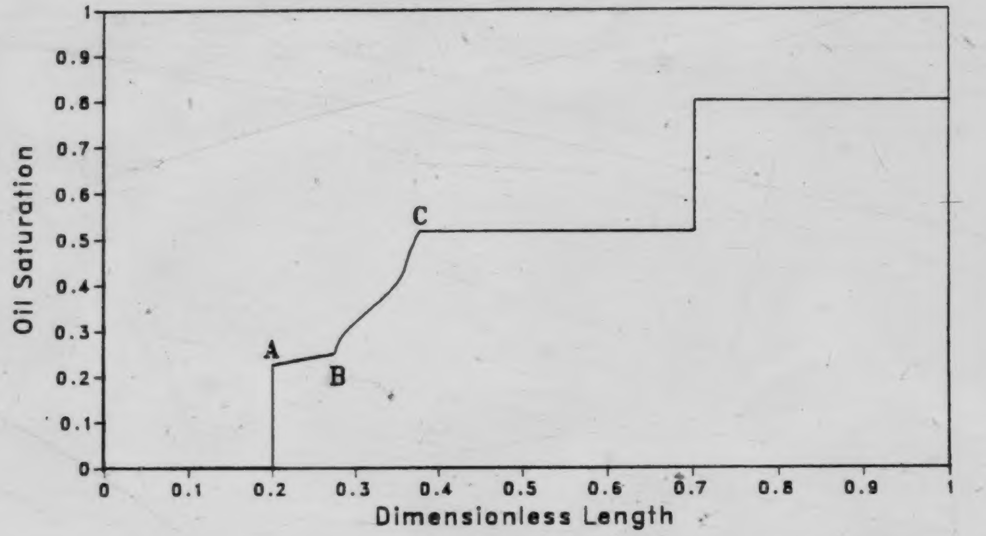

% Recovery of In–Place n–Decane
vs. Pore Volume Injection

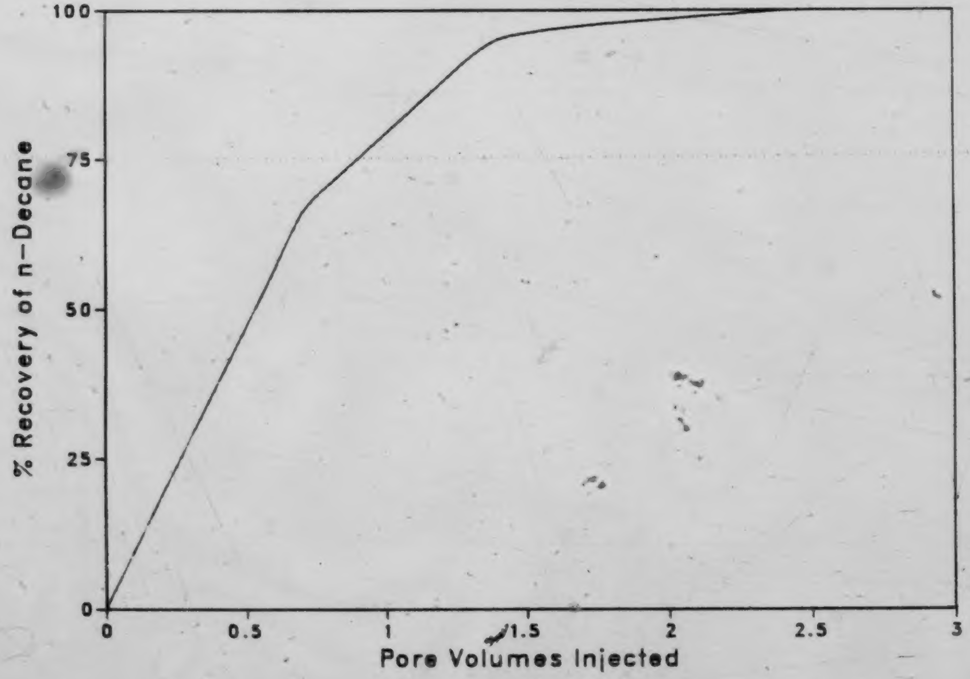

1.5.2 Vaporizing Gas Drive Case

In this case the production rate was specified, and the solution path was obtained starting from the production point to the injection point, thus working backwards. Figure 1-5 shows the projection of the solution path on the composition plane. The composition route jumps from the injection gas composition to the slow path point A. At point A the composition route changes to a fast path that, by extension, goes through the reservoir oil. Because of this change, a bank is formed. Since the velocities along the fast path between A and B decrease, the composition route jumps straight to B, which gives rise to another shock front. Hence, the cross-over between the bounding tie-lines occurs, in this case, over an interval of zero width. From point B to C the composition route travels along the tie-line with oil saturation as the only changing variable (see Figures 1-6 and 1-7). At point C the composition route jumps to the reservoir oil composition which also results in a shock front. The recovery as a function of pore volumes injected is shown on Figure 1-7. Note that recovery after breakthrough is much lower than for the condensing gas drive case. This may be due to the closer proximity of the two bounding tie-lines, which results in less mass transfer between the co-currently flowing oil and gas phases. Also, it may be observed that the evaporation front of the condensing gas drive travels at a faster rate than that of the vaporizing gas drive.

Table 1-2

Input Data for Vaporizing Gas Drive

Relative permeability data:

absolute permeability (darcy) = 0.100

maximum oil relative permeability = 0.800

maximum gas relative permeability = 0.800

N_o = oil relative permeability exponent = 3.0

N_g = gas relative permeability exponent = 3.0

irreducible oil saturation = 0.05

irreducible water saturation = 0.20

Reservoir data:

porosity = 0.25

length (m) = 100.0

gravitational acceleration (cm/s^2) = 981.0

angle of dip (rads) = 4.7124

Injection gas composition:

light component mole fraction = 0.990

intermediate component mole fraction = 0.010

In place oil composition:

light component mole fraction = 0.450

intermediate component mole fraction = 0.300

Production phase velocity (m/day) = 0.450

Production time (days) = 50.0

Figure 1–5

Vaporizing Gas Drive Case: Composition Route

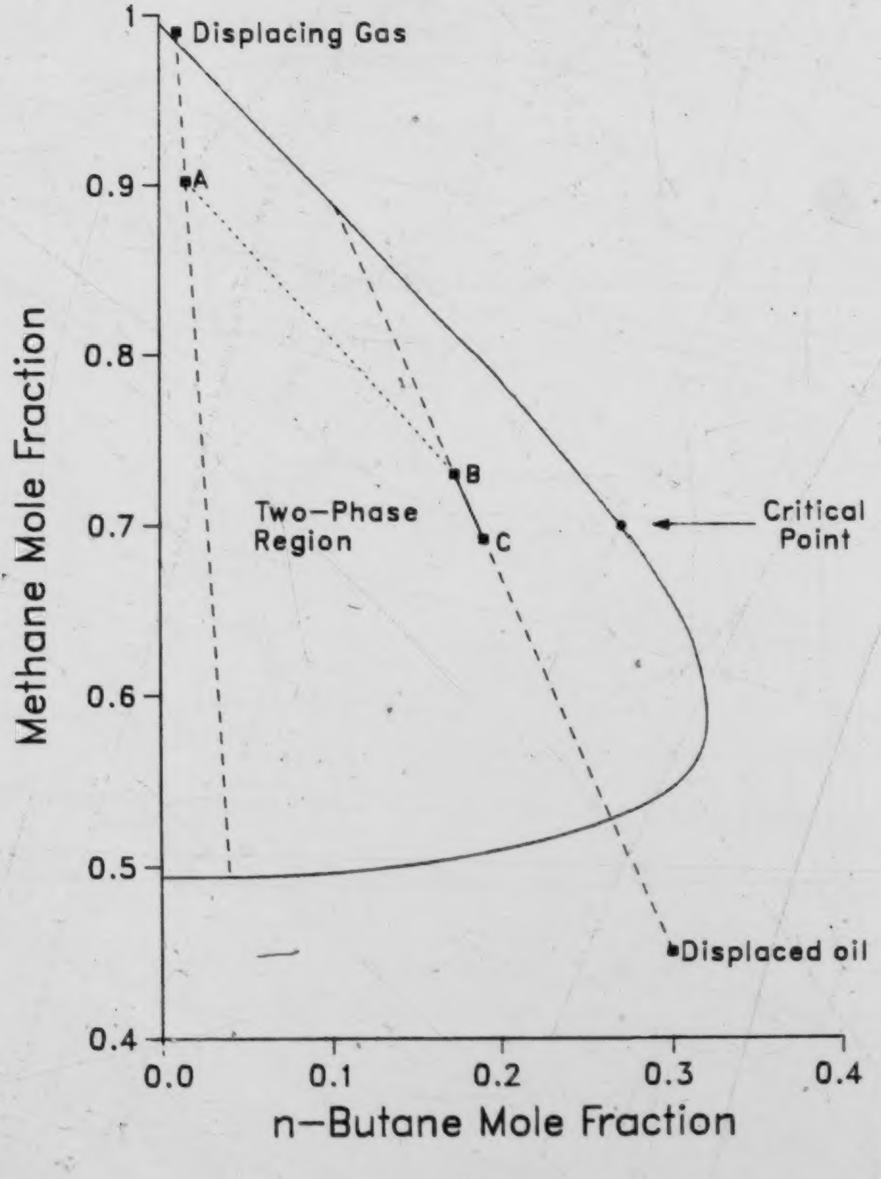

Figure 1–6
Vaporizing Gas Drive Case:
Phase Composition and Normalized Velocity
vs. Dimensionless Length (at 0.5 Pore Volume Injection)

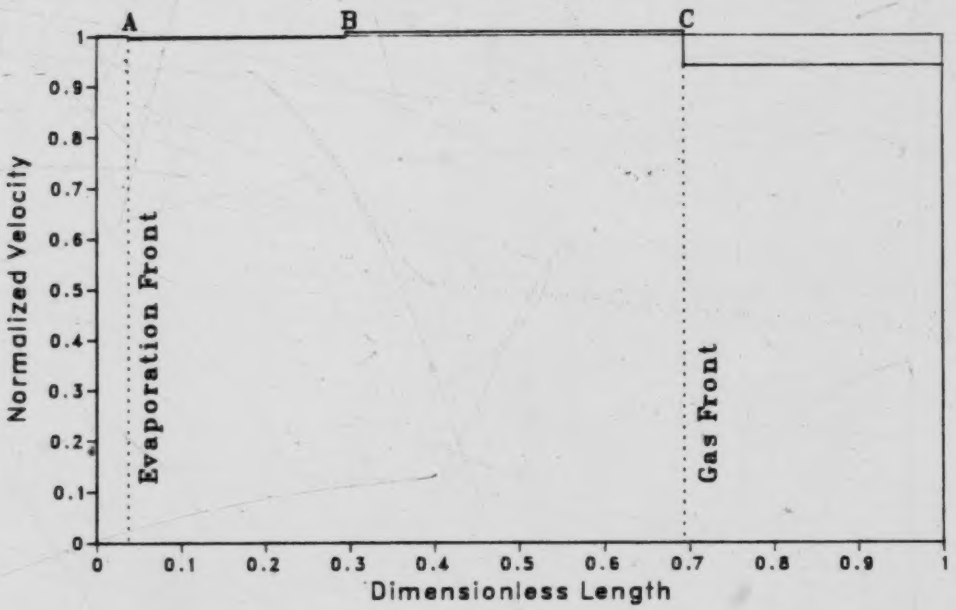

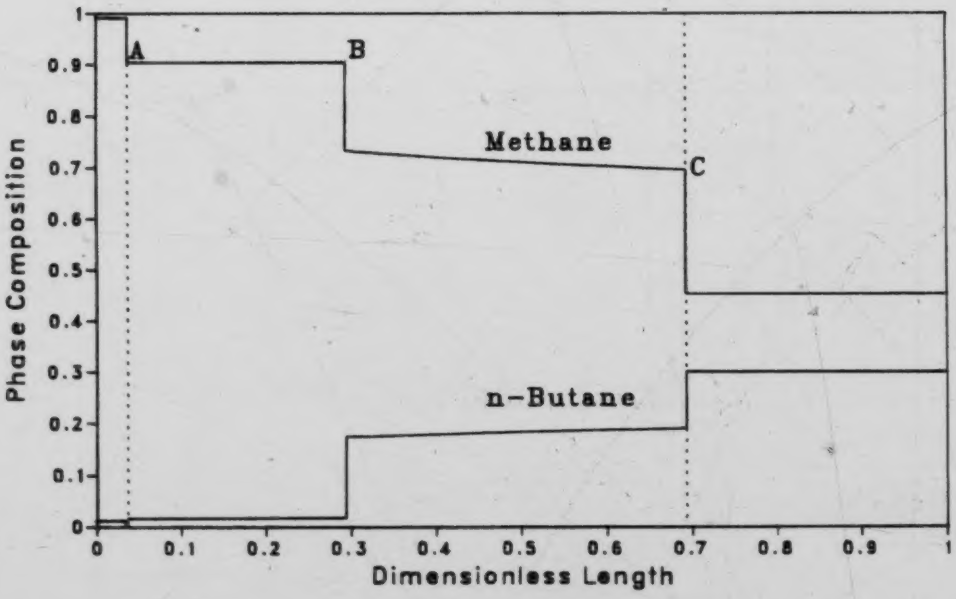

Figure 1–7
Vaporizing Gas Drive Case:

Oil Saturation vs. Dimensionless Length
(at 0.5 Pore Volume Injection)

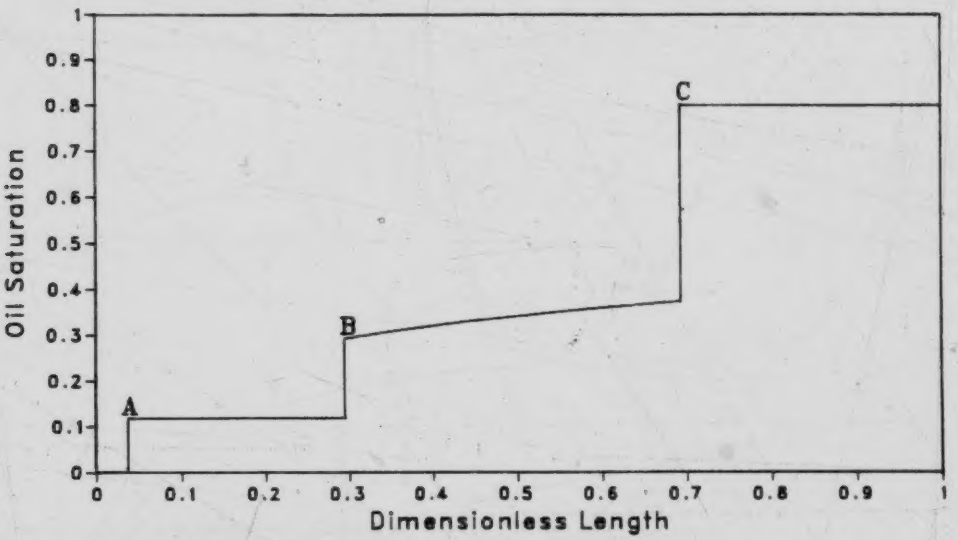

% Recovery of In–Place n–Decane
vs. Pore Volume Injection

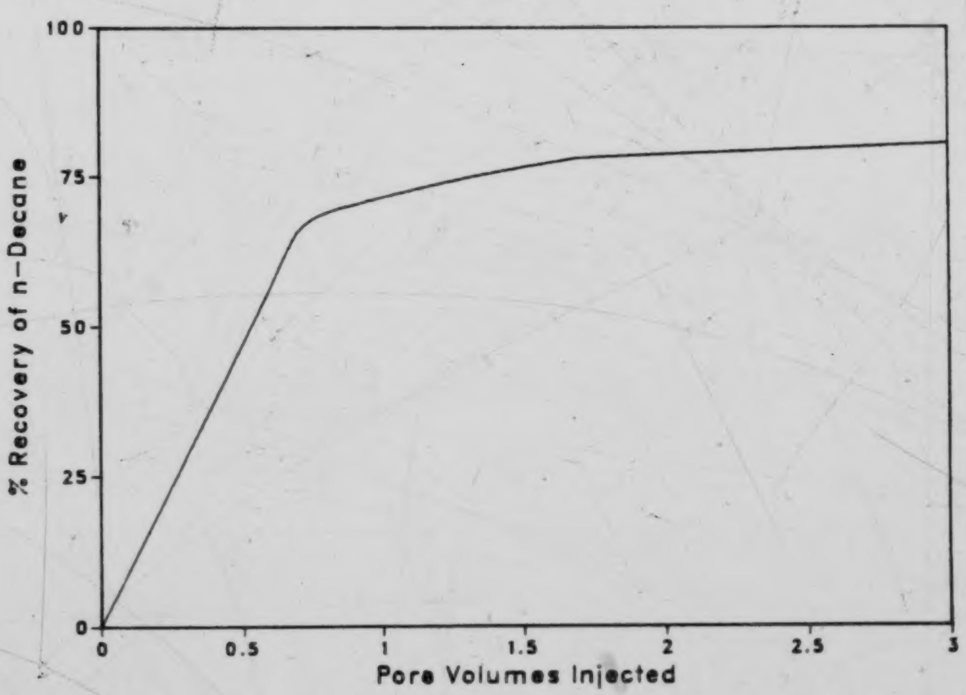

Appendix 2

Properties of Extensive Variables

2.1 Introduction

In the following, for the purposes of clarity, the dependent variable and the functional relationship relating it to the independent variables will be designated by different symbols. Furthermore, since the systems of interest are multicomponent systems at fixed pressure and temperature, the latter variables (P and T) will be omitted in the functional relationship. Although the results presented herein may be extented to other extensive variables[1], the discussion will be restricted to the case of the Gibbs free energy.

2.2 Properties of Homogeneous Functions

Let the Gibbs free energy, G, of an n-component system containing $N_1, N_2 \ldots, N_n$ moles of components $1,2,\ldots,n$ at some fixed pressure and temperature, be given by the following functional relationship:

$$G = F(N_1,N_2,\ldots,N_n)$$

Since G is an extensive variable, the function F is a homogeneous function of degree 1, having the following property:

for any positive λ,

$$F(\lambda N_1,\lambda N_2,\ldots,\lambda N_n) = \lambda \cdot F(N_1,N_2,\ldots,N_n) = \Phi(\lambda,N_1,N_2,\ldots,N_n)$$

where Φ, represents the functional relationship between the variables $\lambda, N_1, N_2, \ldots, N_n$. Using the above property, one may obtain the following results by direct differentiation (Euler's theorem)

$$\frac{\partial \Phi}{\partial \lambda} = F(N_1,N_2,\ldots,N_n) = \sum_{i=1}^{n} N_i \frac{\partial F}{\partial \lambda N_i} (\lambda N_1,\lambda N_2,\ldots,\lambda N_n) \qquad (2\text{-}1)$$

and

$$\frac{\partial \Phi}{\partial N_i} = \lambda \frac{\partial F}{\partial N_i} = \lambda \frac{\partial F}{\partial \lambda N_i} \qquad (2\text{-}2)$$

where Equation 2-2 implies that

$$\frac{\partial F}{\partial N_i} (N_1,N_2,\ldots,N_n) = \frac{\partial F}{\partial \lambda N_i} (\lambda N_1,\lambda N_2,\ldots,\lambda N_n) \qquad (2\text{-}3)$$

Substituting Equation 2-3 into Equation 2-1, one obtains an expression for the Gibbs free energy in terms of the chemical potentials

$$G = F(N_1,N_2,\ldots,N_n) = \sum_{i=1}^{n} N_i \frac{\partial F}{\partial N_i} = \sum_{i=1}^{n} N_i \mu_i \qquad (2\text{-}4)$$

where

$$\mu_i = \frac{\partial F}{\partial N_i}$$

In particular, for $\lambda = 1/N$, where N is the total number of moles present in the system, one obtains the molar Gibbs free energy, g,

$$g = \frac{G}{N} = F(\frac{N_1}{N}, \frac{N_2}{N}, \ldots, \frac{N_n}{N})$$

and defining the mole fraction X_i by

$$X_i = \frac{N_i}{N} \quad \text{and} \quad \sum_{i=1}^{n} X_i = 1$$

and using the relationship 2-3 for $\lambda = 1/N$, one obtains

$$\mu_i = \frac{\partial F}{\partial N_i}(N_1,N_2,\ldots,N_n) = \frac{\partial F}{\partial X_i}(X_1,X_2,\ldots,X_n) \qquad (2\text{-}5)$$

Since only n-1 variables between the quantities X_i are independent, one may obtain a functional relationship in terms of $X_1,X_2,\ldots,X_{n-1}$ for the molar Gibbs free energy

$$g = F(X_1,X_2,\ldots,X_{n-1}, X_n = 1 - \sum_{i=1}^{n-1} X_i) = f(X_1,X_2,\ldots,X_{n-1}) \qquad (2\text{-}6)$$

and from Equation 2-4

$$g = \sum_{i=1}^{n} X_i \mu_i \qquad (2\text{-}7)$$

Furthermore, a relationship exists between the partial derivatives of the Gibbs free energy and its molar counterpart

$$g_i = \frac{\partial f}{\partial X_i} = \frac{\partial F}{\partial X_i} + \frac{\partial F}{\partial X_n}\frac{\partial X_n}{\partial X_i} = \frac{\partial F}{\partial X_i} - \frac{\partial F}{\partial X_n} \qquad i=1,n-1$$

or, using the relationship 2-5

$$g_i = \mu_i - \mu_n \qquad i=1,n-1 \qquad (2\text{-}8)$$

Equation 2-7 may also be written as follows

$$g = \sum_{i=1}^{n} X_i \mu_i = \sum_{i=1}^{n-1} X_i \mu_i + X_n \mu_n = \sum_{i=1}^{n-1} X_i \mu_i + (1 - \sum_{i=1}^{n-1} X_i)\mu_n$$

or

$$g = \mu_n + \sum_{i=1}^{n-1} X_i(\mu_i - \mu_n)$$

and substituting Equation 2-8, one obtains the following result

$$g = \mu_n + \sum_{i=1}^{n-1} X_i g_i$$

or

$$\mu_n = g - \sum_{i=1}^{n-1} X_i g_i \tag{2-9}$$

2.3 Properties of the Gibbs Surface in the Heterogeneous Region

Let the Gibbs surface be the hypersurface represented by the functional relationship, $g=f(Z_1,Z_2,...,Z_{n-1})$, which relates the molar Gibbs free energy, g, to the composition of an n-component system given by the mole fractions $Z_1,Z_2,..,Z_{n-1}$ of the components 1,2,...,n-1, at some fixed pressure and temperature. Consider now a mixture $(Z_1{}^m,Z_2{}^m,...,Z_{n-1}{}^m)$ of the above system which results in a coexistence of a liquid phase of composition $(X_1,X_2,...,X_{n-1})$ and a vapor phase of composition $(Y_1,Y_2,...,Y_{n-1})$ at equilibrium. The phases in equilibrium must satisfy the criteria of equality of the chemical potential of each component in each phase:

$$\mu_i{}^l = \mu_i{}^v \qquad i=1,n$$

where μ_i refers to the chemical potential of component i and superscripts l and v refer respectively to the liquid and vapor phases of the system considered.

Using the results of Equation 2-8, it follows that

$$g_i^l = g_i^v \qquad i=1,n-1 \tag{2-10}$$

Since the chemical potentials of component n in the liquid and vapor phases are equal, one obtains the following equality using Equation 2-9

$$g^l - \sum_{i=1}^{n-1} X_i g_i^l = g^v - \sum_{i=1}^{n-1} Y_i g_i^v \tag{2-11}$$

where g^l and g^v refer respectively to the molar Gibbs free energy of the liquid and vapor phases.

The tangent plane to the Gibbs surface at the point $(X_1,X_2,...,X_{n-1},g^l)$ representing the liquid phase is given by

$$(g - g^l) - \sum_{i=1}^{n-1} (Z_i - X_i) g_i^l = 0 \tag{2-12}$$

Substituting Equation 2-10 into Equation 2-11, the following is obtained

$$(g^v - g^l) - \sum_{i=1}^{n-1} (Y_i - X_i) g_i^l = 0 \qquad (2\text{-}13)$$

The result given in Equation 2-13 shows, therefore, that the point $(Y_1, Y_2, \ldots, Y_{n-1}, g^v)$ representing the vapor phase on the Gibbs surface satisfies Equation 2-12. Hence, the point representing the vapor phase belongs to the plane tangent to the Gibbs surface at the point representing the liquid phase. Furthermore, as a consequence of the relationship given in Equation 2-11, this plane is also tangent to the Gibbs surface at the point representing the vapor phase. One may also show that the point $(Z_1^m, Z_2^m, \ldots, Z_{n-1}^m, g^m)$ representing the overall system on the Gibbs surface belongs necessarily to the above double-tangent plane. Let nl be the liquid mole fraction of the overall system, the molar Gibbs free energy of the overall system is given by

$$g^m = nl \cdot g^l + (1-nl) g^v$$

and from material balance,

$$Z_i^m = nl \cdot X_i + (1-nl) Y_i \qquad i=1,n-1$$

Substituting the expressions of g^m and Z_i^m into the left hand side of Equation 2-12, one obtains

$$(g^m - g^l) - \sum_{i=1}^{n-1} (Z_i^m - X_i) g_i^l = (g^v - g^l) - \sum_{i=1}^{n-1} (Y_i - X_i) g_i^l + nl[(g^l - g^v) - \sum_{i=1}^{n-1} (X_i - Y_i) g_i^l]$$

and using Equations 2-12 and 2-13 one obtains that

$$(g^m - g^l) - \sum_{i=1}^{n-1} (Z_i^m - X_i) g_i^l = 0 \qquad (2\text{-}14)$$

The result shown in Equation 2-14 shows, therefore, that the point $(Z_1^m, Z_2^m, \ldots, Z_{n-1}^m, g^m)$ representing the overall system on the Gibbs surface satisfies Equation 2-12. Hence, the point representing the overall system belongs also to the double-tangent plane to the Gibbs surface at the points representing the liquid and vapor phases in equilibrium.

Appendix 3

Stability Analysis of Homogeneous Phases

The criteria that need to be satisfied by locally stable systems are considered herein. The systems of interest are multicomponent systems, at constant pressure and temperature, representing the homogeneous portion of the primitive Gibbs surface. It was shown, in Appendix 2, that the molar Gibbs free energy of an n-component sytem composed of species 1,2,.. and n may be expressed as

$$g = \mu_n + \sum_{i=1}^{n-1} X_i g_i \tag{3-1}$$

where g_i is the partial derivative of the molar Gibbs free energy with respect to the mole fraction of species i, and μ_n is the chemical potential of component n.

As stated before, the equilibrium criterion requires that the Gibbs surface be above its tangent plane at a point representing a homogeneous system (refer to section 5.2). Consider such a system and its representation on the Gibbs surface given by a point of coordinates $(X_1, X_2, \ldots, X_{n-1}, g)$. To inquire whether the system is stable, one only needs to apply the above criterion with respect to any other adjacent stable phase[5], as follows

$$g - \sum_{i=1}^{n-1} X_i g_i - \mu_n = 0 \tag{3-2}$$

and

$$g' - \sum_{i=1}^{n-1} X_i' g_i - \mu_n > 0 \tag{3-3}$$

where the superscript (') refers to the adjacent phase. The inequality (3-3) expresses the condition that the Gibbs surface be above its tangent plane at the point representing the considered system. This relationship (using Equation 3-2) may be simplified to

$$(g'-g) - \sum_{i=1}^{n-1} (X_i'-X_i) g_i > 0 \tag{3-4}$$

The reciprocal is also true, meaning that if the system considered is stable, than any other stable phase (indicated by the superscript ') must satisfy the following

$$(g-g') - \sum_{i=1}^{n-1} (X_i-X_i') g_i' > 0 \tag{3-5}$$

and the following relationship is obtained by adding expressions 3-4 and 3-5

$$\sum_{i=1}^{n-1} \Delta X_i \Delta g_i > 0 \qquad (3\text{-}6)$$

where

$$\Delta X_i = X_i' - X_i$$

$$\Delta g_i = g_i' - g_i$$

If one fixes the values of $X_2, X_3, \ldots, X_{n-1}$, equation 3-6 becomes

$$\Delta X_1 \Delta g_1 > 0$$

and dividing by ΔX_1^2 and taking the limit as ΔX_1 tends to zero, one obtains

$$\frac{\partial^2 g}{\partial X_1^2} \Big| X_2, \ldots, X_{n-1} > 0 \qquad (3\text{-}7)$$

Interchanging the rôles played by components 1,2... and n-1, one also obtains that

$$\frac{\partial^2 g}{\partial X_i^2} \Big| X_j > 0 \quad j \neq i \qquad (3\text{-}8)$$

Similarly, if one fixes the values of g_1, $X_3, \ldots, X_{n-1}$, one obtains

$$\frac{\partial^2 g}{\partial X_2^2} \Big| g_1, X_3, \ldots, X_{n-1} > 0 \qquad (3\text{-}9)$$

The following relationships may also be obtained by fixing respectively $(g_1, g_2, X_4, \ldots, X_{n-1})$, ..., $(g_1, g_2, \ldots, g_{n-2})$

$$\frac{\partial^2 g}{\partial X_3^2} \Big| g_1, g_2, X_4, \ldots, X_{n-1} > 0$$

$$\vdots$$

$$\frac{\partial^2 g}{\partial X_{n-1}^2} \Big| g_1, g_2, \ldots, g_{n-2} > 0 \qquad (3\text{-}10)$$

Similar results may also be obtained by interchanging the roles played by components 1 to n-1.

Considering $X_1, X_2, \ldots X_{n-1}$ as the independent variables, one obtains the following set of equations in the neighborhood of a system at fixed pressure and temperature

$$dg_1 = g_{11} dX_1 + \ldots + g_{1,n-1} dX_{n-1}$$

$$\vdots$$

$$dg_{n-1} = g_{n-1,1} dX_1 + \ldots + g_{n-1,n-1} dX_{n-1} \qquad (3\text{-}11)$$

where the general term g_{ij} is the second partial derivative of the molar Gibbs free energy with respect to X_i and X_j.

If variations of the system are considered while keeping $g_1, g_2, \ldots, g_{n-2}$ constant, one obtains

$$U_{n-2} dg_{n-1} = U_{n-1} dX_{n-1} \tag{3-12}$$

where U_{n-1} is given by the following determinant:

$$U_{n-1} = \begin{vmatrix} g_{11} & g_{1j} & g_{1,n-1} \\ \vdots & \vdots & \vdots \\ g_{i1} & g_{ij} & g_{i,n-1} \\ \vdots & \vdots & \vdots \\ g_{n-1,1} & g_{n-1,j} & g_{n-1,n-1} \end{vmatrix}$$

and U_{n-2} is the determinant obtained by eliminating the last row and last column of the above determinant U_{n-1}, or

$$\lambda_1 = \frac{\partial^2 g}{\partial X_{n-1}^2} \Big|_{g_1, g_2, \ldots, g_{n-2}} = \frac{U_{n-1}}{U_{n-2}}$$

Similarly, one obtains the following general results

$$\lambda_2 = \frac{\partial^2 g}{\partial X_{n-2}^2} \Big|_{g_1, g_2, \ldots, g_{n-3}, X_{n-1}} = \frac{U_{n-2}}{U_{n-3}}$$

$$\vdots$$

$$\lambda_{n-1} = \frac{\partial^2 g}{\partial X_2^2} \Big|_{g_1, X_3, \ldots, X_{n-1}} = \frac{U_2}{U_1}$$

where U_{n-j} is the determinant obtained by eliminating the last j rows and columns of the determinant U_{n-1}, and

$$U_{n-1} = \lambda_1 \cdot \lambda_2 \cdots \lambda_{n-1}$$

Using the relationships 3-7 through 3-10, the following must be satisfied by a stable system

$$U_1 > 0 \qquad \frac{U_1}{U_2} > 0 \qquad \frac{U_2}{U_3} > 0 \quad \ldots \quad \frac{U_{n-2}}{U_{n-1}} > 0$$

or

$$U_1 > 0 \qquad U_2 > 0 \quad \ldots \quad U_{n-1} > 0$$

One may also show that all the other principal minors of the determinant U_{n-1} are also positive by interchanging the roles played by subscripts 1 to n-1. Therefore, one may conclude that for a system to be locally stable, the determinant U_{n-1} as well as all its principal minors must be positive.

Appendix 4

Gibbs Free Energy From Soave-Redlich and Kwong Equation of State and Related Partial Derivatives

4.1 Molar Gibbs Free Energy From SRK EOS[2]

The construction of the molar Gibbs free energy using a pressure explicit equation of state may be expressed as

$$g(T,P,X_i) = A(T,v,X_i) + Pv \tag{4-1}$$

where the molar Helmholtz free energy (A) is given by

$$A(T,v,X_i) = \int_{\infty}^{v} [\frac{RT}{v} - P]dv - RTLn(\frac{v}{RT}) + \sum_i X_i A_i^{*} + RT\sum_i X_i Ln X_i \tag{4-2}$$

Substituting the expression for P given by the SRK EOS[2] (Equation 52) and carrying out the integration, one obtains

$$A(T,v,X_i) = RTLn(\frac{v}{v-b}) + \frac{a}{b}(\frac{v}{v+b}) - RTLn(\frac{v}{RT}) + \sum_i X_i A_i^{*} + RT\sum_i X_i Ln X_i \tag{4-3}$$

where b and a (Equations 53 and 54) are given by

$$b = \sum_i\sum_j X_i X_j b_{ij}, \quad b_{ij} = \frac{b_i + b_j}{2} \tag{4-3-a}$$

and

$$a = \sum_i\sum_j X_i X_j a_{ij}, \quad a_{ij} = \sqrt{a_i a_j}\cdot(1-\delta_{ij}) \tag{4-3-b}$$

One may note that for the specific case where $b_{ij} = (b_i + b_j)/2$, the expression for b simplifies to

$$b = \sum_i X_i b_i \tag{4-3-c}$$

4.2 Partial Derivatives of the Molar Gibbs Free Energy

The expression for the molar Gibbs free energy, obtained upon substitution of Equation 4-3 into Equation 4-1, is implicit in pressure through the variable v. Moreover, the independent variables of the function g are $T, P, X_1, X_2, \ldots X_{n-1}$ ($X_n = 1 - X_1 - X_2 - \ldots X_{n-1}$), where n is the number of components. The first partial derivative of the molar Gibbs free energy with respect to the mole fraction X_i ($i=1,n-1$) is given by

$$\frac{\partial g}{\partial X_i} = \frac{\partial A}{\partial X_i} + \frac{\partial A}{\partial v}\frac{\partial v}{\partial X_i} + P\frac{\partial v}{\partial X_i} \tag{4-4}$$

where $\frac{\partial A}{\partial v} = -P$ (4-4-a)

and $\frac{\partial v}{\partial X_i} = -\frac{\partial P}{\partial X_i}/\frac{\partial P}{\partial v}$ (4-4-b)

Substituting Equations 4-4-a and 4-4-b into Equation 4-4, the expression for the first partial derivative simplifies to

$$\frac{\partial g}{\partial X_i} = \frac{\partial A}{\partial X_i} \tag{4-5}$$

The second partial derivative of the molar Gibbs free energy with respect to the mole fractions X_i and X_j ($i=1,n-1$, $j=1,n-1$) is given by

$$\begin{aligned}\frac{\partial^2 g}{\partial X_i \partial X_j} &= \frac{\partial^2 A}{\partial X_i \partial X_j} + \frac{\partial^2 A}{\partial X_i \partial v}\frac{\partial v}{\partial X_j} \\ &= \frac{\partial^2 A}{\partial X_i \partial X_j} - \frac{\partial P}{\partial X_i}\frac{\partial v}{\partial X_j} \\ &= \frac{\partial^2 A}{\partial X_i \partial X_j} + \frac{\partial P}{\partial X_i}\frac{\partial P}{\partial X_j}/\frac{\partial P}{\partial v}\end{aligned} \tag{4-6}$$

Using Equations 4-3 and 52, one obtains the following expressions for the partial derivatives of the molar Helmholtz free energy and pressure

$$\frac{\partial A}{\partial X_i} = \beta_i\frac{RT}{(v-b)} + \alpha_i \mathrm{Ln}(\frac{v}{v+b}) + \frac{\gamma_i}{(v+b)} + A_i^{\bullet} + RT\mathrm{Ln}(\frac{X_i}{X_n}) \quad i=1,n-1 \tag{4-7}$$

$$\frac{\partial^2 A}{\partial X_i \partial X_j} = \beta_{ij}\frac{RT}{(v-b)^2} + \alpha_{ij}\mathrm{Ln}(\frac{v}{v+b}) + \frac{\gamma_{ij}}{(v+b)} + \frac{\theta_{ij}}{(v+b)^2} + RT(\frac{\epsilon_{ij} X_n + X_i}{X_i X_n}) \quad i=1,n-1 \; j=1,n-1 \tag{4-8}$$

$$\frac{\partial P}{\partial X_i} = \beta_i\frac{RT}{(v-b)^2} - \frac{1}{v(v+b)}[\xi_i - \frac{a\beta_i}{v+b}] \quad i=1,n-1 \tag{4-9}$$

$$\frac{\partial P}{\partial v} = -\frac{RT}{(v-b)^2} + \frac{a}{v(v+b)}[\frac{1}{v} + \frac{1}{v+b}] \tag{4-10}$$

where

$$X_n = 1 - \sum_{i=1}^{n-1} X_i$$

$$\beta_i = b_i - b_n$$

$$\alpha_i = w_i - w_n$$

$$\gamma_i = w(b_n - b_i)$$

$$\xi_i = u_i - u_n$$

$$\beta_{ij} = b_i b_j - b_i b_n - b_j b_n + b_n b_n$$

$$\alpha_{ij} = w_{ij} - w_{in} - w_{jn} + w_{nn}$$

$$\gamma_{ij} = -[w_i b_j + w_j b_i - b_n (w_i + w_j) - w_n (b_i + b_j) + 2 w_n b_n]$$

$$\theta_{ij} = w \beta_{ij}$$

$$\epsilon_{ij} = 1 \ (i=j)$$

$$\epsilon_{ij} = 0 \ (i \neq j)$$

and

$$u_i = 2 \sum_{r=1}^{n} X_r a_{ir}$$

$$w = a/b$$

$$w_i = \frac{u_i}{b} - \frac{w b_i}{b}$$

$$w_{ij} = (2a_{ij} - w_i b_j - w_j b_i)/b$$

Appendix 5

A New Equation of State for Pure Components

The use of equations of state has taken an ever increasing role in the prediction of phase behavior and fluid properties. Among them, the SRK[2] and PR[20] equations of state have gained popularity in chemical and petroleum engineering. These equations of state consist of modifications of the attractive term of the van der Waals equation which was made temperature dependent. However, Henderson[64] has shown that the major weakness of these empirical equations of state is the retaining of the van der Waals free volume term $(v-b)^{-1}$ for the representation of the repulsive forces which was shown to be inadequate in the dense fluid region. Henderson[64] suggested the use of the $v^3/(v-b)^4$ term which is a good approximation to the hard sphere fluid. Following the above suggestion, an attempt was made to develop a relatively simple equation in order to improve the representation of the dense fluid region, as well as the critical compressibility (Zc) of pure components. Initially the term $v^3/(v-b)^4$ was considered. However, the replacement of the above repulsive term by $v^5/(v-b)^6$ allowed a better correlation of the characteristic parameters of a pure fluid in terms of the reduced temperature. For a pure fluid, the equation developed in this study is given by

$$P = RT\frac{V^5}{(V-b)^6} - \frac{1}{(V+b)^2}\left(a + \frac{c}{V^2} + \frac{d}{V^3} + \frac{e}{V^4}\right) \tag{5-1}$$

where the parameters a, b, c, d and e are characteristic of a given fluid and are expressed in terms of the critical properties and reduced temperature as follows:

1. for subcritical temperatures, Tr ≤ 1:

$$b = Bc(Zc \cdot RTc/Pc)$$

$$a = Ac(Zc \cdot RTc/Pc)^2[1 + A1(1-Tr) + A2(1-Tr)^2] \cdot Pc$$

$$c = Cc(Zc \cdot RTc/Pc)^4[1 + A1(1-Tr) + A2(1-Tr)^2] \cdot Pc$$

$$d = Dc(Zc \cdot RTc/Pc)^5[1 + A1(1-Tr) + A2(1-Tr)^2] \cdot Pc$$

$$e = Ec(Zc \cdot RTc/Pc)^6[1 + A3(1-Tr)] \cdot Pc \tag{5-2}$$

2. for supercritical temperatures, $Tr \geq 1$:

$$b=Bc(Zc{\cdot}RTc/Pc)$$

$$a=Ac(Zc{\cdot}RTc/Pc)^2[1+AV1(1-Tr)+AV2(1-Tr)^2]{\cdot}Pc$$

$$c=Cc(Zc{\cdot}RTc/Pc)^4[1+AV3(1-Tr)]{\cdot}Pc$$

$$d=Dc(Zc{\cdot}RTc/Pc)^3[1+AV4(1-Tr)]{\cdot}Pc$$

$$e=Ec(Zc{\cdot}RTc/Pc)^6{\cdot}Pc \qquad (5\text{-}3)$$

Equation 5-1 was constrained to the critical point conditions:

$$\left(\frac{\partial P}{\partial V}\right)_{Tc} = 0$$

$$\left(\frac{\partial^2 P}{\partial V^2}\right)_{Tc} = 0$$

and

$$Zc = Zc(\text{experimental}) \qquad (5\text{-}4)$$

Satisfying the conditions given by Equations 5-4 results in the following expressions for Cc, Dc and Ec in terms of parameters Ac and Bc

$$Cc = 6Y1 - 4Y2 + Y3 - 6Ac$$

$$Dc = -8Y1 + 7Y2 - 2Y3 + 8Ac$$

$$Ec = 3Y1 - 3Y2 + Y3 - 3Ac$$

where

$$Y1 = T1$$

$$Y2 = (T2 - 2T1)/(1+Bc)$$

$$Y3 = (T1 - 2T2 + T3)/(1+Bc)^2$$

and

$$T1 = (1+Bc)^3/(1+Bc)^6/Zc - (1+Bc)^2$$

$$T2 = [6/(1-Bc)^7 - 5/(1-Bc)^6]{\cdot}(1+Bc)^3/Zc$$

$$T3 = [10/(1-Bc)^6 - 30/(1-Bc)^7 + 21/(1+Bc)^8]{\cdot}(1+Bc)^4/Zc$$

For subcritical temperatures, the parameters Bc, A1, A2 and A3 for normal alkanes (C1 to C16) were correlated as a function of the acentric factor ω, and are given by:

$$Bc = 0.0750$$

$$A1 = C11 + C12\omega + C13\omega^2 + C14\omega^3$$

$$A2 = C21 + C22\omega + C23\omega^2 + C24\omega^3$$

$$A3 = C31 + C32\omega + C33\omega^2 + C34\omega^3$$

where

C11 = 0.1375442 C21 = 0.1954498 C31 = 0.03490
C12 = 0.9635242 C22 = -0.0575359 C32 = 0.10965
C13 = 0.1886594 C23 = 1.3482324 C33 = 2.55142
C14 = -0.4096685 C24 = -1.7412168 C34 = -2.85363

For supercritical temperatures, the parameters AV1, AV2, AV3 and AV4 for methane to n-pentane, for which experimental data is available, are given by:

Component	AV1	AV2	AV3	AV4
methane	0.1945	0.0169	0.5552	0.3635
ethane	0.2677	-0.0181	0.6831	0.4525
propane	0.3671	-0.0007	0.9572	0.6183
n-butane	0.4074	0.0278	0.9332	0.6018
n-pentane	0.5351	2.0417	0.8938	0.6200

The parameter Ac, the acentric coefficient ω and the critical pressure (Pc), critical temperature (Tc) and critical compressibility (Zc) for the above normal alkanes are listed in Table 5-1. The acentric factors of methane to n-butane were obtained from Goodwin[65-68], while for the other n-alkanes the values were taken from Passut and Danner[73].

Nitrogen was the only non-hydrocarbon component considered in this study. The parameters for nitrogen are given by:

Bc=0.0750
Ac=5.76004 AV1=0.23773 Pc=3399.9 kPa
A1=0.17669 AV2=0.02945 Tc=126.80 K
A2=0.22807 AV3=0.50129 Zc=0.28910
A3=0.04419 AV4=0.34891

Table 5-1

Acentric Coefficients and Critical Properties

Component	ω	Pc,kPa	Tc,K	Zc	Ac	Source
methane	0.0105	4598.8	190.55	0.29027	5.70000	65
ethane	0.0991	4871.4	305.33	0.28220	5.99194	66
propane	0.1523	4247.5	369.85	0.27625	6.21813	67
n-butane	0.1991	3796.0	425.16	0.27394	6.30368	68
n-pentane	0.2530	3374.0	469.77	0.26863	6.51901	69
n-hexane	0.2957	3031.0	507.85	0.26390	6.70413	70
n-heptane	0.3506	2736.0	540.16	0.25975	6.87716	70
n-octane	0.3942	2496.0	569.35	0.25630	7.02354	70
n-nonane	0.4437	2288.0	595.15	0.25127	7.25250	70
n-decane	0.4840	2117.0	619.15	0.24792	7.40709	70
n-undecane	0.5349	1945.0	640.15	0.24101	7.70890	70
n-dodecane	0.5666	1813.0	659.15	0.23775	7.91946	70
n-tridecane	0.6340	1720.0	677.15	0.23467	8.11323	70
n-tetradecane	0.6797	1620.0	695.15	0.23168	8.30872	70
n-pentadecane	0.7060	1510.0	710.15	0.22634	8.62758	70
n-hexadecane	0.7418	1420.0	725.15	0.22221	8.91808	70

In Table 5-2, the calculated pressure is compared with the experimental value for nitrogen and methane to n-decane. Comparing pressures instead of volumes for the given reduced temperature range results in a much harder test, especially in the dense fluid region whereby a slight decrease in volume is accompanied by a large increase in pressure. For nitrogen and methane to n-pentane, the AAD between calculated and experimental data is less than 5%, which is in good agreement considering that a good portion of the data points were in the dense fluid region. The good quantitative agreement is better illustrated in Figures 5-1 to 5-6, where various isotherms are shown on the Pr vs. Vr diagram. Only the dense fluid region was experimentally investigated for n-hexane to n-decane. A larger deviation is observed between calculated and experimental data for these components. As it is shown in Figures 5-7 to 5-11, the isotherms become almost vertical in the dense fluid region, which puts a very hard constraint on any equation of state. A study of Figures 5-7 to 5-11 shows clearly that if the volumes were compared, instead of pressures, a much better agreement would have resulted.

The comparison between calculated and experimental saturated properties is shown in Table 5-3. It may be observed that the vapor pressures and saturated liquid and vapor volumes are well represented by Equation 5-1. The saturated liquid and vapor branches are also shown in Figures 5-1 to 5-11 as well as the experimental data points. Also, the calculated vapor pressures (Pr^S vs. Tr) are graphically compared with the experimental data points in Figure 5-12 for various components.

For the components considered, it appears then that a good representation of the PVT and saturated properties is obtained using Equation 5-1. However, additional work is necessary for the development of appropriate mixing rules for its application to mixtures, as well as extensive testing and comparison with experimental data. It is anticipated that liquid densities of mixtures (dense fluid region) will be well represented by Equation 5-1, which is much needed in reservoir engineering calculations.

Table 5-2

Comparison Between Calculated and Experimental PVT Data

Component	Tr range	Pr range	AAD%	Source
nitrogen	0.62-2.20	0.01-20	3.90	72
methane	0.63-2.62	0.02-15	1.81	65
ethane	0.59-1.96	0.01-15	2.02	66
propane	0.65-1.89	0.02-17	2.63	67
n-butane	0.66-1.65	0.02-19	2.35	68
n-pentane	0.66-1.09	0.03-20	4.76	49
n-hexane	0.61-1.01	0.40-23	3.86	73
n-heptane	0.46-0.97	1.80-18	6.18	70
n-octane	0.65-0.97	0.80- 8	11.98	70
n-nonane	0.52-0.86	0.60-30	8.71	74
n-decane	0.50-0.83	0.00-32	17.30	49

Table 5-3

Comparison Between Calculated and Experimental Saturated Properties

Component	Tr range	AAD% Vapor pressure	AAD% Saturated liquid volume	AAD% Saturated vapor volume	Source
nitrogen	0.53-0.97	0.62	0.35	0.71	72
methane	0.50-0.99	0.59	0.45	1.23	65
ethane	0.49-0.98	0.75	0.26	1.37	66
propane	0.50-0.99	0.76	0.46	1.67	67
n-butane	0.52-0.99	0.74	0.33	1.58	68
n-pentane	0.58-0.97	0.93	0.50	2.50	49
n-hexane	0.54-0.97	0.76	0.55	3.80	70
n-heptane	0.50-0.99	0.90	0.53	3.25	70
n-octane	0.48-0.97	1.08	0.94	5.82	70
n-nonane	0.46-0.85	0.73	0.25	-	70
n-decane	0.47-0.83	0.65	0.52	-	49
n-dodecane	0.47-0.72	1.68	0.75	-	70
n-tridecane	0.51-0.74	0.98	1.07	-	70
n-tetradecane	0.57-0.75	0.59	0.53	-	70
n-pentadecane	0.58-0.76	0.90	0.55	-	70
n-hexadecane	0.64-0.76	1.07	0.25	-	70

Figure 5–1
Comparison of PVT Data: Methane

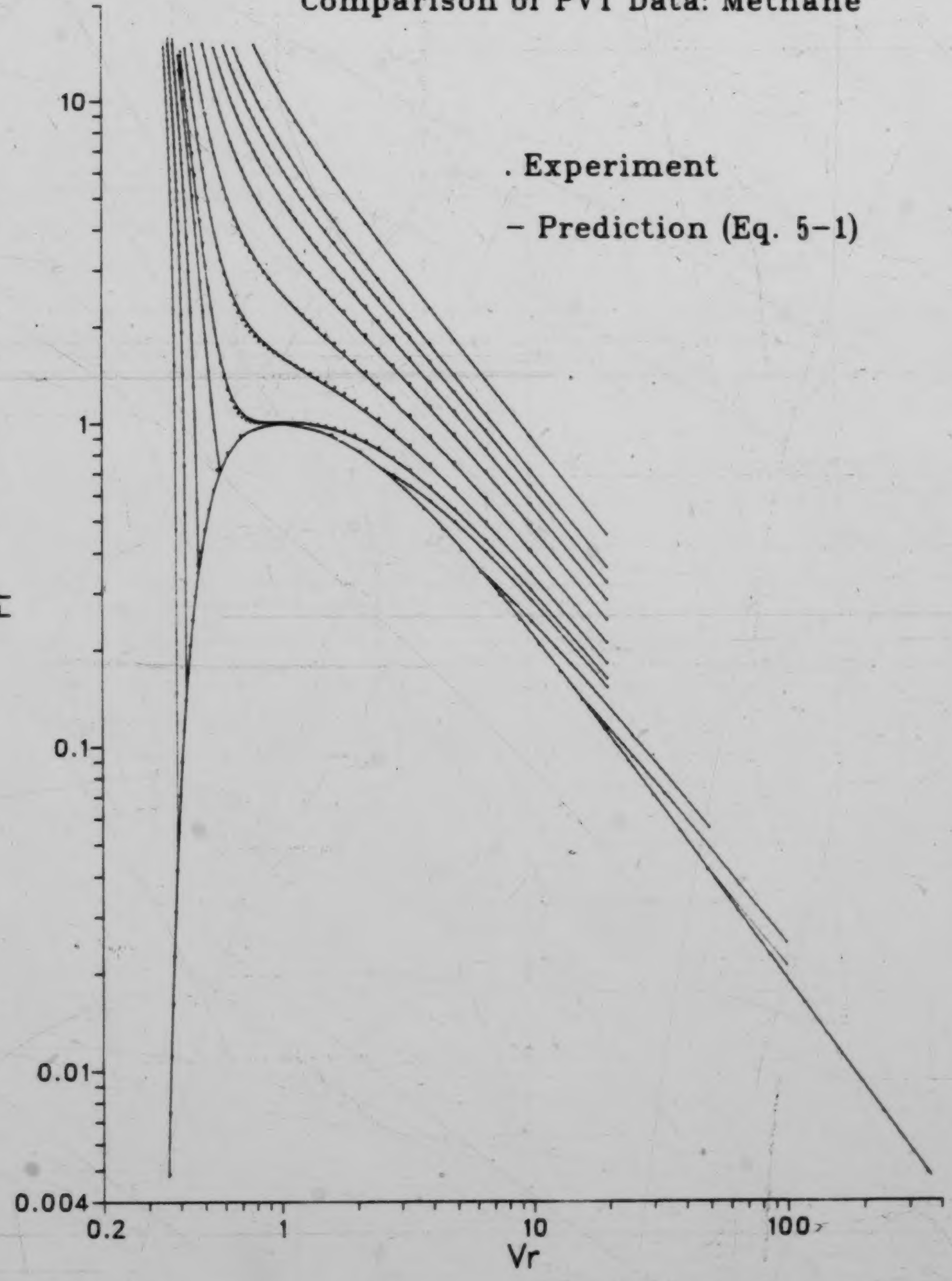

Figure 5-2

Comparison of PVT Data: Nitrogen

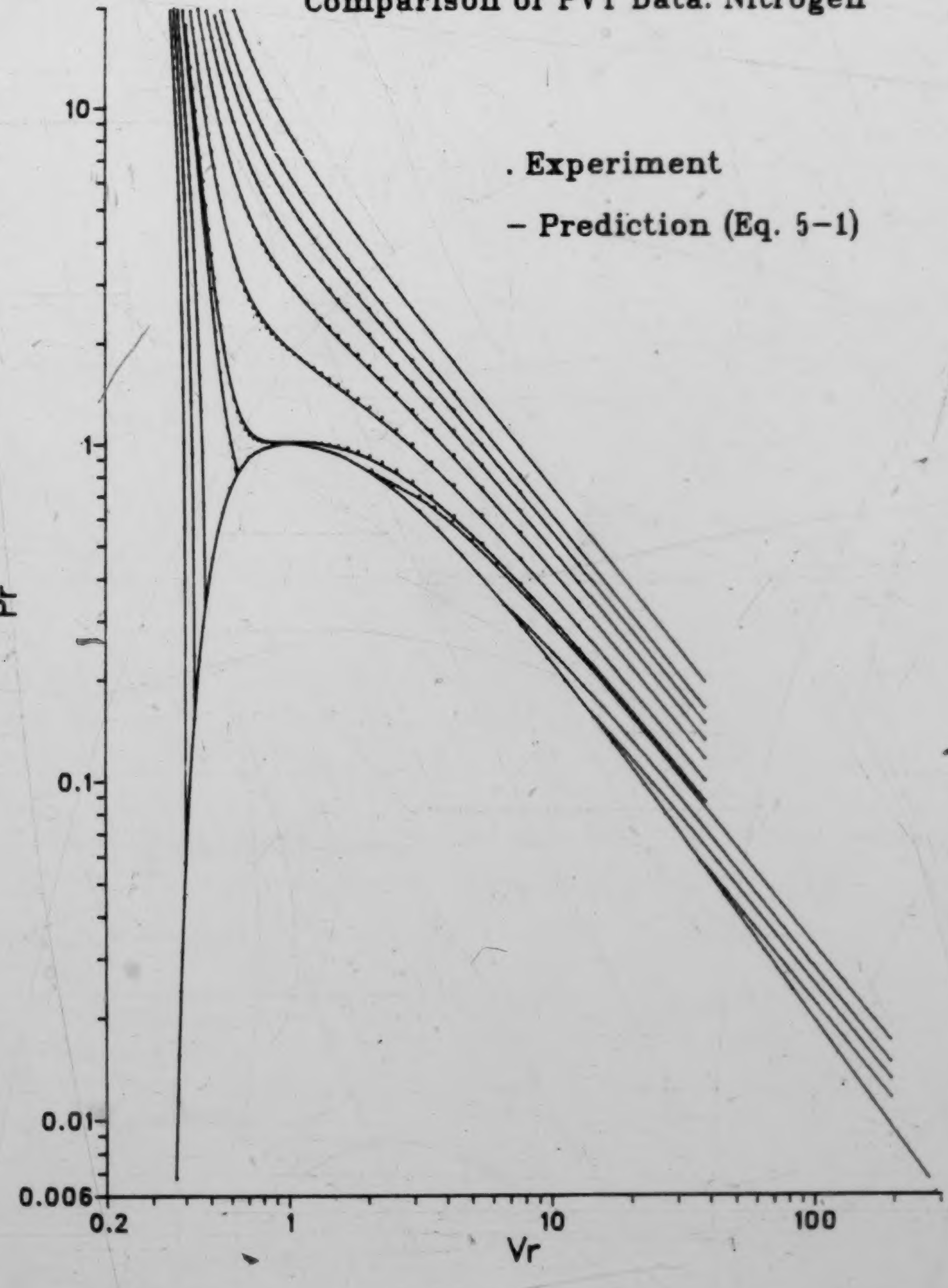

Figure 5-3
Comparison of PVT Data: Ethane

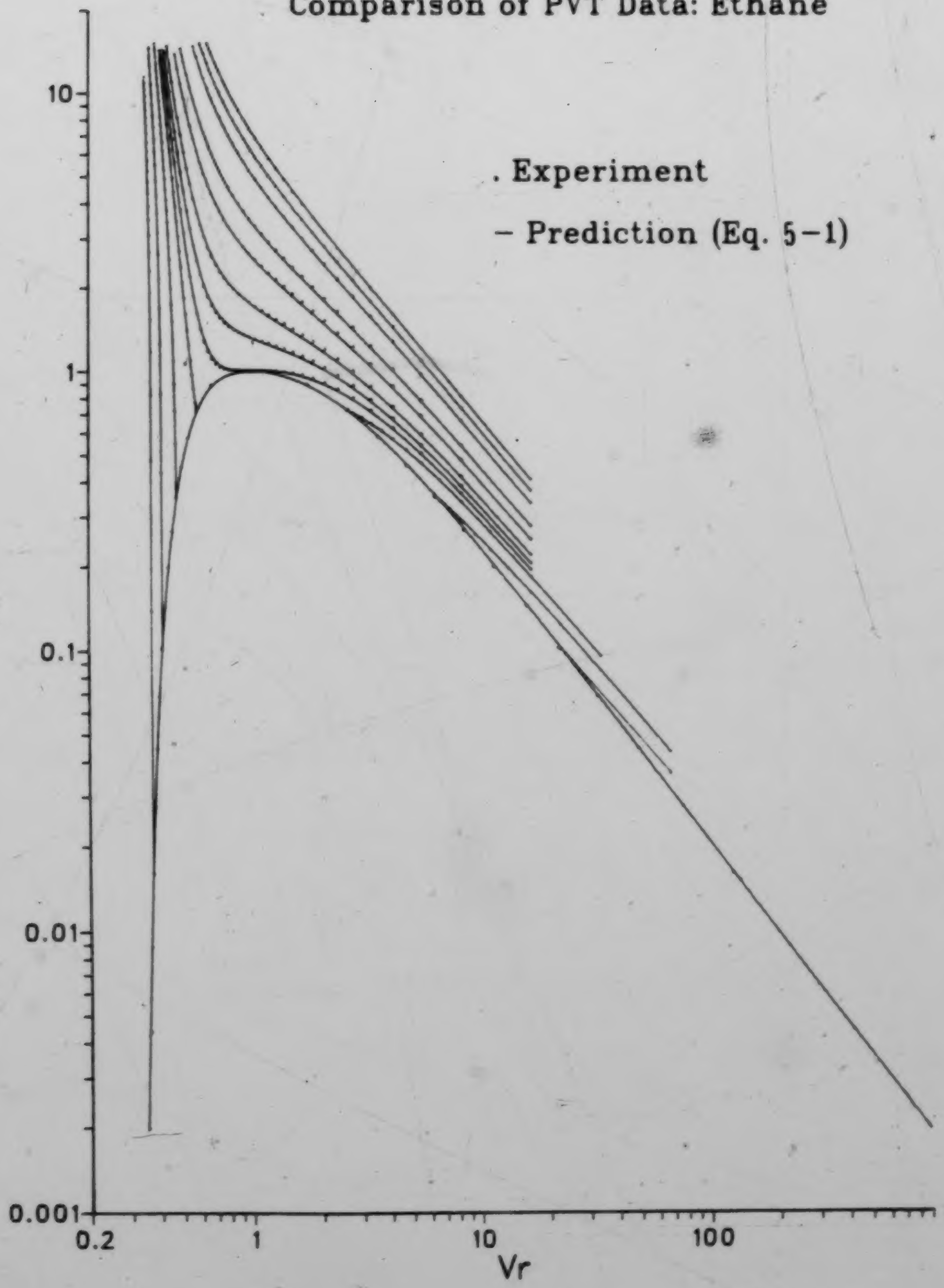

Figure 5-4
Comparison of PVT Data: Propane

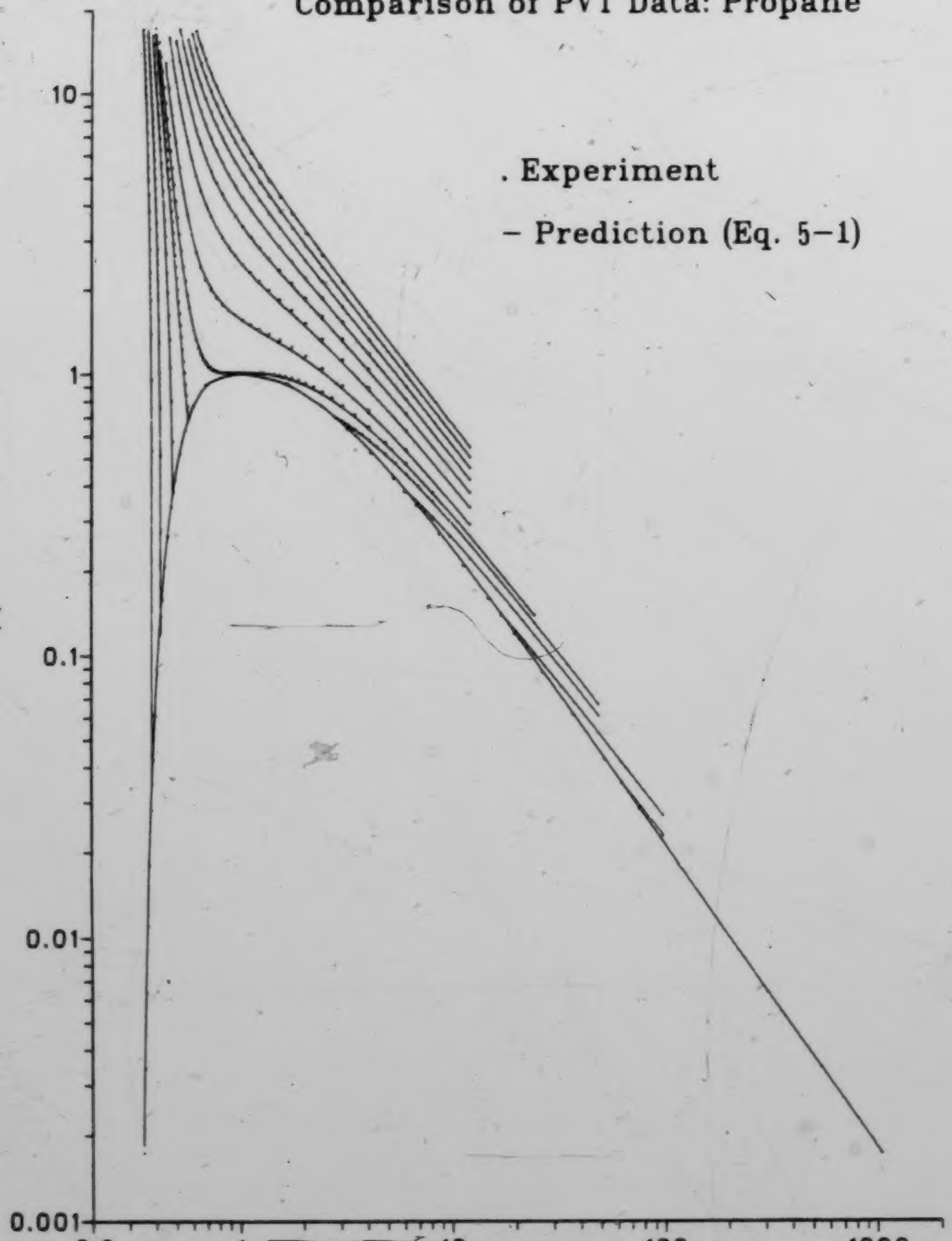

Figure 5–5
Comparison of PVT Data: n–Butane

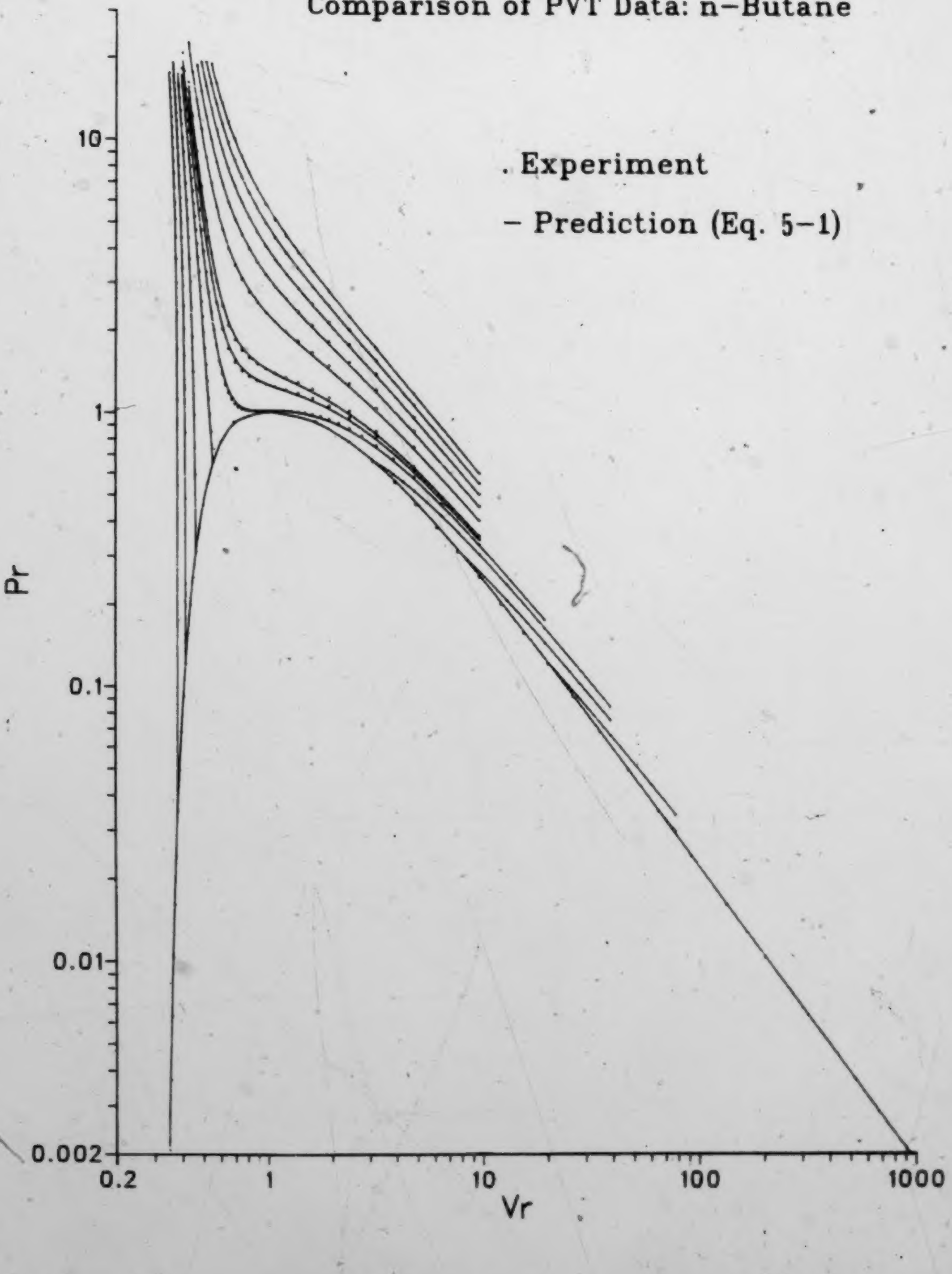

Figure 5-6
Comparison of PVT Data: n-Pentane

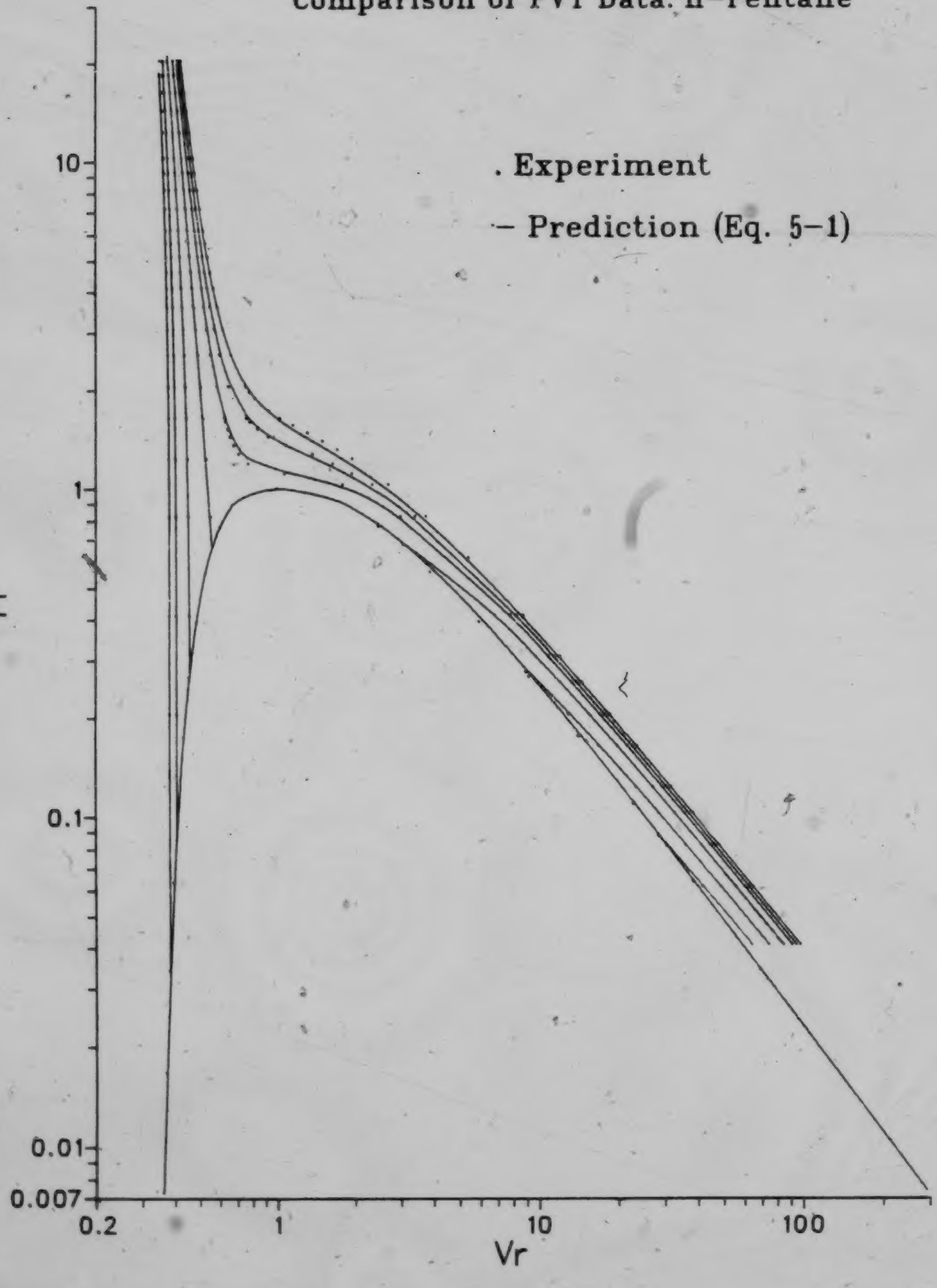

Figure 5-7
Comparison of PVT Data: n-Hexane

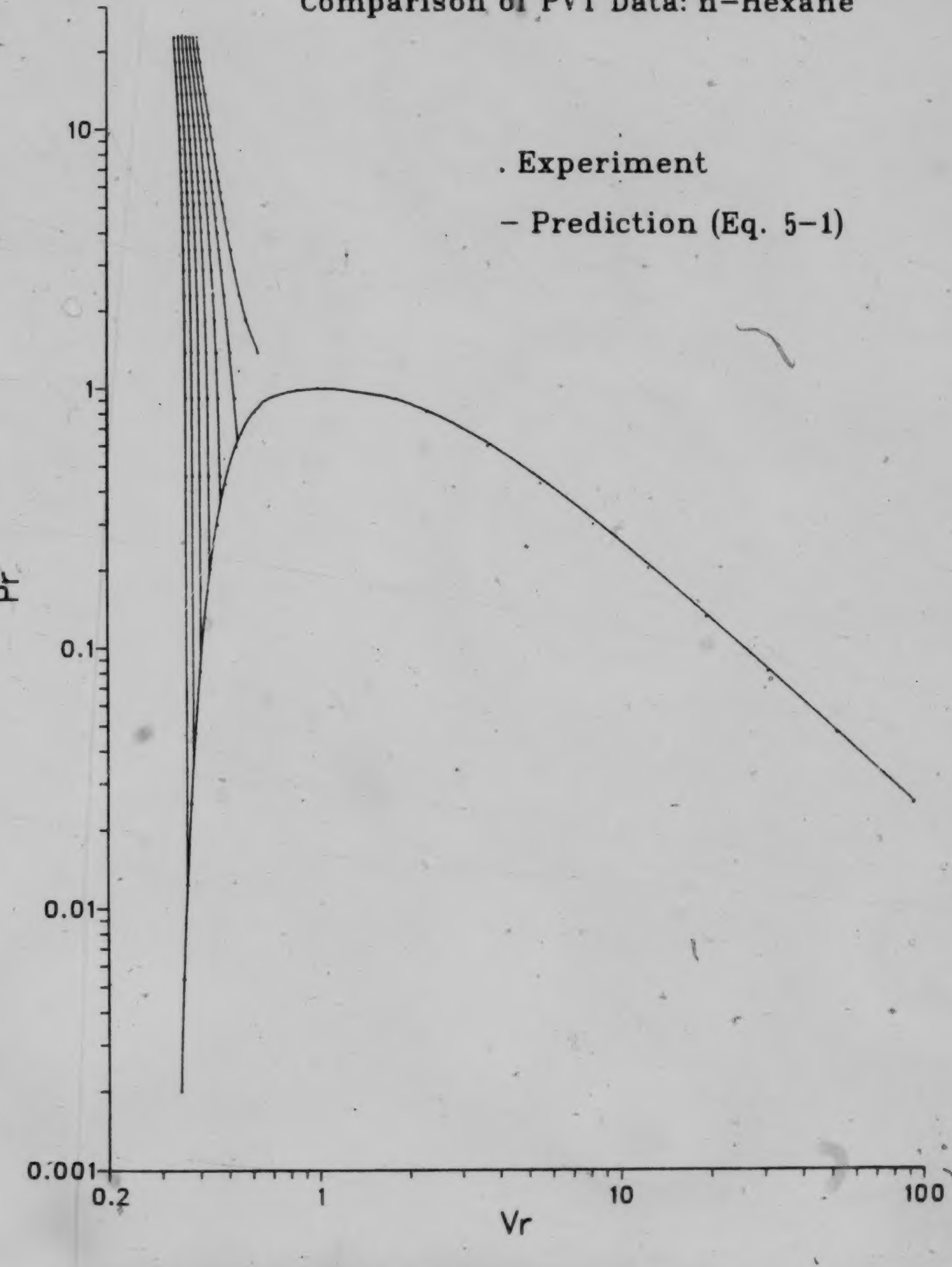

Figure 5-8
Comparison of PVT Data: n-Heptane

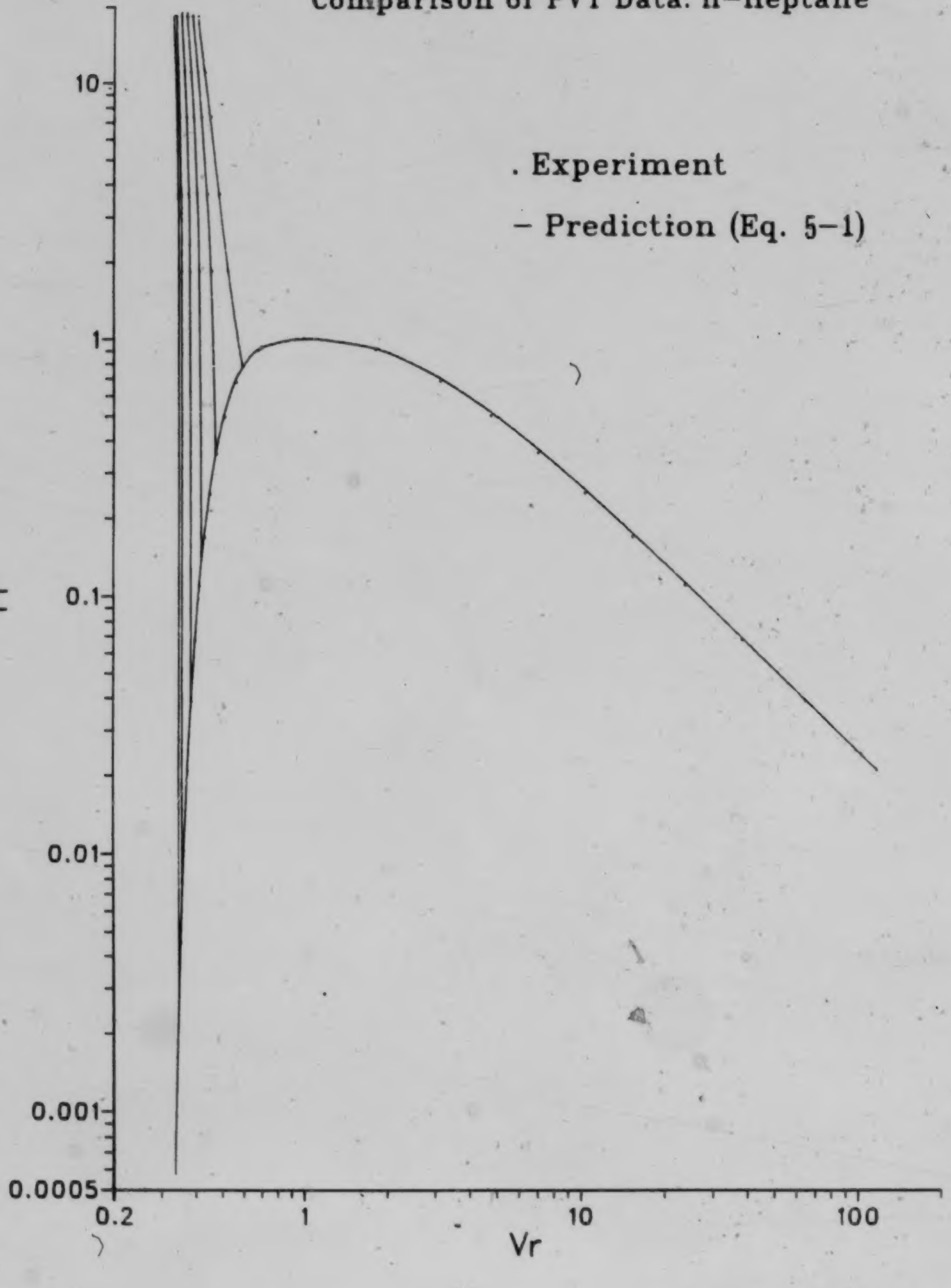

Figure 5-9
Comparison of PVT Data: n-Octane

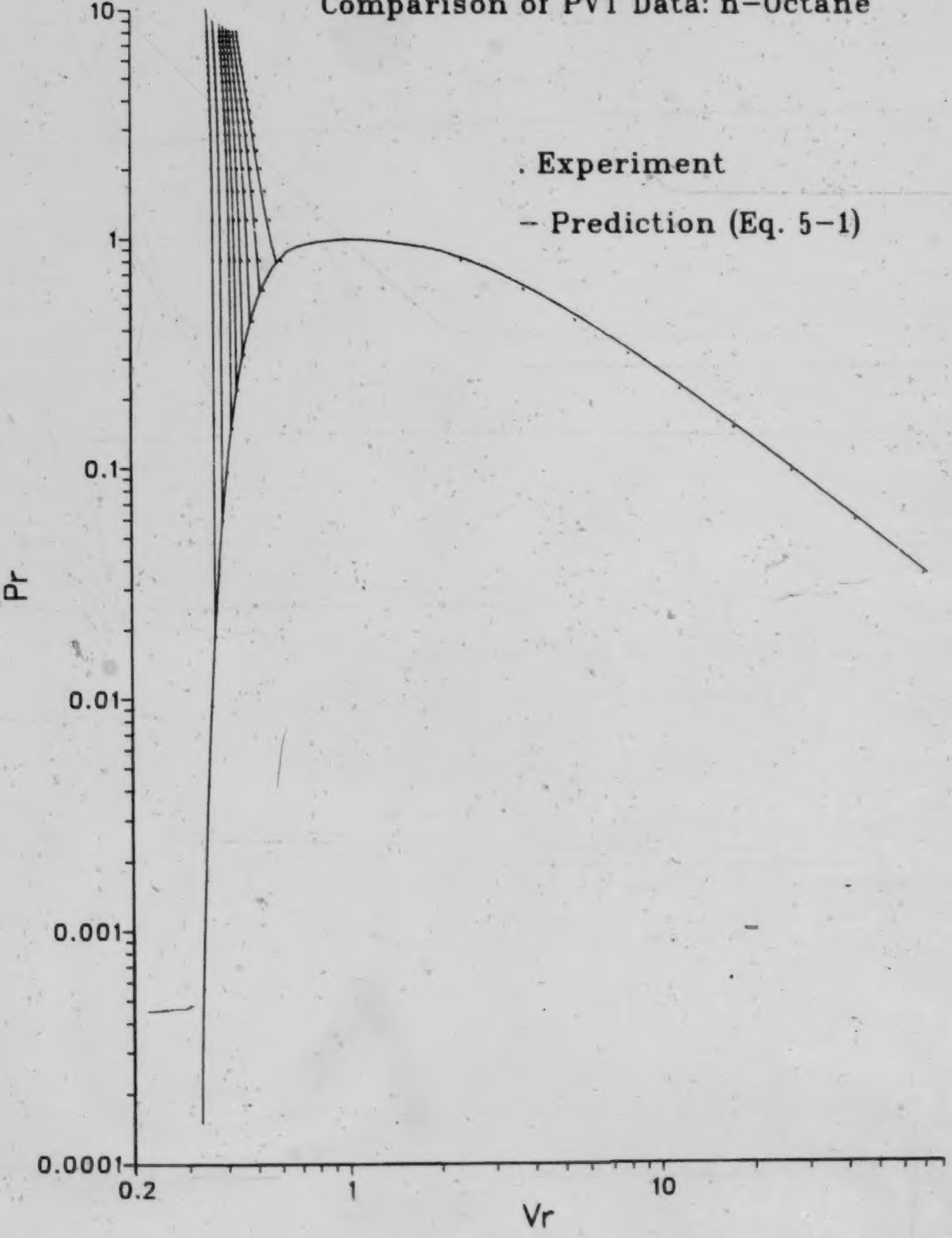

Figure 5–10
Comparison of PVT Data: n–Nonane

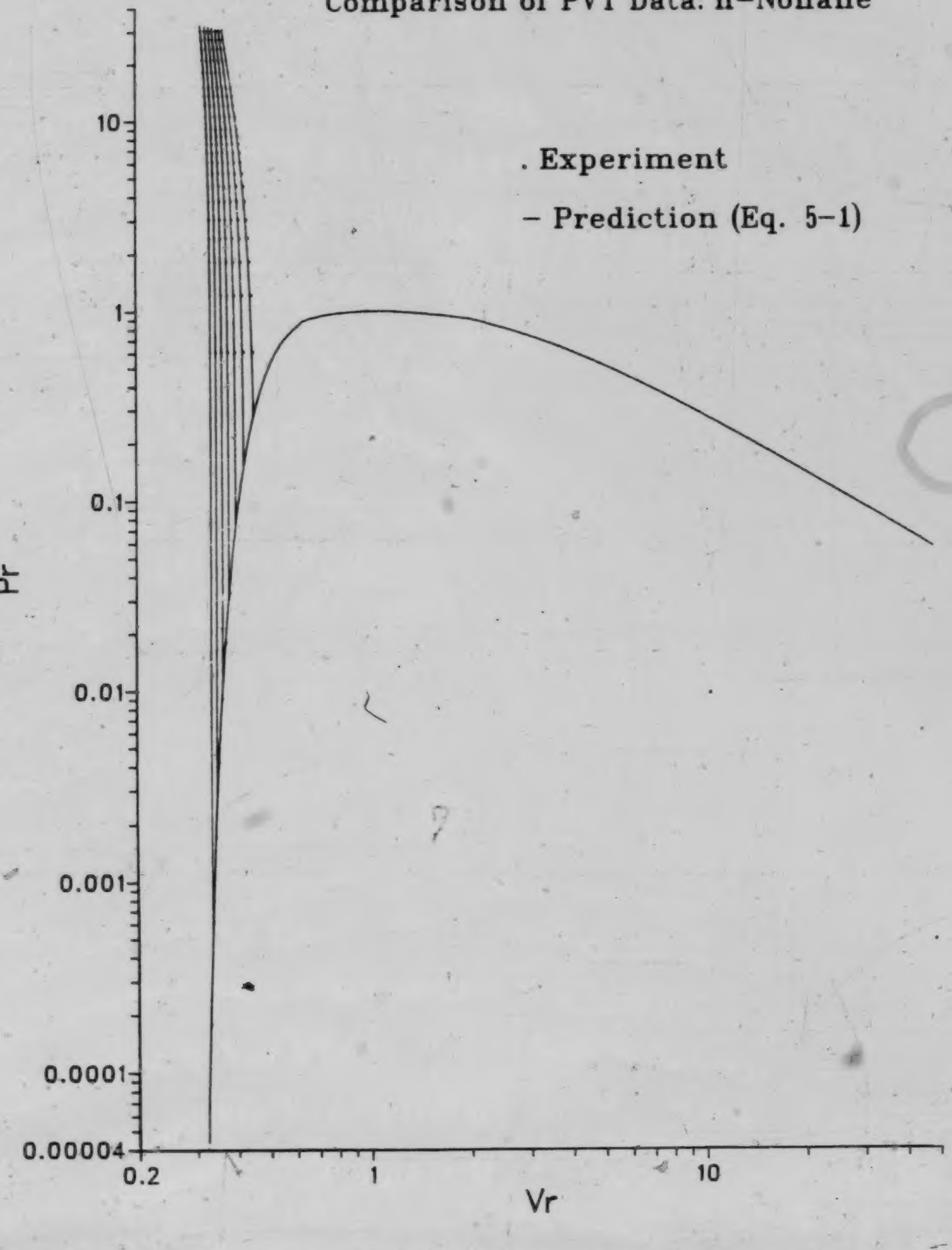

Figure 5–11
Comparison of PVT Data: n–Decane

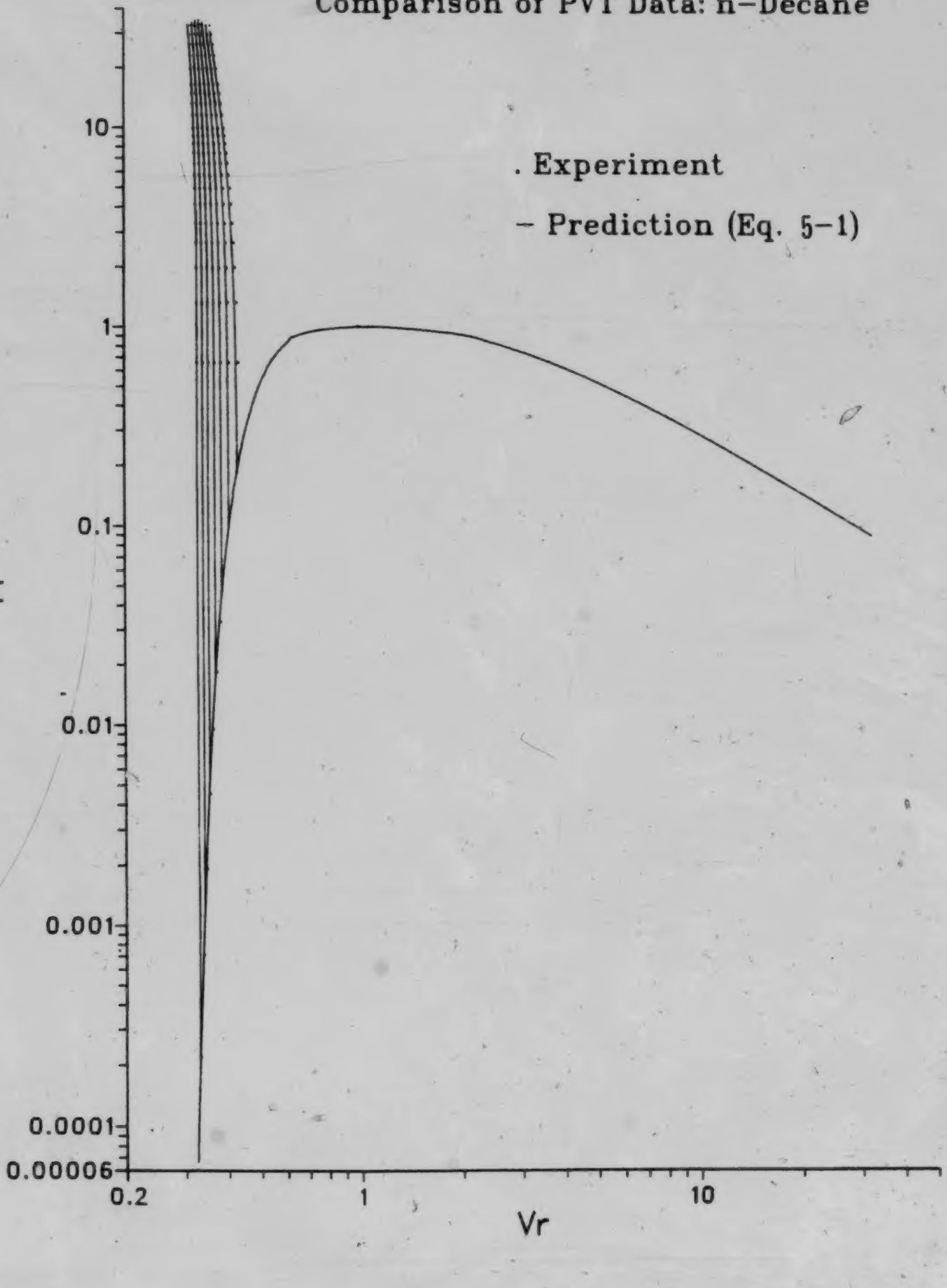

Figure 5–12
Comparison of Vapor Pressures

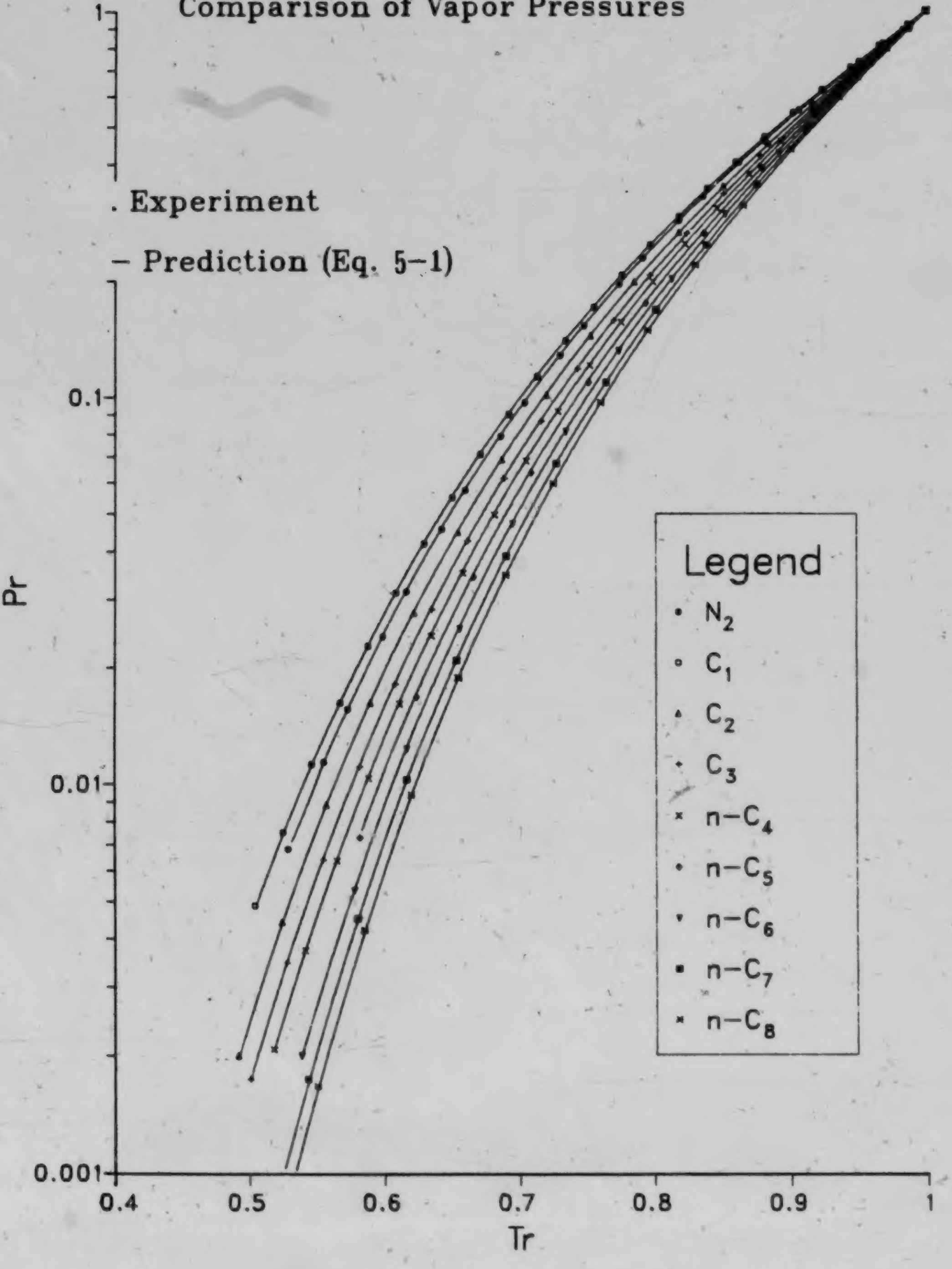

Appendix 6

Prediction of the MMP of a Methane VGD

Numerical Application and Related Table and Figures

A numerical application of the method, showing the various steps involved, when predicting the MMP of a multicomponent oil displaced by a lean hydrocarbon gas is described herein. The case considered has been investigated by Koch and Hutchinson[11], and the reported data is as shown below:

	Oil Composition (mole fraction)	Lean Gas Composition (mole fraction)
N2	0	0.010
CO2	0	0.021
C1	0.427	0.880
C2	0.125	0.086
C3	0.102	0.003
C4's	0.062	0
C5's	0.038	0
C6's	0.033	0
C_7^+	0.213	0
	1.000	1.000
MWC_7^+	191	

T = 60 °C

After grouping the intermediate and heavy fractions of the oil, one obtains:

	Mole Fraction	AMW
light fraction (C1)	0.427	16
Intermediate fraction (C2-C6)	0.360	48
Heavy fraction (C_7^+)	0.213	191

The four ternary systems that circumscribe the above hypothetical ternary are:

SYSTEM	MWI	MWH
C1 - C3 - C12	44	170
C1 - C3 - C15	44	212
C1 - C4 - C12	58	170
C1 - C4 - C15	58	212

For each of the above ternaries, the coefficients xic, a_1, a_2 and b_1 are obtained from Table 6-1. Solving Equation 61 (refer to section 6.2.2) for each case, one obtains four values of X_{Ic} corresponding to the above four ternaries. The next step is to select the appropriate figure and curve (Figures 6-1 to 6-10) corresponding to each of the above ternaries, at a temperature of 60 °C, and the MMP is read from the graph at the value obtained for X_{Ic}, as is shown below:

Case	MWI	MWH	X_{Ic}	MMP (MPa)	From Figure
1	44	170	0.228	23.8	6-5-a
2	44	212	0.225	27.5	6-5-a
3	58	170	0.160	25.6	6-5-b
4	58	212	0.158	29.2	6-5-b

Interpolating the MMP between cases 1 and 2, and cases 3 and 4 at a MWH of 191, one obtains:

Case	MWI	MWH	MMP(MPa)
5	44	191	25.65
6	58	191	27.40

Finally, interpolating the MMP between cases 5 and 6 at a MWI of 48, one obtains the desired MMP:

MWI	MWH	Predicted MMP (MPa)	Reported MMP (MPa)
48	191	26.1	24.2

Table 6-1
Coefficients of Equations 58 and 59
(lean hydrocarbon vaporizing gas drive)

T (°C)	MWI	MWH	xic	b_1	a_1	a_2	AAD% EQ58	AAD% EQ59
30	44	114	0.3820	-0.734	2.792	0.527	0.2	2.1
		142	0.3820	-0.781	3.305	1.915	0.5	3.9
		170	0.3820	-0.820	3.095	1.444	0.5	5.8
		212	0.3820	-0.855	3.220	1.845	0.6	7.8
	58	114	0.2288	-0.555	4.758	1.848	0.2	1.6
		142	0.2288	-0.643	5.016	3.132	0.4	3.3
		170	0.2288	-0.700	5.240	4.269	0.5	4.9
		212	0.2288	-0.759	5.501	5.614	0.5	7.1
	72	114	0.1747	-0.426	5.647	-0.290	0.1	0.9
		142	0.1747	-0.543	5.774	0.631	0.2	2.0
		170	0.1747	-0.618	5.904	1.585	0.3	3.1
		212	0.1747	-0.694	6.069	2.835	0.3	4.7
	86	114	0.1354	-0.265	7.553	1.319	0.1	0.4
		142	0.1354	-0.415	7.736	2.904	0.1	1.2
		170	0.1354	-0.511	7.989	5.075	0.2	2.3
		212	0.1354	-0.606	8.420	8.762	0.3	4.0
45	44	114	0.4664	-0.770	2.026	-0.211	0.1	1.7
		142	0.4664	-0.814	2.389	0.589	0.4	2.9
		170	0.4664	-0.848	2.186	0.207	0.4	4.8
		212	0.4664	-0.878	2.259	0.408	0.5	6.5
	58	114	0.2660	-0.593	3.762	0.099	0.2	1.2
		142	0.2660	-0.679	3.893	0.690	0.3	2.5
		170	0.2660	-0.733	4.027	1.299	0.4	3.9
		212	0.2660	-0.786	4.196	2.077	0.5	5.7
	72	114	0.1947	-0.449	4.886	-1.180	0.1	0.7
		142	0.1947	-0.568	4.916	-0.881	0.2	1.7
		170	0.1947	-0.642	4.981	-0.393	0.3	2.7
		212	0.1947	-0.716	5.077	0.339	0.3	4.2
	86	114	0.1489	-0.284	6.709	0.034	0.1	0.3
		142	0.1489	-0.438	6.768	0.606	0.1	1.0
		170	0.1489	-0.535	6.921	1.857	0.2	2.0
		212	0.1489	-0.629	7.222	4.262	0.3	3.5
60	44	114	0.5719	-0.801	1.474	-0.450	0.0	1.7
		142	0.5719	-0.842	1.724	-0.003	0.3	2.5
		170	0.5719	-0.872	1.532	-0.305	0.3	4.4
		212	0.5719	-0.898	1.566	-0.215	0.4	5.9
	58	114	0.3096	-0.627	2.976	-0.764	0.1	1.0
		142	0.3096	-0.710	3.013	-0.580	0.2	2.1
		170	0.3096	-0.761	3.080	-0.295	0.3	3.3
		212	0.3096	-0.811	3.177	0.116	0.4	4.9

Table 6-1 (continued)
Coefficients of Equations 58 and 59
(lean hydrocarbon vaporizing gas drive)

T (°C)	MWI	MWH	xic	b_1	a_1	a_2	AAD% EQ58	AAD% EQ59
60	72	114	0.2177	-0.472	4.212	-1.679	0.1	0.7
		142	0.2177	-0.592	4.163	-1.799	0.2	1.5
		170	0.2177	-0.665	4.171	-1.646	0.2	2.4
		212	0.2177	-0.736	4.208	-1.291	0.3	3.8
	86	114	0.1643	-0.303	5.934	-0.880	0.0	0.3
		142	0.1643	-0.462	5.891	-1.011	0.1	0.9
		170	0.1643	-0.558	5.958	-0.435	0.2	1.7
		212	0.1643	-0.651	6.148	1.018	0.3	3.1
75	44	114	0.7087	-0.829	1.073	-0.454	0.2	2.1
		142	0.7087	-0.866	1.235	-0.222	0.2	2.7
		170	0.7087	-0.893	1.051	-0.456	0.2	4.5
		212	0.7087	-0.916	1.057	-0.429	0.3	5.9
	58	114	0.3617	-0.659	2.345	-1.121	0.0	0.9
		142	0.3617	-0.739	2.313	-1.167	0.2	1.9
		170	0.3617	-0.787	2.328	-1.078	0.2	2.9
		212	0.3617	-0.833	2.369	-0.895	0.3	4.3
	72	114	0.2444	-0.495	3.613	-1.906	0.1	0.6
		142	0.2444	-0.616	3.500	-2.289	0.1	1.4
		170	0.2444	-0.688	3.460	-2.365	0.2	2.2
		212	0.2444	-0.756	3.447	-2.276	0.3	3.5
	86	114	0.1817	-0.322	5.234	-1.448	0.0	0.2
		142	0.1817	-0.484	5.108	-2.045	0.1	0.8
		170	0.1817	-0.581	5.102	-1.948	0.2	1.6
		212	0.1817	-0.672	5.198	-1.194	0.2	2.8
90	44	114	0.8943	-0.856	0.786	-0.350	0.4	3.1
		142	0.8943	-0.889	0.876	-0.876	0.1	3.4
		170	0.8943	-0.912	0.699	-0.431	0.0	5.0
		212	0.8943	-0.932	0.681	-0.440	0.2	6.4
	58	114	0.4257	-0.689	1.828	-1.193	0.0	1.0
		142	0.4257	-0.767	1.745	-1.745	0.1	1.8
		170	0.4257	-0.812	1.720	-1.385	0.2	2.7
		212	0.4257	-0.854	1.719	-1.340	0.3	4.0
	72	114	0.2762	-0.519	3.063	-1.979	0.0	0.6
		142	0.2762	-0.640	2.900	-2.512	0.1	1.3
		170	0.2762	-0.710	2.821	-2.731	0.2	2.1
		212	0.2762	-0.776	2.766	-2.822	0.2	3.3
	86	114	0.2016	-0.341	4.602	-1.751	0.0	0.2
		142	0.2016	-0.507	4.407	-2.646	0.1	0.7
		170	0.2016	-0.603	4.341	-2.877	0.2	1.4
		212	0.2016	-0.693	4.357	-2.621	0.2	2.6
							0.2	2.7

Minimum Miscibility Pressure vs Intermediate Mole Fraction
at Critical Point
T=30°C

Fig. 6-1-a

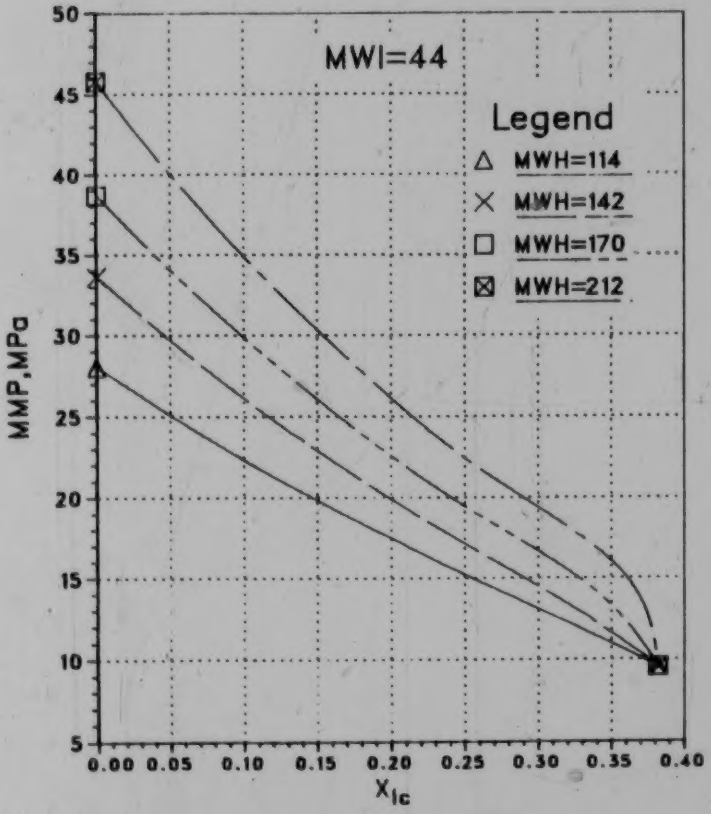

Fig. 6-1-b

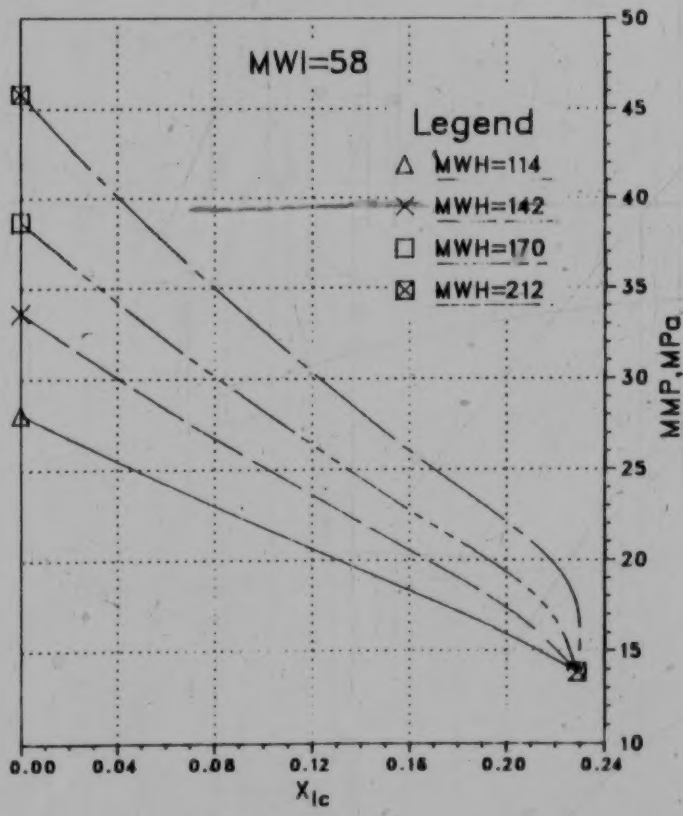

Minimum Miscibility Pressure vs Intermediate Mole Fraction at Critical Point
T=30°C

Fig. 6–2–a

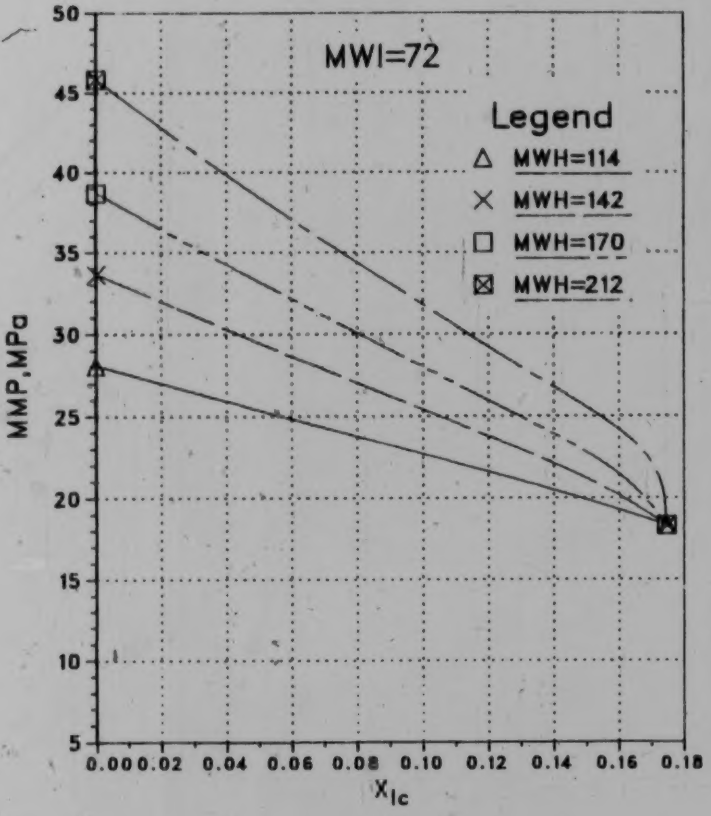

Fig. 6–2–b

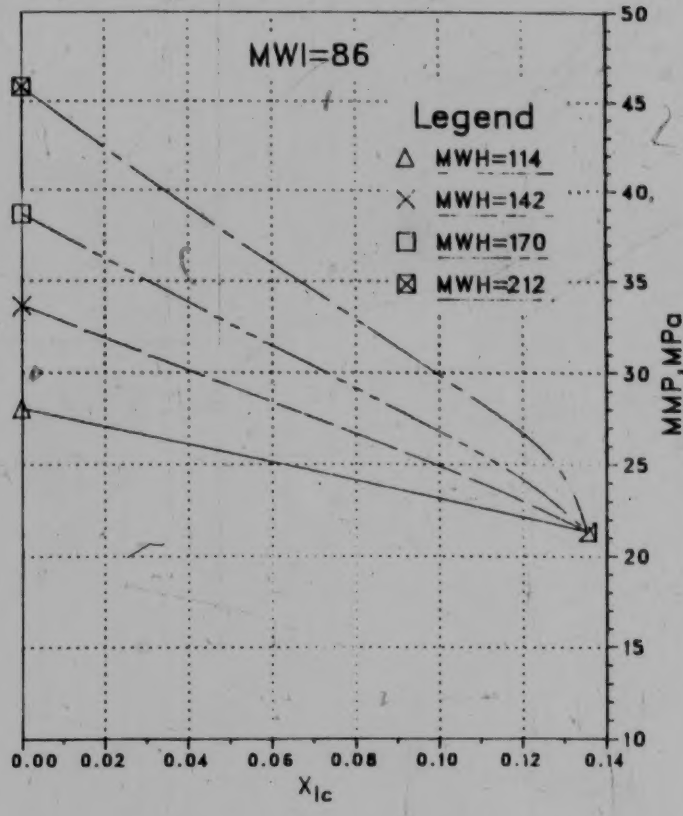

Minimum Miscibility Pressure vs Intermediate Mole Fraction
at Critical Point
T=45°C

Fig. 6-3-a

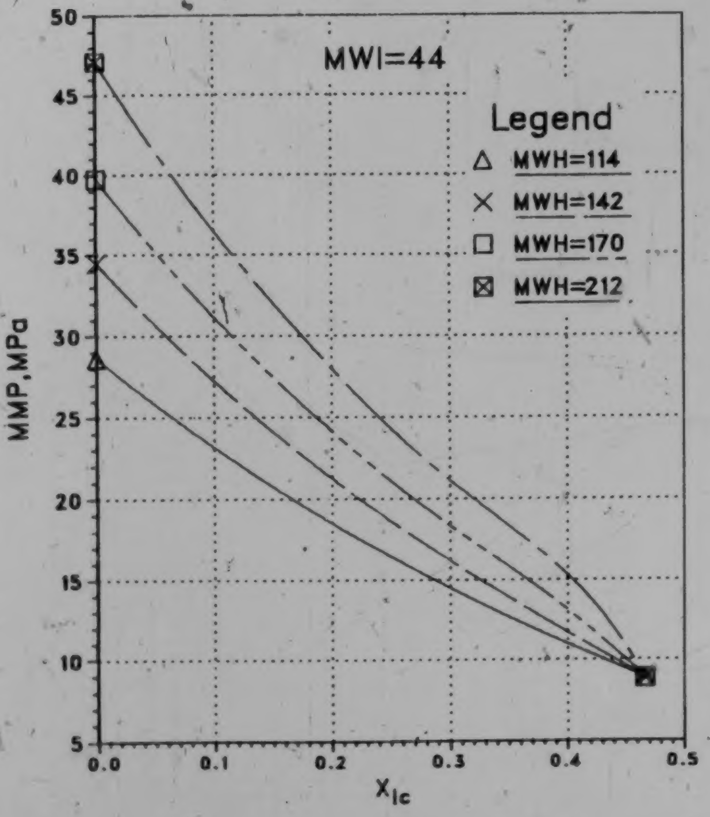

Fig. 6-3-b

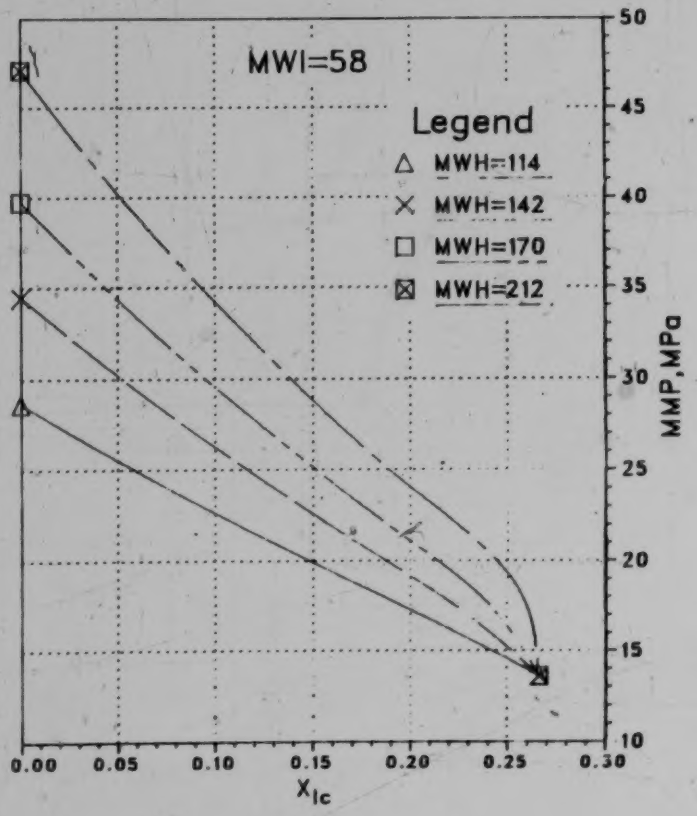

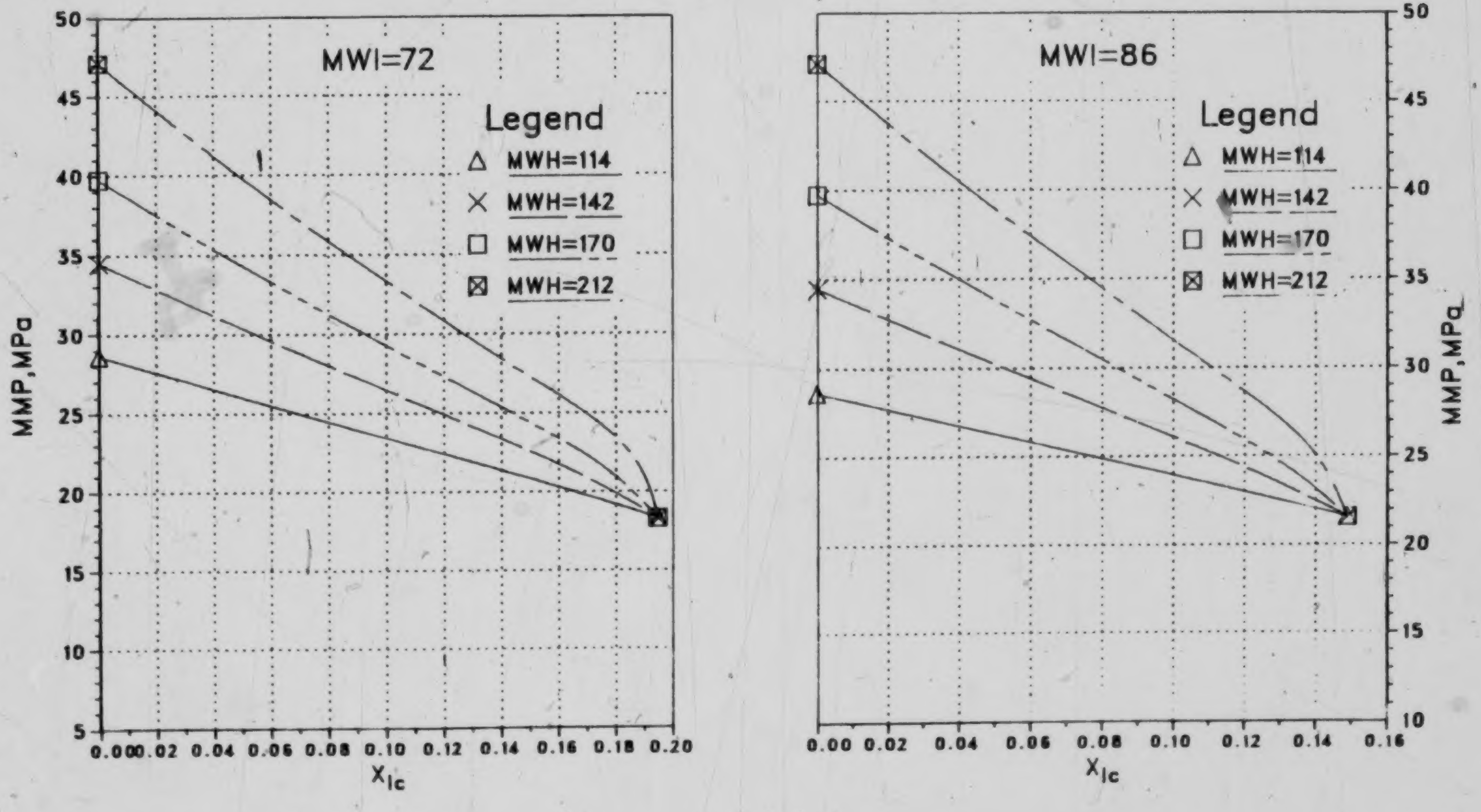

Minimum Miscibility Pressure vs Intermediate Mole Fraction
at Critical Point
T=45°C

Fig. 6-4-a

Fig. 6-4-b

Minimum Miscibility Pressure vs Intermediate Mole Fraction
at Critical Point
T=60°C

Fig. 6-5-a

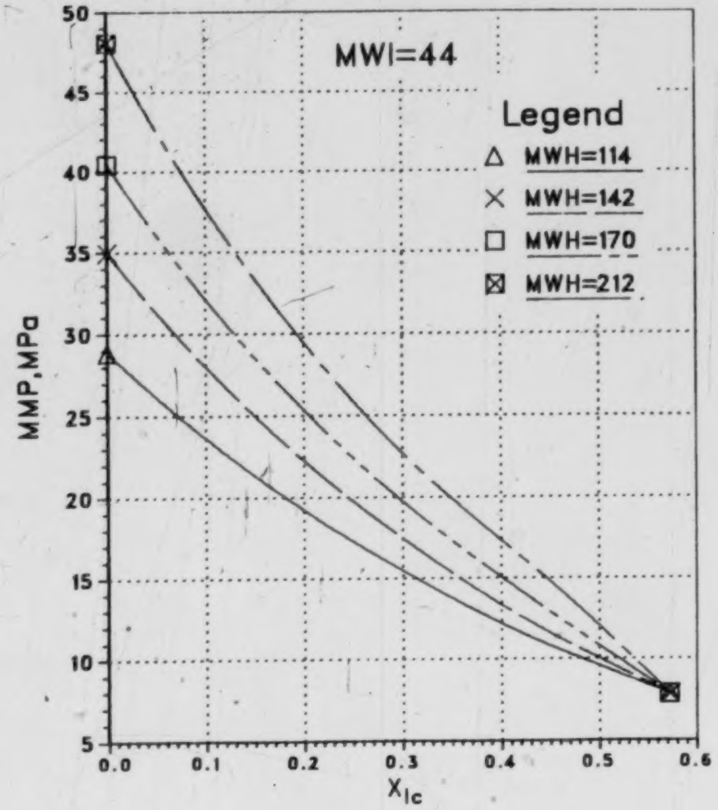

Fig. 6-5-b

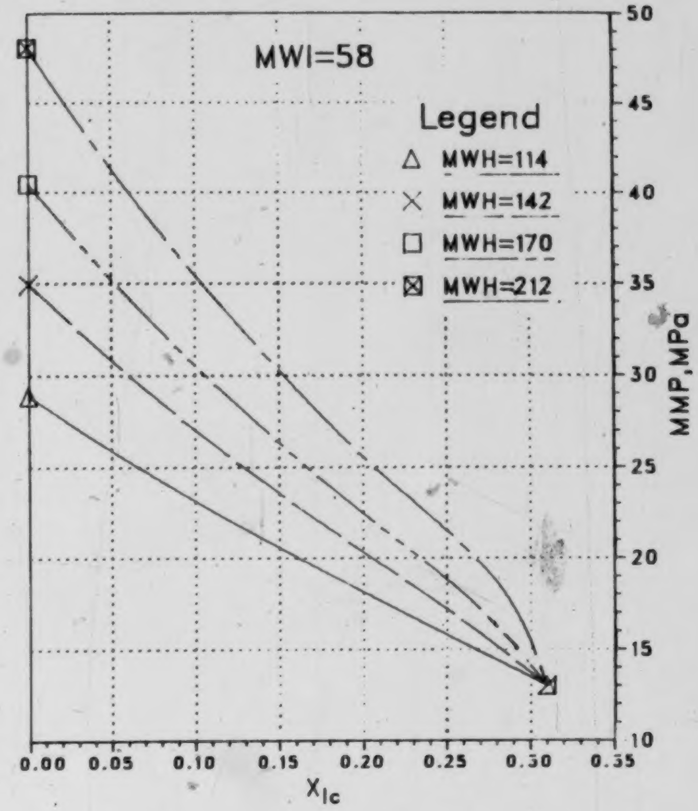

Minimum Miscibility Pressure vs Intermediate Mole Fraction
at Critical Point
T=60°C

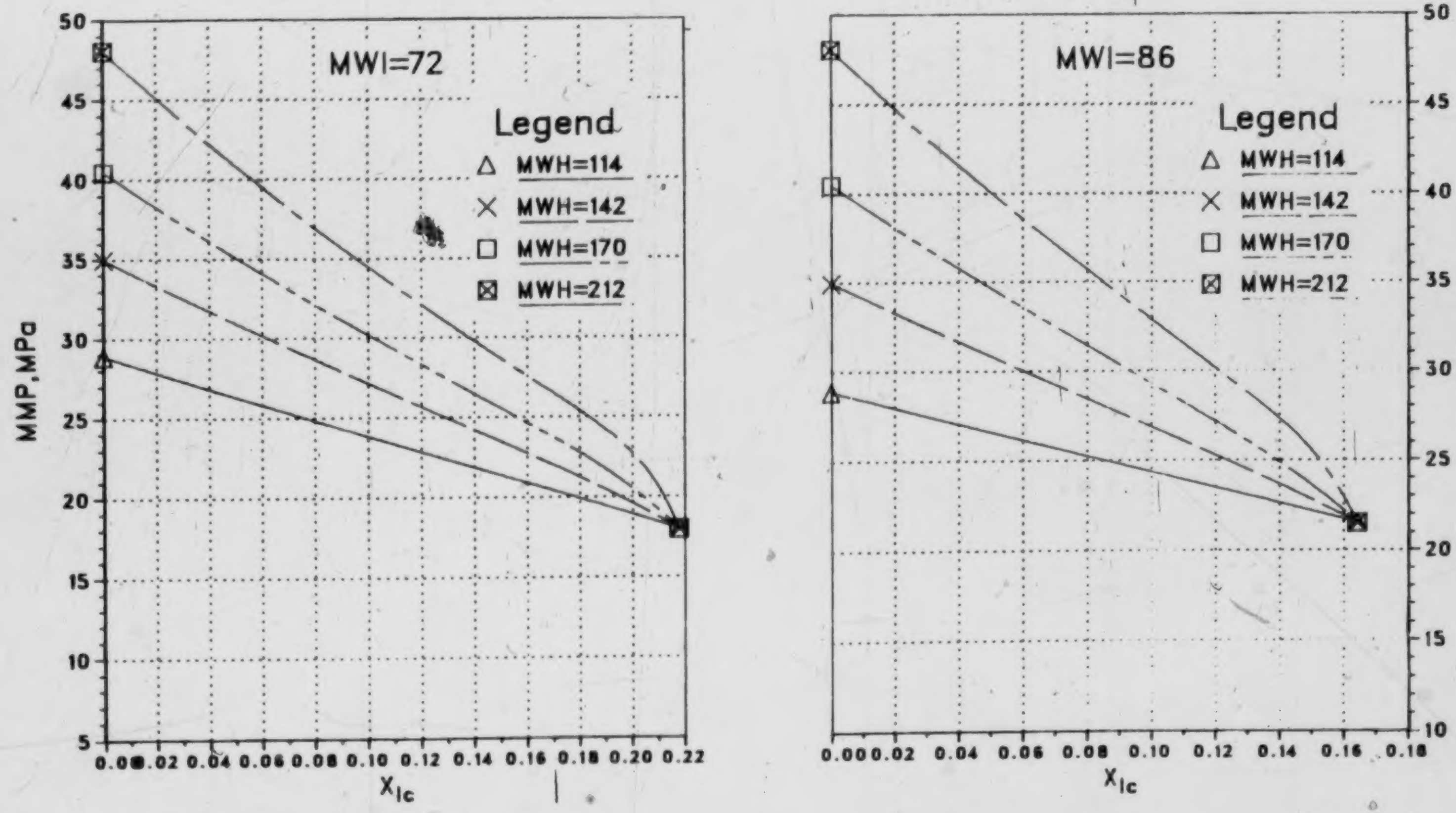

Fig. 6-6-a

Fig. 6-6-b

Minimum Miscibility Pressure vs Intermediate Mole Fraction
at Critical Point
T=75°C

Fig. 6-7-a

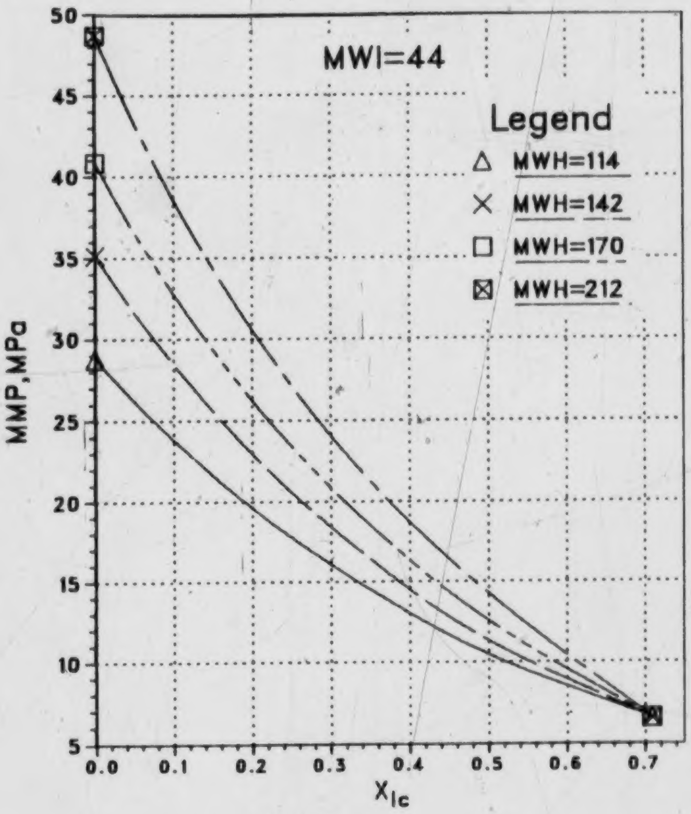

Fig. 6-7-b

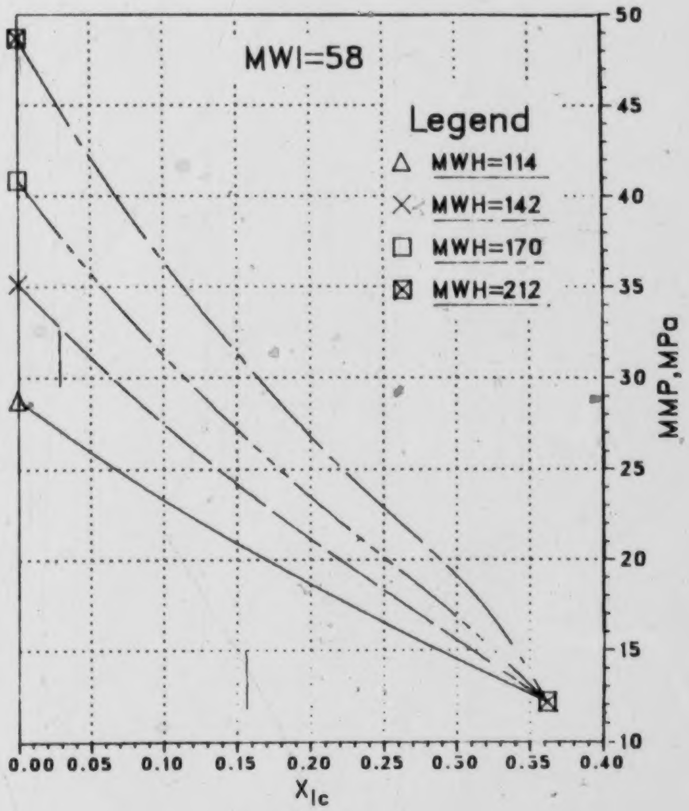

Minimum Miscibility Pressure vs Intermediate Mole Fraction
at Critical Point
T=75°C

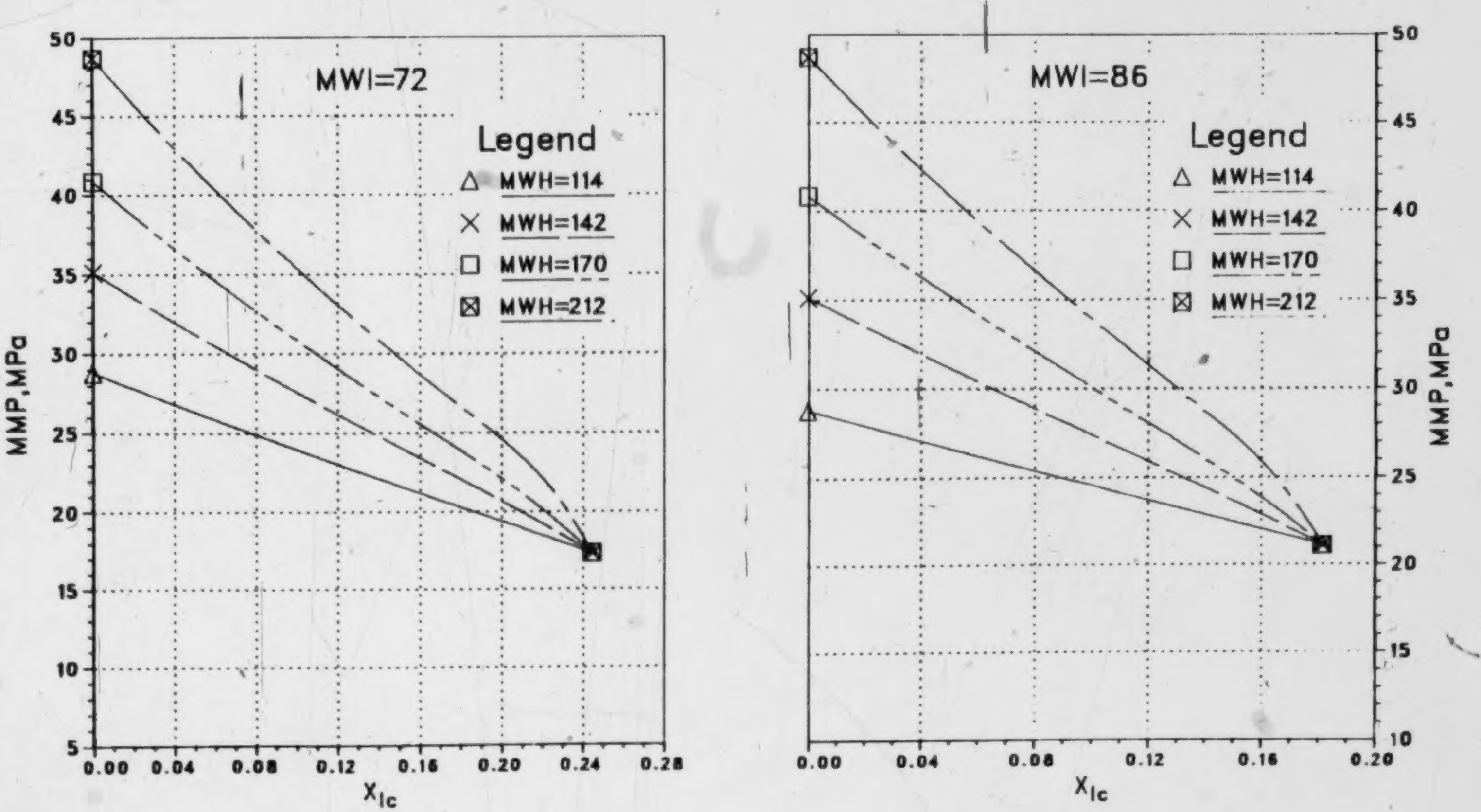

Fig. 6-8-a

Fig. 6-8-b

Minimum Miscibility Pressure vs Intermediate Mole Fraction at Critical Point
T=90°C

Fig. 6–9–a

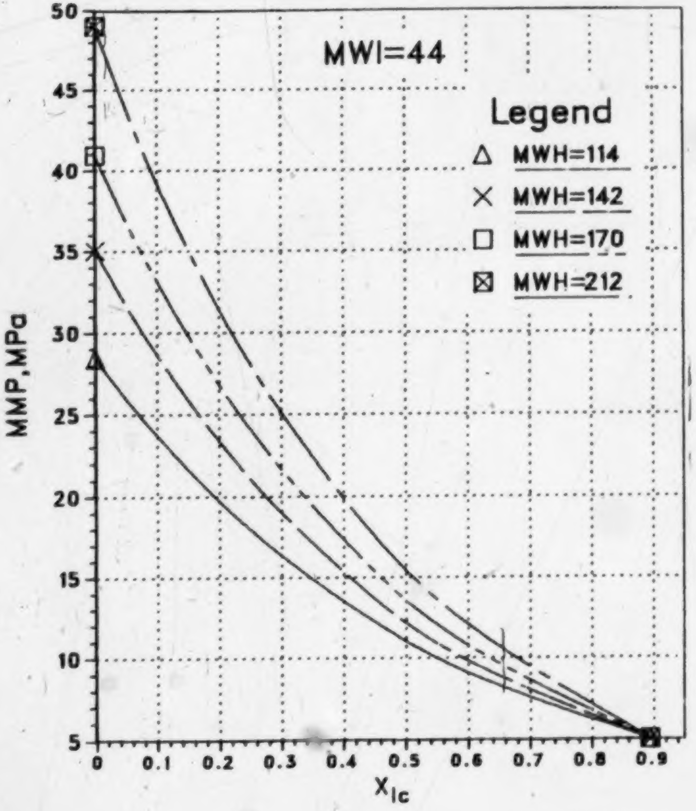

Fig. 6–9–b

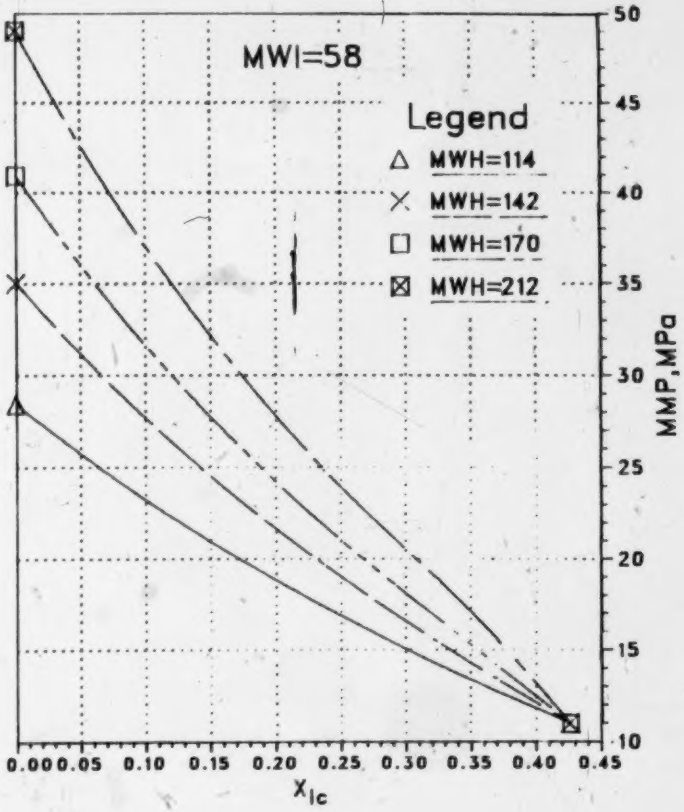

Minimum Miscibility Pressure vs Intermediate Mole Fraction
at Critical Point
T=90°C

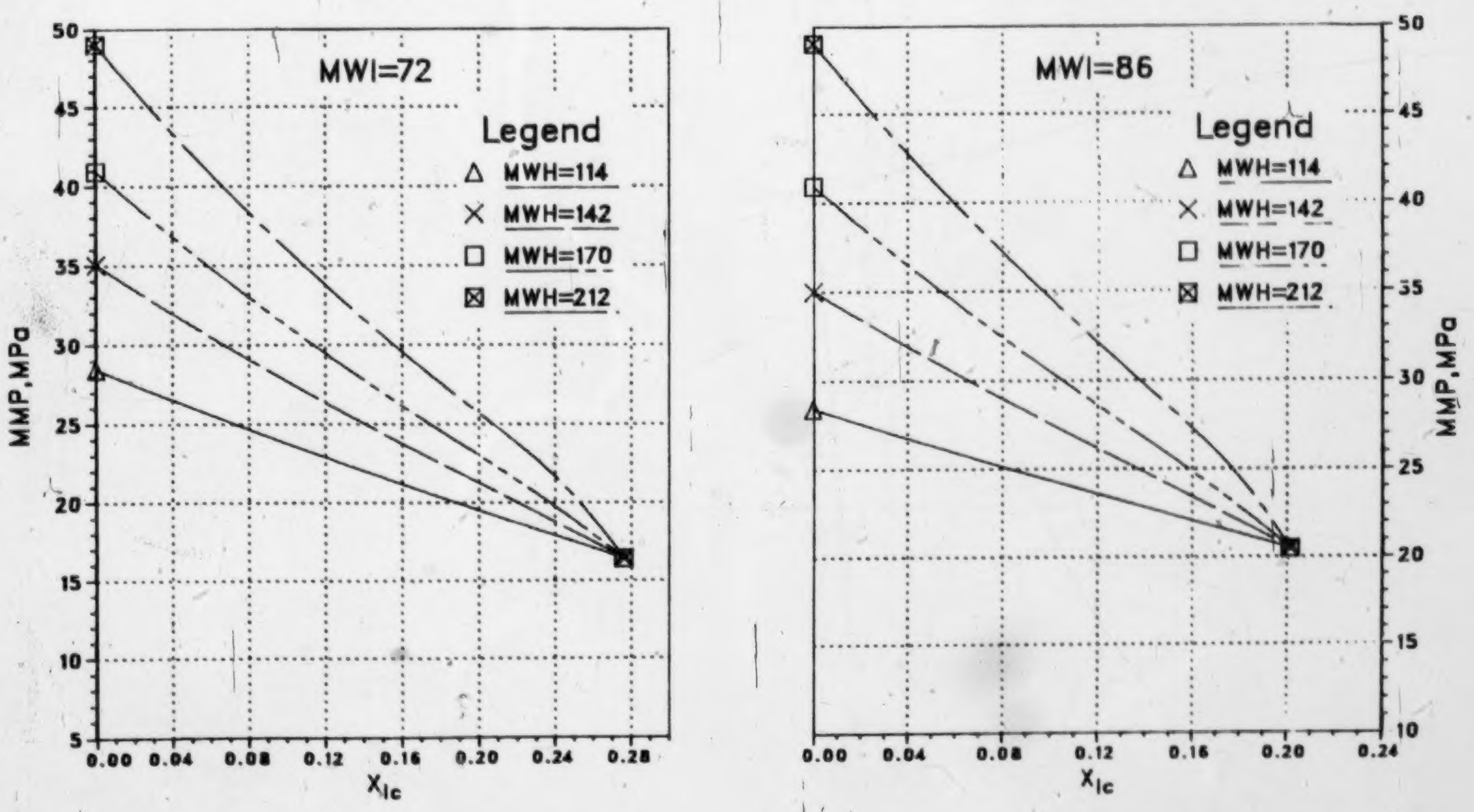
Fig. 6-10-a

Fig. 6-10-b

Appendix 7

Experimental Apparatus & Experimental Procedure

7.1 Description of the Slim-tube Apparatus

The apparatus (see Figure 7-1) is composed of:

a. An injection system which permits displacement at constant injection rate.

b. An unconsolidated porous medium (slim-tube).

c. A sight glass (observation of the transition zone).

d. A back pressure regulator (continuous downstream pressure control).

e. A separator at atmospheric conditions, a condenser and metering devices for the liquid and gaseous phases.

A Ruska positive displacement pump was used as the injection system. This pump was of the double-cylinder type and was geared for discharge rates of from 2.5 to 560 cm^3/h per cylinder and calibrated to 0.01 cm^3.

The slim-tube utilized was 24.4 m long. It consisted of a series of interconnected 6.1 m long, 0.635 cm OD stainless steel tubes. The tubes were dry packed with 100-150 mesh glass beads in a vertical position, before being coiled. This procedure was used as a result of some communication with the technical services of D B Robinson & Associates Laboratory (Edmonton). Packing a pre-coiled tube necessitated a vibrating table which induced stress cracking of the steel tube. A 250 mesh sintered steel filter was placed at each end of the tube and maintained in place by a washer and a 0.635 cm fitting. Each tube was then evacuated for a period of 24 hours before being saturated with distilled water, while a vacuum was maintained at the downstream end. After breakthrough of the water, the vacuum pump was disengaged and a further four pore volumes of water were injected prior to measurements leading to the determination of the liquid permeability. The porosity was determined by the gravimetric method, given the wet weight (saturated tube), dry weight and dimensions of the tube. The tubes were subsequently dried in an oven for a period of 48 hours. The slim-tube

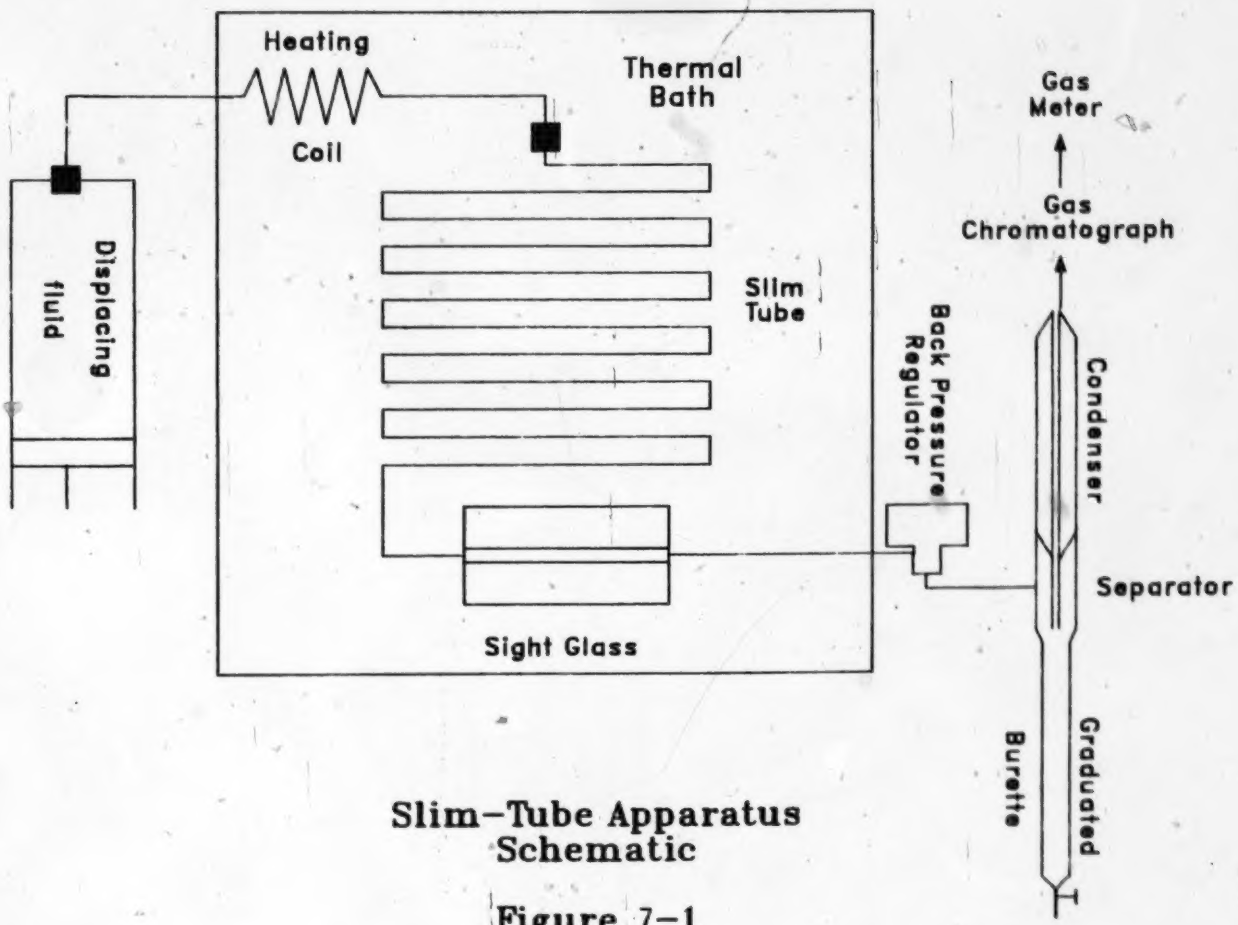

Slim–Tube Apparatus Schematic

Figure 7–1

physical characteristics are presented in Table 7-1:

Table 7-1

Slim-tube Physical Characteristics

Core #	Length (m)	ID (m)	Porosity (%)	Liquid permeability (m^2)
1	6.1	0.457E-2	37.83	10.82E-12
2	6.1	0.457E-2	37.44	09.50E-12
3	6.1	0.457E-2	36.81	10.82E-12
4	6.1	0.457E-2	36.49	10.44E-12

A high pressure sight glass was connected to the downstream end of the slim-tube. It allowed for the observation of the effluent at the operating conditions of pressure and temperature of the displacement. The slim-tube and sight glass were enclosed in a constant temperature air bath.

A back-pressure regulator was used for downstream pressure control. The device, designed by Fausto Nicola (Calgary, Alberta), allowed very accurate control of the downstream pressure to ±0.02 MPa.

7.2 Experimental Procedure

For each test conducted, the displaced oil was composed of methane, propane and n-decane with a composition fixed at 30, 35 and 35 mole%, respectively (it will be subsequently referred to as the live oil). N-decane (99% minimum purity) was purchased from Fisher Scientific Ltd (Edmonton). Propane (99.5% minimum purity) was purchased from Matheson Ltd (Edmonton). The methane-propane-n-decane mixture was prepared by

Matheson Ltd. The mixture was stored in a cylinder and maintained in a single liquid phase under a pressure of 12.4 MPa by injection of water at the bottom of the cylinder. The displacing fluids were methane and nitrogen.

Prior to the initiation of a displacement, the slim-tube apparatus was thoroughly checked for leaks, then evacuated for 2 hours. The coil was saturated with toluene at the desired test temperature and pressure. The toluene was subsequently displaced with the live oil at the same operating conditions. Approximately 1.6 pore volumes of live oil were injected. This saturation procedure was used in order to prevent phase separation of the live oil, the test pressure always being above its bubble-point pressure. The system was then allowed to equilibrate at the test temperature overnight. The pressure of the displacing fluid was brought to the desired test pressure. The displacing fluid was allowed to equilibrate at the test temperature in the heating coil upstream of the slim-tube inlet, during which displacing and displaced fluids were isolated by a valve. At equilibrium, the displacement proceeded at the desired injection rate, while the downstream pressure was continuously monitored by adjusting the back pressure regulator. The effluent was flashed to atmospheric conditions, and the separator gas flow rate and liquid volume were recorded with time, using a bubble flow meter and a 100 cm^3 graduated burette. The transition zone was monitored by observing the phase condition of the effluent as it flowed in the high pressure sight glass. The observations of the transition zone effluent were noted. After breakthrough of the transition zone, the liquid production decreased rapidly to a point where only a gaseous phase was being produced, at which time the test was terminated.

For the purposes of calculating the recovery of the IOIP versus the pore volume injected, the following calculations were necessary. The amount of the gas phase injected was obtained using the real gas law

$$Vh = \frac{(P\ Vr)}{(Zr\ Tr)} \frac{(Zh\ Th)}{P} = \frac{Zh\ Th}{Zr\ Tr} Vr \tag{7-1}$$

where

Th = test temperature, K

Tr = room temperature, K

P = test pressure (constant throughout the test), kPa

Vr = volume of gas displaced from the external gas cylinder at Tr and P, m^3

Vh = volume of gas injected at Th and P, (accounts for thermal expansion in the temperature bath), m^3

Zr = compressibility of methane at P and Tr

Zh = compressibility of methane at P and Th

The compressibilities for methane and nitrogen were obtained from Sage and Lacey[49].

The volume of oil displaced at test temperature and pressure was calculated by multiplying the produced separator liquid volume by a predetermined volume factor (VF):

$$\% \text{ recovery of IOIP} = \frac{(\text{Separator Liq Volume})\cdot \text{VF}}{\text{Pore Volume}} 100 \tag{7-2}$$

This factor was calculated from a knowledge of the phase and volumetric behavior of the methane-propane-n-decane system at atmospheric conditions and at test temperature and pressure[45]. The compositions of the dead oil (separator liquid of a flashed live oil at atmospheric conditions) and liberated gas at atmospheric conditions showed that the gas phase was mainly composed of methane and propane, and that virtually no decane was present.

Therefore, a material balance on n-decane was performed and the volume factor (VF) was found to be

$$\text{VF} = \frac{\text{X10d}}{\text{X10l}} \frac{\overline{\text{Vl}}}{\overline{\text{Vd}}} \tag{7-3}$$

where

X10l = mole fraction of decane in live oil (0.35)

X10d = mole fraction of decane in dead oil (0.871)

$\overline{\text{Vl}}$ = molar volume of live oil at test pressure and temperature, m^3/mole

$\overline{\text{Vd}}$ = molar volume of dead oil at atmospheric conditions, m^3/mole

Vl = volume of oil at test pressure and temperature, m^3

Vd = liquid volume when Vl is flashed to atmospheric conditions, m^3

It may be observed that this method assumed that after breakthrough of the displacing fluid, the liquid produced had the same composition to that prior to breakthrough. This assumption was not very restrictive since the liquid volume produced after breakthrough was small compared to the total liquid volume ultimately recovered. A more accurate material balance would have required a knowledge of the composition of the liquid produced after breakthrough. Furthermore, as long as the same calculation procedure is utilized, a comparison of results obtained from different tests is possible.

Appendix 8

Fortran Program for the Determination of the MMP of a Nitrogen VGD

```
C
C
C PREDICTION OF THE MMP USING ROUTINE MINMP
C
C   THE ARGUMENTS OF THE ROUTINE MINMP ARE:
C
C   XL : MOLE FRACTION OF METHANE IN THE OIL
C   XI : MOLE FRACTION OF INTERMEDIATES IN THE OIL
C      (C2-C6)
C   MWI: APPARENT MOLECULAR WEIGHT OF INTERMEDIATES
C      IN THE OIL
C   MWH: APPARENT MOLECULAR WEIGHT OF HEAVIES (C7+)
C      IN THE OIL
C   T : TEMPERATURE (CELCIUS)
C   MMP: RETURNED VALUE OF THE MINIMUM MISCIBILITY
C      (kPa)
C
        SUBROUTINE MINMP(XL,XI,MWI,MWH,T,MMP)
        REAL XL,XI,MWI,MWH,T,MMP,A,B,C,D
        IF(T.LE.60.1) GO TO 100
        IF(T.GT.60.1) GO TO 200
        100 CONTINUE
        IF(MWH.LE.184.1) GO TO 110
        IF(MWH.GT.184.1) GO TO 120
        110 CONTINUE
        CALL MNP1TL(XL,XI,PP1L)
        CALL MNP1TM(XL,XI,PP1M)
        CALL MNP2TL(XL,XI,PP2L)
        CALL MNP2TM(XL,XI,PP2M)
        CALL MNB1TL(XL,XI,PB1L)
        CALL MNB1TM(XL,XI,PB1M)
        CALL MNB2TL(XL,XI,PB2L)
        CALL MNB2TM(XL,XI,PB2M)
        D=(PB2L-PB1L-PP2L+PP1L)/(14*14)
        C=(PP2L-PP1L)/14-44*D
        B=(PB2L-184*C-58*184*D-PP1L+170*C+44*170*D)/14
        A=-44*B+PP1L-170*C-44*170*D
        PL=A+B*MWI+C*MWH+D*MWI*MWH
```

```
D=(PB2M-PB1M-PP2M+PP1M)/(14*14)
C=(PP2M-PP1M)/14-44*D
B=(PB2M-184*C-58*184*D-PP1M+170*C+44*170*D)/14
A=-44*B+PP1M-170*C-44*170*D
PM=A+B*MWI+C*MWH+D*MWI*MWH
MMP=(PM-PL)*(T-30)/30+PL
RETURN
120 CONTINUE
CALL MNP2TL(XL,XI,PP2L)
CALL MNP2TM(XL,XI,PP2M)
CALL MNP3TL(XL,XI,PP3L)
CALL MNP3TM(XL,XI,PP3M)
CALL MNB2TL(XL,XI,PB2L)
CALL MNB2TM(XL,XI,PB2M)
CALL MNB3TL(XL,XI,PB3L)
CALL MNB3TM(XL,XI,PB3M)
D=(PB3L-PB2L-PP3L+PP2L)/(14*14)
C=(PP3L-PP2L)/14-44*D
B=(PB3L-198*C-58*198*D-PP2L+184*C+44*184*D)/14
A=-44*B+PP2L-184*C-44*184*D
PL=A+B*MWI+C*MWH+D*MWI*MWH
D=(PB3M-PB2M-PP3M+PP2M)/(14*14)
C=(PP3M-PP2M)/14-44*D
B=(PB3M-198*C-58*198*D-PP2M+184*C+44*184*D)/14
A=-44*B+PP2M-184*C-44*184*D
PM=A+B*MWI+C*MWH+D*MWI*MWH
MMP=(PM-PL)*(T-30)/30+PL
RETURN
200 CONTINUE
IF(MWH.LE.184) GO TO 210
IF(MWH.GT.184) GO TO 220
210 CONTINUE
CALL MNP1TM(XL,XI,PP1M)
CALL MNP1TH(XL,XI,PP1H)
CALL MNP2TM(XL,XI,PP2M)
CALL MNP2TH(XL,XI,PP2H)
CALL MNB1TM(XL,XI,PB1M)
CALL MNB1TH(XL,XI,PB1H)
CALL MNB2TM(XL,XI,PB2M)
CALL MNB2TH(XL,XI,PB2H)
D=(PB2M-PB1M-PP2M+PP1M)/(14*14)
C=(PP2M-PP1M)/14-44*D
B=(PB2M-184*C-58*184*D-PP1M+170*C+44*170*D)/14
A=-44*B+PP1M-170*C-44*170*D
PM=A+B*MWI+C*MWH+D*MWI*MWH
D=(PB2H-PB1H-PP2H+PP1H)/(14*14)
```

```
      C=(PP2H-PP1H)/14-44*D
      B=(PB2H-184*C-58*184*D-PP1H+170*C+44*170*D)/14
      A=-44*B+PP1H-170*C-44*170*D
      PH=A+B*MWI+C*MWH+D*MWI*MWH
      MMP=(PH-PM)*(T-60)/30+PM
      RETURN
      220 CONTINUE
      CALL MNP2TM(XL,XI,PP2M)
      CALL MNP2TH(XL,XI,PP2H)
      CALL MNP3TM(XL,XI,PP3M)
      CALL MNP3TH(XL,XI,PP3H)
      CALL MNB2TM(XL,XI,PB2M)
      CALL MNB2TH(XL,XI,PB2H)
      CALL MNB3TM(XL,XI,PB3M)
      CALL MNB3TH(XL,XI,PB3H)
      D=(PB3M-PB2M-PP3M+PP2M)/(14*14)
      C=(PP3M-PP2M)/14-44*D
      B=(PB3M-198*C-58*198*D-PP2M+184*C+44*184*D)/14
      A=-44*B+PP2M-184*C-44*184*D
      PM=A+B*MWI+C*MWH+D*MWI*MWH
      D=(PB3H-PB2H-PP3H+PP2H)/(14*14)
      C=(PP3H-PP2H)/14-44*D
      B=(PB3H-198*C-58*198*D-PP2H+184*C+44*184*D)/14
      A=-44*B+PP2H-184*C-44*184*D
      PH=A+B*MWI+C*MWH+D*MWI*MWH
      MMP=(PH-PM)*(T-60)/30+PM
      RETURN
      END
C
C
      SUBROUTINE MNP1TL(XL,XI,MMP)
      INTEGER N
      REAL XL,XI,MMP,AM(12),BM(12),AN(12),BN(12),P(12)
      DATA AM/-0.63035,-0.55317,-0.48142,-0.41177,-0.34222,
      $-0.27136,-0.19808,-0.12143,-0.04050,0.0,0.0,0.0/
      DATA BM/0.71747,0.64219,0.56721,0.49073,0.41158,
      $0.32878,0.24147,0.14879,0.04984,0.0,0.0,0.0/
      DATA AN/-1.52307,-1.49449,-1.47553,-1.45403,-1.43629,
      $-1.42250,-1.41172,-1.40314,-1.39615,-1.39027,-1.37269,
      $-1.35228/
      DATA BN/1.03056,0.99755,0.97013,0.94413,0.92038,0.89861,
      $0.87839,0.85936,0.84125,0.82388,0.75938,0.64439/
      DATA P/17500.0,20000.0,22500.0,25000.0,27500.0,30000.0,
      $32500.0,35000.0,37500.0,40000.0,50000.0,70000.0/
      N=12
      CALL FINDP(XL,XI,N,AM,BM,AN,BN,P,MMP)
      RETURN
      END
C
C
      SUBROUTINE MNP2TL(XL,XI,MMP)
      INTEGER N
      REAL XL,XI,MMP,AM(12),BM(12),AN(12),BN(12),P(12)
      DATA AM/-0.64196,-0.57335,-0.51011,-0.44918,-0.38873,
      $-0.32756,-0.26472,-0.19944,-0.13102,-0.05875,0.0,0.0/
      DATA BM/0.73376,0.66756,0.60209,0.53574,0.46749,
      $0.39654,0.32223,0.24387,0.16081,0.07235,0.0,0.0/
      DATA AN/-1.52982,-1.48897,-1.46068,-1.43288,-1.41171,
      $-1.39604,-1.38417,-1.37488,-1.36741,-1.36127,-1.34400,
      $-1.32404/
      DATA BN/1.03075,0.99729,0.97006,0.94486,0.92251,0.90241,
      $0.88397,0.86676,0.85048,0.83495,0.77779,0.67680/
      DATA P/17500.0,20000.0,22500.0,25000.0,27500.0,30000.0,
      $32500.0,35000.0,37500.0,40000.0,50000.0,70000.0/
      N=12
      CALL FINDP(XL,XI,N,AM,BM,AN,BN,P,MMP)
      RETURN
      END
C
C
      SUBROUTINE MNP3TL(XL,XI,MMP)
      INTEGER N
      REAL XL,XI,MMP,AM(12),BM(12),AN(12),BN(12),P(12)
      DATA AM/-0.65151,-0.58905,-0.53147,-0.47600,-0.42101,
      $-0.36538,-0.30831,-0.24910,-0.18712,-0.12178,0.0,0.0/
      DATA BM/0.74620,0.68622,0.62690,0.56682,0.50507,
      $0.44096,0.37389,0.30330,0.22860,0.14920,0.0,0.0/
      DATA AN/-1.53096,-1.47915,-1.44264,-1.41064,-1.38802,
      $-1.37196,-1.36005,-1.35086,-1.34354,-1.33756,-1.32124,
      $-1.30269/
      DATA BN/1.02998,0.99628,0.96918,0.94484,0.92382,0.90519,
      $0.88821,0.87242,0.85752,0.84331,0.79118,0.69916/
      DATA P/17500.0,20000.0,22500.0,25000.0,27500.0,30000.0,
      $32500.0,35000.0,37500.0,40000.0,50000.0,70000.0/
      N=12
      CALL FINDP(XL,XI,N,AM,BM,AN,BN,P,MMP)
      RETURN
      END
C
C
      SUBROUTINE MNP1TM(XL,XI,MMP)
      INTEGER N
      REAL XL,XI,MMP,AM(12),BM(12),AN(12),BN(12),P(12)
      DATA AM/-0.59574,-0.53033,-0.46901,-0.40916,-0.34917,
     $-0.28791,-0.22451,-0.15820,-0.08827,-0.01404,0.0,0.0/
      DATA BM/0.71529,0.64775,0.57982,0.51034,0.43844,
     $0.36338,0.28450,0.20111,0.11251,0.01793,0.0,0.0/
      DATA AN/-1.45473,-1.43518,-1.41739,-1.40314,-1.39185,
     $-1.38279,-1.37539,-1.36922,-1.36401,-1.35954,-1.34496,
     $-1.32649/
      DATA BN/0.95843,0.93211,0.90785,0.88548,0.86460,0.84488,
     $0.82607,0.80801,0.79056,0.77362,0.70940,0.59200/
      DATA P/17500.0,20000.0,22500.0,25000.0,27500.0,30000.0,
     $32500.0,35000.0,37500.0,40000.0,50000.0,70000.0/
      N=12
      CALL FINDP(XL,XI,N,AM,BM,AN,BN,P,MMP)
      RETURN
      END
C
C
      SUBROUTINE MNP2TM(XL,XI,MMP)
      INTEGER N
      REAL XL,XI,MMP,AM(12),BM(12),AN(12),BN(12),P(12)
      DATA AM/-0.60699,-0.54873,-0.49462,-0.44218,-0.38993,
     $-0.33685,-0.28222,-0.22540,-0.16584,-0.10300,0.0,0.0/
      DATA BM/0.73253,0.67270,0.61296,0.55224,0.48977,
     $0.42493,0.35718,0.28600,0.21085,0.13116,0.0,0.0/
      DATA AN/-1.44777,-1.41915,-1.39666,-1.37991,-1.36719,
     $-1.35723,-1.34923,-1.34265,-1.33713,-1.33242,-1.31830,
     $-1.30042/
      DATA BN/0.95933,0.93367,0.91078,0.89008,0.87100,0.85314,
     $0.83620,0.82000,0.80440,0.78930,0.73250,0.62942/
      DATA P/17500.0,20000.0,22500.0,25000.0,27500.0,30000.0,
     $32500.0,35000.0,37500.0,40000.0,50000.0,70000.0/
      N=12
      CALL FINDP(XL,XI,N,AM,BM,AN,BN,P,MMP)
      RETURN
      END
C
C
      SUBROUTINE MNP3TM(XL,XI,MMP)
      INTEGER N
      REAL XL,XI,MMP,AM(12),BM(12),AN(12),BN(12),P(12)
      DATA AM/-0.61619,-0.56331,-0.51424,-0.46669,-0.41932,
     $-0.37125,-0.32177,-0.27036,-0.21653,-0.15981,0.0,0.0/
      DATA BM/0.74566,0.69128,0.63706,0.58202,0.52546,
     $0.46685,0.40570,0.34156,0.27396,0.20243,0.0,0.0/
      DATA AN/-1.43617,-1.40047,-1.37546,-1.35783,-1.34483,
      $-1.33483,-1.32689,-1.32041,-1.31501,-1.31043,-1.29712,
      $-1.28055/
      DATA BN/0.95908,0.93418,0.91263,0.89344,0.87587,0.85949,
      $0.84399,0.82919,0.81495,0.80117,0.74944,0.65567/
      DATA P/17500.0,20000.0,22500.0,25000.0,27500.0,30000.0,
      $32500.0,35000.0,37500.0,40000.0,50000.0,70000.0/
      N=12
      CALL FINDP(XL,XI,N,AM,BM,AN,BN,P,MMP)
      RETURN
      END
C
C
      SUBROUTINE MNP1TH(XL,XI,MMP)
      INTEGER N
      REAL XL,XI,MMP,AM(12),BM(12),AN(12),BN(12),P(12)
      DATA AM/-0.51568,-0.46692,-0.41875,-0.36992,-0.31958,
      $-0.26713,-0.21203,-0.15379,-0.09194,-0.02596,0.0,0.0/
      DATA BM/0.68452,0.62283,0.55996,0.49519,0.42792,
      $0.35760,0.28368,0.20562,0.12282,0.03465,0.0,0.0/
      DATA AN/-1.39247,-1.37997,-1.36967,-1.36119,-1.35413,
      $-1.34817,-1.34306,-1.33864,-1.33477,-1.33134,-1.31928,
      $-1.30268/
      DATA BN/0.88758,0.86536,0.84439,0.82443,0.80528,0.78680,
      $0.76888,0.75142,0.73437,0.71767,0.65338,0.53338/
      DATA P/17500.0,20000.0,22500.0,25000.0,27500.0,30000.0,
      $32500.0,35000.0,37500.0,40000.0,50000.0,70000.0/
      N=12
      CALL FINDP(XL,XI,N,AM,BM,AN,BN,P,MMP)
      RETURN
      END
C
C
      SUBROUTINE MNP2TH(XL,XI,MMP)
      INTEGER N
      REAL XL,XI,MMP,AM(12),BM(12),AN(12),BN(12),P(12)
      DATA AM/-0.52776,-0.48540,-0.44369,-0.40149,-0.35807,
      $-0.31294,-0.26565,-0.21585,-0.16316,-0.10720,0.0,0.0/
      DATA BM/0.70558,0.65082,0.59536,0.53856,0.47988,
      $0.41887,0.35508,0.28808,0.21743,0.14265,0.0,0.0/
      DATA AN/-1.37465,-1.35936,-1.34743,-1.33793,-1.33020,
      $-1.32376,-1.31832,-1.31365,-1.30958,-1.30600,-1.29452,
      $-1.27861/
      DATA BN/0.89195,0.87146,0.85234,0.83426,0.81701,0.80042,
      $0.78439,0.76881,0.75363,0.73879,0.68203,0.57672/
      DATA P/17500.0,20000.0,22500.0,25000.0,27500.0,30000.0,
      $32500.0,35000.0,37500.0,40000.0,50000.0,70000.0/
      N=12
      CALL FINDP(XL,XI,N,AM,BM,AN,BN,P,MMP)
      RETURN
      END
C
C
      SUBROUTINE MNP3TH(XL,XI,MMP)
      INTEGER N
      REAL XL,XI,MMP,AM(12),BM(12),AN(12),BN(12),P(12)
      DATA AM/-0.53765,-0.50016,-0.46306,-0.42538,-0.38650,
     $-0.34598,-0.30349,-0.25872,-0.21133,-0.16104,0.0,0.0/
      DATA BM/0.72157,0.67174,0.62138,0.56987,0.51675,
     $0.46160,0.40404,0.34371,0.28020,0.21310,0.0,0.0/
      DATA AN/-1.35597,-1.33938,-1.32691,-1.31720,-1.30941,
     $-1.30301,-1.29763,-1.29304,-1.28906,-1.28558,-1.27483,
     $-1.26012/
      DATA BN/0.89498,0.87602,0.85843,0.84187,0.82609,0.81094,
     $0.79631,0.78212,0.76828,0.75477,0.70316,0.60751/
      DATA P/17500.0,20000.0,22500.0,25000.0,27500.0,30000.0,
     $32500.0,35000.0,37500.0,40000.0,50000.0,70000.0/
      N=12
      CALL FINDP(XL,XI,N,AM,BM,AN,BN,P,MMP)
      RETURN
      END
C
C
      SUBROUTINE MNB1TL(XL,XI,MMP)
      INTEGER N
      REAL XL,XI,MMP,AM(12),BM(12),AN(12),BN(12),P(12)
      DATA AM/-0.83313,-0.72580,-0.62736,-0.53342,-0.44098,
     $-0.34798,-0.25289,-0.15438,-0.05128,0.0,0.0,0.0/
      DATA BM/0.85921,0.76329,0.67042,0.57762,0.48287,
     $0.38468,0.28186,0.17331,0.05794,0.0,0.0,0.0/
      DATA AN/-2.05186,-1.92935,-1.84280,-1.78319,-1.74025,
     $-1.70793,-1.68269,-1.66242,-1.65199,-1.64559,-1.61913,
     $-1.58668/
      DATA BN/1.35338,1.26920,1.20605,1.15706,1.11678,1.08211,
     $1.05129,1.02322,0.99951,0.97815,0.89759,0.75729/
      DATA P/17500.0,20000.0,22500.0,25000.0,27500.0,30000.0,
     $32500.0,35000.0,37500.0,40000.0,50000.0,70000.0/
      N=12
      CALL FINDP(XL,XI,N,AM,BM,AN,BN,P,MMP)
      RETURN
      END
C
C
```

```
      SUBROUTINE MNB2TL(XL,XI,MMP)
      INTEGER N
      REAL XL,XI,MMP,AM(12),BM(12),AN(12),BN(12),P(12)
      DATA AM/-0.84426,-0.74609,-0.65814,-0.57547,-0.49503,
     $-0.41489,-0.33367,-0.25026,-0.16371,-0.07312,0.0,0.0/
      DATA BM/0.87057,0.78443,0.70284,0.62242,0.54115,
     $0.45766,0.37094,0.28011,0.18433,0.08277,0.0,0.0/
      DATA AN/-2.12097,-1.93911,-1.82548,-1.75250,-1.70209,
     $-1.66514,-1.63682,-1.61435,-1.60223,-1.59495,-1.56641,
     $-1.53196/
      DATA BN/1.37674,1.27190,1.20152,1.15055,1.11039,1.07681,
     $1.04756,1.02133,0.99951,0.98008,0.90761,0.78408/
      DATA P/17500.0,20000.0,22500.0,25000.0,27500.0,30000.0,
     $32500.0,35000.0,37500.0,40000.0,50000.0,70000.0/
      N=12
      CALL FINDP(XL,XI,N,AM,BM,AN,BN,P,MMP)
      RETURN
      END
C
C
      SUBROUTINE MNB3TL(XL,XI,MMP)
      INTEGER N
      REAL XL,XI,MMP,AM(12),BM(12),AN(12),BN(12),P(12)
      DATA AM/-0.85166,-0.76014,-0.67936,-0.60390,-0.53076,
     $-0.45810,-0.38463,-0.30935,-0.23141,-0.15001,0.0,0.0/
      DATA BM/0.87821,0.79895,0.72485,0.65222,0.57905,
     $0.50407,0.42635,0.34510,0.25960,0.16912,0.0,0.0/
      DATA AN/-2.20565,-1.94644,-1.80718,-1.72396,-1.66872,
     $-1.62923,-1.59948,-1.57618,-1.56326,-1.55506,-1.52577,
     $-1.49222/
      DATA BN/1.40508,1.27353,1.19641,1.14416,1.10449,1.07207,
     $1.04425,1.01956,0.99917,0.98106,0.91418,0.80167/
      DATA P/17500.0,20000.0,22500.0,25000.0,27500.0,30000.0,
     $32500.0,35000.0,37500.0,40000.0,50000.0,70000.0/
      N=12
      CALL FINDP(XL,XI,N,AM,BM,AN,BN,P,MMP)
      RETURN
      END
C
C
      SUBROUTINE MNB1TM(XL,XI,MMP)
      INTEGER N
      REAL XL,XI,MMP,AM(12),BM(12),AN(12),BN(12),P(12)
      DATA AM/-0.81546,-0.71917,-0.62999,-0.54483,-0.46131,
     $-0.37767,-0.29258,-0.20493,-0.11372,-0.01799,0.0,0.0/
      DATA BM/0.85198,0.76730,0.68368,0.59952,0.51348,
      $0.42446,0.33155,0.23388,0.13058,0.02077,0.0,0.0/
      DATA AN/-1.74025,-1.71461,-1.68506,-1.65888,-1.63683,
      $-1.62467,-1.62145,-1.61585,-1.60960,-1.60349,-1.57956,
      $-1.54989/
      DATA BN/1.16739,1.12852,1.09184,1.05855,1.02819,1.00199,
      $0.97950,0.95723,0.93546,0.91430,0.83454,0.69264/
      DATA P/17500.0,20000.0,22500.0,25000.0,27500.0,30000.0,
      $32500.0,35000.0,37500.0,40000.0,50000.0,70000.0/
      N=12
      CALL FINDP(XL,XI,N,AM,BM,AN,BN,P,MMP)
      RETURN
      END
C
C
      SUBROUTINE MNB2TM(XL,XI,MMP)
      INTEGER N
      REAL XL,XI,MMP,AM(12),BM(12),AN(12),BN(12),P(12)
      DATA AM/-0.82772,-0.73912,-0.65875,-0.58310,-0.50972,
      $-0.43694,-0.36352,-0.28849,-0.21102,-0.13036,0.0,0.0/
      DATA BM/0.86435,0.78810,0.71417,0.64068,0.56625,
      $0.48988,0.41075,0.32816,0.24143,0.14990,0.0,0.0/
      DATA AN/-1.72954,-1.69361,-1.65568,-1.62380,-1.59788,
      $-1.58317,-1.57779,-1.57007,-1.56198,-1.55434,-1.52948,
      $-1.49889/
      DATA BN/1.16532,1.12510,1.08821,1.05571,1.02676,1.00228,
      $0.98156,0.96107,0.94114,0.92189,0.85073,0.72628/
      DATA P/17500.0,20000.0,22500.0,25000.0,27500.0,30000.0,
      $32500.0,35000.0,37500.0,40000.0,50000.0,70000.0/
      N=12
      CALL FINDP(XL,XI,N,AM,BM,AN,BN,P,MMP)
      RETURN
      END
C
C
      SUBROUTINE MNB3TM(XL,XI,MMP)
      INTEGER N
      REAL XL,XI,MMP,AM(12),BM(12),AN(12),BN(12),P(12)
      DATA AM/-0.83610,-0.75320,-0.67905,-0.60979,-0.54292,
      $-0.47682,-0.41033,-0.34256,-0.27274,-0.20021,0.0,0.0/
      DATA BM/0.87288,0.80264,0.73535,0.66887,0.60179,
      $0.53314,0.46218,0.38827,0.31082,0.22924,0.0,0.0/
      DATA AN/-1.72807,-1.67868,-1.63222,-1.59547,-1.56668,
      $-1.55014,-1.54300,-1.53376,-1.52451,-1.51604,-1.49081,
      $-1.46142/
      DATA BN/1.16520,1.12252,1.08507,1.05316,1.02533,1.00218,
      $0.98272,0.96351,0.94492,0.92706,0.86184,0.74894/
      DATA P/17500.0,20000.0,22500.0,25000.0,27500.0,30000.0,
      $32500.0,35000.0,37500.0,40000.0,50000.0,70000.0/
      N=12
      CALL FINDP(XL,XI,N,AM,BM,AN,BN,P,MMP)
      RETURN
      END
C
C
      SUBROUTINE MNB1TH(XL,XI,MMP)
      INTEGER N
      REAL XL,XI,MMP,AM(12),BM(12),AN(12),BN(12),P(12)
      DATA AM/-0.75133,-0.66711,-0.58813,-0.51192,-0.43663,
      $-0.36090,-0.28364,-0.20393,-0.12095,-0.03390,0.0,0.0/
      DATA BM/0.81027,0.73423,0.65776,0.57989,0.49978,
      $0.41666,0.32982,0.23859,0.14224,0.04005,0.0,0.0/
      DATA AN/-1.59365,-1.58646,-1.58601,-1.59105,-1.58906,
      $-1.58418,-1.57841,-1.57260,-1.56713,-1.56209,-1.54224,
      $-1.51577/
      DATA BN/1.05250,1.02384,0.99821,0.97529,0.95212,0.92926,
      $0.90694,0.88522,0.86408,0.84348,0.76489,0.62133/
      DATA P/17500.0,20000.0,22500.0,25000.0,27500.0,30000.0,
      $32500.0,35000.0,37500.0,40000.0,50000.0,70000.0/
      N=12
      CALL FINDP(XL,XI,N,AM,BM,AN,BN,P,MMP)
      RETURN
      END
C
C
      SUBROUTINE MNB2TH(XL,XI,MMP)
      INTEGER N
      REAL XL,XI,MMP,AM(12),BM(12),AN(12),BN(12),P(12)
      DATA AM/-0.76738,-0.69018,-0.61898,-0.55114,-0.48480,
      $-0.41865,-0.35169,-0.28311,-0.21223,-0.13839,0.0,0.0/
      DATA BM/0.82674,0.75867,0.69111,0.62300,0.55349,
      $0.48187,0.40755,0.32996,0.24856,0.16276,0.0,0.0/
      DATA AN/-1.56446,-1.55425,-1.55164,-1.55457,-1.54993,
      $-1.54263,-1.53484,-1.52744,-1.52069,-1.51464,-1.49477,
      $-1.46812/
      DATA BN/1.05044,1.02313,0.99920,0.97804,0.95661,0.93556,
      $0.91515,0.89541,0.87633,0.85784,0.78830,0.66284/
      DATA P/17500.0,20000.0,22500.0,25000.0,27500.0,30000.0,
      $32500.0,35000.0,37500.0,40000.0,50000.0,70000.0/
      N=12
      CALL FINDP(XL,XI,N,AM,BM,AN,BN,P,MMP)
      RETURN
      END
```

```
C
C
        SUBROUTINE MNB3TH(XL,XI,MMP)
        INTEGER N
        REAL XL,XI,MMP,AM(12),BM(12),AN(12),BN(12),P(12)
        DATA AM/-0.77877,-0.70682,-0.64118,-0.57908,-0.51864,
        $-0.45858,-0.39797,-0.33606,-0.27221,-0.20587,0.0,0.0/
        DATA BM/0.83843,0.77607,0.71467,0.65308,0.59045,
        $0.52609,0.45946,0.39005,0.31738,0.24096,0.0,0.0/
        DATA AN/-1.54434,-1.53041,-1.52525,-1.52570,-1.51857,
        $-1.50928,-1.50007,-1.49168,-1.48426,-1.47775,-1.45812,
        $-1.43281/
        DATA BN/1.04903,1.02253,0.99976,0.97982,0.95961,0.93988,
        $0.92086,0.90259,0.88501,0.86804,0.80475,0.69132/
        DATA P/17500.0,20000.0,22500.0,25000.0,27500.0,30000.0,
        $32500.0,35000.0,37500.0,40000.0,50000.0,70000.0/
        N=12
        CALL FINDP(XL,XI,N,AM,BM,AN,BN,P,MMP)
        RETURN
        END
C
C
        SUBROUTINE FINDP(X,Y,N,AM,BM,AN,BN,P,MMP)
        INTEGER N,I1,I2
        REAL X,Y,AM(N),BM(N),AN(N),BN(N),P(N),MMP,XINT(12),
        $YINT(12),YT,PAV,AMAV,BMAV,ANAV,BNAV,XINTAV,YINTAV,
        $P1,AM1,BM1,AN1,BN1,XINT1,YINT1,
        $P2,AM2,BM2,AN2,BN2,XINT2,YINT2
        DO 1 I=1,N
        XINT(I)=-(BN(I)-BM(I))/(AN(I)-AM(I))
        YINT(I)=-(AM(I)*BN(I)-AN(I)*BM(I))/(AN(I)-AM(I))
        1 CONTINUE
        IF(X.LT.XINT(1)) YT=AN(1)*X+BN(1)
        IF(X.GE.XINT(1)) YT=AM(1)*X+BM(1)
        IF(Y.GE.YT) GO TO 10
        IF(X.LT.XINT(N)) YT=AN(N)*X+BN(N)
        IF((X.LT.XINT(N)).AND.(Y.LE.YT)) GO TO 20
        DO 2 I=2,N
        IF(X.LT.XINT(I)) YT=AN(I)*X+BN(I)
        IF(X.GE.XINT(I)) YT=AM(I)*X+BM(I)
        IF(Y.GE.YT) GO TO 3
        2 CONTINUE
        3 CONTINUE
        I1=I-1
        I2=I
        ITER=0
```

```
P1=P(I1)
AM1=AM(I1)
BM1=BM(I1)
AN1=AN(I1)
BN1=BN(I1)
XINT1=XINT(I1)
YINT1=YINT(I1)
P2=P(I2)
AM2=AM(I2)
BM2=BM(I2)
AN2=AN(I2)
BN2=BN(I2)
XINT2=XINT(I2)
YINT2=YINT(I2)
4 IF(ITER.GT.20) GO TO 7
ITER=ITER+1
XINTAV=(XINT1+XINT2)/2
YINTAV=(YINT1+YINT2)/2
PAV=(P1+P2)/2
AMAV=(AM1+AM2)/2
BMAV=(BM1+BM2)/2
ANAV=(AN1+AN2)/2
BNAV=(BN1+BN2)/2
IF(X.LT.XINTAV) YT=ANAV*X+BNAV
IF(X.GE.XINTAV) YT=AMAV*X+BMAV
IF(Y.GE.YT) GO TO 5
IF(Y.LT.YT) GO TO 6
5 CONTINUE
XINT2=XINTAV
YINT2=YINTAV
P2=PAV
AM2=AMAV
BM2=BMAV
AN2=ANAV
BN2=BNAV
GO TO 4
6 CONTINUE
XINT1=XINTAV
YINT1=YINTAV
P1=PAV
AM1=AMAV
BM1=BMAV
AN1=ANAV
BN1=BNAV
GO TO 4
7 CONTINUE
```

```
MMP=PAV
RETURN
10 CONTINUE
AINT=(YINT(1)-YINT(2))/(XINT(1)-XINT(2))
BINT=YINT(2)
YT=AINT*X+BINT
IF((YT+X).GT.1.0) GO TO 11
IF((X.LT.XINT(1)).AND.(Y.LT.YT)) GO TO 11
IF(Y.GE.YT) GO TO 12
11 CONTINUE
Y1=AN(1)*X+BN(1)
Y2=AN(2)*X+BN(2)
MMP=(Y-Y1)*(P(1)-P(2))/(Y1-Y2)+P(1)
RETURN
12 CONTINUE
Y1=AM(1)*X+BM(1)
Y2=AM(2)*X+BM(2)
MMP=(Y-Y1)*(P(1)-P(2))/(Y1-Y2)+P(1)
RETURN
20 CONTINUE
Y1=AN(N-1)*X+BN(N-1)
Y2=AN(N)*X+BN(N)
MMP=(Y-Y1)*(P(N-1)-P(N))/(Y1-Y2)+P(N-1)
RETURN
END
```